Microbial Nitrate Dependent Fe^{2+} Oxidation: A Potential Early Mars Metabolism

Thesis

Microbial Nitrate-Dependent Fe^{2+} Oxidation: A Potential Early Mars Metabolism

Alexander Boyd Price

Thesis Submitted for the Degree of
Doctor of Philosophy

Astrobiology

The Open University

April 2020

Abstract

This thesis experimentally investigates the proposition that aqueous environments with anoxic, reducing, circumneutral conditions, inorganic electron donors and oxidants such as nitrate may have allowed chemolithotrophic microbial metabolisms, such as nitrate-dependent Fe^{2+} oxidation (NDFO), to thrive on early Mars.

The NDFO microorganisms, *Acidovorax sp*. strain BoFeN1, *Paracoccus sp*. strain KS1 and *Pseudogulbenkiania sp*. strain 2002, are demonstrated to grow lithoautotrophically with a Mars-relevant olivine Fe^{2+} source and in martian simulant media developed from *in situ* and meteorite geochemical data. Additionally, mixotrophic NDFO with Fe^{2+} and an organic co-substrate as electron donors, was shown to increase the extent of microbial growth, which gains importance in light of the confirmation of complex organics at the martian surface. Biomineralised microbial features were discovered after culture with olivine and the oxidation of Fe^{2+} was measured in heterotrophic cultures. Microfossils and Fe^{3+} compounds in reducing contexts provide targets for biosignature detection missions.

In addition, this work presents findings on the biochemical mechanisms of NDFO, quantifying the relative contributions of the Nar respiratory nitrate reductase enzyme, putative ferroxidases and nitrite accumulation to Fe^{2+} oxidation during nitrate reduction. Gene knockout experiments revealed that Fe^{2+} oxidation in the heterotrophic *Salmonella enterica* Serovar Typhimurium strain SL1344 is largely driven by the production of reactive nitrite ions during Nar activity. Draft genome analysis of *Acidovorax sp*. strain BoFeN1 and *Paracoccus sp*. strain KS1 revealed potential mechanisms of electron acquisition during Fe^{2+} oxidation, underlining that multiple mechanisms of NDFO exist.

The combined findings of this thesis support the plausibility of NDFO in the deep martian past and propose mechanisms by which evidence may be preserved in the geological record of that planet.

Acknowledgements

This thesis was written by my hand but would have been impossible without the guidance and support of so many others, some of whom I would particularly like to highlight.

Firstly, Karen, Vic and Susanne, who have been endlessly patient, supportive, dependable and attentive despite the ever-increasing responsibilities within AstrobiologyOU and elsewhere. I have become an immeasurably better scientist under your watch and could not have imagined a better supervisory team.

The Open University, for supporting my work these past years. The mission to make higher education accessible for all is a worthy and inspiring one that I hope shall endure.

My friends Pegg, Elliot, Megan, Tom and Candice. Your love and support kept me going in the moments I'd rather have been anywhere else. I thank you all for that.

Chris, Stacy, Paul, Jack, Andrew, Rhian, Leanne, Frances and other past and present denizens of K-Block, Gass and Hooke. Your endless supply of wit, niche conversation and general inane wittering has sustained me through many a long day.

Sammy and Leo the cat, for making the socially-distanced write-up feel a little less isolated. I can't wait to find out where our adventures take us.

Laurie, for giving a quiet, moody teenager the confidence to follow his passions.

My parents, Don and Carole, for raising me to be endlessly curious and for giving me the chance to pursue the things that matter to me.

My brothers, Dan and Tom, sister-in-law Laura and my amazing god-daughter Emilia, for inspiring me to be the best version of myself.

Lastly, to my grandmother, Dorothy. You taught me the value of kindness, honesty and service to others. You will never be forgotten. Thank you.

Table of Contents

List of Figures

List of Tables

Equations

Cell density

$$T = N \times \frac{A}{a} \div V \quad (1)$$

where

T = number of cells mL^{-1}

N = mean number of cells per field of view

A = surface of filtration (mm^2)

a = the area of the microscopic field (mm^2)

V = volume of sample filtered (mL)

Maximum specific growth rate

$$\mu_{max} = \frac{\ln x - \ln x_0}{t} \quad (2)$$

where

μ_{max} = maximum specific growth rate

x_0 = cell density at the start of the exponential phase

x = cell density at the end of exponential phase

t = time between measurement of x_0 and x

Declaration

This composition of this thesis has been solely my own work. Where samples or results have been obtained through the work of other researchers or technical staff, their contributions are made clear in the text as appropriate. I have conducted all subsequent processing and analysis of data myself.

Two first-authored papers containing content held within this thesis have been published during the course of writing. A condensed version of the literature review (Chapter 1) was published as a hypothesis paper. Additionally, the draft genomes sequenced for Chapter 4 have been published together as a genome announcement paper. These publications are listed below:

1) Price, A., Pearson, V. K., Schwenzer, S. P., Miot, J., & Olsson-Francis, K. (2018). Nitrate-dependent iron oxidation: a potential Mars metabolism. *Frontiers in Microbiology*, *9*, 513.
2) Price, A., Macey, M. C., Miot, J., & Olsson-Francis, K. (2018). Draft Genome Sequences of the Nitrate-Dependent Iron-Oxidizing Proteobacteria *Acidovorax sp*. Strain BoFeN1 and *Paracoccus pantotrophus* Strain KS1. *Microbiology Resource Announcements*, *7*(10), e01050-18.

I hereby confirm that no part of this thesis has been submitted for any other qualification.

“He was determined to discover the underlying logic behind the universe.

Which was going to be hard, because there wasn't one.”

~ Terry Pratchett

1. Literature Review

1.1 Introduction

Throughout human history, questions around the uniqueness, or otherwise, of life on Earth have defined and permeated cultures and religions. It is only in recent decades, with the return of a wealth of data from probes, satellites, space telescopes, orbiters and landers that we have begun to approach questions of habitability in answerable terms. These questions are of great philosophical, as well as scientific, importance. The field of astrobiology applies the knowledge and principles of terrestrial biology to the questions of possible origin, development and persistence of organisms in extraterrestrial environments. This pursuit is the underlying thread running through this thesis, setting the course for the experiments undertaken, and guiding the focus of interpretation and discussion of results.

Mars has inspired the search for extraterrestrial life since the early days of the telescope. Perceptions of its habitability – or even inhabitation – have fluctuated with advances in our exploration capabilities and increased knowledge of martian environments (Filiberto and Schwenzer, 2018). The martian "channels" described by Giovanni Schiaparelli in the 19th century led to a wave of public interest in Mars and imagined civilisations there, helped, in part, by the mistranslation of his description to "canals", implying deliberately constructed features. This was perpetuated by the astronomer Percival Lowell's claims to have seen these supposed alien structures for himself. Though these claims proved to be unfounded, the idea of martian life persisted in popular culture through literature such as HG Wells' famed novel *The War of the Worlds*. Any question of a civilisation was, however, firmly put to rest by the early ventures of the space age beyond the Earth-Moon system.

The first space missions to Mars confirmed our near neighbour to be a cold, dry world, heavily cratered and bathed in radiation that penetrates the thin, anoxic atmosphere (Kliore et al., 1965; Leighton et al., 1965). Over the intervening decades since Mariner 4, fly-bys,

orbiters, landers and rovers have allowed us to build up the story of Mars' history; one which points to a once warmer and wetter environment than today, a potential haven for early microbial life (Craddock and Howard, 2002; Ehlmann et al., 2011).

This project relates specifically to early Mars as a habitat for known terrestrial microbial metabolisms. The resulting body of work provides new knowledge pertaining to the suitability and feasibility, in simulated martian environmental conditions, of known terrestrial microbial metabolisms, particularly those that utilise substrates that are known to exist on Mars. Specifically, this thesis will investigate whether biotic Fe^{2+} oxidation could have occurred on Mars, building on previous work relating to microbial iron (Fe) reduction and attempting to close the hypothetical loop of biotic Fe cycling in the martian crust (Nixon, 2014). The results extend our knowledge of relatively understudied forms of microbial Fe^{2+} oxidation on Earth, as well as informing design of - and targets for - future life detection missions to Mars.

1.1 Mars

1.1.1 A brief history

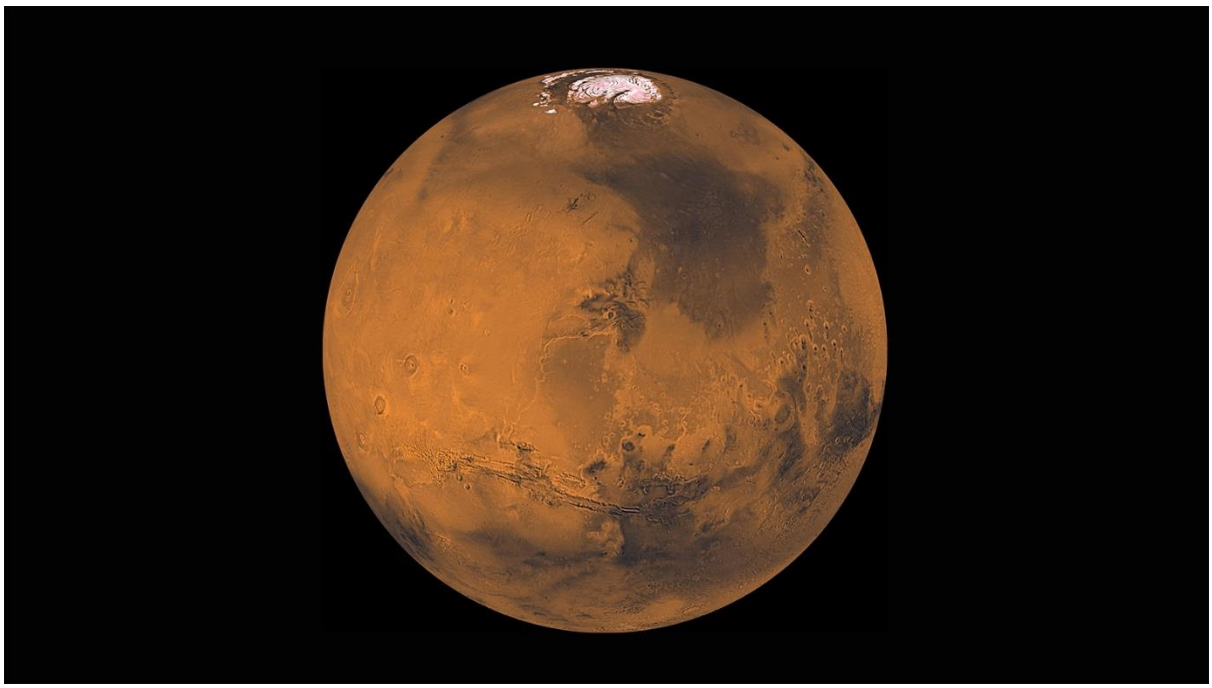

Figure 1.1 Global mosaic image of Mars from Viking orbiter images. Centred at 20° latitude and 60° longitude (Image credit: NASA/JPL/USGS).

Mars (Figure 1.1) is the outermost of the rocky planets within our Solar System, formed by accretion, along with the other planets, within the protoplanetary disc orbiting our young Sun around 4.6 Ga. Owing to its relatively small size (0.107 Earth masses), Mars cooled more rapidly than our own planet, meaning that a global magnetic field is unlikely to have have been active beyond its first few hundred million years (Chassefière and Leblanc, 2004). The period immediately following this initial cooling, termed the Noachian (4.1–3.7 Ga), was characterised by high impact, erosion and valley formation rates. Widespread hydrous weathering products formed at that time suggest at least occasional warm and wet conditions at the surface, resulting from the effects of impacts or volcanism (Schwenzer and Kring, 2009; Halevy and Head III, 2014). The existence of liquid water is critical to assessing habitability, as an essential solvent for biochemistry and requirement for all known life.

Either through heavy bombardment or the lack of a protective magnetic field to resist the solar wind, the atmosphere was largely stripped away over time (Jakosky and Phillips, 2001; Chassefière and Leblanc, 2004), exposing the surface to intense solar radiation and cosmic rays. Since then, liquid water has been unstable under surface conditions because of the low atmospheric pressure (increasing sublimation), ionising radiation (which splits water molecules into free radicals) and low average global temperatures. However, infrequent catastrophic outflow events (Tanaka et al., 2005) during the Hesperian period (3.7-3.0 Ga), upwelling of groundwater in deep basins and impact-generated hydrothermal systems may have allowed for large volumes of water to form at the surface, with circulation perhaps persisting over millions of years (Marzo et al., 2010; Schwenzer et al., 2012; Michalski et al., 2013; Osinski et al., 2013).

In the period from 3 Ga to the present day (the Amazonian), conditions are thought to have been broadly similar to the cold, desiccated and irradiated environment we currently observe (Carr and Head, 2010). Volcanic activity decreased and episodic floods represent the most notable large-scale aqueous activity at the surface during this time (Carr and Head, 2010), though evidence of recent wet-based glaciation is now mounting (Butcher et al., 2017). Today, liquid groundwater is proposed to be the source of seasonal recurring slope lineae (RSL) features (Ojha et al., 2015) although estimates of water volume therein are no more than 3 wt% (Edwards and Piqueux, 2016). Despite the present surface conditions on Mars posing challenges to the existence of extant life there, the well-preserved geological record of the broadly stable cold and dry surface conditions of the last three billion years offers an opportunity to investigate features from time periods which are difficult to access in the terrestrial rock record.

1.1.2 Habitable worlds in parallel?

Efforts to find convincing evidence of the earliest terrestrial life are hampered by the continual reprocessing of the crust by the action of plate tectonics. All but a few traces of the early Earth's crust have been destroyed, and the remaining material is heavily altered, making all current evidence for life in the early Archaean period (Figure 1.2) inherently questionable. The oldest undisputed evidence for microbial life on Earth falls at ~3.5 Ga (Westall et al., 2006; Noffke et al., 2013), within the martian Hesperian period. However, a more recent study proposes stromatolites in Isua supracustal belt rock of 3.7 Ga age (Nutman et al., 2016), there is geochemical evidence of microbially-induced carbon isotope fractionation on Earth at ~3.8 Ga and putative microfossils in Nuvvuagittuq supracrustal belt rock at >3.77 Ga (Mojzsis et al., 1996; Dodd et al., 2017). This older evidence corresponds to the late Noachian period on Mars, meaning that life may have been established on Earth while Mars still harboured a thick atmosphere and standing liquid water. Mars has not experienced plate tectonics (McSween et al., 2009), so if life ever existed there, those ancient rocks, and thus any biosignatures preserved within, may be good targets for investigation.

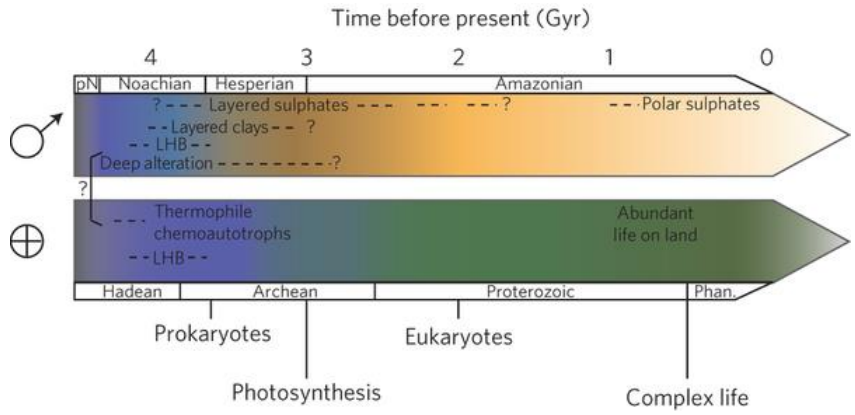

Figure 1.2. Geological timescale for Mars with proposed dates for formation of features on Mars (top) and milestones of evolution of life on Earth (bottom). The coincidence of peak activity of deep alteration processes on Mars and the first prokaryotic life on Earth is noted. "pN" =pre-Noachian. "Phan."= Phanerozoic. Taken from (Michalski et al., 2013).

1.1.3 Hydrothermal habitats on early Mars

During the Noachian period, more hospitable surface environments for life may have prevailed (Carr and Head, 2010; Mangold et al., 2012), including: large-scale fluvial systems (Malin and Edgett, 2003; Irwin et al., 2005; Fassett and Head, 2008; Mangold et al., 2012; Williams et al., 2013), and impact-generated hydrothermal, lacustrine and groundwater systems (Schwenzer and Kring, 2009; Osinski et al., 2013; Grotzinger et al., 2014b; Rampe et al., 2017). Evidence for these environments comes from lake bed sediments, such as those identified at Gale Crater, which the NASA Mars Science Laboratory rover (Curiosity) is investigating in detail (e.g., Grotzinger et al., 2015). Phyllosilicates and other hydrated minerals have also been observed from orbit (Gendrin et al., 2005; Bibring et al., 2006; Chevrier et al., 2007) and from the ground (Squyres et al., 2004b; Ehlmann et al., 2011). Despite this wealth of evidence for a range of habitable environments, hydrothermal systems are of intense astrobiological interest due to the temperature, redox and chemical gradients which drive productive microbial ecosystems here on Earth (e.g., Moyer et al., 1995; Konhauser and Ferris, 1996; Brazelton et al., 2006).

On Earth, active hydrothermal systems are linked to tectonic processes or volcanism, which drive water circulation; there is no evidence of a sufficiently large and sufficiently young crater on the Earth's surface in which an active impact-generated hydrothermal system could exist (Osinski et al., 2013). However, evidence for past hydrothermal systems is observed in the form of hydrothermal mineral veins around many ancient terrestrial craters, e.g., Chicxulub, Manicouagan, Sudbury and others (see Pirajno (2009) and Osinski et al. (2013) for reviews). On Mars, hydrothermal systems caused by large impacts craters (>30 km) could provide warm water conditions even in periods of cold climate (Abramov and Kring, 2005).

Hydrothermal fluids dissolve bedrock and precipitate secondary mineral phases as conditions change throughout their lifetime and, thus, contain abundant bioessential elements (carbon, hydrogen, oxygen, nitrogen and sulfur) that support diverse microbial communities (Arnold and Sheppard, 1981; Welhan and Craig, 1983; Charlou and Donval, 1993; Wheat et al., 1996; Konn et al., 2009). With estimated life-times of 150,000-200,000 years even for modest craters (100-180 km diameter) the size of Gale, and with cycles of continuous mineral dissolution and precipitation maintaining the availability of inorganic substrates for microorganisms during that time, impact-generated hydrothermal systems could have provided localised hospitable zones (Abramov and Kring, 2005; Schwenzer and Kring, 2009).

To better understand the conditions of impact-generated systems on early Mars, some previously characterised, potentially habitable environments are be discussed here: (1) the ancient lake at Gale Crater investigated by the Curiosity rover (Palucis et al., 2016); (2) the hydrothermal environment discovered in the rim of Endeavour Crater by the MER Opportunity rover (Squyres et al., 2012; Arvidson et al., 2014; Grotzinger et al., 2014b; Fox et al., 2016), and (3) the hydrothermal fluids which altered the nakhlite meteorites (Changela and Bridges, 2010; Hicks et al., 2014; Schwenzer et al., 2016).

1.1.3.1 Gale crater lake hydrothermal system

The ancient lake bed at Gale Crater is likely to be one of many that formed within impact craters on Mars (Cabrol and Grin, 1999). Conglomerates, cross-bedded sandstones, siltstones, and mudstones have been identified by the Curiosity rover, allowing for a detailed understanding of water flow, standing water conditions and even temporary periods of desiccation (Vaniman et al., 2013; Williams et al., 2013; Grotzinger et al., 2014b; Grotzinger et al., 2015; Palucis et al., 2016; Hurowitz et al., 2017). The mineralogy

and geochemistry of Gale Crater sediments suggest that the conditions in this ancient lake were temperate and pH-neutral, suitable for the maintenance of life in the water table and water column over the 10,000-10,000,000 year lifetime of the active system (Grotzinger et al., 2014b; Grotzinger et al., 2015). However, excursions to, or local areas of, mildly acidic (pH > 2) conditions are evidenced by the discovery of jarosite (Rampe et al., 2017), but these would not pose an insurmountable obstacle to the continued existence of a microbial biosphere, as has been demonstrated using simulated Mars conditions previously (Bauermeister et al., 2014).

Post-depositional diagenetic and alteration processes, such as the dissolution of primary minerals, the formation of calcium-sulfate veins, cementation, desiccation, or even changes to the chemistry of the incoming sediment load due to external silicic volcanism, will have changed the lake's environmental conditions multiple times, leading to complex environmental conditions variable in space and time (Bridges et al., 2015; Johnson et al., 2016; Schwenzer et al., 2016; Frydenvang et al., 2017; Nachon et al., 2017; Rampe et al., 2017; Yen et al., 2017). Further, Gale Crater sediments are reported to contain bioessential elements such as hydrogen, phosphorus, oxygen and nitrogen, and Fe and sulfur in variable oxidation states that could provide possible energy sources (Vaniman et al., 2013; Grotzinger et al., 2014b; Stern et al., 2015; Morris et al., 2016; Sutter et al., 2016). Complex organic molecules are also reported to be present at concentrations that could have supported past life (Eigenbrode et al., 2018).

1.1.3.2 Endeavour crater hydrothermal system

Orbital observations have shown that many craters on Mars bear evidence of impact-generated hydrothermal activity (Marzo et al., 2010; Mangold et al., 2012), and ground based exploration by the MER rover Opportunity revealed an impact-generated

hydrothermal system at Endeavour Crater, where localized zinc enrichments and aluminium-rich smectites in fractures suggest hydrothermal alteration. From the geochemical data collected by Opportunity, the original fluids in the system are predicted to have been low-temperature and slightly acidic to circumneutral pH, amenable to microbial life (Squyres et al., 2012; Arvidson et al., 2014; Fox et al., 2016).

1.1.3.3 Hydrothermal alteration in nakhlite meteorites

Characteristic products of hydrothermal alteration, namely carbonates and clay minerals, are also found within martian meteorites; the most complete succession of martian minerals ascribed to impact-generated hydrothermal activity are specifically found in the nakhlite martian meteorites (Changela and Bridges, 2010; Bridges and Schwenzer, 2012; Hicks et al., 2014). These rocks formed at ~1.3 Ga and were ejected from Mars around 11 Myr ago (Nyquist L.E., 2001), with hydrothermal alteration occurring some time since 670 Ma (Swindle et al., 2000). While these meteorites have an unknown martian provenance, and thus their geological context remains an informed guess, the opportunity to investigate the succession of minerals with Earth-based instrumentation adds significant detail to an understanding of the compositional, reduction-oxidation (redox) and pH evolution of such alteration processes. For example, the alteration reactions evident in the nakhlites indicate a change in redox conditions as evidenced by a shift from Fe^{2+}-precipitates to Fe^{3+}-precipitates over the course of the formation of the assemblage (Bridges and Schwenzer, 2012; Hicks et al., 2014). Investigating such details is, to date, beyond the capability of current rovers and landers, but future *in situ* collection of this information would represent a major advance in assessing the habitability of a site during and after hydrothermal activity.

These examples of martian environments (impact-generated hydrothermal lacustrine and groundwater systems) demonstrate the abundance of potentially habitable environments (as we understand them) on ancient Mars.

1.2 Finding model organisms for Mars

1.2.1 Extremophiles

All life on Earth falls somewhere within a set of ranges relating to physical and chemical variables (e.g., temperature, salinity, pressure, radiation), which are constantly being refined and updated. Organisms which thrive best when one or more of these parameters is outside of what is considered to be the norm, are termed "extremophilic" (extreme-loving).

These extremophiles are of great interest to astrobiologists, as many of the potential niches for life in extraterrestrial environments fall within some combination of extremes. For example, the surface of Mars today is cold, so any extant life there could be expected to be psychrophilic (cold-loving) (Reid et al., 2006). Due to the low temperature, any fluids near the surface are predicted to exist predominantly as acidic, concentrated brines (Fairén et al., 2009), and so organisms would also need to be both acidophilic (acid-loving) and halophilic (salt-loving) (Mancinelli et al., 2004; Amils et al., 2011; Oren et al., 2014).

As an alternative example, the pressure and high temperature around putative hydrothermal deep-sea vents on Saturn's moon, Enceladus (Hsu et al., 2015; Waite et al., 2017), would select for barophilic (pressure-loving) and thermophilic (heat-loving) life forms (Taubner et al., 2016; Taubner et al., 2018). In order to identify model organisms for the combinations of extremes reported for extraterrestrial environments, it is possible to investigate the microbes inhabiting analogous locations on Earth.

1.2.2 Terrestrial analogue sites

Terrestrial analogue sites are those that exhibit environmental conditions or processes comparable with those found in extraterrestrial environments. Many of these sites are 'extreme' in terms of temperature, salinity, pH or other physicochemical parameters. Some offer a combination of relevant environmental stressors, and others may simply offer a specific or rare characteristic (Preston and Dartnell, 2014). For microbiologists, terrestrial analogues of extraterrestrial environments are a source of model organisms, and those isolated from extreme environments have often developed adaptations that can be used to inform our understanding of the potential for life in extraterrestrial locations.

Popular regions for Mars analogues include the Antarctic Dry Valleys (exhibiting low temperatures, desiccation and irradiation) (Wynn-Williams and Edwards, 2000; Gilichinsky et al., 2007), the Rio Tinto mine drainage site (with low pH) (Amils et al., 2007; Amils et al., 2011; Preston et al., 2011), the Atacama Desert (desiccation and irradiation) (Connon et al., 2007; Ewing et al., 2008; Valdivia-Silva et al., 2011) and deep-sea hydrothermal vent systems (high pressure and temperature) (Amador et al., 2017). Iceland offers sites with many of these characteristics, with an added benefit - it is one of the few land masses on Earth which is primarily basaltic, compositionally similar to the crust of Mars. For a comprehensive list of current astrobiologically-relevant sites, see (Preston et al., 2012).

It is important to note that, although many analogues are considered extreme environments by the standards of terrestrial life, more clement locations can also be used to yield insights into potential martian metabolisms. One example of this would be the River Dee estuarine environment, which has been characterised as an analogue for early martian lacustrine environments such as at Gale crater (Curtis-Harper et al., 2018).

1.2.3 Appropriate martian metabolic strategies

In early martian surface environments, where the conditions were more conducive to life than the present day, both phototrophic (solar energy-driven) and chemotrophic (chemical energy-driven) primary producers may have been viable, possibly producing enough organic carbon for the subsequent development of heterotrophy (using organic carbon molecules as electron donors) and a complex web of microbial life (Westall et al., 2015). As the environment evolved from "warm and wet" to "cold and dry", life would have likely become limited to the sub-surface environment (Nixon et al., 2012). Here, they would be protected from the adverse surface conditions and, as such, may have become limited to light-independent chemolithotrophic metabolisms (those that harvest energy from redox reactions using inorganic substrates) (Nixon et al., 2012). This metabolic strategy involves the transfer of electrons donated by the inorganic substrate, through the electron transport chain for adenosine tri-phosphate (ATP) production, to a final acceptor (Figure 1.3).

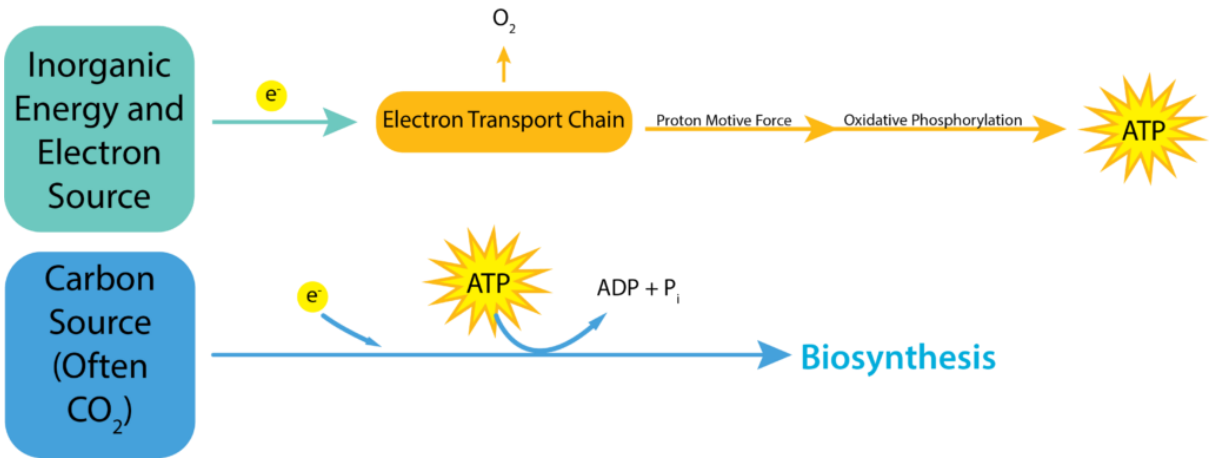

Figure 1.3. Summary of electron and carbon sources for chemolithotrophic energy production and biosynthetic pathways. e^- = electron. ADP = adenosine diphosphate. ATP = adenosine triphosphate. P_i = inorganic phosphate (Bruslind, 2019).

On Earth, chemolithotrophy is pivotal for biogeochemical cycling (e.g., of Fe, nitrogen and sulfur) (Madigan et al., 2008). Laboratory-based Mars simulation experiments, using

analogue regolith or brine, and theoretical modelling, have suggested that chemolithotrophic life driven by Fe and sulfur cycling or methanogenesis could persist in the sub-surface martian environment across a wide range of pH, salinity, desiccation and temperature (Parnell et al., 2004; Amils et al., 2007; Jepsen et al., 2007; Gronstal et al., 2009; Chastain and Kral, 2010; Smith, 2011; Popa et al., 2012; Hoehler and Jørgensen, 2013; Montoya et al., 2013; Summers, 2013; Bauermeister et al., 2014; Oren et al., 2014; King, 2015; Fox-Powell et al., 2016; Schuerger and Nicholson, 2016). Hence, understanding the role of Fe in the martian crust is crucial for astrobiological studies.

1.3 Fe chemolithotrophy

On early Earth, Fe biogeochemical cycling and the occurrence of Fe redox-couples were crucial to the evolution of the biosphere, both in microbial metabolism and also as a cofactor in metalloproteins such as cytochromes, nitrogenases and hydrogenases (Canfield et al., 2006; Hoppert, 2011; Raiswell and Canfield, 2012). In metabolism, Fe can act as either an electron acceptor or donor, dependent on its redox state (Miot and Etique, 2016). Fe-oxidising microorganisms (Section 1.3.2.1) have been shown to utilise Fe^{2+} once released by dissolution from minerals such as olivine (Santelli et al., 2001) and a similar process may have operated within potentially habitable environments on Mars. Conversely, microbial Fe reduction commonly utilises electrons donated from organic substrates, H_2 or S^0, with oxidised Fe^{3+} as the final electron acceptor (Lovley and Phillips, 1988; Lovley et al., 1989) and the plausibility of Fe reduction on Mars has been appraised previously (Nixon et al., 2012; Nixon et al., 2013; Nixon, 2014).

1.3.1 Fe in the martian crust

The crust of Mars is Fe-rich, as evidenced by the largely reddish colouration of the surface, an effect resulting from the oxidation of reduced Fe, Fe^{2+}, within basaltic bedrock to form Fe^{3+}-compounds in the uppermost rock and dust layers, often only a few millimetres in

depth (Grotzinger et al., 2014b). The FeO content of the basalts, which dominate martian geology because of the lack of plate tectonics, is roughly twice that observed in comparable basalts on Earth (Bertka and Fei, 1998). Fe^{2+} can exist as little as a few centimetres beneath the surface, as evidenced by the Mars Science Laboratory (MSL) drill holes, 'John Klein' and 'Cumberland' (Vaniman et al., 2013), and Fe^{2+}-bearing minerals such as olivine ($(Mg^{2+}, Fe^{2+})_2SiO_4$) have been detected across large areas of the martian surface (Hoefen et al., 2003). It is also likely that large amounts of basaltic glass (amorphous Fe^{2+}-containing material) is contained within martian crustal rocks (McSween et al., 2009). It has also been suggested that Fe^{2+}-bearing minerals may be released during weathering by the current martian atmosphere (Chevrier et al., 2006), although acid-sulfate weathering is thought by some to have been more prevalent in the Noachian period of early Mars history (Bibring et al., 2006; Zolotov and Mironenko, 2007) even in a broadly circumneutral global context (Andrews-Hanna and Lewis, 2011).

Owing to its abundance, availability and role in terrestrial biogeochemical cycling, Fe is an inviting starting point when considering energy sources for a biosphere on Mars. Further, Fe-rich terrestrial fluids and sediments can be of use as sources of model organisms for microbiologists assessing Mars as a habitat.

1.3.2 A potential Mars Fe cycle

The Fe-rich nature of Mars raises possibilities regarding the feasibility of Fe biogeochemical cycling. An active hydrological cycle, combined with prevailing reducing conditions during the Noachian period, are likely to have facilitated large-scale transport of Fe through enhanced dissolution and limitation of abiotic oxidation respectively (Figure 1.4).

A hypothetical 'loop' of biologically-mediated martian Fe cycling (Figure 1.5) was first proposed by Nealson (1997), which included both Fe reduction and also phototrophic Fe^{2+}-oxidation (Ehrenreich and Widdel, 1994). Nealson's model assumed a habitable photic zone on early Mars that cannot be applied to present-day Mars, because of the surface conditions that prevent closure of this 'loop' for biogeochemical Fe cycling.

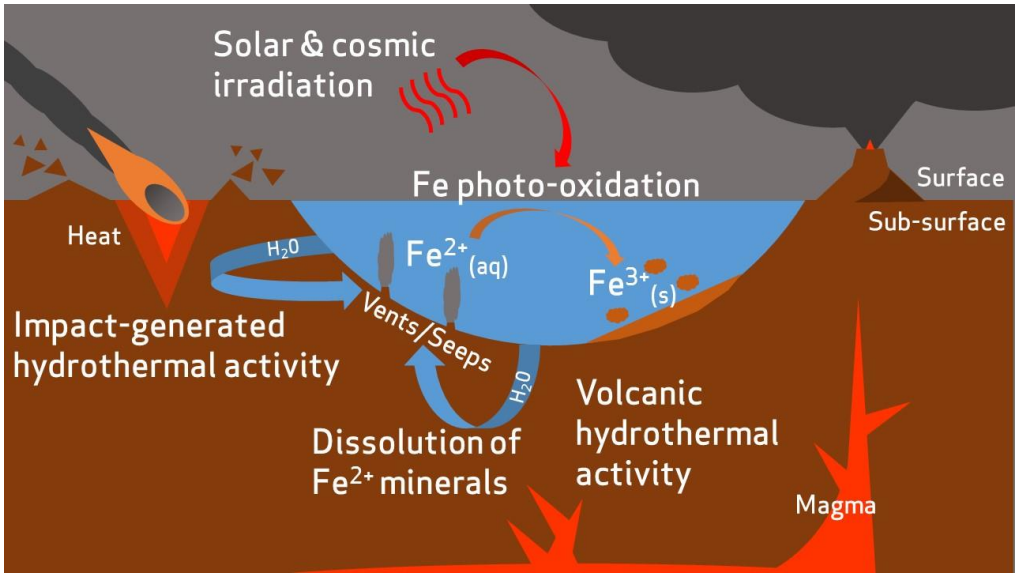

Figure 1.4. Hypothetical transport of Fe on early Mars. Reduced Fe is released into aqueous environments by dissolution of ferrous minerals. This process could be accelerated by volcanic or impact-generated hydrothermal activity (McSween et al., 2009). Some dissolved Fe may be photo-oxidised by solar UV radiation to ferric compounds and deposited as sediments (Nie et al., 2017).

Although research suggests that phototrophs may be sufficiently protected inside various micro-habitats (e.g., within ice, halite, Fe^{3+}-rich sediments and impact-shocked rocks) to withstand modern martian UV flux and remain photosynthetically productive (Cockell and Raven, 2004), the effect of desiccation, in combination with UV irradiation, would prevent dispersal and negatively impact viability (Cockell et al., 2005). Additionally, a lack of liquid water at the surface of Mars would be detrimental to any form of life (Martín-Torres et al., 2015).

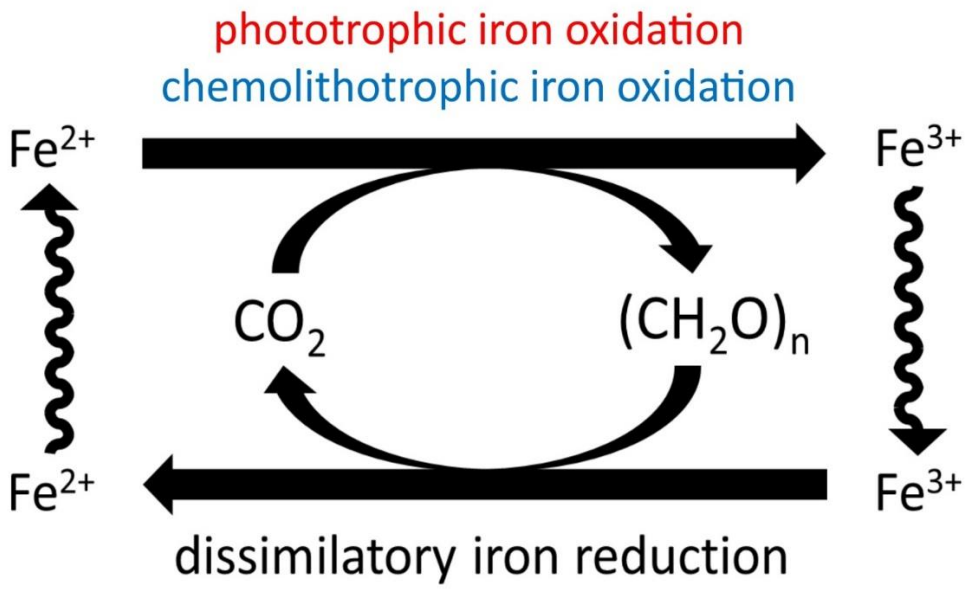

Figure 1.5. Hypothetical martian biogeochemical cycle of Fe. Nealson (1997) suggested combination of phototrophic Fe^{2+} oxidation (Ehrenreich and Widdel, 1994) and heterotrophic Fe reduction (Myers and Nealson, 1988) to give a hypothetical Fe cycle. Carbon cycles are driven by solar and chemical energy sources. Fe is both the oxidant and the reductant for the cycle. Chemolithotrophic Fe^{2+} oxidation is proposed as an alternative to phototrophic Fe^{2+} oxidation, as the post-Noachian Mars surface environment may restrict opportunities for phototrophy, and any mechanism of Fe^{2+} oxidation in more recent periods may necessarily be light-independent.

A plausible alternative to a phototrophic Fe-oxidiser would be a chemolithotrophic Fe-oxidiser, which can obtain energy from redox reactions involving inorganic substances. This would allow for a light-independent Fe cycle, which could have existed at the surface or in the sub-surface of early Mars and even continue today in deep sub-surface groundwaters (Michalski et al., 2013).

1.3.2.1 Chemolithotrophic Fe^{2+} oxidation

Abiotic Fe^{2+} oxidation occurs as a function of oxidant concentration, pH, temperature and Fe^{2+} concentration (Ionescu et al., 2015). On Earth, low pH (<4) prevents the abiotic oxidation of Fe^{2+} by atmospheric O_2 (Morgan and Lahav, 2007) (Figure 1.6), allowing biotic oxidation (using oxygen as the electron acceptor) to dominate in aerobic, acidic

environments such as acid mine drainage sites like Rio Tinto (Amils et al., 2007; Amils et al., 2011; Preston et al., 2011). Acidophilic (low pH-adapted) microbes take advantage of the high proton gradient to synthesise ATP. The influx of protons is balanced with electrons sourced by the oxidation of Fe^{2+} (Hedrich et al., 2011).

Evidence from evaporitic palaeo-environments on Mars suggest historic low pH (<3.5) conditions existed in certain regions (Gendrin et al., 2005; Squyres and Knoll, 2005; Ming et al., 2006), although neutral-alkaline pH-associated clays are also observed in older terrains (Bibring et al., 2006). The transition to more arid conditions is thought to have coincided with a general shift from widespread clay formation to evaporitic sulfate precipitation at the surface (Bibring et al., 2006; Chevrier et al., 2007), resulting in increasingly acidic brines that may have promoted this form of biotic Fe^{2+} oxidation (Tosca and McLennan, 2006; 2009). Given that only trace quantities (1450 ppm) of oxygen exist in the modern martian atmosphere (Mahaffy et al., 2013), the idea of aerobic, acidophilic Fe^{2+} oxidation at the surface today has been largely dismissed (Bauermeister et al., 2014). However, modelling approaches have suggested that enough oxygen could be dissolved in perchlorate brines to support oases of aerobic metabolism in the martian subsurface (Stamenković et al., 2018), albeit at temperatures largely below the currently known limits for microbial growth (Clarke et al., 2013).

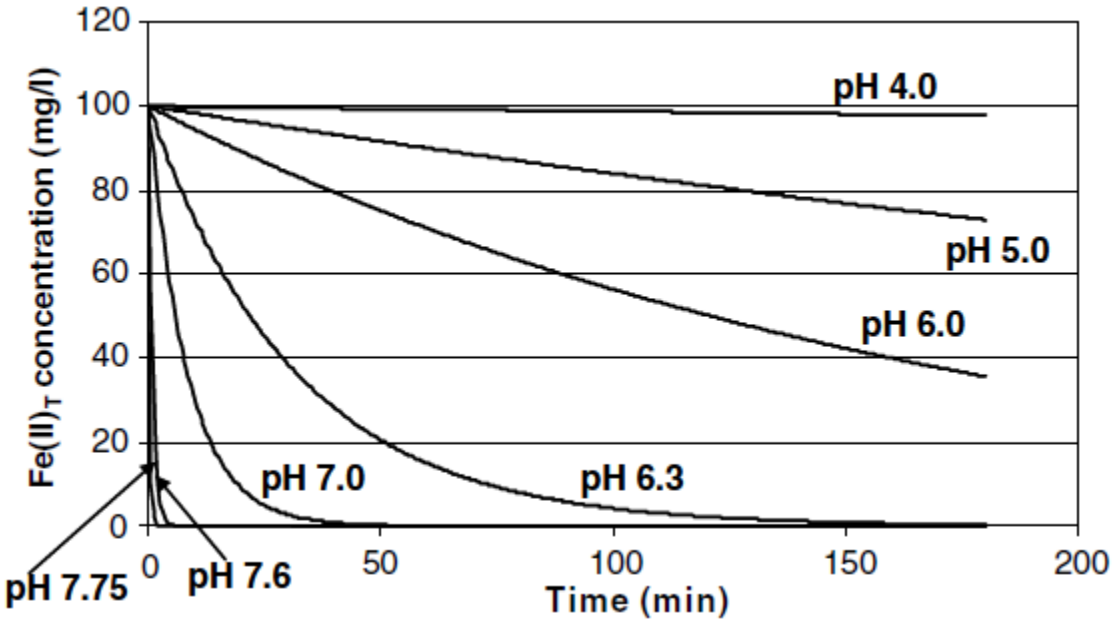

Figure 1.6. Oxidation rate of soluble Fe^{2+} by O_2 in aqueous solution as a function of pH. Taken from Morgan and Lahav (2007).

An alternative to aerobic Fe-oxidisers is microaerophilic (requiring < 21 % oxygen to survive) neutrophilic Fe-oxidisers (NFeOs), which are able to compete with abiotic oxidation at near neutral pH. On Earth, this form of metabolism is largely restricted to oxic-anoxic boundary zones, where oxidation is much slower (Roden et al., 2004). Phylogenetic studies have identified NFeOs in a variety of terrestrial environments including arctic tundra, Icelandic streams, deep-ocean vents, Fe-rich soils and temperate ground waters (Emerson and Moyer, 2002; Edwards et al., 2003; Emerson and Weiss, 2004; Cockell et al., 2011; Hedrich et al., 2011; Emerson et al., 2015). Many NFeOs are psychrophilic (Edwards et al., 2003; Edwards et al., 2004), which could be linked to the much lower rate of abiotic Fe^{2+}-oxidation at low temperatures (Millero et al., 1987). Fe-bearing minerals such as olivine can be biologically oxidised by a neutrophilic Fe-oxidiser under a 1.6 % oxygen headspace gas (Popa et al., 2012).

On Mars, regions of the modern sub-surface have been proposed as tolerable for some extreme microaerophiles today (Fisk and Giovannoni, 1999). King (2015) also argued that microaerophilic activity could be supported by the modern oxygen concentrations recorded by the Curiosity rover (Mahaffy et al., 2013; Franz et al., 2015); however, this metabolism would be restricted, since oxygen diffusion distances in sediments are often limited to a few millimeters (Revsbech et al., 1980; Reimers et al., 1986; Visscher et al., 1991). Furthermore, there is evidence to suggest that redox stratification, seen in standing water bodies on Earth (Comeau et al., 2012), also occurred in martian lakes such as Gale Crater, resulting in an anoxic bottom layer (Hurowitz et al., 2017). Even assuming an oxygen-rich early martian atmosphere, such as that suggested by Tuff et al. (2013), deeper waters, sediments and the sub-surface would have been largely anoxic. As such, whatever the martian atmospheric oxygen concentration, potential habitats for anaerobically respiring chemolithotrophs would have been prevalent on ancient Mars and could have persisted in the deep sub-surface to the present day (Michalski et al., 2013).

Further, anaerobic chemotrophic Fe^{2+} oxidation is known to occur in terrestrial anoxic waters and sediments of approximately circumneutral pH (Straub et al., 1996; Benz et al., 1998; Kappler and Straub, 2005; Chakraborty and Picardal, 2013). Data from Curiosity at Gale Crater has shown that the Sheepbed mudstone formation at Yellowknife Bay contains abundant clay minerals, indicating a circumneutral pH environment during sedimentation (Vaniman et al., 2013; Grotzinger et al., 2014b; Bridges et al., 2015; Schwenzer et al., 2016). The conditions associated with Gale Crater are not unique and can be inferred for other sites on Mars. For example, circumneutral aqueous alteration during both the Noachian and across the Noachian-Hesperian boundary have been proposed based on orbital data of Jezero crater (Ehlmann et al., 2008a; Ehlmann et al., 2009), indicating further environments which could have supported anaerobic Fe^{2+} oxidation.

1.3.2.2 Electron acceptors for anaerobic Fe^{2+} oxidation

In the absence of molecular oxygen, chemolithotrophic Fe-oxidisers would be limited by the availability of alternative electron acceptors, such as perchlorate and nitrate, for metabolic redox reactions (Straub et al., 1996; Benz et al., 1998; Kappler and Straub, 2005; Chakraborty and Picardal, 2013). Of these, perchlorate is the stronger oxidant.

Studies at multiple locations on Mars have confirmed the presence of perchlorate (Hecht et al., 2009; Navarro-González et al., 2010; Glavin et al., 2013; Kounaves et al., 2014). Terrestrial perchlorate-reducing microorganisms have been shown to grow at up to 0.4 M perchlorate, which exceeds concentrations found on Mars and suggests the strong oxidative capability and toxicity associated with perchlorates would not be prohibitive to life there (Oren et al., 2014; Stern et al., 2017). Many perchlorate-reducing microorganisms are able to promote Fe^{2+}-oxidation when perchlorate or nitrate is provided as an electron acceptor (Bruce et al., 1999; Chaudhuri et al., 2001; Lack et al., 2002), though energy conservation leading to growth is yet to be described in the case of perchlorate-reduction coupled to Fe^{2+}-oxidation. For example, *Dechloromonas agitata* strain CKB (Bruce et al., 1999) and *Azospira suillum* strain PS (*Dechlorosoma suillum*) (Lack et al., 2002) have both been shown to conduct perchlorate-dependent Fe^{2+}-oxidation, but only in stationary phase and with organic carbon source in the form of acetate. Thus, other electron acceptors may be more applicable in driving potential growth in early martian contexts than perchlorate.

Nitrate is a more feasible electron acceptor for martian Fe^{2+}-oxidation, as it has been observed as the electron receptor in Fe^{2+}-oxidising metabolisms of growth-phase cultures (Hafenbradl et al., 1996; Straub et al., 1996; Benz et al., 1998; Straub and Buchholz-Cleven, 1998). However, until the recent discovery of nitrates on the surface of Mars (Stern et al., 2015), nitrate-reducers have been largely overlooked with regard to Mars

astrobiology. The following sections discuss the discovery of nitrates on Mars and the feasibility of nitrate-dependent Fe^{2+} oxidation (NDFO) as a plausible metabolism for now closing the biological Fe 'loop' on Mars (Figure 1.5).

1.3.2.3 Nitrates and nitrogen cycling on Mars

The geochemical evidence for nitrates on the surface of Mars comes from *in-situ* analysis of mudstone at Gale Crater by Curiosity (Stern et al., 2015) and from analysis of the EETA79001 and Nakhla martian meteorites (Grady et al., 1995; Kounaves et al., 2014). It has been proposed that these nitrates may have formed through photochemical processing (Smith et al., 2014) of the low abundance (1.9 %) molecular nitrogen in the martian atmosphere (Mahaffy et al., 2013), volcanic-induced lightning or thermal shock from impacts (Stern et al., 2015), and may have resulted in large accumulated quantities of nitrates during the early history of the planet (Manning et al., 2009; Stern et al., 2017) (Figure 1.7). The concentration of nitrates detected at Gale Crater (Stern et al., 2015) is consistent with predictions of a 5×10^{15} mol global nitrate reservoir from past impact processing (Manning et al., 2009). Although it is not believed that nitrate deposition currently operates on the martian surface (Stern et al., 2015), interest in the martian nitrogen cycle has been reignited because of recent spacecraft observations of atmospheric nitrogen in the upper atmosphere (Stevens et al., 2015).

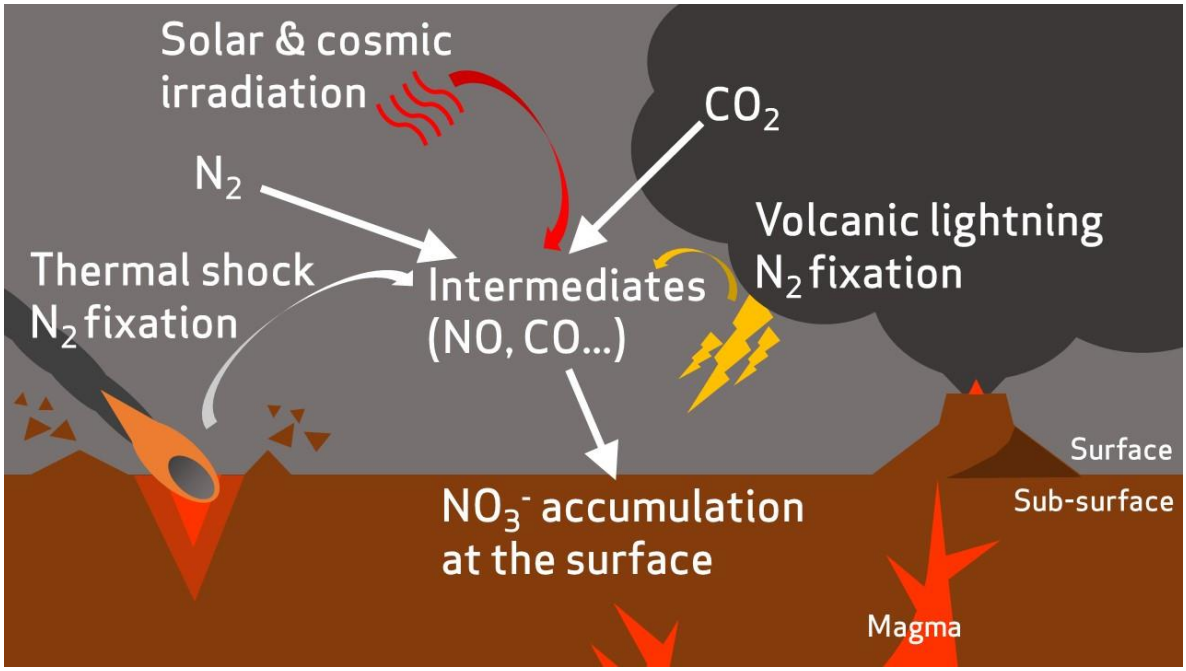

Figure 1.7. A hypothetical incomplete nitrogen cycle on early Mars. Atmospheric nitrogen is fixed to oxidised nitrogen species via abiotic processes such as volcanic lightning (Stern et al., 2015), thermal shock during impacts (Summers and Khare, 2007) and irradiation from solar and cosmic sources (Smith et al., 2014).

On Earth, the production of molecular nitrogen is primarily facilitated by microbes through denitrification (Fowler et al., 2013). Biological denitrification on Mars could have contributed to an early nitrogen cycle during the Noachian period, although Mars' atmosphere (including its primordial atmosphere) has long been suspected to have had a low nitrogen abundance relative to Earth (Fox, 1993). Nevertheless, the presence of nitrates as a plausible electron acceptor expands the range of microbial metabolisms that could be considered potentially viable on Mars.

With Fe^{2+} and nitrates abundant on the surface of Mars, it is therefore prudent to study the coupling of nitrate reduction to Fe^{2+} oxidation as a potential metabolism for Mars. This is the overall focus of this thesis.

1.4 Nitrate-dependent Fe^{2+} oxidation (NDFO)

NDFO metabolism was identified on Earth two decades ago (Straub et al., 1996), yet the detailed biochemical mechanisms involved are still unresolved (e.g., Carlson et al., 2013). Early studies reported Fe^{2+}-oxidation balanced with nitrate reduction in mixed cultures and isolates from anaerobic freshwater, brackish water and marine sediment (Hafenbradl et al., 1996; Straub et al., 1996; Benz et al., 1998). There are only a few known isolates capable of this metabolism (see Table 1.1), but this is likely to be an under-representation of the true diversity and prevalence of these organisms (Straub and Buchholz-Cleven, 1998). The terrestrial NDFO microbes described in the literature are phylogenetically diverse, including an archaeal species and representatives of the alpha-, beta-, gamma- and delta-proteobacteria (Hafenbradl et al., 1996; Kappler et al., 2005; Kumaraswamy et al., 2006; Weber et al., 2009; Chakraborty et al., 2011). The isolation of a member of the euryarchaeota capable of NDFO from a submarine vent system (Hafenbradl et al., 1996) is suggestive that NDFO may have been an early microbial process on Earth, because of the implication of such vents in the earliest evolution of life (Martin et al., 2008).

The mechanisms of NDFO have remained elusive since the process was first described. Several hypotheses have been advanced to account for both the oxidation of Fe during nitrate reduction and the observed associated benefit for growth (Carlson et al., 2012).

The first of these is that a dedicated ferroxidase enzyme is present in all NDFO species, which catalyses the oxidation of Fe^{2+} to Fe^{3+} resulting in the release and conservation of electrons for energy metabolism (Figure 1.8A). Enzymatic Fe^{2+} oxidation by NDFO has never been proven and a detailed proteomic study of the NDFO species *Acidovorax ebreus* definitively demonstrated that this strain lacks any specific Fe^{2+}-oxidoreductase (Carlson et al., 2013). A second possibility is that Fe^{2+} oxidation is catalysed by a secondary action of

the respiratory nitrate reductase (Nar) enzyme (Figure 1.8B), providing a less efficient pathway for electron acquisition, thus NDFO may actually be an innate capability of all respiratory nitrate reducers (Carlson et al., 2013; Etique et al., 2014). Alternatively, abiotic side reactions between Fe^{2+} and reactive nitrogen species (NO, NO_2^-) produced upon nitrate reduction could also account for Fe^{2+} oxidation (Carlson et al., 2013; Klueglein et al., 2014; Klüglein et al., 2015).

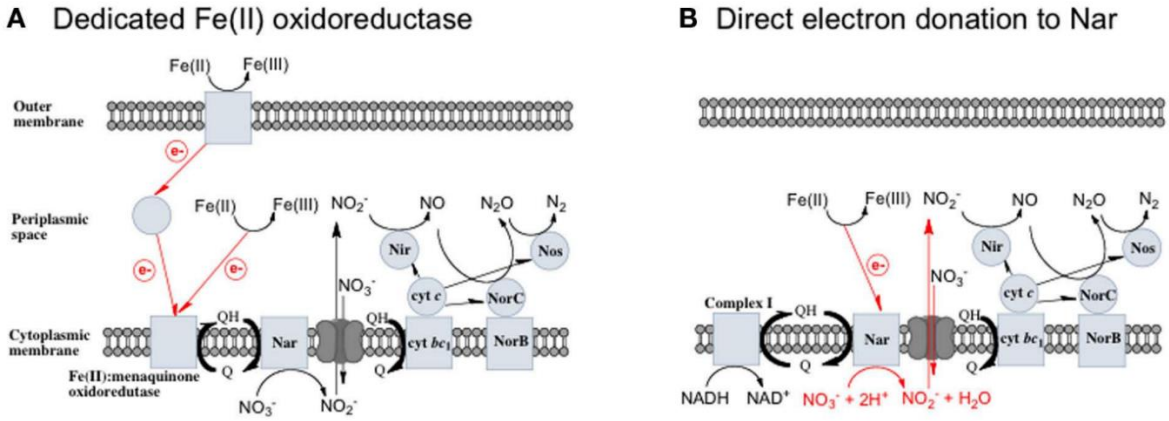

Figure 1.8. Potential mechanisms of nitrate-dependent Fe oxidation, from Carlson et al. (2012). (A) An Fe^{2+} oxidoreductase enzyme accepts electrons from extracellular Fe^{2+} for the electron transport chain. (B) Electrons released by oxidation of Fe^{2+} in the periplasm are accepted by the Nar respiratory nitrate reductase, which consumes protons to generate a proton motive force.

NDFO microorganisms must balance (a) a potential energy gain from coupled Fe oxidation and nitrate reduction and (b) energy consumption to overcome the toxicity of Fe^{2+} and reactive nitrogen species (Carlson et al., 2012; Carlson et al., 2013). Although Fe^{2+} oxidation coupled to nitrate reduction to nitrite provides less energy (-481.15 kJ mol^{-1} NO_3^-) than both organotrophic denitrification (oxidation of organics coupled to reduction of nitrate to nitrogen gas) (-556 kJ mol^{-1} NO_3^-) and organotrophic nitrate ammonification (oxidation of organics coupled to reduction of nitrate to ammonia) (-623 kJ mol^{-1} NO_3^-) (Strohm et al., 2007). This reaction is exergonic (energy-producing) at circumneutral pH (-481.15 kJ mol^{-1} NO_3^-), and may theoretically provide enough energy to sustain growth under mixotrophic (with an organic carbon source) or autotrophic

(lacking organic carbon) conditions (Muehe et al., 2009; Weber et al., 2009; Laufer et al., 2016a). At the same time, ferruginous conditions stimulate metal efflux pumping and stress response pathways to overcome toxicity (Carlson et al. 2013), potentially further impairing the efficiency of NDFO as an energy metabolism under such conditions.

Ilbert and Bonnefoy (2013) postulated that the mechanisms of biological anaerobic Fe^{2+} oxidation may have arisen independently several times on Earth in an example of convergent evolution (i.e., similar strategies are adopted by genetically distant species). This widespread phylogeny, plus evidence from Fe palaeochemistry, physiology, and redox protein cofactors involved in these pathways suggests that NDFO may be the most ancient Fe^{2+} oxidation pathway in terrestrial life (Ilbert and Bonnefoy, 2013). Indeed, NDFO microbes have been implicated, alongside anoxygenic Fe^{2+}-oxidising phototrophy, in Fe cycling and the production of early banded Fe formations prior to the full oxygenation of the atmosphere on Earth (Weber et al., 2006a; Busigny et al., 2013; Ilbert and Bonnefoy, 2013). Thus, NDFO may be relevant to any putative early biosphere on Mars, where the conditions are favourable to this metabolism.

Table 1.1 Examples of microbial species capable of nitrate-dependent Fe^{2+} oxidation.

Isolate	Respiration	e^- donor	e^- acceptor	Optimum pH	Optimum temperature (°C)	Metabolism	NDFO Growth	Reference
Thiobacillus denitrificans	obligate anaerobe	S/Fe^{2+}	NO_3^-	6.90	30	autotrophic	Unclear	Straub et al., 1996
Pseudogulbenkiania sp. strain 2002	facultative aerobe	Fe^{2+}	NO_3^-	6.75-8.00	37	autotrophic	Yes	Weber et al., 2006
Paracoccus sp. strain KS1	facultative aerobe	Organics/S/ Fe^{2+}	NO_3^-	7.00	37	heterotrophic	No	Kumaraswamy et al., 2005
Acidovorax sp. strain BoFeN1	facultative anaerobe	Organics/ Fe^{2+}	NO_3^-	6.80	30	mixotrophic	Unclear	Kappler et al., 2005
Ferroglobus placidus	obligate anaerobe	$Fe^{2+}/H_2/S^{2-}$	NO_3^-	7.00	85	autotrophic	Yes	Hafenbradl et al., 1995
Azospira sp. strain PS	facultative anaerobe	Fe^{2+}/humic acids	NO_3^-/ClO_4^-	7.00	26	mixotrophic	No	Lack et al., 2002; Byrne-Bailey & Coates, 2012
Acidovorax sp. strain BrG1	facultative anaerobe	Organics/ Fe^{2+}	NO_3^-	6.70	28-35	heterotrophic	No	Straub et al., 1996; Straub et al., 2004
Aquabacterium sp. strain BrG2	facultative anaerobe	Organics/ Fe^{2+}	NO_3^-	6.40.-6.70	28	heterotrophic	Unclear	Straub et al., 1996; Straub et al., 2004
Thermomonas sp. strain BrG3	facultative anaerobe	Organics/ Fe^{2+}	NO_3^-	6.70	32-35	heterotrophic	No	Straub et al., 1996; Straub et al., 2004
Klebsiella mobilis	facultative aerobe	Organics	NO_3^-	7.00	30	heterotrophic	No	(Etique et al., 2014)

1.4.1 Feasibility of NDFO on early Mars

The relevance of NDFO as a plausible metabolism for putative life on Mars had, until recently, been overlooked because of a lack of evidence of nitrogen species , although the theoretical possibility of NDFO was explored using numerical modelling with hypothetical nitrate sources (Jepsen et al., 2007). The newly-detected availability of nitrates (Stern et al., 2015) helps to close the 'loop' of potential chemotrophic Fe cycling on Mars (Figure 1.5), since it could provide a ready source of electron acceptors for NDFO organisms (Figure 1.9). It should be noted that the highest nitrate concentrations (1,100 ppm) determined by Curiosity at Gale crater were present in sedimentary rocks with the most limited evidence of subsequent alteration, suggesting a period of nitrate production during sediment deposition followed by variable leaching of sediments and nitrate loss (Stern et al., 2015).

The modern martian atmosphere is 95.9 % CO_2 (Mahaffy et al., 2013), and CO_2 is likely to have also formed a major proportion of the denser early Mars atmosphere (Ramirez et al., 2014; Jakosky et al., 2017; Kurokawa et al., 2018) (Figure 1.10). Microbes that can utilise inorganic atmospheric carbon would therefore hold an advantage in the Mars environment. Although a low energy-yielding metabolism, some species (*Pseudogulbenkiania sp.* strain 2002 and the hyperthermophilic archaeon *Ferroglobus placidus*) have been found to fix carbon autotrophically from CO_2 and other inorganic sources during growth by NDFO (Hafenbradl et al., 1996; Weber et al., 2006b; Weber et al., 2009), providing an alternative carbon assimilatory capability relevant for the early and current Mars environments. Further, although nitrate reduction can be coupled to anaerobic oxidation of methane (Raghoebarsing et al., 2006; Ettwig et al., 2008), the ability of NDFO strains to use C1 organic compounds as carbon sources has not been investigated. This could prove an important capability when considering the martian environment, given the, as yet

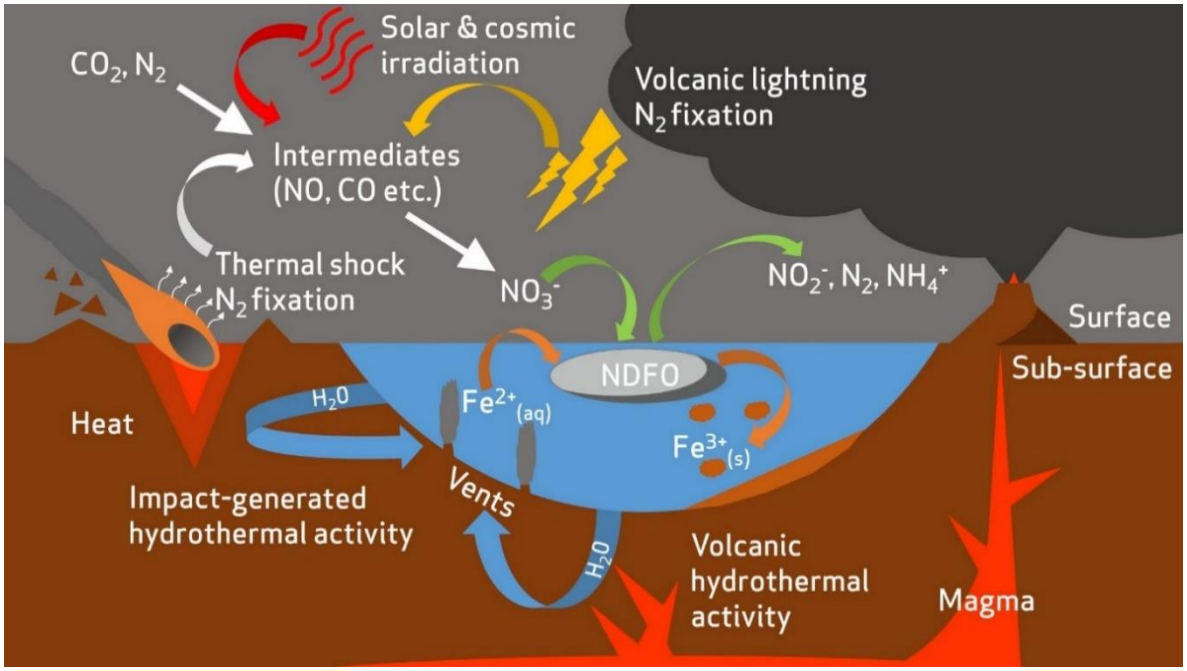

Figure 1.9. Overview of potential redox substrate sources for nitrate-dependent Fe^{2+}-oxidising microorganisms in the early Mars environment. Nitrates are produced from an atmospheric nitrogen reservoir by fixation from volcanic lightning (Stern et al., 2015), thermal shock during impacts (Summers and Khare, 2007) and irradiation from solar and cosmic sources (Smith et al., 2014). Reduced Fe^{2+} is released into aqueous environments by mineral dissolution, a process accentuated by hydrothermal activity (Emerson and Moyer, 2002; McSween et al., 2009). A fuller description of abiotic nitrogen fixation pathways is available in Summers et al. (2012).

unexplained and variable, detections of methane in the modern atmosphere (Formisano et al., 2004; Webster et al., 2015; Webster et al., 2018; Korablev et al., 2019), and should be investigated further. Most NDFOs are heterotrophic and require an organic carbon source (Chaudhuri et al., 2001; Kappler et al., 2005; Muehe et al., 2009). Organic carbon has been reported on the martian surface and in martian meteorites (Sephton et al., 2002; Steele et al., 2012b; Ming et al., 2014; Eigenbrode et al., 2018). This may be endogenous (Steele et al., 2012a) or have been delivered into the martian crust by meteoritic input (~2.4×10^5 kg yr^{-1} (Yen et al., 2006)) (Figure 1.10). Sutter et al. (2016) calculated that < 1 % of the total carbon detected in sedimentary rocks at Gale Crater would have been sufficient to support 10^5

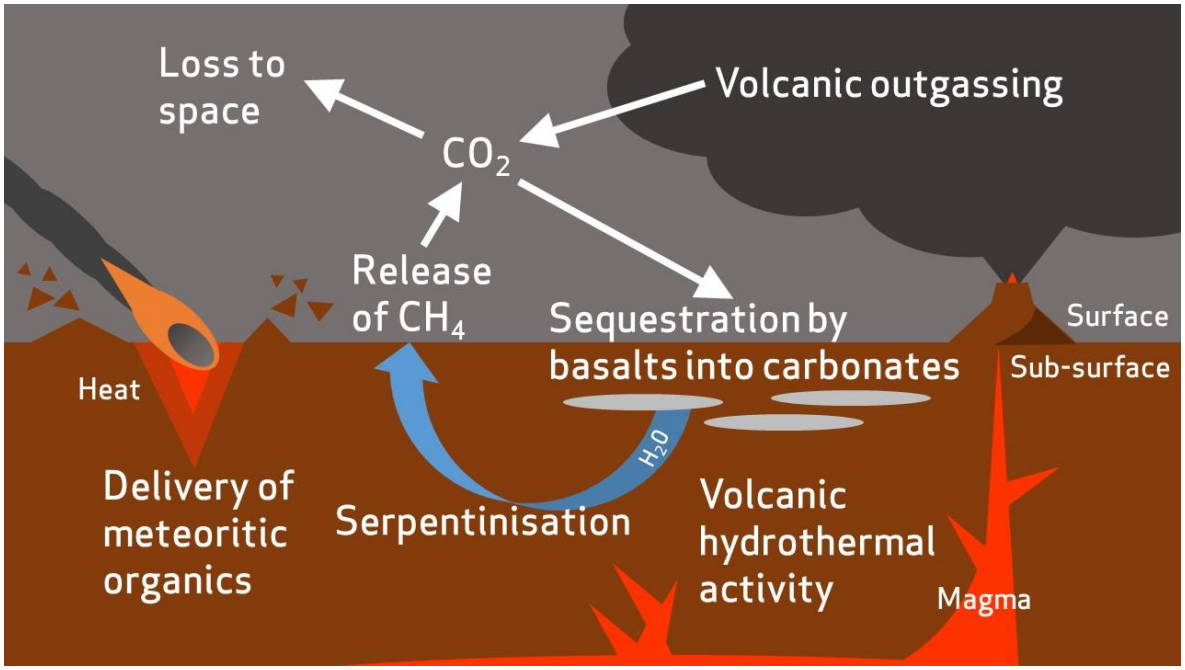

Figure 1.10. Summary of proposed processes in carbon cycling on early Mars. Atmospheric carbon dioxide is sequestered by basalts to form carbonate minerals (Edwards and Ehlmann, 2015). The carbon is then remobilised by hydrothermal fluids and incorporated into simple organic compounds, such as methane, by serpentinisation reactions (Chassefière and Leblanc, 2011). Carbon dioxide is gradually lost to space due to erosion of the atmosphere by solar winds. Meteorites are also likely to have delivered an inventory of organic carbon to the surface and sub-surface of Mars (Yen et al., 2006).

cells g^{-1} sediment if present as biologically available organics in the earlier lacustrine environment, and hence could well have sustained heterotrophic NDFOs.

Aside from metabolic requirements, life also needs an environment which falls within other sets of physical parameters that are conducive to life, which means protecting it from the radiation environment of the martian surface. In contrast to phototrophic Fe-oxidisers, NDFO could have occurred in near-surface ground waters (Straub et al., 1996), which would have protected the microorganisms even if the surface radiation of early Mars was as intense as it is today (Dartnell et al., 2007b). In the deep sub-surface, neutral-alkaline, Fe^{2+}-rich ground waters could have persisted long after the evaporation of most surface bodies (Michalski et al., 2013), greatly extending the period across which NDFO could have been viable, possibly to the present day. In addition, cell encrustation by iron

minerals may have protected them against UV irradiation at the near-unattenuated levels proposed on the early Earth (Gauger et al., 2016), which are comparable to the present flux on Mars (Cockell and Raven, 2004).

Although the modern martian surface environment is oxidising due to irradiation, even modest levels of volcanism over the last 3.5 billion years are likely to have produced CO_2 at levels that contributed to periodically reducing conditions (Sholes et al., 2017), favouring NDFO by limiting abiotic Fe^{2+} oxidation. However, there has also been a suggestion that certain locations on the ancient surface (>3.5 billion years ago) were, at one point, oxidising (Lanza et al., 2016). In practical terms, oxidising atmospheric conditions and potential redox stratified water bodies, such as the palaeolake at Gale crater (Hurowitz et al., 2017) would not preclude the viability of NDFO, but merely restrict it to anoxic sediment and water layers, as is the case on Earth.

1.4.1 Biomineralisation and preservation in the rock record

Under Fe^{2+}-rich (>5 mM) conditions, a major limiting factor for the growth of NDFO populations is the progressive encrustation of the periplasm and outer membrane by insoluble Fe^{3+}-compounds (Figure 1.11), resulting in a decline in individual metabolic activity and cell death (Miot et al., 2015). Even the lithoautotrophic *Pseudogulbenkiania sp*. strain 2002 shows evidence of encrustation after batch culture (Klueglein et al., 2014) (Figure 1.11C). Although the mechanisms behind this remain unexplained, various extracellular Fe^{3+}-mineral precipitates also form as by-products of NDFO metabolism, either due to the interaction of released Fe^{3+} ions with dissolved phosphate, sulfate and carbonate ions, or by oxidation of extracellular Fe^{2+}-bearing minerals (Miot et al., 2009b). Persistence of a low proportion of cells that escape encrustation ensures the viability of

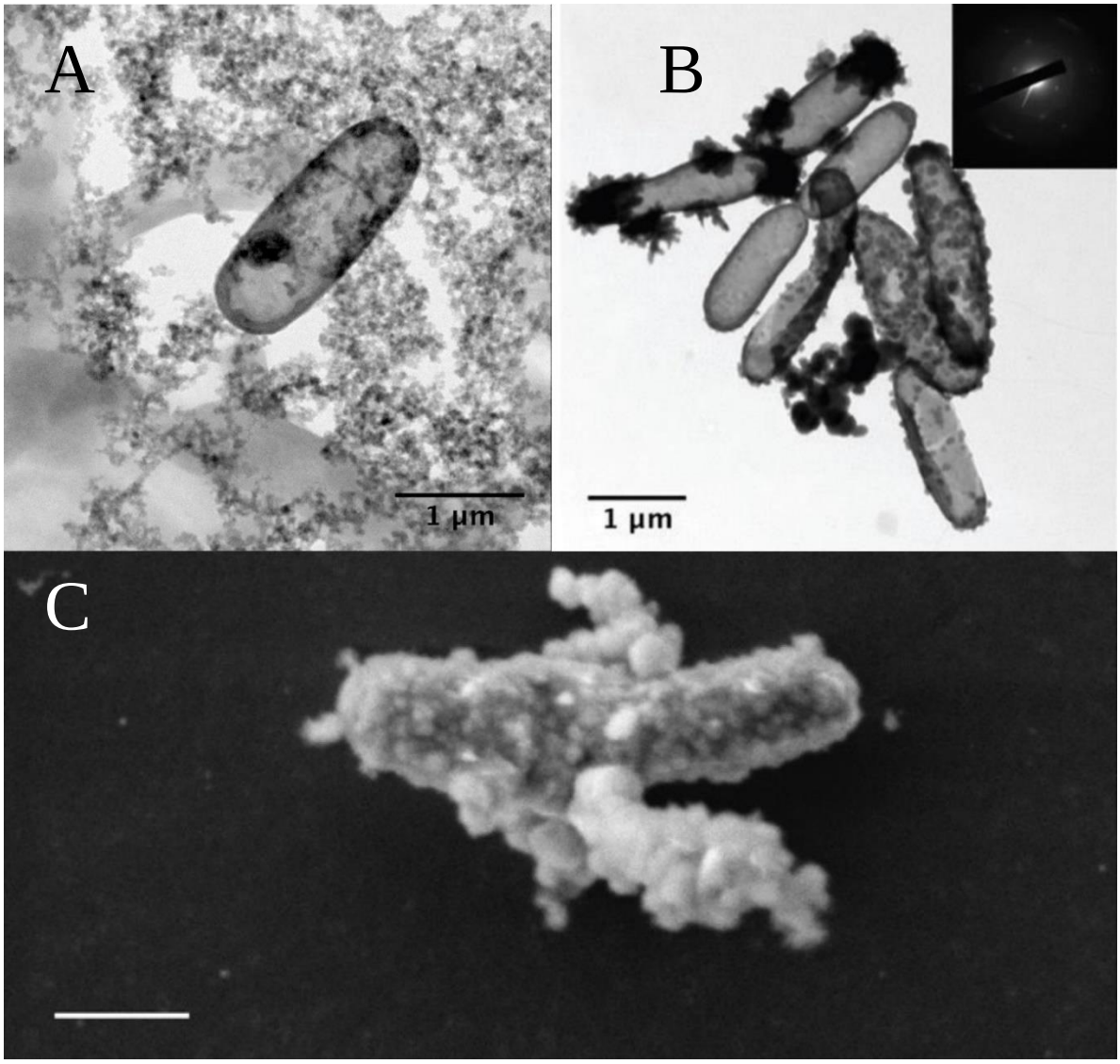

Figure 1.11. (A) Transmission electron microscopy image of an Fe-encrusted cell from an NDFO enrichment culture from the anoxic layer of the ferruginous Lake Pavin, France (Jennyfer Miot, personal communication). (B) TEM of *Acidovorax sp*. BoFeN1 cells fully, partially and non-encrusted with goethite (from Miot et al. (2015)). (C) SEM of encrusted *Pseudogulbenkiania sp*. 2002 cells (from Klueglein et al. (2014)) (scale bar = 500 nm).

NDFO microorganisms at the population scale, thus accounting for their occurrence in ferruginous habitats on modern Earth (Miot et al., 2016). The membrane-associated and extracellular mineral precipitates associated with NDFO metabolism may also present plausible biosignatures that may be detectable by future life detection missions, provided they persist over geological time. In particular, periplasmic encrustation leads to mineral shells that entrap protein globules and which display a constant thickness (around 40 nm)

(Miot et al., 2011). The minerals formed have been shown to be dependent on both the local chemical composition and the pH environment. *Acidovorax sp*. strain BoFeN1, one of the best studied NDFO species, has been found to produce either lepidocrocite (γ-FeO(OH)) at pH 7 (Miot et al., 2014b) or a mixture of lepidocrocite and magnetite (Fe_3O_4) at pH 7.6 (Miot et al., 2014a). Likewise, changing the chemical composition of the culture medium at pH 7 results in the precipitation of either Fe^{3+}-phosphates (Miot et al., 2009), goethite (α-FeO(OH)) (Kappler et al., 2005; Schädler et al., 2009), or green rust (mixed Fe^{2+}/Fe^{3+} hydroxides) (Pantke et al., 2012).

It is also becoming apparent that encrustation is less likely in environments with low Fe^{2+} concentrations (50-250 µM), i.e., conditions more representative of many terrestrial environments in which NDFO is prevalent (Chakraborty et al., 2011). Encrustation may occur only when solutions become highly concentrated (millimolar) with Fe^{2+} ions, as could have occurred on Mars in hydrothermal and stratified lake settings (Hurowitz et al., 2017) or in evaporitic environments during the desiccation of the surface (Tosca and McLennan, 2009). Oxide-encrusted cells in both contexts could have been deposited and preserved during sedimentation (Fig. 4). If deposited and lithified as macroscopic flocs or bands within an otherwise generally reducing sedimentary geological context, these oxidised mineral features may be visible in exposed strata and would serve as prime initial targets for further astrobiological investigation.

Alternative mineralisation processes such as pyritisation (saturation and replacement of biological structures with FeS_2) or silicification (saturation and replacement of biological structures with silica) could also contribute to nonspecific morphological preservation of microbes in Fe- and sulfur-rich, predominantly basaltic, early martian environments. Microbial silicification has been observed on Earth *in situ* and *in vivo* around hot springs

and under simulated conditions as well as in the fossil record (Toporski et al., 2002a; Konhauser et al., 2004) whereas microbial pyritisation is recognised only in the context of microfossils (Schieber, 2002; Wacey et al., 2013). Given the ability of microbial communities to thrive in conditions which encourage geologically rapid mineralisation of biological material over days, these processes should not be viewed as prohibitive to microbial life on early Mars and are beneficial to the search for any traces of early life.

Formation of organo-ferric complexes have also been demonstrated to facilitate the preservation of organic molecules in soils and sediment over geological timescales on Earth (Lalonde et al., 2012), raising the possibility that encrustation of NDFO cells by Fe^{3+}-bearing minerals and subsequent complexation may be beneficial to the preservation of organic biosignatures. At the same time, depending on the nature of encrusting minerals and diagenetic (T, P) conditions, association with Fe^{3+} minerals may enhance the thermal maturation of organic matter and partly degrade organic biosignatures (Miot et al. in revision).

It may be possible for the Mars Organics Molecule Analyser (MOMA) and Raman Laser Spectrometer (RLS) aboard the ESA ExoMars Rosalind Franklin rover, to detect biogenic organic molecules co-located with Fe^{3+} minerals in Fe-rich drill samples and laser targets respectively (Lopez-Reyes et al., 2013; Goetz et al., 2016). However, these instruments are not specific enough to distinguish evidence of NDFO microbes from other potentially biological material encrusted in Fe minerals (e.g., Kish et al., 2016; Mirvaux et al., 2016).

Specific evidence of NDFO metabolism in the geological record on Earth or Mars may, however, come from isotopes. NDFOs have been shown to produce distinctive $^{56}Fe/^{54}Fe$ fractionation patterns, discernible from other processes (Kappler et al., 2010). These variations may be detected, for example in returned samples, using isotope ratio mass

spectrometry (Anand et al., 2006; Czaja et al., 2013). The preservation of isotopic anomalies in martian sediments could provide detectable supporting evidence of NDFO on early Mars.

1.4.2 Summary of NDFO as a Mars metabolism

NDFO microorganisms oxidise Fe^{2+} compounds while also reducing nitrates under anaerobic, circumneutral conditions. These environments are proposed to have existed on Mars, providing the electron donors and acceptors required for NDFO metabolism. This implies that NDFO is a feasible and logical avenue for investigating hypothetical early martian life.

The discovery of nitrates establishes NDFO as a viable mechanism for hypothetical, biological Fe^{2+} oxidation on present-day Mars. NDFO could help to close a chemotrophic 'loop' of biogeochemical Fe cycling on Mars, by providing a potential mechanism for Fe^{2+} oxidation, and allowing chemotrophic Fe cycling to occur in both circumneutral ancient surface waters and deep sub-surface waters throughout martian history.

1.5 Thesis objectives and outline

To test the validity of this overarching hypothesis, that NDFO provides an avenue for microbial metabolism in early martian environments, different aspects of the feasibility of NDFO metabolism in early Mars environments have been investigated and answered experimentally, including:

- The ability of NDFO strains to utilise Fe^{2+} for growth from a Mars-relevant mineral substrate
- The capability of NDFO strains to metabolise and grow under simulated chemical conditions of ancient martian fluids
- The extent of biomineralisation processes associated with NDFO growth in the above conditions as a formation mechanism for morphological biomarkers
- The underlying mechanisms of NDFO energy metabolism and therefore the feasibility for NDFO-based primary production to drive an early martian biosphere

Chapter 2 presents an investigation into whether multiple NDFO strains can grow autotrophically using a solid olivine Fe^{2+} substrate, representative of one of the main Fe^{2+}-carriers in unaltered martian magmatic rocks. The study determines the suitability of these microorganisms to metabolise Fe^{2+} from crystalline sources abundant on Mars and whether biomineralised structures form upon desiccation which may act as morphological biosignatures.

Chapter 3 builds on this, presenting an evaluation of whether these strains are resistant to the chemical environments of early Mars. This is tested through growth experiments using media with compositions based on fluids evolved from aqueous alteration of different martian geological contexts, as established by thermochemical modelling.

In order to move our understanding beyond the survival of particular strains under martian conditions, we need to understand whether this process could ever have driven a martian biosphere, and so Chapter 4 investigates the underlying mechanism of NDFO, presenting draft genome sequencing of two strains and analysis of available NDFO genomes to allow for hypothetical mechanisms of electron acquisition in NDFO based on dedicated enzymatic pathways to be investigated. It also describes a knockout mutant study undertaken to quantify the relative contributions of the respiratory nitrate reductase enzyme and nitrite ions to the Fe^{2+} oxidation witnessed in NDFO.

Finally, Chapter 5 summarizes how the outcomes of these experiments taken together advance our understanding of NDFO as a process on Earth, as a hypothetical driver of life on early Mars and as a formation mechanism of morphological biosignatures which will inform target selection for future life detection missions.

2. Growth of NDFO bacteria on olivine

2.1 Introduction

Fe is a key driver of microbial metabolisms in diverse and widespread environments on Earth, acting as both an electron donor for Fe-oxidisers and an electron acceptor for Fe-reducers (Lovley et al., 2004; Hedrich et al., 2011). This flexibility to perform as both an electron donor and acceptor is owing to the existence of both the reduced (Fe^{2+}) and oxidised (Fe^{3+}) redox states. The reduced Fe^{2+} state provides a source of electrons for aerobic Fe-oxidising microorganisms in acidic, oxygenated and neutral and microoxic conditions (Emerson and Moyer, 2002; Amils et al., 2011) whereas abiotic oxidation is limited by the concentration of available oxygen. Circumneutral, anaerobic conditions provide niches for both anoxygenic phototrophs and nitrate-reducers to utilise Fe^{2+} as an electron donor in the relative absence of competing oxidation from elemental oxygen (Widdel et al., 1993; Weber et al., 2006a).

It has been proposed that the properties of dominant minerals and rocks can affect both the extent of microbial colonisation and community composition, a so-called "mineralosphere" effect (Uroz et al., 2015). Thus, any early martian biosphere would be shaped by the geological properties of the planet. Mars' surface is dominated by Fe-rich basaltic material with Fe^{2+} present in olivine ($(Fe^{2+}Mg)_2SiO_4$; mainly forsterite, Fo_{64}, for example at Gale Crater (Bish et al., 2013)) and other minerals such as pyrite (FeS_2) (Ehlmann and Edwards, 2014). The interaction of Fe-bearing minerals with circumneutral fluids of low ionic strength, such as those proposed for Gale Crater (Bristow et al., 2015), leads to mineral dissolution and the liberation of Fe^{2+} into the aqueous environment, where it is more readily available for utilisation by microbes (Santelli et al., 2001). Evidence of circumneutral fluids in temperate fluvial and lacustrine systems suggest that abiotic dissolution would have been widespread during the hydrologically-active Noachian (4.1-3.7 Ga) and early Hesperian (3.7-3.1 Ga) periods of early martian history (Hartmann and

Neukum, 2001). Given the necessity of free liquid water as a solvent for all known biochemical processes, Mars was most conducive to the development of life as we understand it at this time (McLennan et al., 2014; Grotzinger et al., 2015; Westall et al., 2015; Davis et al., 2016). Though the ability of oxygen-respiring microorganisms to utilise olivine-derived Fe at pH 7 has been documented (Popa et al., 2012), the low solubility of olivine under neutral conditions (Wogelius and Walther, 1991) raises a serious question as to whether simple abiotic dissolution could provide a sufficient concentration of Fe^{2+} ions to sustain microbial growth, for example, that of anaerobic neutrophilic Fe-oxidisers. To this end, it is necessary to conduct experiments to verify the capability of microbes to subsist on low Fe^{2+}quantities in solution in order to demonstrate the applicability of Fe oxidation metabolisms to circumneutral martian environments.

The primary oxidant for microbial Fe^{2+} oxidation - molecular oxygen - is a trace gas in the modern martian atmosphere and is unlikely to have ever been a major component (Mahaffy et al., 2013). In the near-absence of molecular oxygen, an alternative electron acceptor would be required. Nitrates are one plausible alternative. The abundance and speciation of nitrogen on Mars has been poorly constrained, but *in-situ* analysis by the Mars Science Laboratory (MSL) Curiosity rover has found nitrate to be present in both modern and ancient martian geology at Gale Crater (Stern et al., 2015). Nitrate is the only acceptor, besides molecular oxygen, known to be coupled to chemotrophic microbial growth by Fe^{2+} oxidation on Earth (Hafenbradl et al., 1996; Straub et al., 1996). Microbial perchlorate (ClO_4^-) reduction has also been shown to be associated with Fe^{2+} oxidation, but there is no evidence of Fe^{2+} oxidation driving active growth in perchlorate-reducing organisms (Bruce et al., 1999).

Biosynthesis refers to the production of complex molecules by living organisms from various substrates. Microbial Fe^{2+} oxidation metabolisms can be either heterotrophic

(requiring organic carbon for biosynthesis) or autotrophic (able to use inorganic carbon for biosynthesis) and there is evidence for both inorganic and organic carbon on the surface of Mars. Organic carbon has been detected in martian meteorites and on the surface of Mars (Sephton et al., 2002; Ming et al., 2006; Steele et al., 2012b), for example, within mudstones in the Murray formation at Pahrump Hills, Gale crater analysed by the Curiosity rover (Eigenbrode et al., 2018). In addition, seasonal peaks of atmospheric methane have recently been described at Gale Crater, adding a gaseous source to the suite of available organics in the modern martian environment (Webster et al., 2018). Furthermore, carbonates have been detected from orbit, by *in-situ* measurements, and in martian meteorites (Bridges and Grady, 2000; Ehlmann et al., 2008b; Boynton et al., 2009; Morris et al., 2010; Wray et al., 2016). CO_2 represents another important carbon source on Mars, constituting 95.9 % of the modern atmosphere (Mahaffy et al., 2013), and likely formed a major component of the early atmosphere (Ramirez et al., 2014; Jakosky et al., 2017). Carbonates are also present, though the global extent is a subject of debate (Morris et al., 2010; Wray et al., 2016). Although some nitrate-dependent Fe^{2+} oxidising (NDFO) microorganisms are heterotrophic or mixotrophic, two species (*Ferroglobus placidus* and *Pseudogulbenkiania sp.* strain 2002) have previously been demonstrated to grow autotrophically using CO_2 as a carbon source (Hafenbradl et al., 1996; Weber et al., 2006b).

On Earth, NDFO microbes inhabit a plethora of niches including seafloor hydrothermal vent systems, anoxic marine and freshwaters and anaerobic sediments (Hafenbradl et al., 1996; Straub et al., 1996; Benz et al., 1998; Straub and Buchholz-Cleven, 1998). The common features of all these environments are the availability of reduced Fe^{2+} species, the absence of molecular oxygen and the presence of nitrates. Given the presence of these features on Mars (McSween et al., 2009; Mahaffy et al., 2013; Stern et al., 2017), NDFO

metabolism could hypothetically have occurred on the early martian surface, but this must be assessed experimentally to add credence to such claims.

This Chapter explores the hypothesis that Fe^{2+} bearing minerals akin to those available on early Mars could provide sufficient Fe^{2+} to drive NDFO metabolism under anaerobic conditions. To address this hypothesis, the following objectives are addressed:

- To determine whether NDFO-capable microorganisms can grow under anoxic, autotrophic conditions relevant to early Mars, with olivine as the sole Fe^{2+} source.
- To correlate the depletion of dissolved Fe^{2+} and nitrate to any observed growth
- To assess the potential production of biogenic morphological features on mineral surfaces following culturing with NDFO microorganisms, which may serve as biosignatures in a martian context.

2.2 Methods

2.2.1 Microorganisms

Four NDFO strains: *Pseudogulbenkiania sp*. strain 2002 (DSM-18807), *Paracoccus sp*. strain KS1 (DSM-11072), *Thiobacillus denitrificans* (DSM-12475) and *Acidovorax sp*. strain BoFeN1 were used in this Chapter. The isolates were purchased from the DSMZ (Deutsche Sammlung von Mikroorganismen und Zellkulturen GmbH) culture collection in Leibniz, Germany, with the exception of *Acidovorax sp*. strain BoFeN1, which was gifted by Jennyfer Miot at IMPMC (Institut de Minéralogie, de Physique des Matériaux et de Cosmochimie) in Paris, France.

The four strains represent the diverse range of metabolic and environmental requirements for NDFO microorganisms. This includes a mix of obligate and facultative anaerobes, with autotrophy, heterotrophy or mixotrophy capability, which are listed in Table 2.1.

Table 2.1. Basic metabolic information for four nitrate-dependent Fe^{2+} oxidising microorganisms.

Isolate	Respiration	e^- donor	e^- acceptor	Optimum pH	Optimum temperature (°C)	Metabolism	Lithoautotrophic NDFO Growth	Reference
Thiobacillus denitrificans	obligate anaerobe	S-species/Fe^{2+}	NO_3^-	6.90	30	autotrophic	unclear	(Straub et al., 1996)
***Pseudogulbenkiania sp.* strain 2002**	facultative aerobe	Fe^{2+}	NO_3^-	6.75-8.00	37	autotrophic	yes	(Weber et al., 2006b)
***Paracoccus sp.* strain KS1**	facultative aerobe	Organics/S/Fe^{2+}	NO_3^-	7.00	37	heterotrophic	no	(Kumaraswamy et al., 2006)
***Acidovorax sp.* strain BoFeN1**	facultative aerobe	Organics/Fe^{2+}	NO_3^-	6.80	30	mixotrophic	unclear	(Kappler et al., 2005)

2.2.2 Anaerobic culturing technique

The modern martian atmosphere is predominantly anaerobic; the concentration of free oxygen is only 0.145 % and it is mainly (96.0 %) CO_2 (Mahaffy et al., 2013). Therefore, all the isolates listed in Table 2.1 were grown under anaerobic conditions throughout this study.

2.2.2.1 Gas flushing

To ensure anaerobic conditions, all media preparation was conducted under a continuous flow of O_2-scrubbed N_2 gas, which was used to prevent intrusion of oxygen with needles for inflow and escape of gas through the septum (Figure 2.1). All subsequent media manipulation, including dispensing into Wheaton bottles and inoculation, were performed in a COY anaerobic glove box under an 85:10:5 N_2:CO_2:H_2 atmosphere, with a palladium catalyst, to maintain anaerobic conditions.

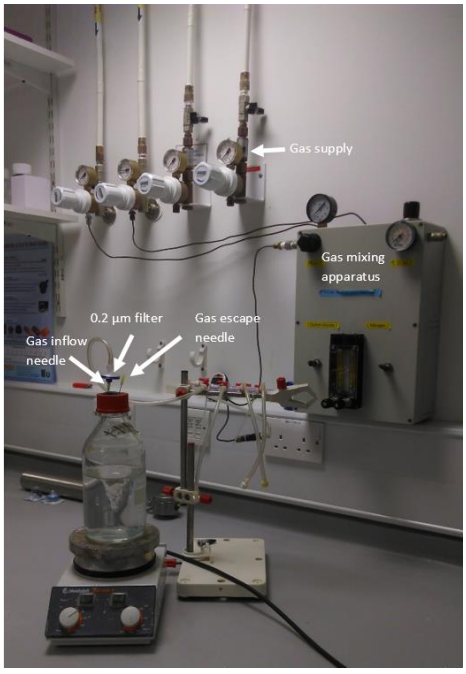

Figure 2.1. Gas supply (top) and mixing apparatus (right) were used to provide anaerobic conditions in media preparation and culturing. Bottles were gas-flushed via sterile-filtered needles.

2.2.2.2 Anaerobic media preparation

Anaerobic media was prepared by heating 800 mL of distilled water in a microwave for 2 minutes until boiling, followed by purging with N_2 gas for 10 minutes. The resultant deoxygenated water was transferred to a water bath to cool under constant flow of N_2 gas. Once cool, the redox indicator Resazurin (Dien et al., 2000) was added in order to monitor the redox potential throughout the experiment and ensure that anaerobic conditions were employed. Under oxygenated conditions, Resazurin is light blue, changing to pink and then to colourless as partially oxygenated and anaerobic conditions are reached, respectively. Other media components were added subsequently, either as powders or as filter-sterilised, deoxygenated solutions.

2.2.2.3 Growth media

Nutrient medium was used for routine growth of *Pseudogulbenkiania sp*. strain 2002, *Paracoccus sp*. strain KS1 and *Acidovorax sp*. strain BoFeN1. The medium (L^{-1}: 5.0 g of peptone, 3.0 g of meat extract, 5.0 g of $Na_2S_2O_3.5H_2O$) was prepared under anaerobic conditions, as described in Section 2.2.2.2. In solution, $Na_2S_2O_3.5H_2O$ dissociates to produce $S_2O_3^{2-}$ ions, which acts as a reducing agent.

Thiobacillus denitrificans was grown in S-8 medium, prepared as in Section 2.2.2.2 that consisted of the following (L^{-1}): 2.0 g of KH_2PO_4, 2.0 g of KNO_3, 1.0 g of NH_4Cl, 0.8 g of $MgSO_4.7H_2O$, 5.0 g of $Na_2S_2O_3.5H_2O$, 1.0 g of $NaHCO_3$, 2.0 mg of $FeSO_4.7H_2O$, 1.0 mL of 1N H_2SO_4 L^{-1}, 2.0 mL of trace element solution SL-4 (as described in Appendix A).

The media were prepared in 1 L Schott bottles under continuous N_2-flushing and altered to pH 7 by the addition of 0.1 M NaOH and 0.1 M HCl (Figure 2.1). The media were sealed with butyl rubber stoppers with screw-caps, using the Hungate technique (Hungate, 1950), then flushed with filter-sterilised N_2 gas. After autoclaving at 121 °C for 15 minutes, 50

mL aliquots of the medium were dispensed into autoclaved 125 mL Wheaton bottles under an 85:10:5 N_2:CO_2:H_2 atmosphere in the anaerobic chamber. The bottles were sealed with butyl stoppers and aluminium crimped caps. The Wheaton bottles had been acid washed with 3 % HNO_3, rinsed with milliQ water, and autoclaved prior to filling. The sealed, media-filled Wheaton bottles were then removed from the anaerobic chamber and each flushed with a 90:10 N_2:CO_2 (1 bar) headspace *via* the 70% ethanol-wiped septum using a 0.2 µm-filtered sterile gas inflow line with an oxygen trap and needles to allow escape of excess pressure.

2.2.2.4 Inoculation

For routine growth, the medium was inoculated with 100 µL of culture. For this, a sterilised N_2-flushed syringe with a 1.1 µm gauge needle *via* the butyl rubber septum was used. The septum was sterilised by applying and igniting 70 % ethanol solution on it, before inserting the needle. Once inoculated, the *Acidovorax sp*. strain BoFeN1 and *T. denitrificans* cultures were incubated at 30 °C, and the strain *Paracoccus sp*. strain KS1 and *Pseudogulbenkiania sp*. strain 2002 cultures were incubated at 37 °C.

2.2.3 Experimental set up

2.2.3.1 Minimal medium

A minimal medium was developed to promote NDFO metabolism over alternative pathways, based on the work of Emerson and Floyd (2005). This medium had been used in previous NDFO substrate experiments, which allowed comparison with other, similar studies (Miot et al., 2016; Tominski et al., 2018).

The minimal media (L^{-1}: 0.3 g of NH_4Cl, 0.4 g of $MgCl_2.6H_2O$, 0.1 g of $CaCl_2.2H_2O$, 0.6 g of K_2HPO_4, 50 mg of $MgSO_4$, 30 mL of 1 M $NaHCO_3$, 4 mL of 1 M $NaNO_3$) was

prepared using the anaerobic technique described in Section 2.2.2.2, with the NH_4Cl, $MgCl_2.6H_2O$, $CaCl_2.2H_2O$, K_2HPO_4 and $MgSO_4$ components added prior to autoclaving at 121 °C for 15 minutes. After cooling, 30 mL L^{-1} of sterile, 0.2 µm-filtered, anoxic 1 M $NaHCO_3$ solution and 4 mL L^{-1} of an anoxic 1 M $NaNO_3$ solution were added in the anaerobic chamber to achieve final concentrations of 30 mM bicarbonate and 4 mM nitrate in the medium. The medium was altered to pH 7 using 0.1 M HCL or 0.1 M NaOH. No organic carbon source was added to the medium. Instead, carbon was supplied as CO_2 gas and the bicarbonate buffer, which selected for autotrophic growth.

2.2.3.2 Olivine substrate characterisation

As a dominant primary mineral in many locations on Mars (McSween et al., 2009), olivine is an important potential Fe^{2+} source for putative NDFO microorganisms. Therefore, it was selected as a relevant Fe^{2+}-bearing mineral substrate for this analogue experiment. The olivine-rich rock, which was available partly as a coherent sample and partly granular material (Figure 2.2A), was originally sourced from the Upper Loire region of France and purchased from Richard Tayler Minerals. The elemental composition of the olivine was determined by Electron Probe Micro-Analysis (EPMA; Cameca SX 100 microprobe). Standard silicate analysis conditions were used (column conditions: 20 keV, 20 nA; beam size: 10 µm).

For the experiment, the mineral substrate was prepared by first crushing the coarse granules to 0.5-1 mm grain size using a TEMA rock crusher and then sieving using 1 mm and 0.5 mm sieves to select for 0.5-1 mm diameter grains. The powdered olivine was added to 50 ml of acetone and sonicated for 15 minutes. This process was repeated before rinsing the sample with deionised water and desiccating the powder at 50 °C for 48 hours. Given that the average predicted $Fe^{2+}/Fe^{2+}Mg$ content of martian olivine is predicted to be

higher than terrestrial olivine (McSween et al., 2009; Bish et al., 2013), a small grain size was chosen (hence a large surface area) to facilitate the dissolution of the Fe^{2+}.

Grains were set in an epoxy resin and polished using the Metprep Saphir 520 polishing machine (this was carried out by Michelle Higgins at the Open University). The mount was carbon-coated before analysis, to prevent charging of mineral surfaces.

A sample of 96 grains were analysed by EMPA (five measurements taken per grain) to obtain major element data, including the FeO:MgO ratio. This identified that 74 % of the grains analysed (Table A C.2) were olivine with a forsterite value of Fo_{84}. The olivine substrate is therefore compositionally Fe-poor relative to olivine at Gale Crater, Mars (Bish et al., 2013).

Figure 2.2. Olivine used as the Fe^{2+} substrate in growth experiments. (A) Fine (~1 mm) grains (top left), coarse (~5 mm) granules (right) and main rock sample (bottom left) were processed into (B) a >1 mm powder substrate (right) and 1 cm^3 cubes (left).

In addition, ~1 cm^3 cubes of olivine were prepared, which were added to some of the cultures to ascertain any morphological or mineralogical changes that occurred to the olivine during the experiment. Cubes were cut with an agate and general trimsaw from the main olivine sample (seen in Figure 2.2A). One of the surfaces was polished using Metprep Cameo fixed abrasive grinding laps (carried out by Michelle Higgins at the Open

University) (Figure 2.2B). To remove any organic carbon associated with the surface of the mineral, the cubes were sonicated for 15 minutes in acetone, followed by 15 minutes of sonication in deionised water. The cubes were autoclaved at 121 °C for 15 minutes and desiccated in a drying oven at 50 °C overnight. Under anaerobic conditions, one olivine cube was added to a single bottle of each of the triplicate culture series which correspond to each microorganism and the control. Cubes were analysed using Scanning Electron Microscopy (SEM) (as described in Section 2.2.7) before the experiment, to identify pre-existing features with potentially biogenic appearance which may confound later observations and conclusions.

2.2.3.3 Batch cultures

Batch cultures were prepared in sterilised 125 mL Wheaton bottles. Each bottle contained 5 g of powdered olivine substrate (Section 2.2.3.2) and 50 mL of minimal medium. The medium was dispensed into the Wheaton bottles in the anaerobic chamber under a 85:10:5 N_2:CO_2:H_2 atmosphere.

Samples (1 mL) of growth cultures were washed twice by centrifugation at 3000 × *g* for 10 min under anaerobic conditions to prepare the inoculum. The supernatant was removed, and the pellet was resuspended in 1 ml of minimal media. Cell counts (Section 2.2.4) were used to estimate the viable number of cells in the inoculum.

For each strain, cultures were conducted in triplicate and inoculated to an initial concentration of 10^5 cells mL^{-1}. The media was inoculated, and the cultures were sealed with a sterile butyl stopper and aluminium crimp, before being removed from the chamber. The headspace was flushed with a filter sterilised 90:10 N_2:CO_2 gas mix *via* the septa using sterile syringe needles, and overpressurised to 1.5 bar to prevent intrusion of oxygen. The

microorganisms and abiotic control series were incubated at 21 °C in the dark for the duration of the experiment.

2.2.4 Cell enumeration

A BacLight Bacterial viability kit (Invitrogen) was used to determine viable cell numbers by assessing membrane integrity. This method uses a SYTO 9 green fluorescent nucleic acid stain and propidium iodide (which acts as a red fluorescent nucleic acid stain). SYTO 9 penetrates both live and dead bacteria, while propidium iodide is only able to pass through the membranes of damaged cells. A secondary characteristic of propidium iodide is that it reduces the fluorescence of the SYTO 9 stain when both are present. This results in damaged and/or dead cells fluorescing red while live cells fluoresce green (Figure 2.3). From this, the viable cell density can be calculated from the mean viable cell count, field of view and volume of sample contained between the glass microscope slide and cover slip.

One confounding factor was the autofluorescence of microscopic olivine grains; however, the clear differences in their size (>10 µm for grains vs <2 µm for cells) and morphology (angular, textured grains vs rounded, uniform cells) allowed these to be differentiated from cells.

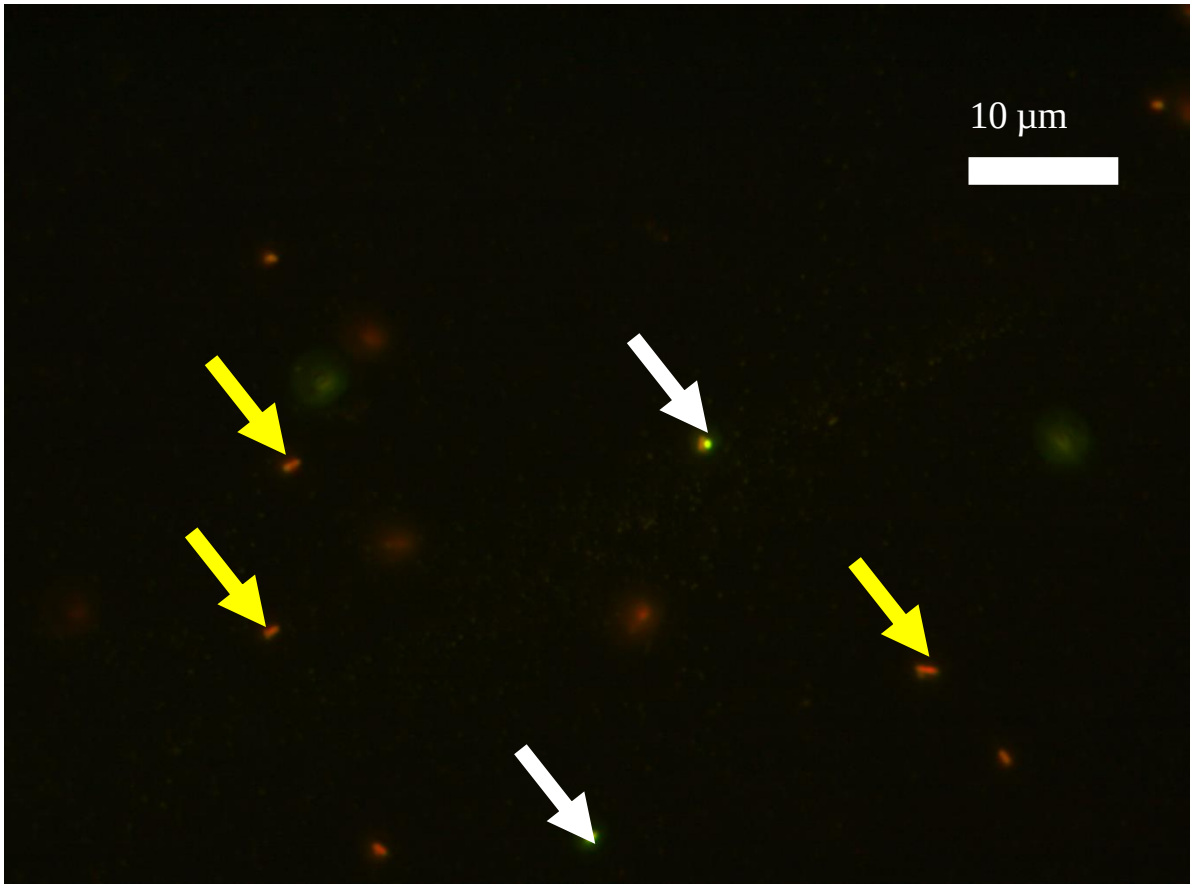

Figure 2.3. Micrograph at x100 magnification of a Live/Dead-stained Thiobacillus denitrificans culture. Intact cells fluoresce green (white arrows) while damaged cells fluoresce red.

To monitor growth, 100 µL of culture was aseptically removed using a N_2-flushed syringe through the rubber septum of the bottle, and dispensed into a sterile, 1.5 mL eppendorf tube. Each sample was mixed with 1 µL of a 1:1 mixture of Component A (SYTO 9 dye (1.67 mM), Propidium iodide (1.67 mM) solution in DMSO) and Component B (SYTO 9 dye (1.67 mM), Propidium iodide (18.3 mM) solution in DMSO) and incubated in the dark for 20 min. Following incubation, 5 µL aliquots of the sample were pipetted onto a sterile glass microscope slide (3 per slide) and a cover slip was added to each. The slides were observed under UV light using a Leica fluorescence microscope at ×100 (oil-immersed) magnification. Data from ten fields of view were collected from across each slide and cells density calculated using equation (1).

Maximum specific growth rates were calculated from the cell counts made during the exponential growth phases of the microorganisms in culture, using equation (2).

2.2.5 Protein concentration

To support the cell count data, protein concentration was monitored as a proxy for accumulation of biomass and thus microbial growth. Aliquots were aseptically removed anaerobically throughout the experiment, as described previously in Section 2.2.4, and analysed using the Bradford colourimetric assay (Bradford, 1976).

To lyse the cells, 500 µL of culture was centrifuged at 15,900 × *g* for 30 min and the pellet were resuspended in 500 µL of 0.1 M NaOH, which was then heated to 60 °C for 6 min. The Bradford reagent solution (Coomassie Brilliant Blue G-250 dye, Sigma) was added to the sample in a 1:1 volume ratio (250 µL + 250 µL). The mixture was dispensed into a clear 1 mL cuvette and after 5 min the optical density at 595 nm was measured using a Camspec M107 visible spectrophotometer. γ-globulin was used as the protein standard, with 0 to 25 µg mL^{-1} prepared in 0.1 M NaOH solution. Standard curves were calculated as shown in Appendix B.

2.2.6 Nitrate measurement

The concentration of nitrate ions in each of the cultures was measured post-inoculation and at the endpoint of the experiment using an ELIT 0821 ion selective nitrate electrode and ELIT 003 lithium acetate reference electrode (Nico2000) connected to a conductivity meter (HANNA instruments). A calibration curve was prepared with 10 µM, 100 µM, 1 mM and 10 mM of $NaNO_3$ dissolved in milliQ water, with the concentration plotted against conductivity (mV). The nitrate concentration was determined using the equation from the standard curve of the calibration graph (Appendix B).

2.2.7 Morphological analysis

Scanning electron microscopy (SEM) was used to search for evidence of biofilm formation or cellular features on the olivine crystal surfaces following incubation with the selected microorganisms and in the abiotic controls. After 146 days, the olivine cubes were aseptically removed and mounted onto aluminium stubs using carbon tape under a 85:10:5 N_2:CO_2:H_2 atmosphere (in the anaerobic chamber). The cubes were then desiccated, before being sealed in glass vials and heat-sealed in air-tight mylar pouches (Fresherpack). The pouches were removed from the chamber and transferred to the electron microscopy suite, where the mounted cubes were briefly (~30 seconds) removed from the anoxic conditions before being gold coated under vacuum for SEM analysis.

The cubes were imaged and analysed under vacuum in a Zeiss Supra 55 VP Field Emission Gun Scanning Electron Microscope (FEG-SEM), using SE2 and Cent detectors at ×100 to ×50,000 magnifications. Working distances of 4.1-10.1 mm and accelerating voltages of 3-20 kV were used for imaging.

Energy-dispersive X-ray spectroscopic (EDS) analysis was performed using the integrated Aztec Energy v3.3 system (Oxford Instruments) to provide qualitative compositional data for Si, Na, K, Al, P, S, Cr, Fe, Ti, Mg, Ca and Cl, allowing composition of potentially biogenic to be compared to the mineral background of each inoculated sample and the control. A working distance of 8.5 mm and an accelerating voltage of 20 kV were used for this analysis with spectra obtained from features of interest and the nearby mineral surface.

2.2.8 Ferrozine assay

The ferrozine colourimetric assay (Stookey, 1970) allows determination of reduced and total Fe concentrations within the medium. This method was used unsuccessfully to quantify the Fe oxidation states throughout the experiment, because the Fe concentrations fell below the detection limits of the method. Inductively-coupled plasma mass spectrometry (ICP-MS) was instead used to determine dissolved Fe concentration.

2.2.9 Inductively-coupled plasma mass spectrometry (ICP-MS)

To measure the chemical composition – particularly relative concentrations of ^{56}Fe and ^{57}Fe – of the media after the experiment, ICP-MS was used as an alternative to the ferrozine assay. An aliquot (9 mL) of each culture and control was extracted under anaerobic conditions using a N_2-flushed sterile syringe at day 146. The samples were filtered through 0.2 µm sterile filters into 1 mL aliquots of 20 % HNO_3 solution, resulting in 2 % final HNO_3 concentration. ICP-MS was conducted using an Agilent 7500s with New Wave 213 laser system, by Sam Hammond at The Open University. Detection limits of the instrument are listed in Table 2.2.

Table 2.2. Detection limits for ions detected by the Agilent 7500s ICP-MS system.

Element	Detection limit (ppm)
Na	3.21
K	2.02
Ca	0.14
Si	0.033
Mg	0.025
^{56}Fe	0.013
^{57}Fe	0.013
Al	0.013
Sr	0.0012
Ba	0.0007
Mn	0.0007

2.2.10 pH measurement

pH was measured using a Thermo Scientific Orion Three Star pH probe with a two-point calibration using Omega Buffer solutions at pH 4 and 7 at the start and end points of the experiment.

2.2.11 Statistics

Observed differences in results between olivine substrate culture series from nitrate analysis, ICP-MS and viable cell counting were tested for significance using the 2-tailed paired Student's t-test. This test was selected as it allows for one reference value to be tested against another value, where the second value may be greater or less than the reference. In this chapter, the test is used to differentiate between data points of the same type, either between two parallel series or between time points.

2.3 Results

2.3.1 Growth with olivine as an Fe source

The collective measurements and assays detailed below assess the capability of the four microorganisms to grow by NDFO metabolism using Fe^{2+} released by dissolution from the olivine substrate.

2.3.1.1 Cell counts

From a starting concentration of 10^5 cells ml^{-1}, both *Pseudogulbenkiania sp*. strain 2002 and *Acidovorax sp*. strain BoFeN1 entered the exponential growth phase immediately and grew to exceed 10^7 cells mL^{-1} by day 4 with specific growth rates of 4.8 and 4.3 day^{-1} respectively (Figure 2.4). Strain BoFeN1 entered stationary phase at 6 x 10^7 cells mL^{-1} after 13 days of incubation, entering a gradual death phase after 28 days to 2.5 x 10^7 cells mL^{-1} by the end of the experiment. Strain 2002 plateaued in stationary phase at 2.3 x 10^7 cells mL^{-1} from day 13 onwards. Neither *Paracoccus sp*. strain KS1 nor *Thiobacillus denitrificans* displayed a clear exponential growth phase in the first 8 days. However, the strain KS1 cell density began an exponential phase at day 13, exceeding 10^7 cells mL^{-1} by day 28 and reaching a concentration of 6.7 x 10^7 cells mL^{-1} by the end of the experiment with a specific growth rate of 0.2 day^{-1} in the exponential phase. *T. denitrificans* maintained a low concentration of cells in stationary phase up to the end-point of the experiment.

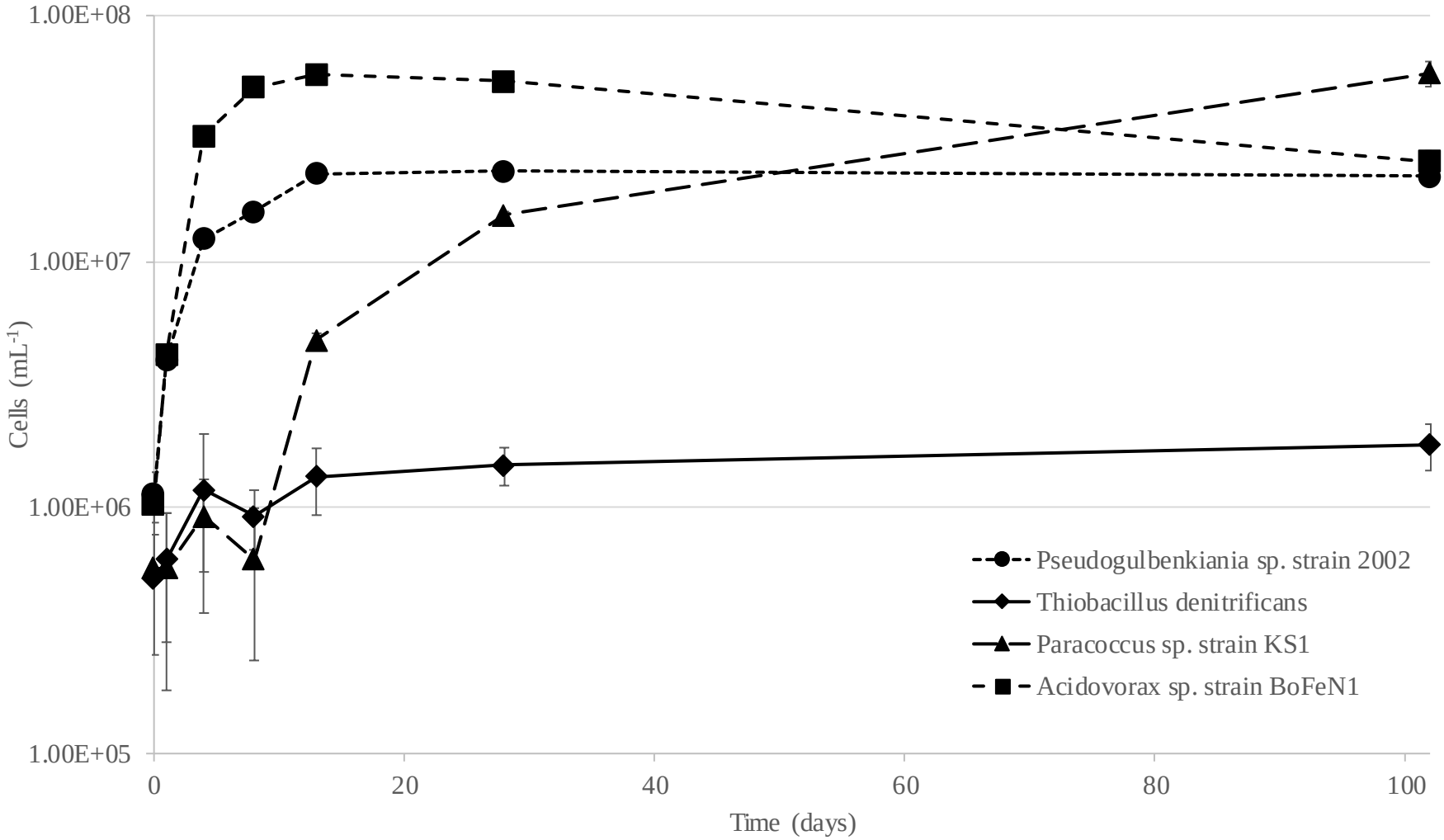

Figure 2.4. Viable cell counts over time for Pseudogulbenkiania sp. strain 2002, Thiobacillus denitrificans, Paracoccus sp. strain KS1 and Acidovorax sp. strain BoFeN1. Error bars represent ± standard error.

2.3.1.2 Protein concentration in culture

Bradford protein assays conducted on samples taken over the first 8 days of the experiment show an increased protein concentration in the strain BoFeN1 cultures (7.72 ±0.56 µg mL^{-1}) and strain 2002 cultures (4.26 ±0.98 µg mL^{-1}) above the abiotic control (2.27 ±0.20 µg mL^{-1}) at day 4, though only the BoFeN1 protein concentration was significantly greater (p<0.05) than the control at this time point (Figure 2.5). The BoFeN1 protein concentration continued to rise to 10.46 ±1.10 µg mL^{-1} at day 8, whilst strain 2002 plateaued at 3.72 ±0.17 µg mL^{-1} although the concentration was significantly (p<0.05) above the abiotic control (1.35 ±0.05 µg mL^{-1}). No significant difference between the strain KS1, *T. denitrificans* and the control at any measured time point.

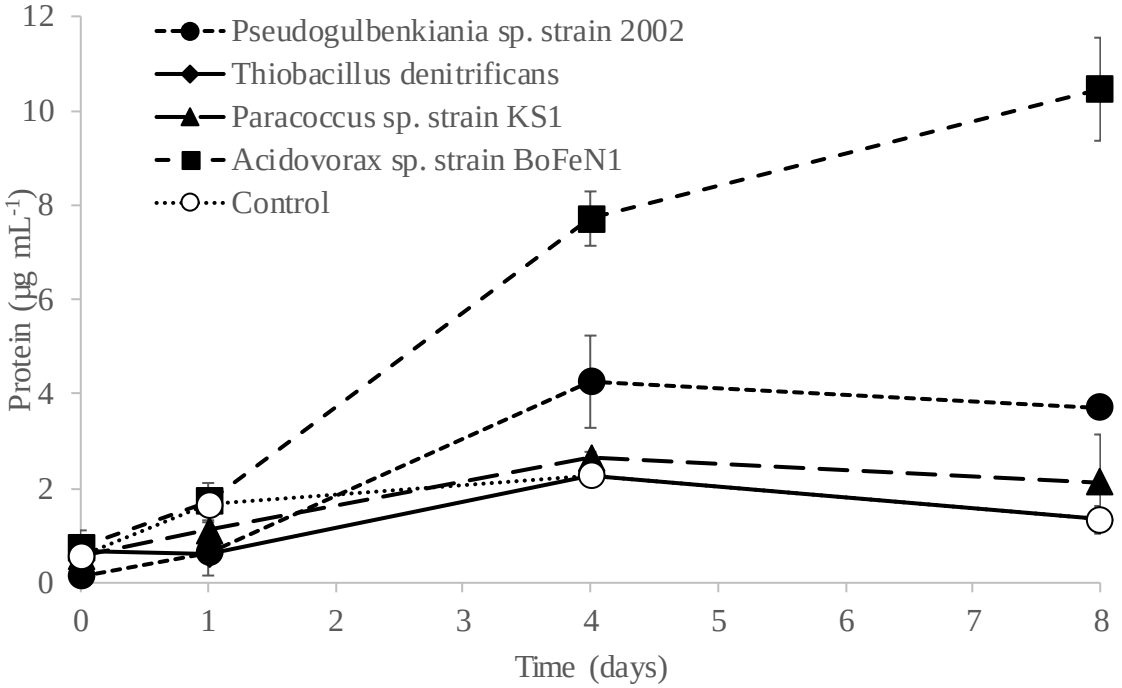

Figure 2.5. Protein concentration over the first 8 days of the experiment for *Pseudogulbenkiania sp*. strain 2002, *Thiobacillus denitrificans*, *Paracoccus sp*. strain KS1, *Acidovorax sp*. strain BoFeN1 and the control. Error bars represent ± standard error.

2.3.1.3 Nitrate depletion

The concentration of nitrate in the growth medium at the end of experiment decreased relative to the starting concentration, even in the control. The control had a nitrate depletion of 10.2 % (±1.0 %) from the initial concentration, with a 13.6 % drop (±0.9 %) observed in *T. denitrificans*, though the difference in relative depletion was not significant (Figure 2.6). In strain BoFeN1 cultures, the nitrate concentration decreased by 27.9 % (±0.8 %), compared with a 34.8 % (±3.1 %) drop in the strain 2002 group and a 40.3 % (±3.8 %) reduction in the strain KS1 group. The end-point nitrate concentration in KS1, 2002 and BoFeN1 cultures was found to be significantly lower ($p<0.05$) than that of *T. denitrificans* and the control groups.

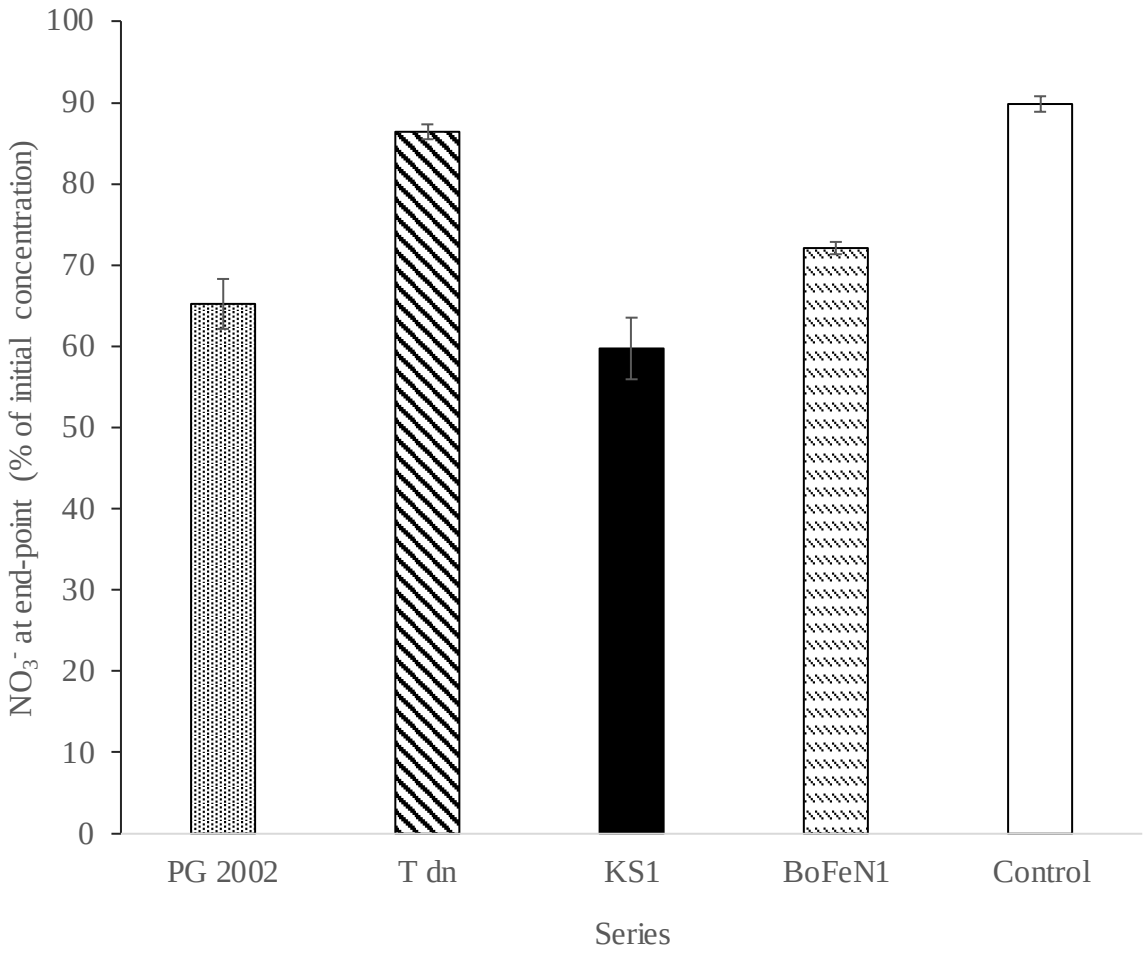

Figure 2.6. End-point nitrate concentrations as a percentage of the initial media concentration by culture series, Pseudogulbenkiania sp. strain 2002 (PG 2002), Thiobacillus denitrificans (T dn), Paracoccus sp. strain KS1, Acidovorax sp. strain BoFeN1 (BoFeN1) and the control. Error bars represent ± standard error.

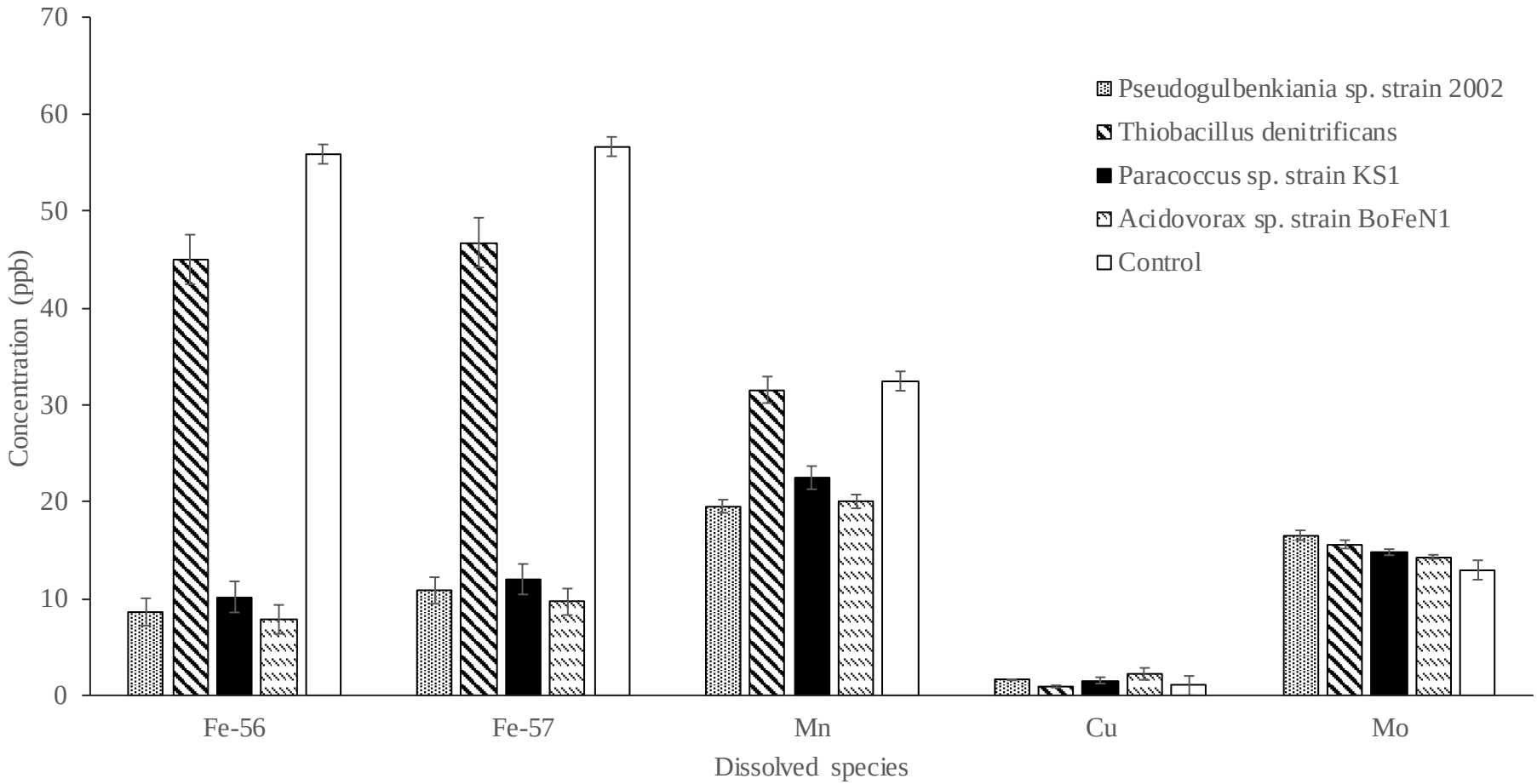

Figure 2.7. Inductively-coupled plasma mass spectrometry (ICP-MS) results for dissolved elemental composition at the end-point of the experiment in *Pseudogulbenkiania sp.* strain 2002, *Thiobacillus denitrificans*, *Paracoccus sp.* strain KS1, *Acidovorax sp.* strain BoFeN1 and the control. Error bars represent ± standard error.

2.3.1.4 End-point dissolved elemental composition

ICP-MS analysis of the end-point media filtrate (Figure 2.7) demonstrated significant differences between the biotic and abiotic controls and between the strains. Importantly, the elements displaying the most significant differences (^{56}Fe and ^{57}Fe, and Mn) are known to be electron donors for microbial energy metabolisms (Tebo et al., 2005; Weber et al., 2006a; Hedrich et al., 2011).

The concentration of ^{56}Fe was lower in all of the biotic experiments, including the non-growing *T. denitrificans* culture (45±2.6 ppb) compared to the abiotic control (55.9±0.9 ppb) ($p<0.05$). Strains BoFeN1 (7.8±1.5 ppb), 2002 (8.6±1.4 ppb) and KS1 (10.2±1.6 ppb) all had lower ^{56}Fe than both *T. denitrificans* and the abiotic control ($p<0.05$).

These ^{56}Fe patterns are mirrored by the heavier ^{57}Fe isotope, with the concentrations associated with the growing cultures lower than that of the abiotic control; the end-point ^{57}Fe concentration in the *T. denitrificans* cultures (46.7±2.6 ppb) was ~83 % of that in the abiotic control (56.6±0.9 ppb). Concentrations of ^{57}Fe in strain BoFeN1 (9.7±1.4 ppb), 2002 (10.8±1.4 ppb) and KS1 (12±1.6 ppb) were significantly lower ($p<0.05$) than both *T. denitrificans* and the control, ranging from 22-27 % of the concentration in the control. It is unlikely that the presence of organisms inhibits the liberation of Fe into the medium, so the lower concentrations of ^{56}Fe and ^{57}Fe compared to the control indicate that Fe is being removed from solution. The most likely explanation in the context of this experiment is that Fe^{2+} is being oxidised during NDFO, resulting in the precipitation of insoluble Fe^{3+} compounds, as has been described extensively in the literature (Miot et al., 2009; Schädler et al., 2009; Pantke et al., 2012; Miot et al., 2014a; Miot et al., 2015).

The $^{57}Fe/^{56}Fe$ ratio varied between cultures with growing microorganisms (strains BoFeN1, KS1 and 2002), the *T. denitrificans* and control cultures. The mean $^{57}Fe/^{56}Fe$ in

the control cultures was 1.014 (±0.001), and 1.039 (±0.003) in *T. denitrificans* cultures. In the growing cultures, the mean $^{56}Fe/^{57}Fe$ was 1.258 (±0.052) for strain 2002, 1.231 (±0.053) for strain BoFeN1 and 1.180 (±0.036) for strain KS1.

Mn concentrations in the abiotic control and *T. denitrificans* cultures were not significantly different. However, there is reduced Mn concentration in strain 2002, BoFeN1 and KS1 relative to the control ($p<0.05$). The Mn concentrations in these three groups are 60-70 % of the control and not significantly different from one another ($p>0.05$).

Although Cu concentrations were similar to the Fe concentrations in their behaviour for each strain, only one significant result ($p<0.05$) was found; the end-point Cu concentration in the strain 2002 series was higher than in *T. denitrificans*.

There was no significant differences in Mo concentrations between the inoculated groups, but the control group had a significantly lower concentration ($p<0.05$).

2.3.2 pH

The pH of all inoculated cultures and abiotic controls increased significantly over the course of the experiment ($p<0.05$), as shown in Table 2.3. However, there were no significant differences in end point pH between any series ($p>0.05$).

Table 2.3. Start and end point mean pH values for inoculated culture series and abiotic control ± standard error of the mean).

Series	pH (start point)	pH (end point)
Pseudogulbenkiania sp. strain 2002	7.00	7.15 ± 0.041
Thiobacillus denitrificans	7.00	7.10 ± 0.003
Paracoccus sp. strain KS1	7.00	7.12 ± 0.003
Acidovorax sp. strain BoFeN1	7.00	7.14 ± 0.019
Control	7.00	7.13 0.011

2.3.3 Morphological features on olivine cubes

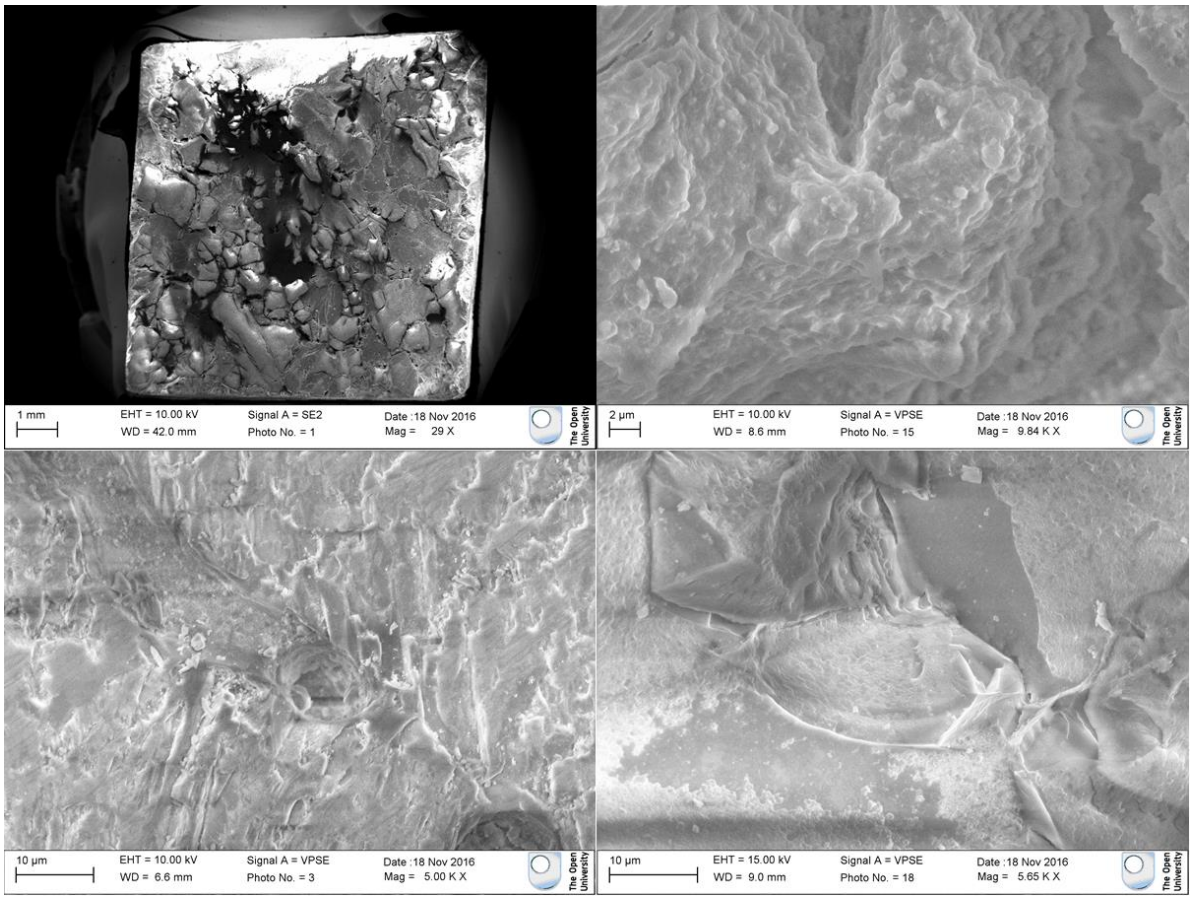

Figure 2.8. Electron micrographs of an un-inoculated olivine cube prior to culture with microorganisms. Clockwise from top left: the whole polished face of the cube, areas of the mineral surfaces at ×5,000-10,000 magnification showing no evidence of pre-existing biogenic features.

Prior to the experiment, no features were observed which suggested biological processes on the mineral surface (Figure 2.8). SEM investigation of the olivine cubes at the end-point of the experiment revealed numerous features that suggested microbial colonisation by some the test strains. Aggregations of globular features, approximately 1.5-2 µm in diameter, were observed to be adhered to the mineral surface after incubation with strain 2002. These aggregations were typically composed of 50-100 globular units and covered by a layer of nanometre-scale dendritic features (Figure 2.9). EDS analysis was used to look for differences in major element composition between the globular features and the background mineral surface. This revealed a co-location between the globular features and regions with elevated carbon (Figure 2.10-Figure 2.12 & Figure A C.1-Figure A C.3).

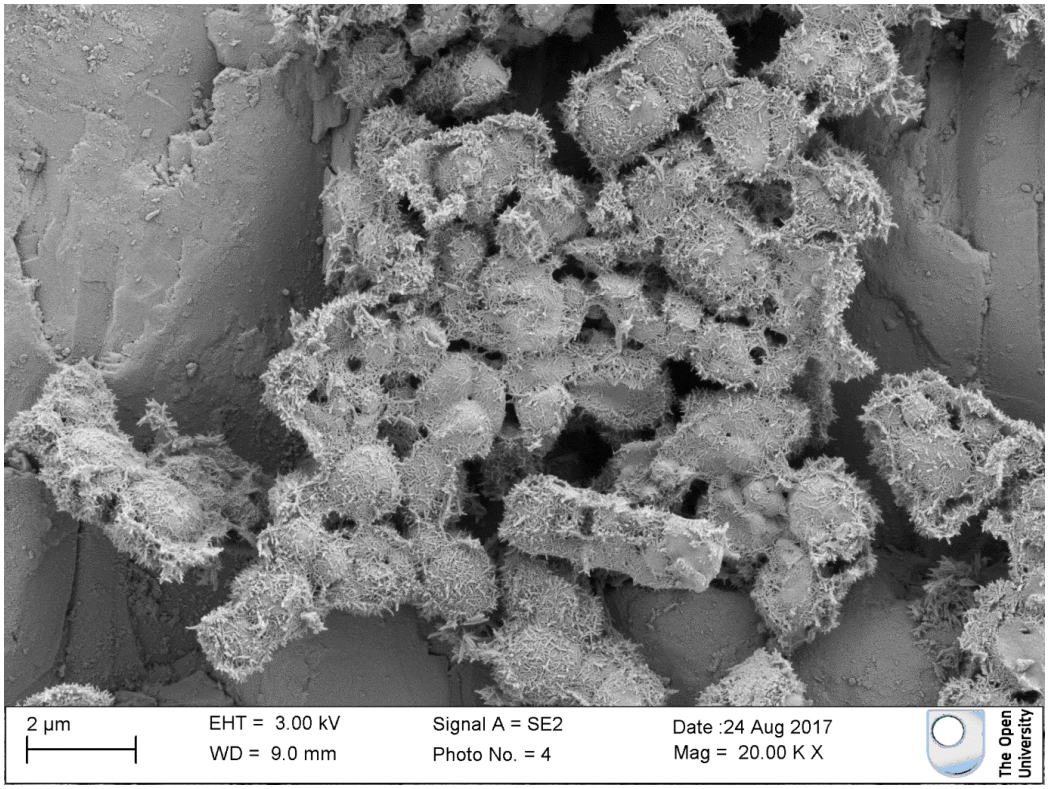

Figure 2.9. Electron micrograph of globular features adhered to olivine after culture with Pseudogulbenkiania sp. strain 2002.

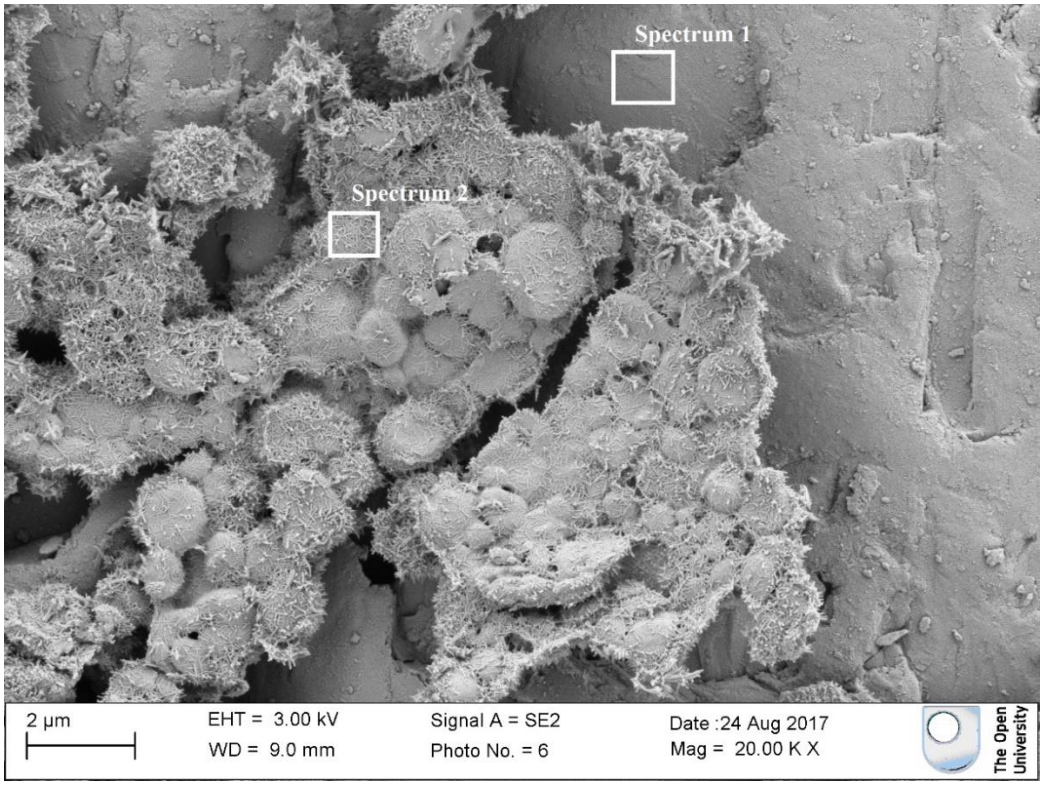

Figure 2.10. Electron micrograph of globular aggregations on olivine surface after culture with Pseudogulbenkiania sp. strain 2002. Target areas for electron dispersive X-ray spectroscopic (EDS) analysis are shown with white boxes.

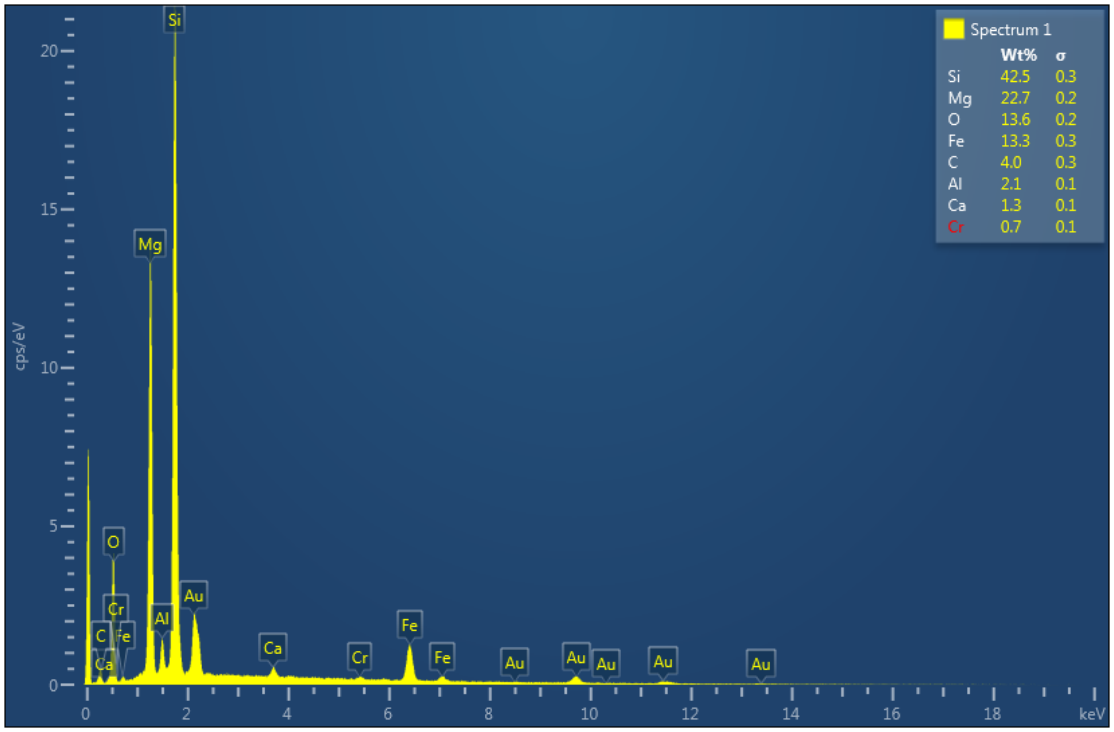

Figure 2.11. Energy dispersive X-ray spectroscopy (EDS) elemental composition output for target area "Spectrum 1" indicated in Figure 2.9.

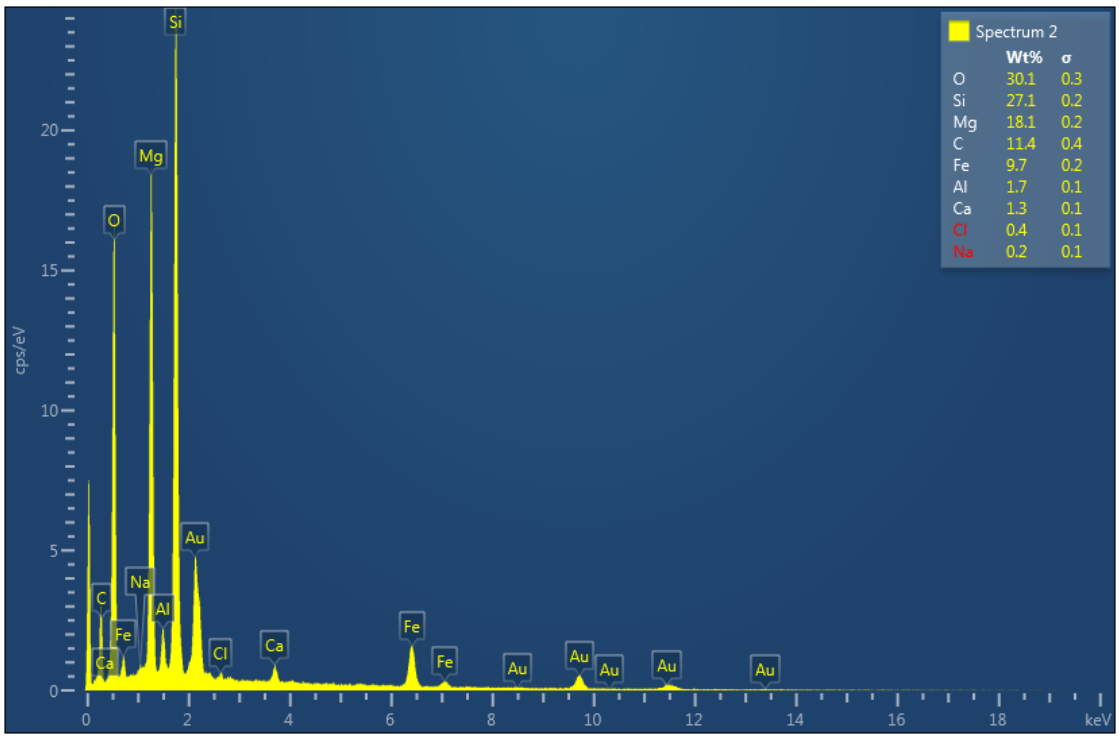

Figure 2.12. Energy dispersive X-ray spectroscopy (EDS) elemental composition output for target area "Spectrum 2" indicated in Figure 2.9.

Individual structures, flattened and ~1 µm in diameter, were also observed attached to the mineral surface of the strain KS1 olivine cube (Figure 2.13). These features were thinnest at the edges, rising in the centre to form irregular convex shapes, reminiscent of round "ravioli" parcels. The thickest of these features were also co-located with areas of elevated carbon (Figure 2.13-Figure 2.15).

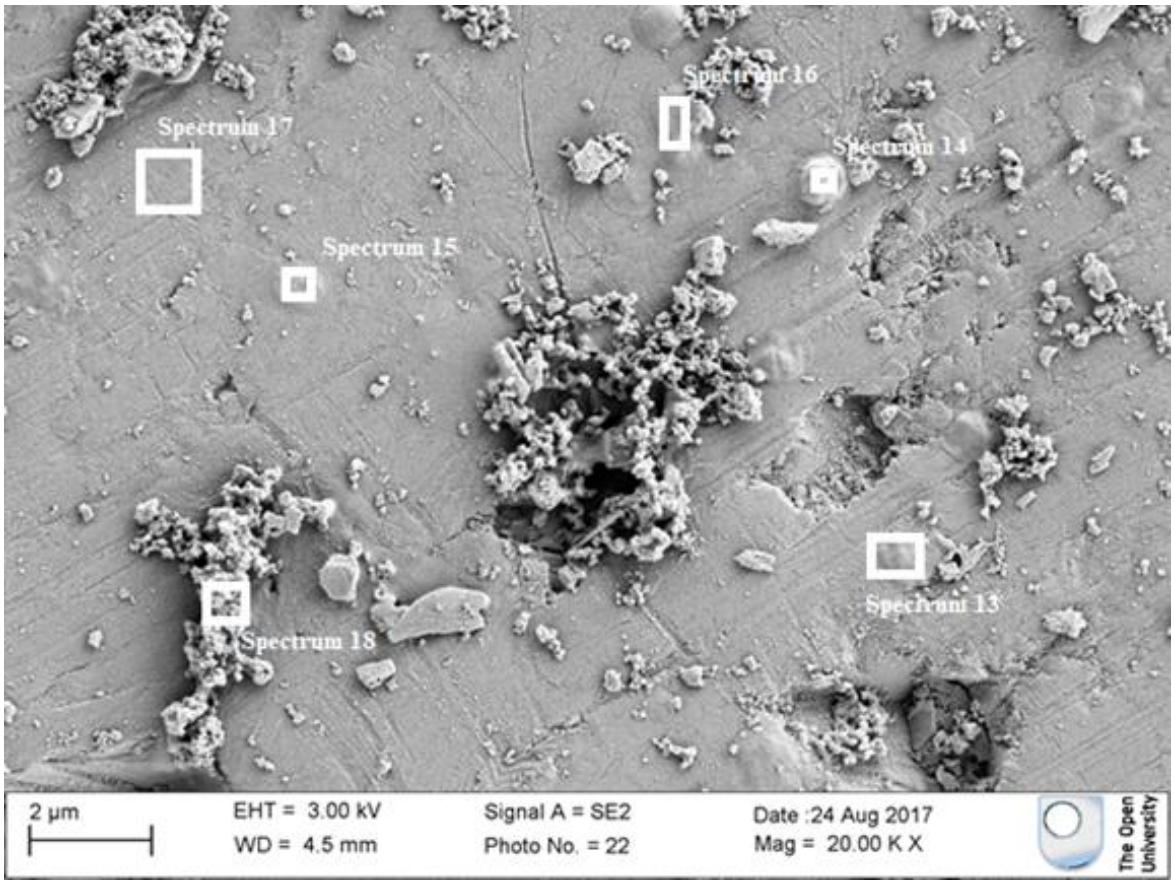

Figure 2.13 Electron micrograph of flattened, rounded features adhered strongly to the olivine surface after culture with Paracoccus sp. strain KS1. Target areas for electron dispersive X-ray spectroscopic (EDS) analysis are shown with white boxes.

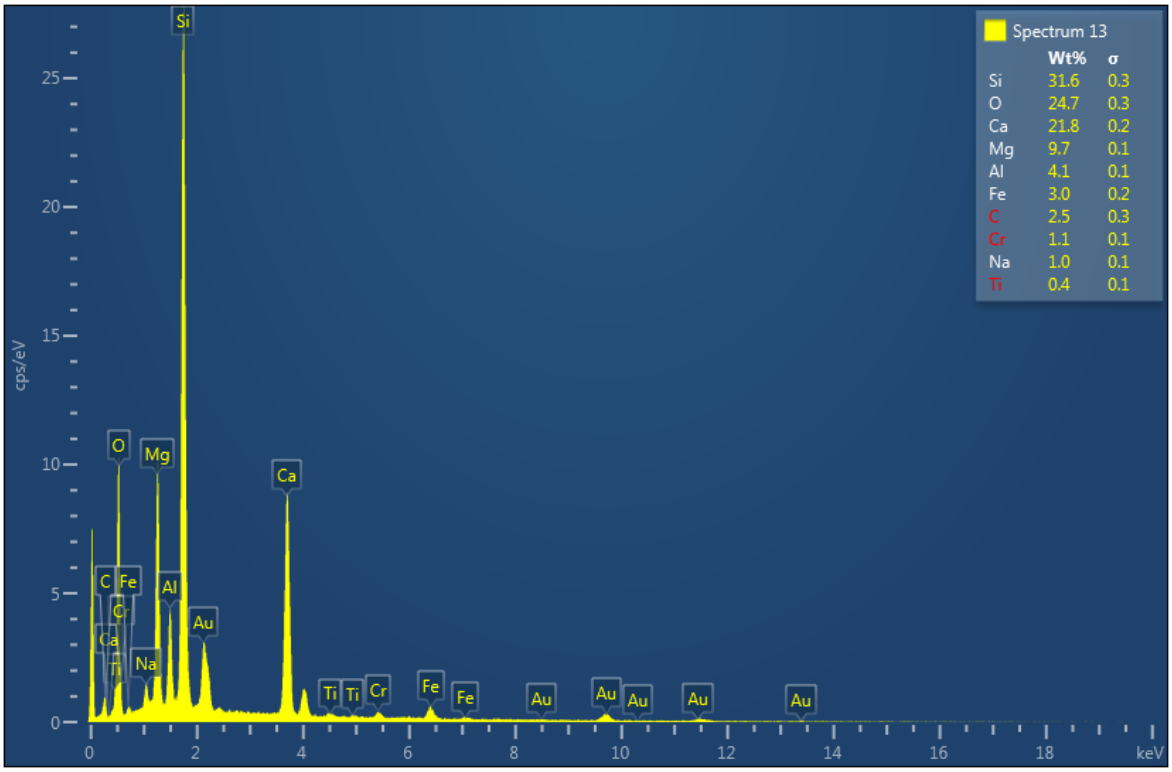

Figure 2.14. Energy dispersive X-ray spectroscopy (EDS) elemental composition output for target area "Spectrum 13" indicated in Figure 2.13.

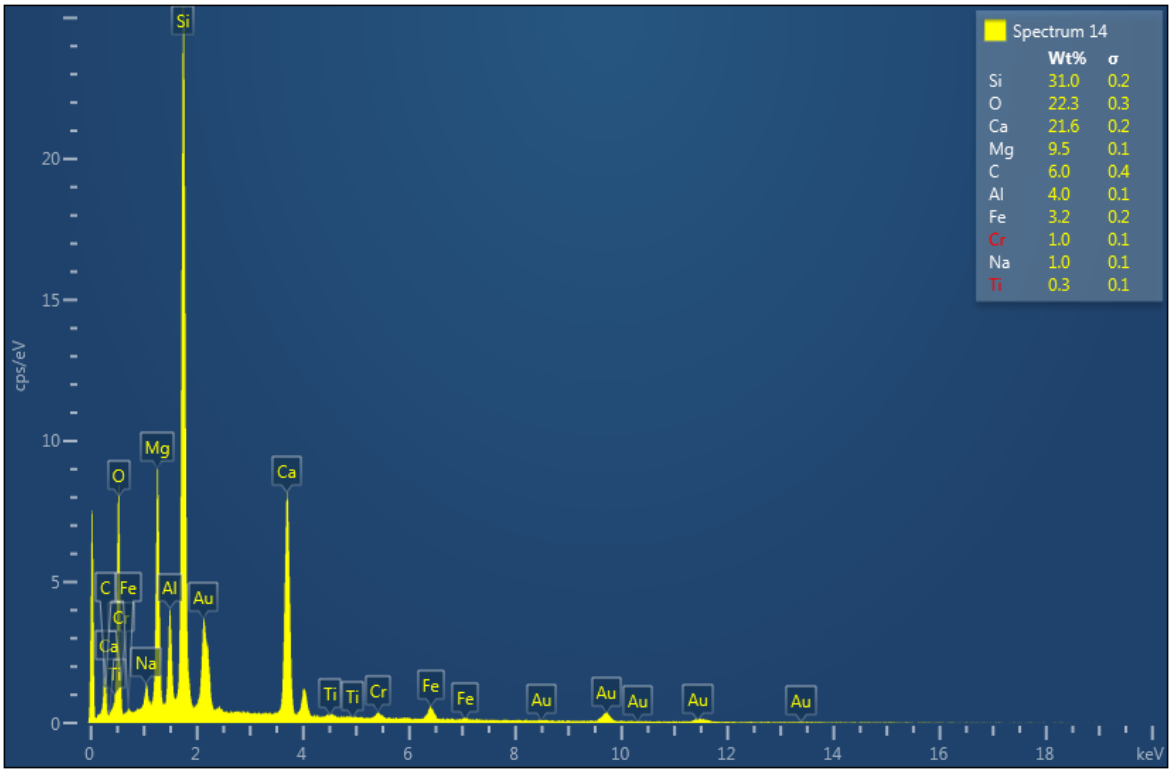

Figure 2.15. Energy dispersive X-ray spectroscopy (EDS) elemental composition output for target area "Spectrum 14" indicated in Figure 2.13.

Rounded structures embedded within a porous or semi-porous matrix were discovered in association with the mineral surfaces of the olivine cube from the KS1, 2002 and BoFeN1 cultures, as well as from the abiotic control. These features were not observed in the *T. denitrificans* culture. On the strain 2002 cube, these features were present in aggregations of several hundred, in recesses (Figure 2.16) and on large flat surfaces (Figure 2.17). EDS analysis revealed that the rounded features, but not the matrix material, were co-located with regions of elevated Ca (Figure 2.18-Figure 2.19 and Figure A C.8-Figure A C.12).

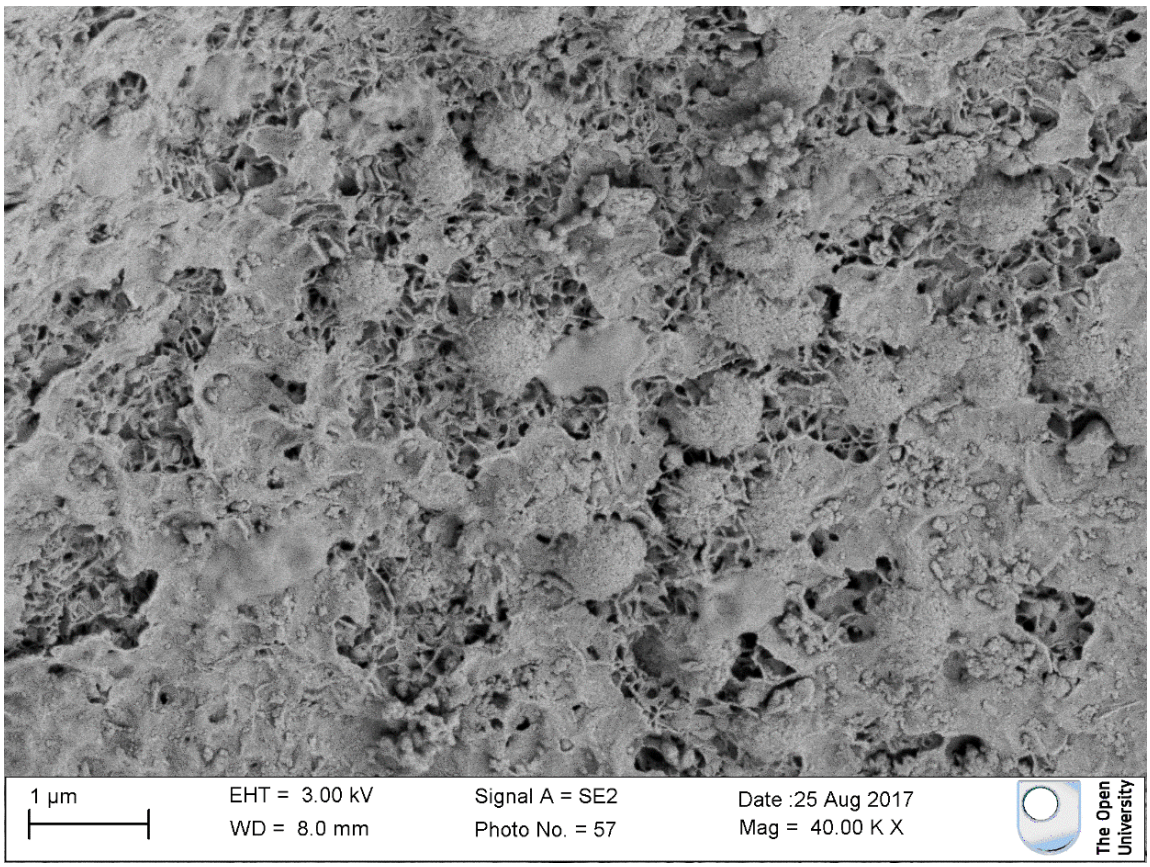

Figure 2.16. Electron micrograph showing rounded features embedded in a porous matrix after culture with Pseudogulbenkiania sp. strain 2002.

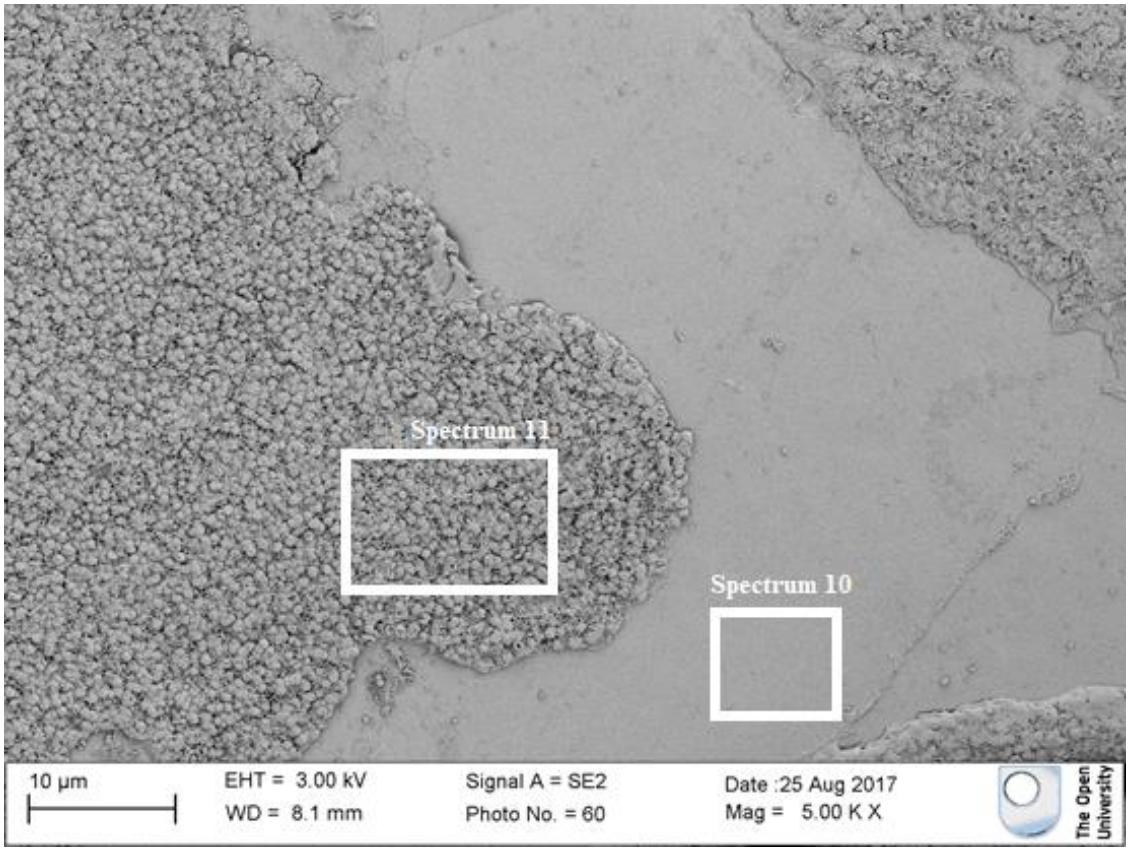

Figure 2.17. Electron micrograph displaying a large aggregation of rounded features (left-hand side) in a single layer adhered to the olivine surface, after culture with Pseudogulbenkiania sp. strain 2002. Target areas for electron dispersive X-ray spectroscopic (EDS) analysis are shown with white boxes.

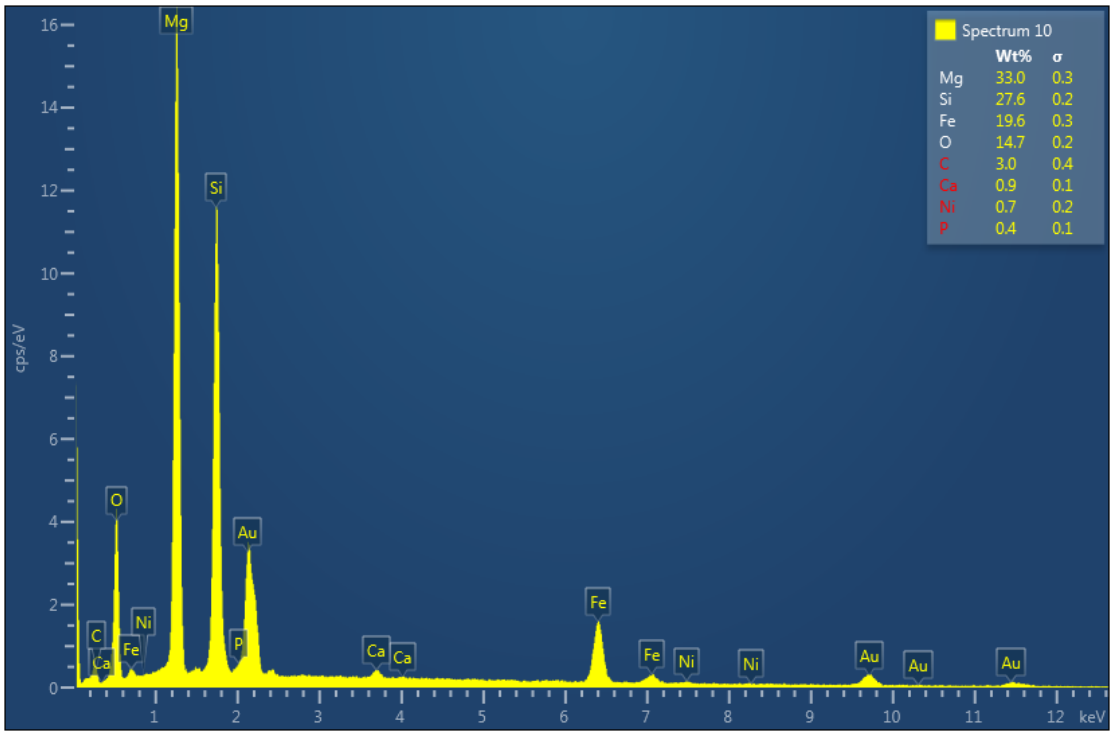

Figure 2.18. Energy dispersive X-ray spectroscopy (EDS) elemental composition output for target area "Spectrum 10" indicated in Figure 2.17.

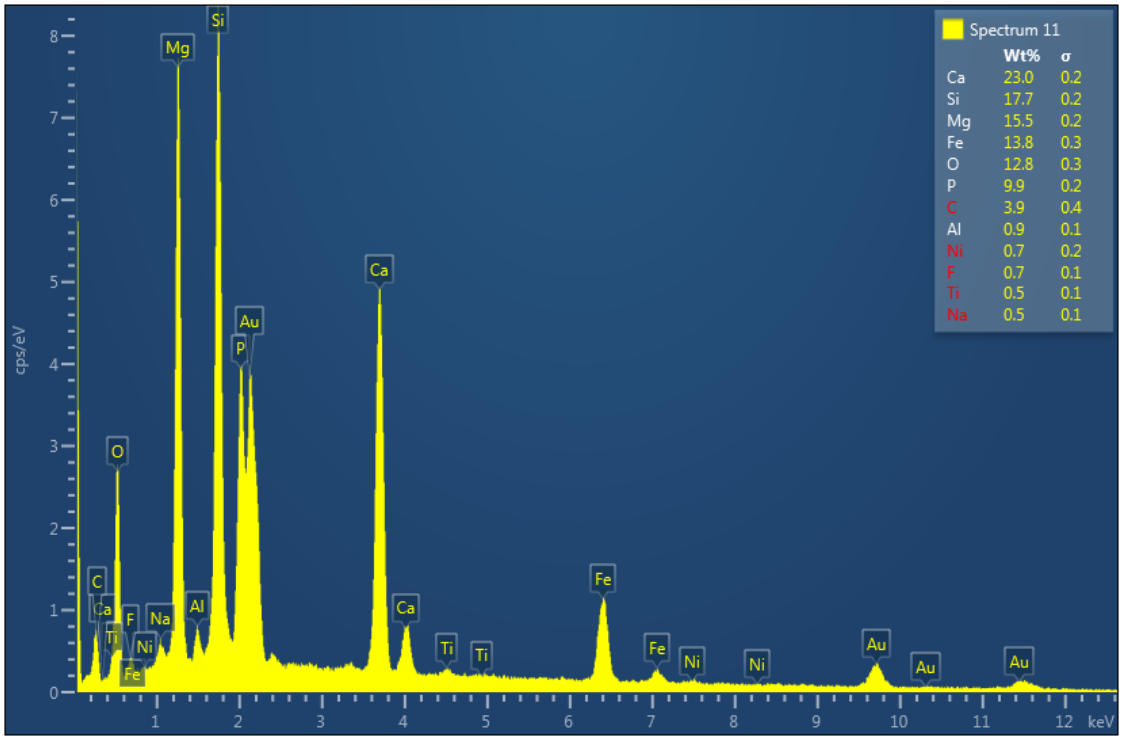

Figure 2.19. Energy dispersive X-ray spectroscopy (EDS) elemental composition output for target area "Spectrum 11" indicated in Figure 2.17.

Several areas of the cube from the strain KS1 culture featured contiguous plaques up to 40 µm diameter (Figure 2.20). These consisted of globular features ~1 µm across, embedded within, and emerging from, an interconnecting matrix. EDS analysis revealed a co-location of the rounded features and elevated Ca, relative to the mineral background (Figure 2.21-Figure 2.23 and Figure A C.13-Figure A C.18).

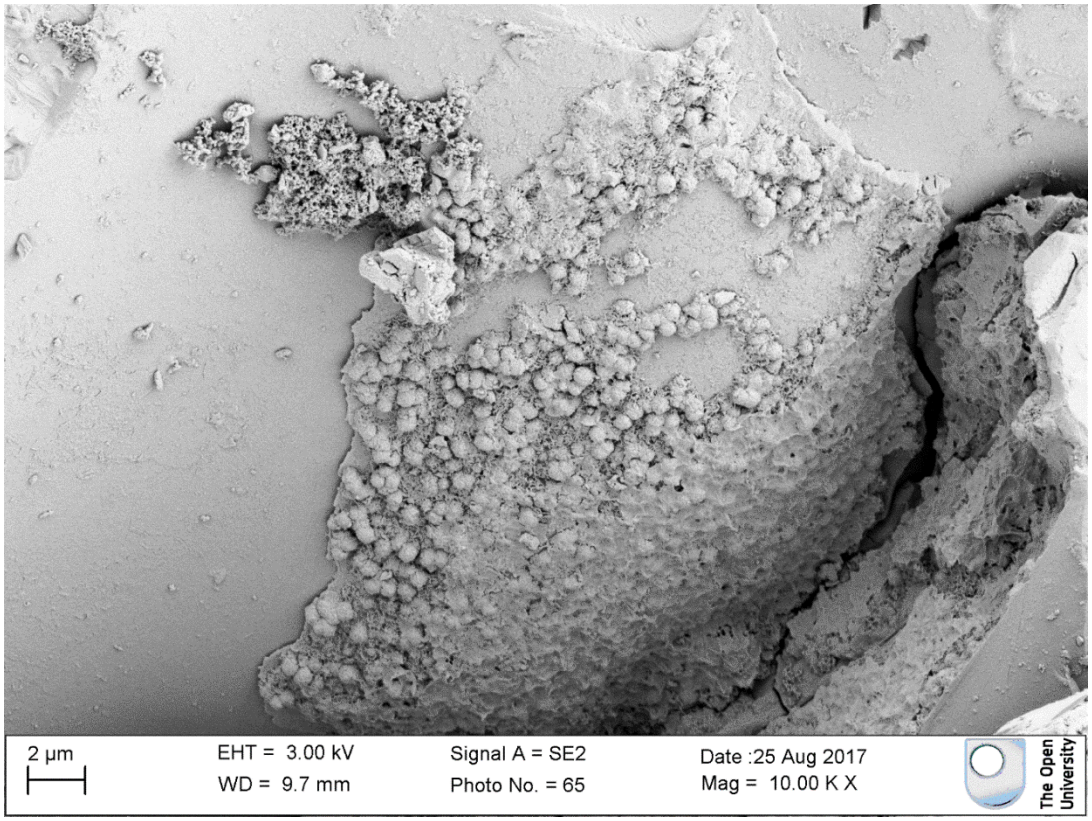

Figure 2.20. Electron micrograph of rounded structures embedded in a semi-porous matrix after culture with Paracoccus sp. strain KS1.

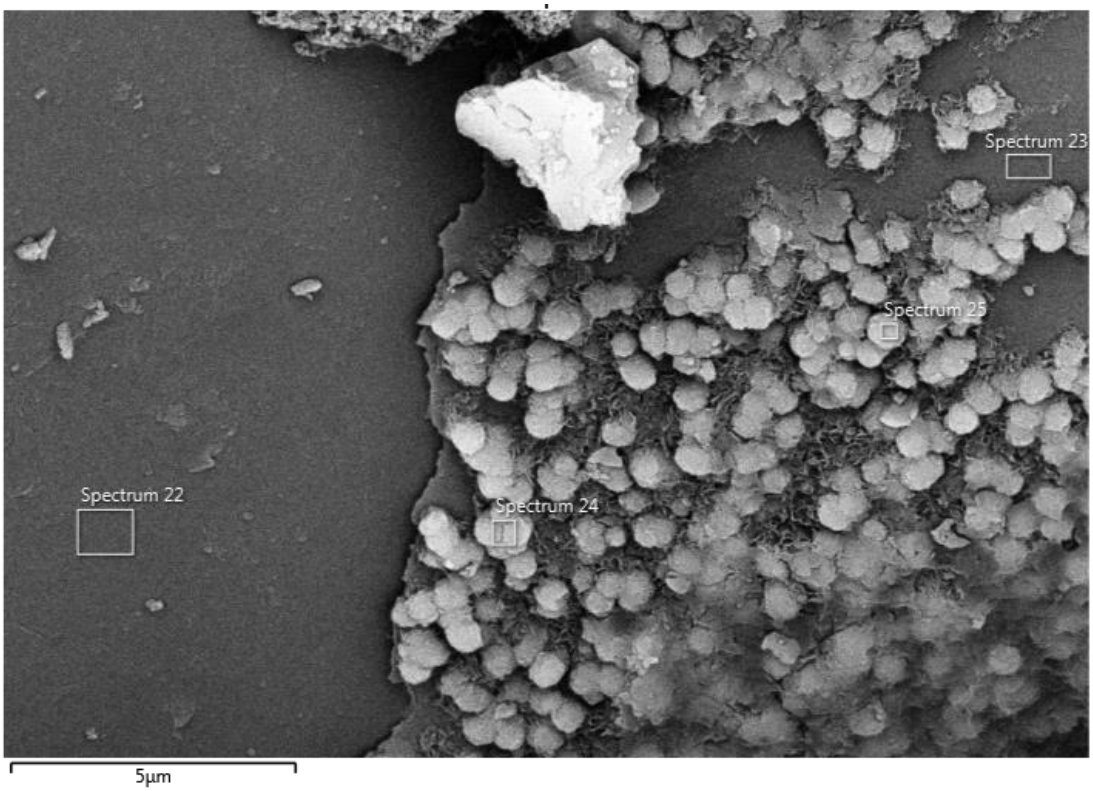

Figure 2.21. Electron micrograph of rounded features in a semi-porous matrix on olivine surface after culture with Paracoccus sp. strain KS1. Target areas for electron dispersive X-ray spectroscopic (EDS) analysis are shown with white boxes.

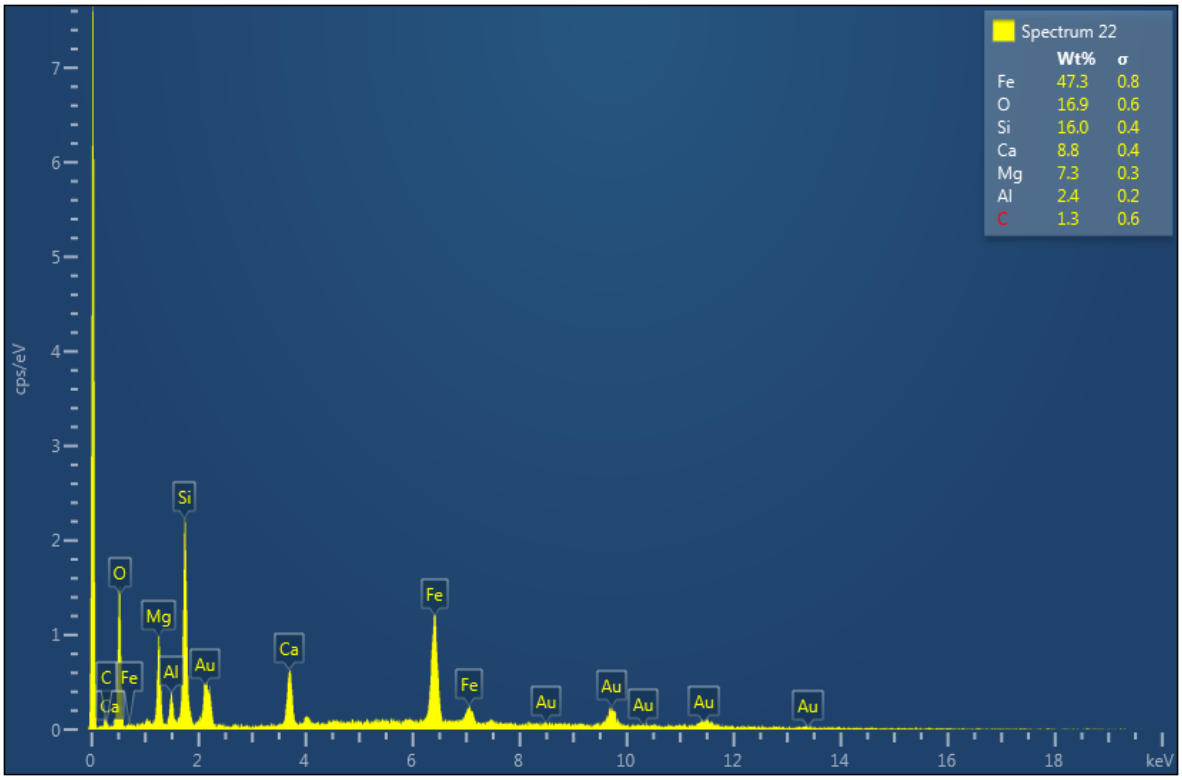

Figure 2.22. Energy dispersive X-ray spectroscopy (EDS) elemental composition output for target area "Spectrum 22" indicated in Figure 2.21.

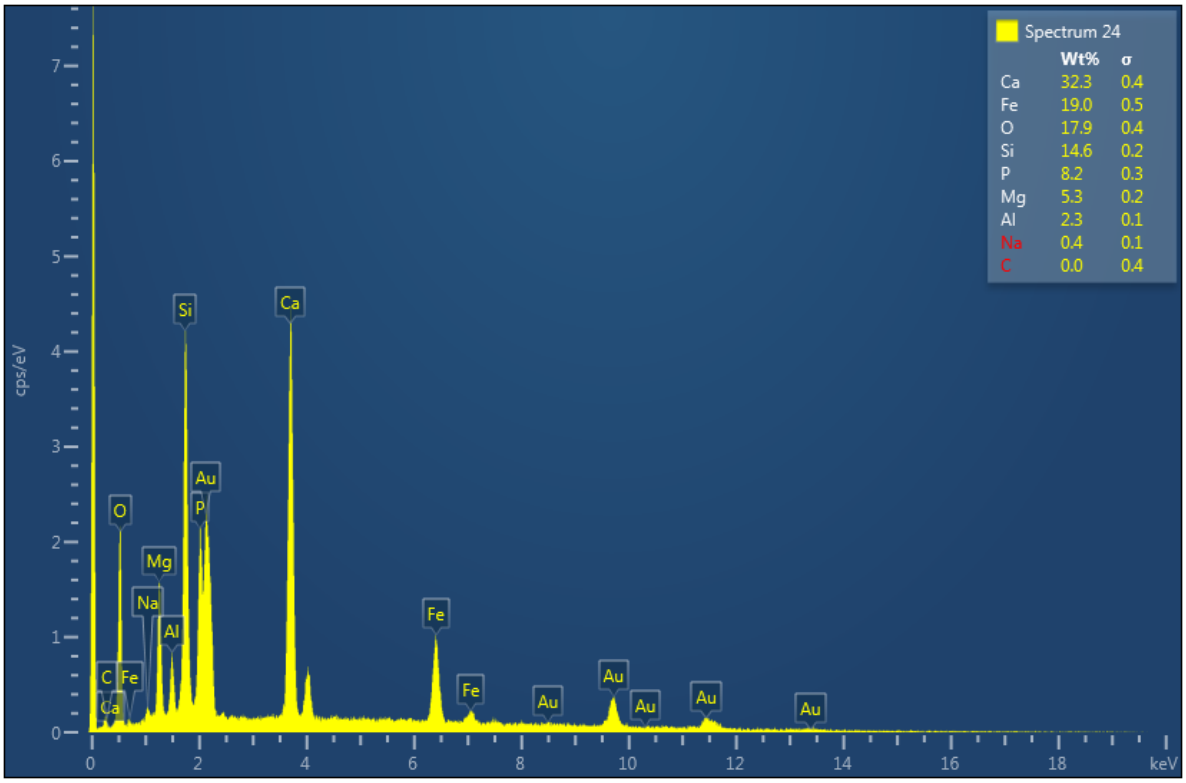

Figure 2.23. Energy dispersive X-ray spectroscopy (EDS) elemental composition output for target area "Spectrum 24" indicated in Figure 2.21.

For the cubes incubated with BoFeN1, the rounded features were mostly found in depressions on exposed flat surfaces (Figure 2.24) and in crevices (Figure 2.25). EDS analysis indicated that the rounded features in some depressions were co-located with slightly elevated Ca concentrations relative to the surface on which they sat. These Ca concentrations were similar to those found at a nearby ridge in the mineral surface (Figure A C.19-Figure A C.23). The grain associated with the rounded features in Figure 2.25 was also found to be enriched in Cr relative to the surface from which it protrudes (Figure 2.26-Figure 2.27 and Figure A C.24-Figure A C.25). The rounded features also appear slightly elevated in both Ca and P, relative to background of the Cr-rich feature.

The rounded features seen in one crevice in the control cube (Figure 2.28) were slightly elevated in Ca relative to the mineral background (Figure 2.29-Figure 2.30).

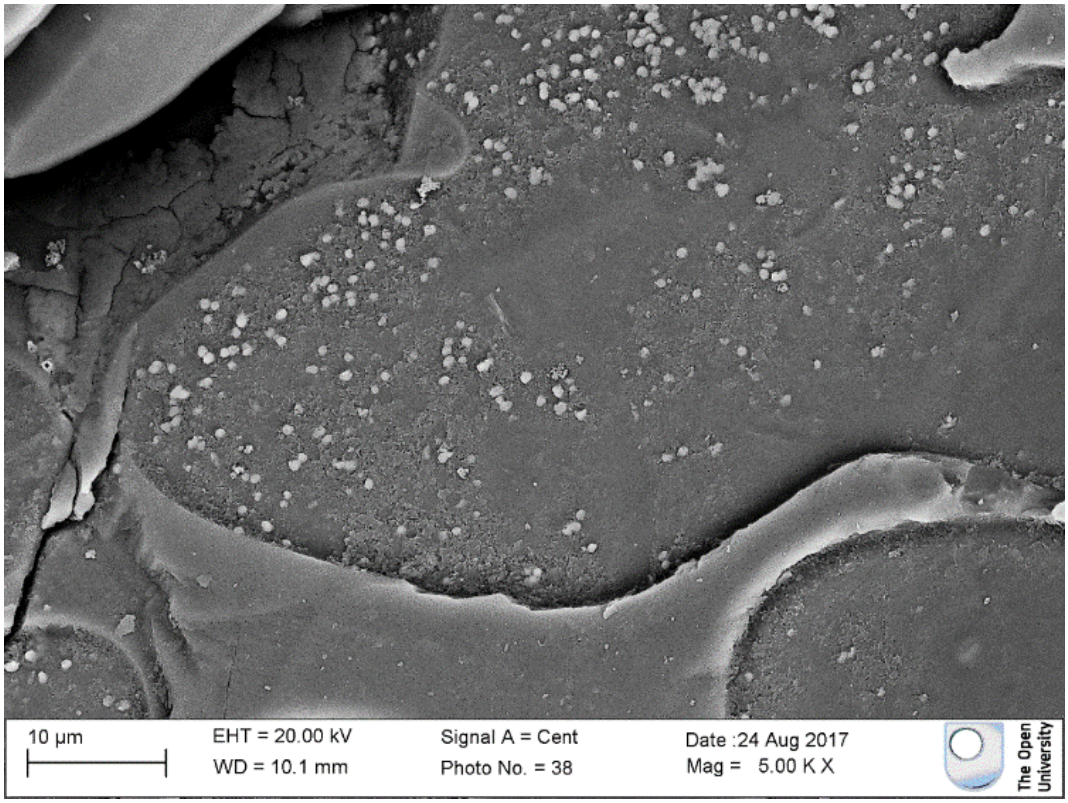

Figure 2.24. Electron micrograph of rounded structures embedded within a semi-porous matrix after culture with Acidovorax sp. strain BoFeN1.

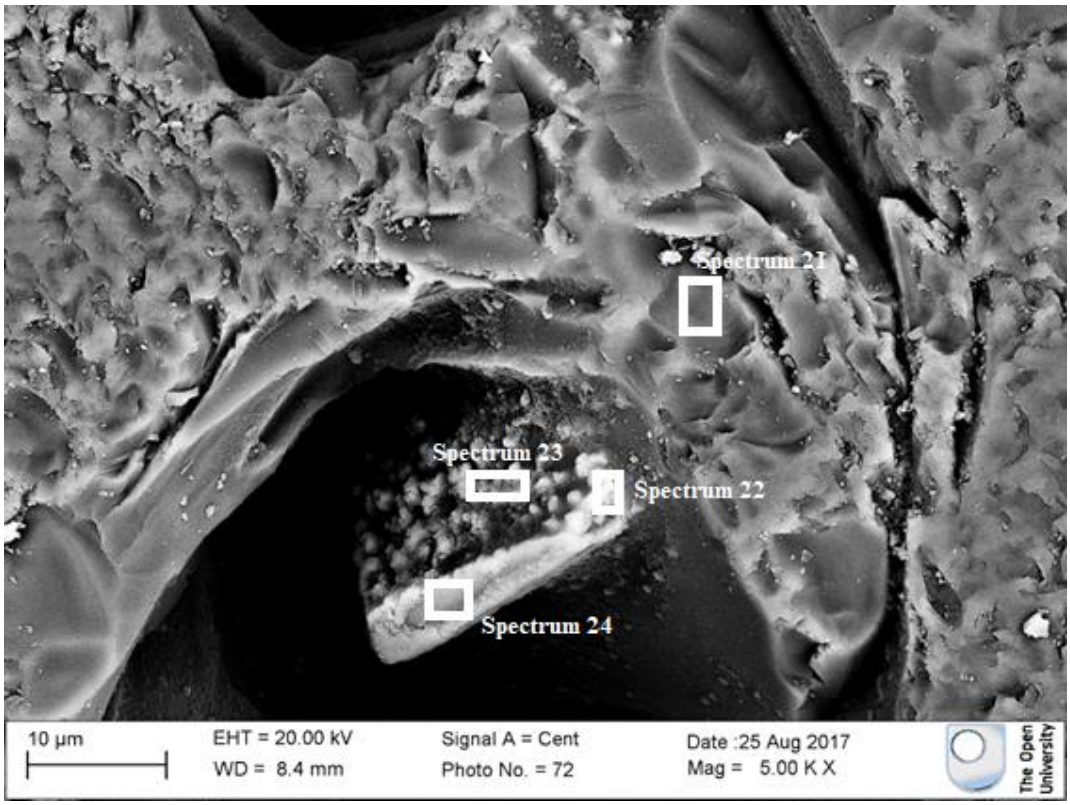

Figure 2.25. Electron micrograph of rounded structures (lower central area of image) associated with the olivine surface after culture with Acidovorax sp. strain BoFeN1. Target areas for electron dispersive X-ray spectroscopic (EDS) analysis are shown with white boxes.

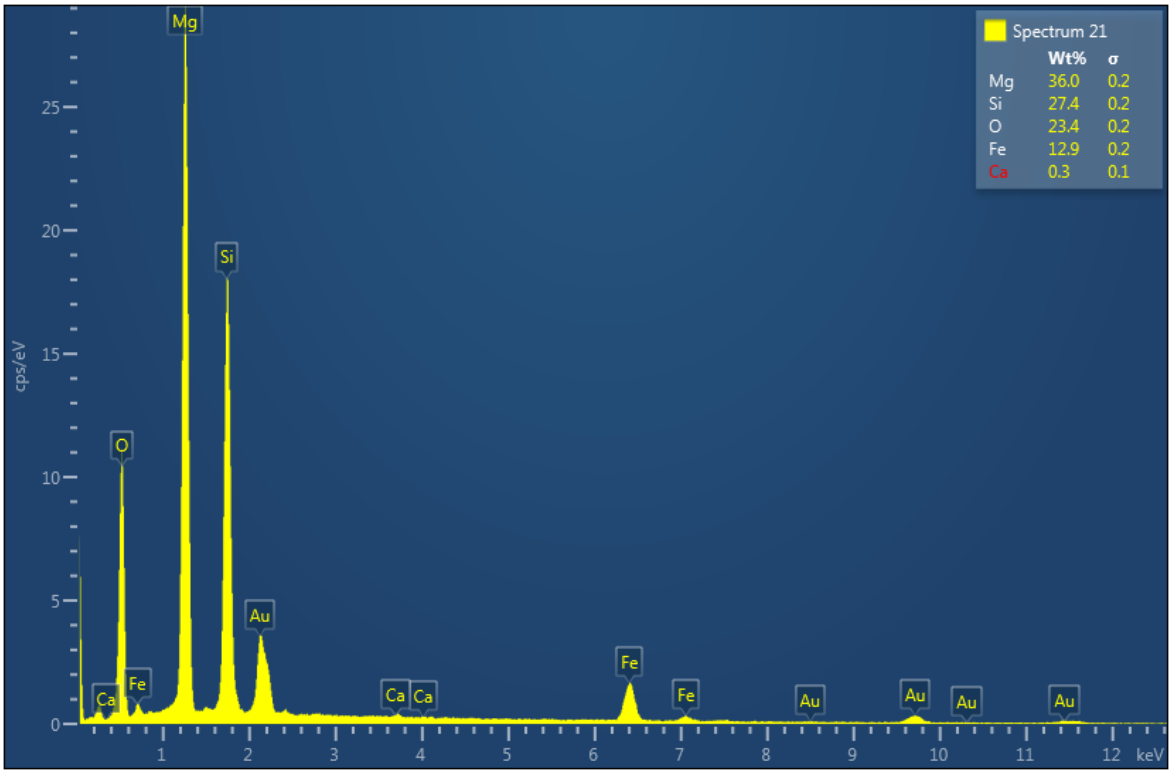

Figure 2.26. Energy dispersive X-ray spectroscopy (EDS) elemental composition output for target area "Spectrum 21" indicated in Figure 2.25.

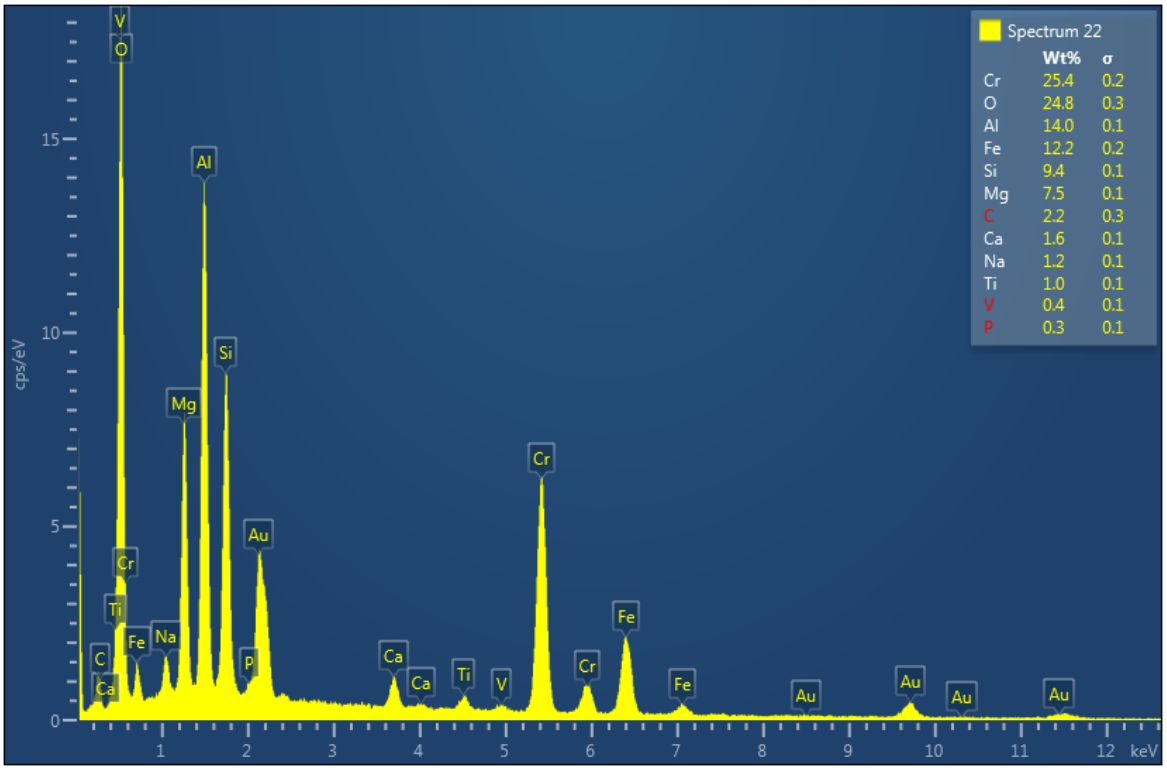

Figure 2.27. Energy dispersive X-ray spectroscopy (EDS) elemental composition output for target area "Spectrum 22" indicated in Figure 2.25.

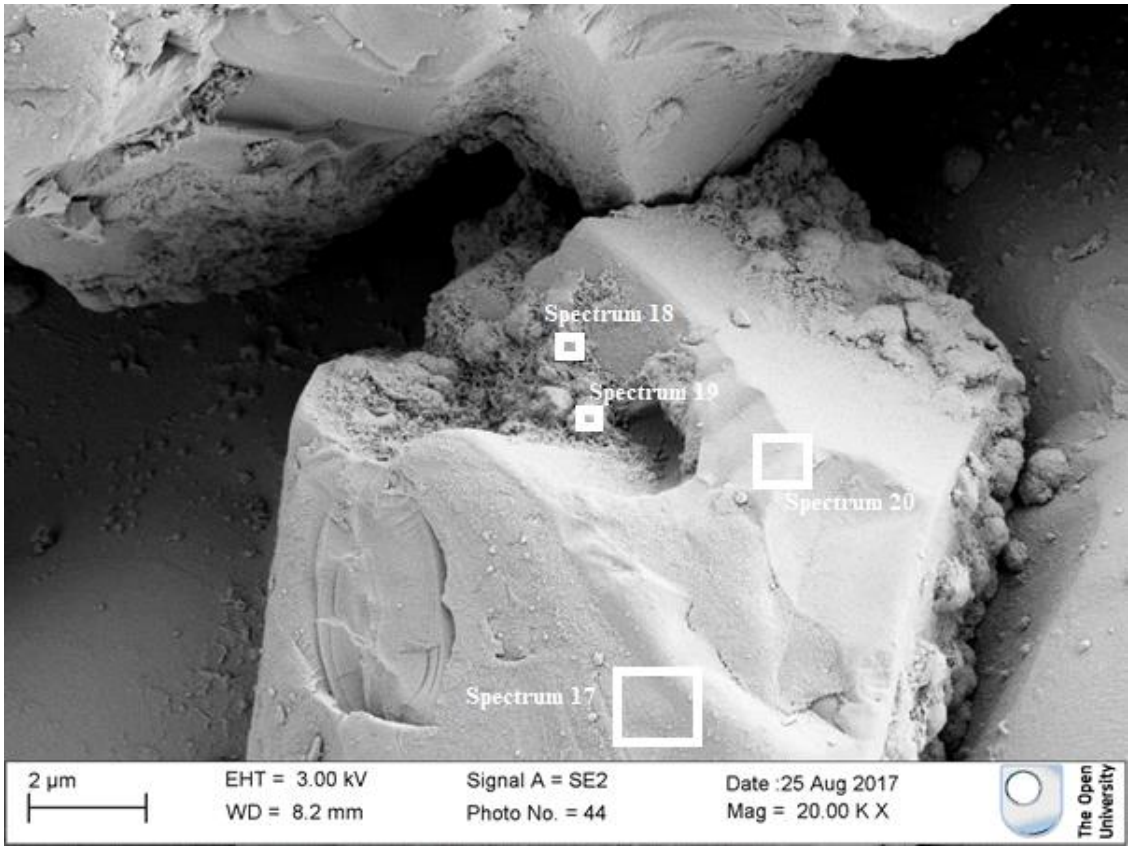

Figure 2.28. Electron micrograph of rounded structures in a porous matrix adhered to the olivine surface in the abiotic control. Target areas for electron dispersive X-ray spectroscopic (EDS) analysis are shown with white boxes.

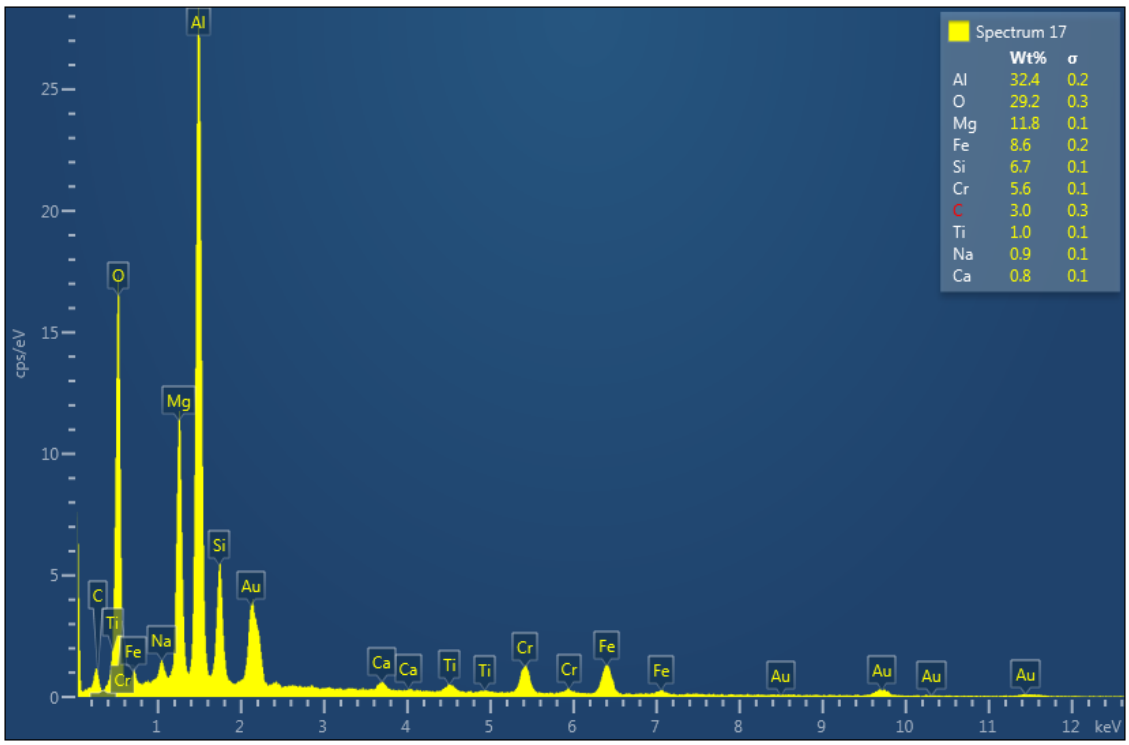

Figure 2.29. Energy dispersive X-ray spectroscopy (EDS) elemental composition output for target area "Spectrum 17" indicated in Figure 2.28.

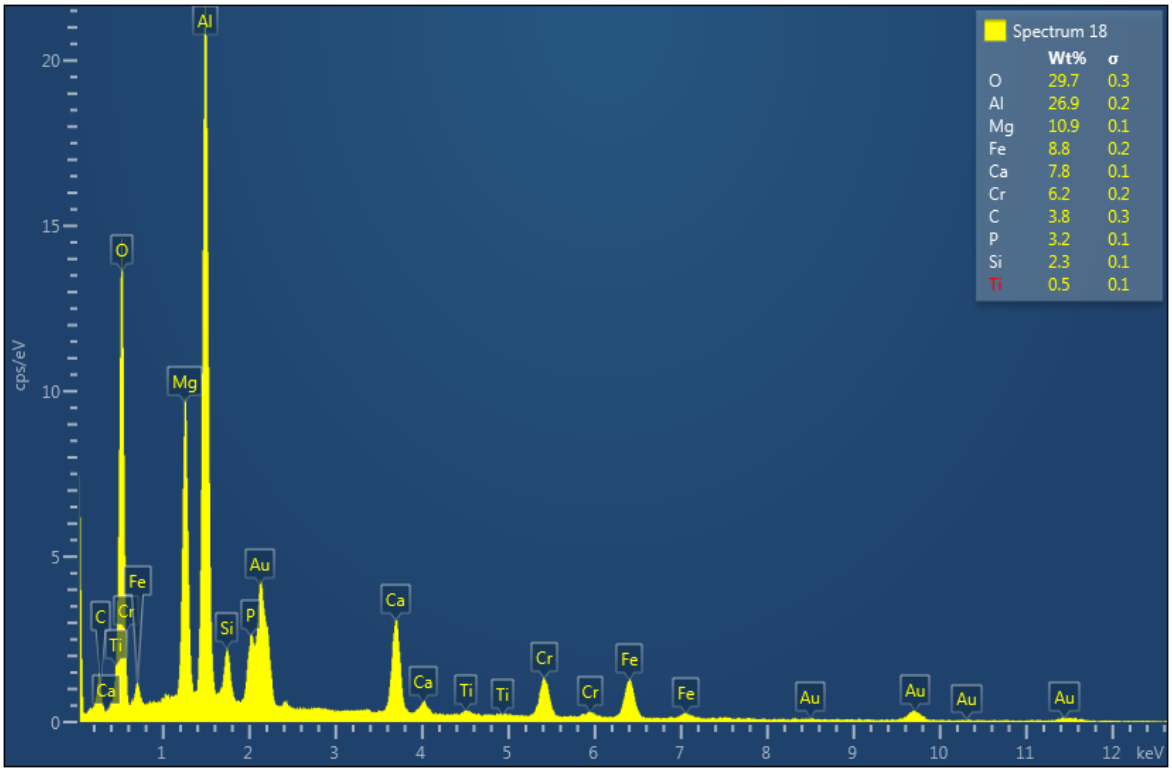

Figure 2.30. Energy dispersive X-ray spectroscopy (EDS) elemental composition output for target area "Spectrum 18" indicated in Figure 2.28.

2.4 Discussion

2.4.1 Growth associated with NDFO

The viable cell counts show clear growth of strains BoFeN1, 2002 and KS1 over the course of the experiment. Cell numbers of BoFeN1 and 2002 increased from time 0 to day 13, demonstrating near-immediate exponential growth phases with similar specific growth rates, before 2002 reached a stationary phase after day 13. Strain BoFeN1 appeared to then enter what could be termed as a death phase, experiencing a 45 % drop in viable cell density between day 13 and the end point. In contrast, the KS1 strain had a much longer lag phase (13 days) compared to BoFeN1 or 2002 and exponential growth was reached at day 13 but with a specific growth rate lower than in BoFeN1 or 2002 (0.19 compared to 4.32 and 4.08, respectively. No clear exponential phase was reached by the *T. denitrificans* cultures, which remained in stationary phase throughout the experiment.

The observations of growth over the first 8 days in strains BoFeN1 and 2002 made from the viable cell counts are supported by the Bradford protein assay results, which suggest biomass increased in both strains BoFeN1 and 2002 between day 1 and day 4. Biomass then stayed constant at day 8 in strain 2002 cultures while continuing to accumulate in strain BoFeN1 cultures. The lack of divergence from the control of protein concentration by strain KS1 and *T. denitrificans* over the first 8 days of culture supports the interpretation of stationary phases for these groups over this period, based on the cell counts. Unfortunately, Bradford assay samples after day 8 were compromised inadvertently by their extended removal from storage temperature (-20°C) prior to analysis, resulting in degradation of protein and unusable data.

The nitrate measurements taken at the end-point verify autotrophic nitrate reduction by the growing cultures of strains BoFeN1, 2002 and KS1; nitrate is depleted in the biotic

experiments relative to both the initial concentration and abiotic control at the end point, as expected for cultures growing by nitrate reduction (Benz et al., 1998). The small drop in end-point nitrate concentration in *T. denitrificans* cultures relative to the control group may indicate a low level of nitrate reduction associated with the maintenance of stationary phase non-growing cells, something which has been observed before in multiple strains (Straub et al., 1996; Chaudhuri et al., 2001; Shelobolina et al., 2003).

The end-point concentration of dissolved Fe was highest in the abiotic control, despite Fe being absent from the components in the preparation of the initial media. It can be assumed that this represents Fe (namely Fe^{2+}) leached abiotically from the olivine substrate over the period of observation, and is in line with olivine dissolution kinetics at circumneutral pH proposed by Wogelius and Walther (1991); circumneutral conditions appear to have been maintained throughout the experiment by the $NaHCO_3$ media component, which counteracted the acidifying effect of the 10 % CO_2 headspace.

If NDFO was taking place in the inoculated culture series, some oxidation of soluble Fe^{2+} to less soluble Fe^{3+} compounds and precipitation may be expected. Although precipitation was not observed, soluble Fe^{2+} concentrations were lower than the control in the actively growing test groups, strains BoFeN1, 2002 and KS1, and to a lesser extent in the *T. denitrificans* cultures. Hence, it could be suggested that growth by NDFO may have occurred; this has only been observed previously in strain 2002 of the microorganisms investigated here (Weber et al., 2006b).

By comparison to the results of this study, the autotrophic growth of strain 2002 by NDFO observed by Weber et al. (2006b) occurred over a shorter time period, with a higher specific growth rate and reached the end of the exponential phase after 2 days (28 days in this experiment). However, there was no limitation on Fe^{2+} in that case, with an initial

concentration of 10 mM. Under the Fe^{2+}-limited conditions of this experiment, it is unsurprising that we observe a longer lag phase. The growth of strain BoFeN1 (previously thought to require an organic co-substrate for NDFO-associated growth, (Kappler et al., 2005) and strain KS1 (previously described as heterotrophic,(Iordan et al., 1995) are more surprising. The non-growth of *T. denitrificans*, meanwhile, supports the suggestion made by Hedrich et al. (2011), that the growth of this species using pyrite (FeS_2) as an electron donor, coupled to nitrate reduction (observed by Juncher Jørgensen et al. (2009)) may have owed more to the oxidation of S^- ions than Fe^{2+} ions. Even so, the growth of strains as metabolically and phylogenetically diverse as strains BoFeN1, 2002 and KS1 under low Fe^{2+} availability and autotrophic, anoxic conditions provides support for the suitability of NDFO organisms to circumneutral early martian environments.

The Fe concentrations accumulated from olivine dissolution over the course of the experiment reached maximum concentrations of ~56 ppb (Figure 2.7), which corresponds to ~1 nM. A similar experiment demonstrated that neutrophilic growth by aerobic bacteria could occur under microoxic (1.6 % O_2), but Mars-relevant, conditions (Popa et al., 2012), using olivine sand as a sole Fe source (although Fo_{91} compared with Fo_{84}) (Popa et al., 2012). That isolate, *Pseudomonas sp*. strain HerB, was able to grow, with the same ratio of olivine mass to media volume, and the same temperature and pH range as in the experiments described in this Chapter. This adds credence to the conclusion that the rate of dissolution and concentration of Fe seen in the results presented here are indeed sufficient to drive microbial growth. Furthermore, the anaerobic conditions and use of nitrate as an electron acceptor in the experiments detailed here more closely match the conditions expected of early martian environments than in Popa et al. (2012).

Other experiments have used media designed to closely mimic fluids modelled for present and past Mars aqueous environments, with Fe concentrations ranging from micromolar to

molar in magnitude (Fox-Powell et al., 2016). These comparatively high-Fe conditions are likely to affect the growth and metabolic behaviour of the microorganisms investigated here and will be investigated in Chapter 3 using media derived from a Mars simulant developed by Nisha Ramkissoon at the Open University. However, it could be proposed that, on the basis of the results presented in this Chapter, NDFO is a possible energy metabolism on early Mars.

2.4.2 Fe isotope disparities

An unexpected result, drawn from the ICP-MS data, is the variation in relative concentrations of dissolved ^{56}Fe and ^{57}Fe. All three strains that showed microbial growth – BoFeN1, KS1 and 2002 – show differences in $^{57}Fe/^{56}Fe$ from that of the control (Table 2.4); this is not observed in the non-growing *T. denitrificans* cultures. That is, there were lower values for ^{56}Fe relative to ^{57}Fe in the medium when microbial growth occurred. Given that all cultures used a homogenised substrate from the same mineral sample, it is unlikely that this variation originates from the olivine itself. Instead, this implies that, there was either a difference in the liberation of ^{56}Fe and ^{57}Fe in cultures, perhaps resulting from chemical changes, or that a biologically-mediated process preferentially removed ^{56}Fe relative to ^{57}Fe.

Table 2.4. $^{57}Fe/^{56}Fe$ ratios for the $Fe_{(aq)}$ component of cultures and controls at the end point of the experiment.

Series	**$^{57}Fe/^{56}Fe$**	**Standard error**
Pseudogulbenkiania sp. strain 2002	1.258	±0.052
Thiobacillus denitrificans	1.039	±0.003
Paracoccus sp. strain KS1	1.180	±0.036
Acidovorax sp. strain BoFeN1	1.231	±0.053
Control	1.014	±0.001

Since there is no difference in either the pH values of the initial media between series and all cultures and controls were produced from the same media stock, it is difficult to imagine that the chemical conditions during dissolution were sufficiently different in these cultures to produce the effect observed.

In an analysis of strategies to gain reliable Fe isotope data from ICP-MS, Vanhaecke et al. (2002) reported that under standard conditions, as were used for this analysis, interference from Ar-based molecular ions could account for up to 17.96% of ^{56}Fe and 16.86% of the ^{57}Fe signals respectively. This finding would confound the results reported here if the objective was to gain accurate information as to $^{57}Fe/^{56}Fe$ in each culture. However, the proposed effect is relative between growing biotic cultures and controls. All ICP-MS samples were run in a single batch under identical conditions, and so any interference effect from the instrument should be mitigated.

In the absence of plausible abiotic explanations for the differences in $^{57}Fe/^{56}Fe$, it must be considered that this may be the result of a biological mechanism. In the context of this experiment, microbial Fe^{2+} oxidation during NDFO.

Fe isotope fractionation associated with different microbial Fe oxidising and reducing metabolisms has been widely reported (Croal et al., 2004; Balci et al., 2006; Crosby et al., 2007), although these studies utilised different isotope systems. In fact, Kappler et al. (2010) have already demonstrated a measurable isotopic shift by strain BoFeN1 during NDFO, using a $^{56}Fe/^{54}Fe$ system.

The effect found here supports the existence of Fe isotope fractionation associated with active NDFO cultures. In the context of astrobiological investigations on Mars, the usefulness of isotopic data as a specific biosignature is limited by our knowledge of

martian abiotic fractionation processes, but may be useful as supporting evidence in concert with other biosignatures (Vago et al., 2017).

2.4.3 Biogenicity of morphological features

If life were to have developed NDFO metabolism on early Mars, the search for evidence may be aided by the phenomenon of biomineralisation. That is, the preservation of microbial morphologies and other characteristics by encrustation and replacement of biological structures with mineral assemblages.

SEM revealed features with aspects suggesting biogenic origin, some of which were supported by results from EDS analyses. The globular aggregations observed on the strain 2002 olivine cube (Figure 2.9) were morphologically similar to that strain (Figure 2.31) (Zhao et al., 2013), with short chains and small clusters of coccobacillal (ovoid) cells. The co-located carbon signature detected by EDS (Figure 2.10-Figure 2.12 and Figure A C.1-Figure A C.3) further supports the biogenicity of these features. EDS was unable to identify the composition of the dendritic features coating the globular aggregations shown in Figure 2.9 however; the small size and thin layering of the dendritic coating may have allowed much of the X-ray beam to penetrate without much stimulation of the features themselves. However, the straight-edged and needle-like appearance of these features (Figure 2.9), suggests they were non-biological and inorganic.

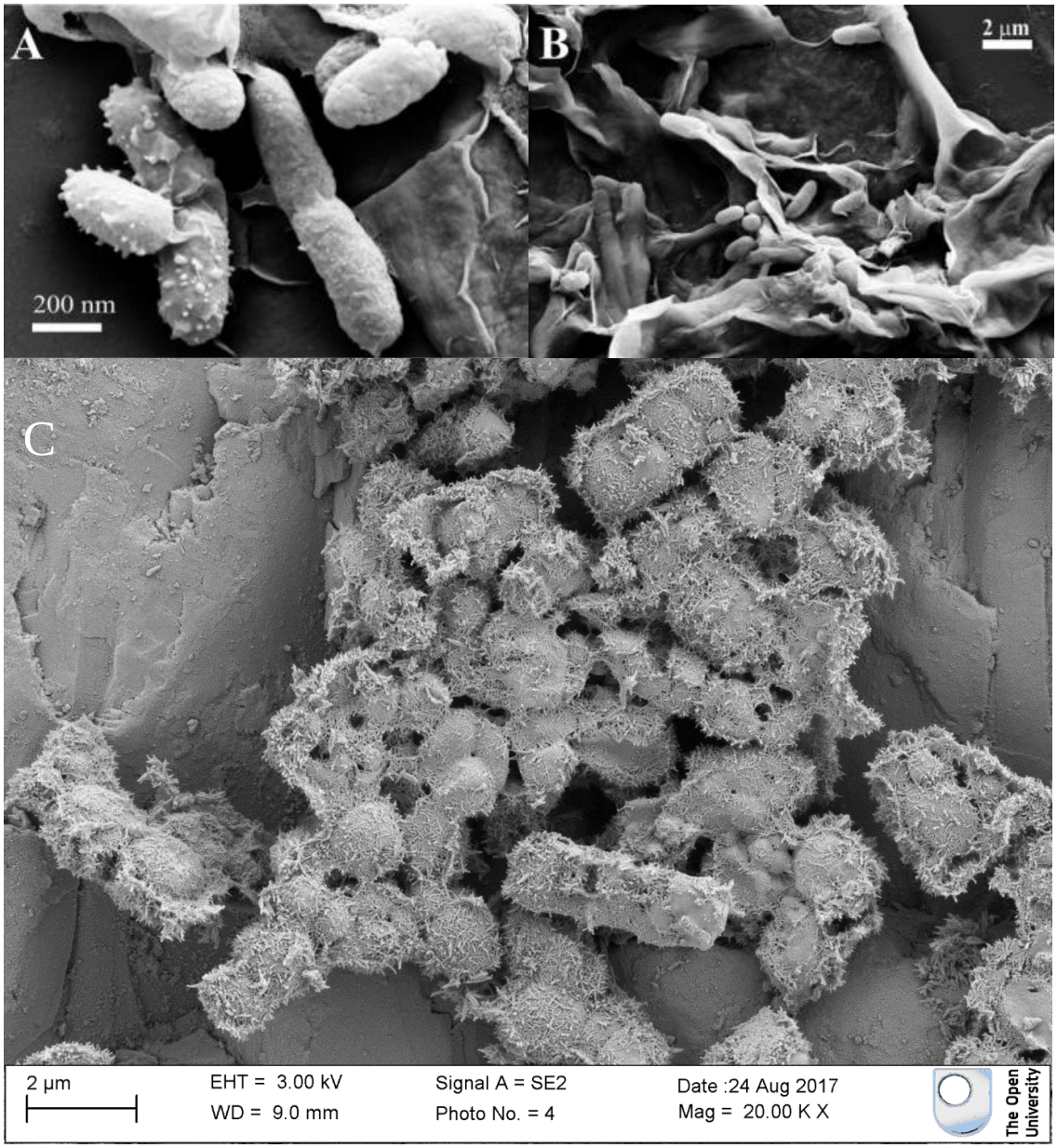

Figure 2.31.(A) SEM image of Pseudogulbenkiania sp., (B) SEM image of strain 2002 cells in association with Fe-rich nontronite clay particles (Zhao et al., 2013) and (C) aggregations of coccobacillal features observed in the Pseudogulbenkiania sp. strain 2002 culture (from Figure 2.9).

The "ravioli" features found after culture with *Paracoccus sp.* strain KS1 (Figure 2.13) were similar in diameter and 2-dimensional shape to the coccoid cells of that strain. The flattened appearance could potentially be a result of cell dehydration during the sample desiccation process, exacerbated by the absence of mineral encrustation. As in the strain 2002 culture, the carbon signature detected in the KS1 culture (Figure 2.14-Figure 2.15 and

Figure A C.4-Figure A C.7) provides supporting evidence for the biogenicity of these features.

The identities of other structures observed are somewhat less certain. The rounded structures, apparently embedded within a porous matrix material in the strain BoFeN1, strain KS1, strain 2002 and control series (Figure 2.16-Figure 2.30), have the superficial appearance of coccoid cells within a biofilm, but were also found in the abiotic control. This suggests that these features may have been present within the parent sample from which the cubes were cut. Adding credence to this, some of the sites where these features are found appear to have been exposed during culture by the removal of a mineral grain from the outer surface of the cube (Figure 2.17 and Figure 2.24). The lack of carbon, and consistent detection of Ca co-located with the rounded features, suggests that the features are either abiotic or are mineralised biofilm structures of previous microbial inhabitants of the olivine substrate (Figure 2.32) that are similar in appearance to what is observed here. The repeated sonification of the olivine cubes in acetone was intended to remove any organic carbon from the substrate before culture to ensure autotrophic conditions, so it is unsurprising that there was an absence of associated carbon.

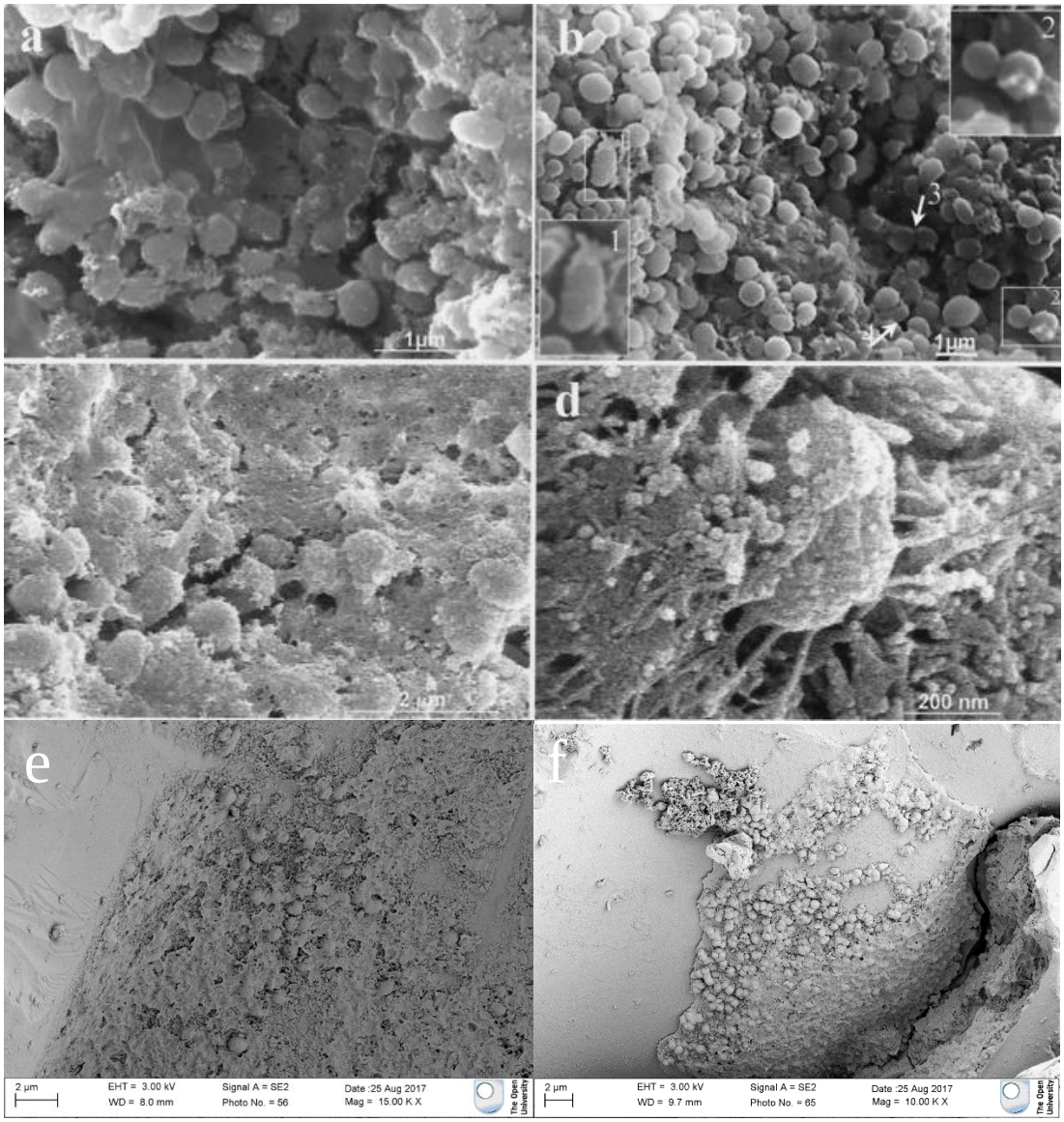

Figure 2.32. Examples of fossil bacterial biofilms. Images A & B show examples of spheres with medial partitioning (inset 1 and arrow 4). Inset 2 and arrow 3 point at two individual cells, which seem to be connected by an thin film. Images C and D depict spheres interpreted as fossil bacterial biofilm (Toporski et al., 2002b). Images E and F are the rounded features embedded in a matrix observed on the olivine substrate surface following the culture experiment (Figure 2.16 and Figure 2.20).

The evident difficulty in determining biogenicity based on morphology, even in batch cultures where the original morphology of the cells is known, serves to highlight the necessity for multiple lines of evidence when investigating potential biosignatures on Earth and Mars. The verification of biogenicity based solely on morphology has led to many contentious claims in both ancient terrestrial rocks and martian meteorites (McKay et al., 1996; Mojzsis et al., 1996). The results of this experiment suggest that pairing with

alternative methods for determining the past presence of biological Fe metabolism, such as isotope fractionation patterns (Anand et al., 2006), should be investigated in order to complement morphological and elemental observations and provide additional tests by which to judge any putative biosignatures.

2.4.4 Future Work

The necessity for a combination approach to biosignature detection is borne out by the results of this Chapter, which demonstrate that individual morphological, elemental and isotopic analyses would not be enough to confirm the biogenicity of preserved biosignatures.

In order to further investigate the findings of this Chapter, it would be necessary to tailor the analytical setup of future experiments using the knowledge gained here. ICP-MS should be used as the primary method for monitoring dissolved Fe throughout culture under oligotrophic conditions, as the micromolar range of concentrations will present challenges to redox sensitive chemical techniques such as the ferrozine assay.

Gas headspaces could also be monitored for consumption of CO_2 during autotrophic growth, as well as the generation of H_2 -an alternative electron donor for microbes – by the abiotic serpentinisation reactions of water and olivine. Serpentinisation has been proposed as an abiotic formation mechanism for methane (CH_4) observed in the martian atmosphere, which is a downstream product of subsequent abiotic reactions between H_2 and CO_2 (Holm et al., 2015).

Lastly, spectroscopic and mineralogical analyses such as could be employed to determine the composition of biomineralised structures observed here. Techniques such as Raman spectroscopy – included in the ExoMars rover design (Beegle et al., 2015; Rull et al., 2017) – and X-ray diffraction crystallography could be employed order to further our

understanding of how traces of NDFO microbes may be preserved or degraded over billions of years in the martian geological record.

2.4.5 Conclusions

Three strains of NDFO microbes - *Pseudogulbenkiania sp.* strain 2002, *Acidovorax sp.* strain BoFeN1 and *Paracoccus sp.* strain KS1- were able to grow under anoxic, autotrophic conditions by respiring nitrate and utilising Fe^{2+} released by dissolution from an olivine substrate. This capability holds implications for the habitability of early Mars, where comparable conditions are likely to have existed.

Aggregations on the olivine surface in the *Pseudogulbenkiania sp.* strain 2002 culture series, inferred to be cells, show signs of biomineralisation. This process could be key to preservation of morphological biosignatures of microbes from the early martian environment for detection in the present day. Non-mineralised, flattened cells were observed after culture with *Paracoccus sp.* strain KS1. However, obvious biogenic features associated with the substrate were not found after culture with the actively-growing *Acidovorax sp.* strain BoFeN1 or non-growing *T. denitrificans*. This demonstrates variability in preservation behaviours between the tested strains under these Fe^{2+}-limited conditions, and so biomineralisation-related features may not be a reliable expectation on Mars if NDFO microbes existed under similar autotrophic conditions.

3. Growth of NDFO microorganisms in Mars simulant-derived media

3.1 Introduction

Evidence for ancient fluvial systems and standing bodies of liquid water exists at various locations across the martian surface (Carr and Head, 2010; Davis et al., 2016; Davis et al., 2019), and have been found by the Opportunity mission at Endeavour and Victoria Crater (Arvidson et al., 2011; Jolliff et al., 2019), and by Curiosity at Gale Crater (Grotzinger et al., 2014a). Additionally, evaporite deposits and mineral veins identified *in situ* on Mars provide evidence of ancient fluid movement at the surface and near-subsurface (Squyres et al., 2004a; Squyres and Knoll, 2005; Ming et al., 2006). In order to determine whether these fluids would have been habitable to life as we understand it, these environments can be simulated in the laboratory to test the growth and response of suitable model martian microorganisms, such as nitrate-dependent Fe^{2+}-oxidising (NDFO) species (Price et al., 2018). As well as testing microbial growth, the identification of distinguishable biosignatures resulting from such biological activity can inform the ongoing search for traces of life on Mars. For example, the biogenic Fe^{3+} minerals, which have been reported in some NDFO cultures, provide one route by which a record of microbial metabolism could be preserved (Miot et al., 2009; Larese-Casanova et al., 2010; Li et al., 2014; Miot et al., 2014a; Miot et al., 2015).

Chapter 2 demonstrated that NDFO microorganisms can utilise a Mars-relevant Fe^{2+} substrate for growth in standard minimal media and that desiccation resulted in possible mineralisation of cells in one tested bacterial strain. To further our understanding of NDFO metabolism plausibility on Mars, more realistic chemical conditions must be imposed to better quantify the ability of this metabolism to support a microbial biosphere as a primary producer.

Previous work to assess the growth of microorganisms and the potential for biosignature generation on Mars have invoked a wide range of chemical, pH, redox and physical conditions. As well as solid simulants (Allen et al., 1997; Peters et al., 2008; Böttger et al., 2012; Stevens et al., 2018), this has featured the development of brines aimed at recreating the aqueous chemistry of martian environments. Tosca et al. (2011) used thermodynamic models to investigate the physicochemical properties, such as water activity and ionic strength, of hypothetical martian brines. Fox-Powell et al. (2016) furthered this work by synthesising the modelled brines as media for use in microbiological studies, identifying ionic strength as a new consideration for the habitability of martian fluids. Despite the contribution made to our understanding of martian fluid chemistry and habitability, these brines were not suitable for the investigation of NDFO for two reasons. Firstly, the concentrated nature of the brines does not broadly apply to the hydrologically-active Noachian period which carries the most interest in terms of NDFO metabolisms and Mars. Secondly, these modelled brines all assume that Fe is present entirely in ferrous form (Fe^{2+}) throughout the evolution of the fluids, which may not be unrealistic when considering the influence that Fe^{2+}-oxidising metabolism could have on the system. To counter this, an alternative set of simulated martian brines with mixed Fe^{2+}/Fe^{3+} balances was required.

A new suite of Mars simulants have been developed by Nisha Ramkissoon at the Open University based on the geochemical composition of three sites on the martian surface and one martian meteorite (Ramkissoon et al., 2019). Data from the NASA Curiosity rover were used from Rocknest at Gale crater (Blake et al., 2013), the same site as the MGS-1 simulant (Cannon et al., 2019), to create a contemporary Mars (CM) simulant. Two further simulants were developed based on the sulfur-rich (SR) Paso Robles site in Columbia Hills, Gusev crater and a haematite-rich (HR) deposit at Meridiani Planum (Rieder et al.,

2004; Lane et al., 2008), respectively investigated by the NASA Mars Exploration Rovers, Spirit and Opportunity. The final simulant was based on geochemical data from a Shergottite (SG) meteorite (Bridges and Warren, 2006), representing basaltic terrain.

This Chapter explores the habitability of martian fluid systems for NDFO microorganisms, by monitoring growth in liquid media derived from the modelled dissolution of these new simulants into solution. Previous studies have used brines that represent ionically concentrated solutions, for example those resulting from evaporitic conditions in Hesperian and Amazonian periods on Mars (e.g. Tosca et al., 2011; Fox-Powell et al., 2016). Though important in understanding the evolution of the martian geological environment and habitability across post-Noachian history, the previously tested brines are not as representative of the expected conditions in the hydrologically-active earlier period as those employed in this study (Grotzinger et al., 2014a; Wordsworth, 2016).

The experiments detailed in this Chapter test the hypothesis that ancient groundwaters on Mars were habitable for NDFO microorganisms to grow and produce detectable shifts in oxidation state from Fe^{2+} to Fe^{3+}, by working through the following objectives:

1) To determine whether selected NDFO-capable microorganisms can grow in liquid media based on brines derived from the geochemistry of four martian environments.
2) To quantify the extent of NDFO by monitoring the relative concentrations of Fe^{2+}/Fe^{3+} and NO_2/NO_3 throughout.
3) To investigate the impact of organic co-substrates and additional Fe^{2+} on growth of NDFO microbes in such a Mars-derived liquid medium.

3.2 Materials and Methods

3.2.1 Mars simulant-based media

Fluid chemistries that would result from dissolution of the simulants at a water/rock ratio (W/R) of 1000 were calculated by Nisha Ramkissoon. This value was chosen as it represents the fluids present within fractures in bedrock during hydrological activity within a near-surface environment. Predicted ion concentrations (shown in Table 3.1) for the fluids were reproduced using media components, which are listed in Table 3.2. A table of the media components in mg L^{-1} is included in Appendix A.

Table 3.1. Predicted ionic concentrations for fluids based on Contemporary Mars (CM), Sulfur-rich (SR), Haematite-rich (HR) and Shergottite (SG) simulants at W/R of 1000. Ions listed in descending order of predicted concentration for CM.

		Simulant			
		CM	SR	HR	SG
Ion		Concentration (mM)			
Si	+	7.351	3.602	6.828	8.585
Fe^{2+}	+	2.618	2.880	1.963	2.254
Mg	+	1.520	1.323	1.724	2.556
Ca	+	1.382	1.511	1.020	1.692
NO_3	-	1.000	1.000	1.000	1.000
Al_2	+	0.989	0.495	0.700	0.635
Na_2	+	0.542	0.309	0.373	0.264
S	-	0.466	3.649	0.534	0.050
K_2	+	0.253	0.164	0.171	0.079
$Fe^{3+}{}_2$	+	0.110	0.105	0.961	0.076
Ti	+	0.092	0.058	0.062	0.032
P_2	-	0.040	0.210	0.036	0.040
Mn	+	0.034	0.016	0.023	0.028
Cl	-	0.029	0.021	0.023	0.020

Table 3.2. Chemical composition of each media based on Contemporary Mars (CM), Sulfur-rich (SR), Haematite-rich (HR) and Shergottite (SG) ion concentrations as listed in Table 3.1.

	Simulant			
	CM	SR	HR	SG
Component	Concentration (µM)			
$NaNO_3$	1000	618.28	746.05	-
$Mg(NO_3)_2$	-	190.86	126.98	500
Na_2S	-	-	11.56	31.59
$MnCl_2$	14.71	10.42	11.56	9.87
K_2HPO_4	19.83	-	72.04	78.70
NaOH	42.45	-	-	461.10
KOH	233.55	-	98.95	-
$Ca(OH)_2$	1381.81	1510.99	1020.33	1692.42
$FeSO_4$	226.29	2300.89	533.84	-
FeO	2392.10	578.66	1429.27	2253.63
Fe_2O_3	-	-	961.19	75.66
$3AL_2O_3.2SiO_2$	329.69	164.92	233.26	211.81
$3MgO.4SiO_2.H_2O$	506.55	-	1597.01	685.33
SiO_2	4665.92	3271.76	-	5420.55
TiOH	92.27	58.41	61.95	31.64
$MnSO_4$	19.04	5.65	746.05	18.59
Na_2HPO_4	-	-	126.98	1.63
$Fe_2(SO_4)_3$	220.41	210.15	11.564	-
KH_2PO_4	-	420.45	11.56	-
$MgSO_4$	-	1131.97	72.04	-

3.2.1.1 Media preparation

Contemporary Mars (CM), Sulfur-rich (SR), Haematite-rich (HR) and Shergottite (SG) media were prepared using the components listed in Table 3.2. Soluble media components were prepared as anoxic stock solutions by dissolving the chemical in deoxygenated distilled water under N_2 gas flushing, as described in Section 2.2.2. The stock solutions were sealed with sterile butyl rubber stoppers, using the Hungate technique (Hungate, 1950), and crimped with aluminium caps.

Table 3.3. Concentrations and volumes of deoxygenated stock solutions used in the preparation of the Contemporary Mars (CM), Sulfur-rich (SR), Haematite-rich (HR) and Shergottite (SG) media.

		Volume to add (mL)			
Compound	Stock concentration (mM)	CM	SR	HR	SG
$NaNO_3$	100	10.000	6.183	7.460	
$Mg(NO_3)_2$	100		1.909	1.270	5.000
Na_2S	100			0.116	0.316
$MnCl_2$	10	1.471	1.042	1.156	0.987
K_2HPO_4	10	1.983		7.204	7.870
NaOH	100	0.424			4.611
KOH	100	2.336		0.989	
$FeSO_4$	1000	0.226	2.301	0.534	
$MnSO_4$	10	1.904	0.565		1.859
Na_2HPO_4	10				0.163
$Fe_2(SO4)_3$	100	2.204	2.101		
KH_2PO_4	100		4.204		
$MgSO_4$	1000		1.132		

Components with low solubility (FeO, Fe_2O_3, $3Al_2O_3{\cdot}2SiO_2$, $3MgO{\cdot}4SiO_2{\cdot}H_2O$, SiO_2, TiOH, $Ca(OH)_2$) were added in powdered form to a sterile 1 L Schott bottle. The chemicals were suspended in deoxygenated water containing resazurin (1 mg L^{-1}) (Chapter 2), under N_2 gas flushing. The bottle was then sealed using the Hungate technique (Hungate, 1950) with a rubber septum and screw-cap, and autoclaved at 121 °C for 15 minutes.

Sterile stock solutions (concentrations listed in Table 3.3) of the soluble components were prepared (Appendix A) and added to the media, *via* sterile 0.2 µm filters, in a COY anaerobic chamber under an 85:10:5 N_2:CO_2:H_2 atmosphere. The volumes used to achieve the final concentrations listed in Table 3.2 are given in Table 3.3.

30 mL aliquots were dispensed into 12 × 50 mL Wheaton bottles for each of the four media (triplicates for each of the three microorganisms and the abiotic control). These were sealed with sterile butyl stoppers and crimped closed with aluminium caps. The headspace

of each was replaced with a 90:10 N_2:CO_2 mixture by inserting a gas line *via* a sterile needle through the rubber septum and an unconnected needle to allow pressure to escape.

3.2.2 Microorganisms

Three microorganisms, *Acidovorax sp*. strain BoFeN1, *Pseudogulbenkiania sp*. strain 2002 (DSM-18807) and *Paracoccus pantotrophus* strain KS1 (DSM-11072) were selected for this experiment as these strains demonstrated autotrophic growth on the olivine substrate in Chapter 2. These strains were maintained in LB media (L^{-1}: 10 g tryptone, 5 g yeast extract, 10 g NaCl) at 30 °C under aerobic conditions prior to the experiment.

3.2.3 Chemolithotrophic growth experiment

3.2.3.1 Inoculation and incubation

Cells (1 mL LB growth culture) were harvested during the exponential phase by centrifugation at 3000 × *g* for 10 minutes, the supernatant was removed and the pellet was resuspended in 1 mL anoxic simulant media. This was repeated twice to wash the cells and prevent carry-over of extracellular nutrients from the LB media into the experiment. Following the wash step, cell suspensions were enumerated using a Baclight Live/Dead stain (Invitrogen) (Section 2.2.4) and optical microscope under UV light.

The medium was inoculated using a sterile syringe and needle to achieve a starting concentration of ~10^7 cells mL^{-1} in cultures and with sterile medium in the controls. Cultures and controls were incubated stationarily at 25 °C in the dark. Samples of 2 mL volume for cell enumerations and chemical analyses were anaerobically collected pre- and post-inoculation, as well as at days 1, 2, 3, 4, 7 and 10.

3.2.3.2 Microbial growth monitoring

In the chemolithotrophic growth experiment, protein concentrations were monitored as a proxy for microbial growth due to the total number of cultures and controls. Samples were reliably stored at -20 °C for later protein analysis, whereas cell counts were performed soon after collection to mitigate the effects of oxygen intrusion to anaerobic redox-sensitive medium.

3.2.3.2.1 Bradford protein assay

The Bradford assay was used as a measure of protein production over the course of the chemolithotrophic experiment, following a protocol developed for Fe-oxidising cultures (Miot et al., 2009).

Aliquots of culture (500 µl) were mixed with 420 µl of Tamm reagent (Appendix A). This reagent served to dissolve amorphous Fe-bearing phases and to lyse cells (Vodyanitskii, 2001). Following this, 80 µl of 6.1 N trichloroacetic acid was added in order to precipitate the proteins from the mixture. The precipitates were pelleted by centrifugation at 15,500 × *g* for 30 minutes, before the supernatant was removed and the pellet was resuspended in 500 µl 0.1 M NaOH. These samples were then heated to 60 °C in a dry bath for 6 minutes.. A 400 µl subsample from each was then mixed with 400 µl of Bradford reagent, and the absorbance at 595 nm measured after 5 minutes in a Camspec M107 visible spectrophotometer. γ-globulin was used as the protein standard, with 0 to 25 µg mL^{-1} prepared in 0.1 M NaOH solution. A standard curve was calculated as shown in Appendix B and sample concentrations calculated using the line equation.

Protein-to-cell density conversion factors for the organisms used in this experiment were created by correlating cell counts and protein concentrations for the three microorganisms during exponential growth phase from Chapter 2. Specific growth rates were then

estimated by applying equation (2) to cell density values converted from the protein concentrations.

3.2.3.3 Chemical analyses

3.2.3.3.1 Ferrozine assay

The ferrozine colourimetric assay was used to determine the reduced and total Fe concentrations in the medium. Ferrozine reagent (3-(2-Pyridyl)-5,6-diphenyl-1,2,4-triazine-p,p′-disulfonic acid monosodium salt) reacts with Fe^{2+} to form a soluble, stable magenta complex species with a peak of maximum absorbance at 562 nm, which may be used for determination of iron in solution (Stookey, 1970).

For this, two 20 µl aliquots of culture were transferred by sterile pipette into two 1.5 mL microcentrifuge tubes, one containing 980 µl of 0.5 M HCl and into another containing 980 µl 0.5 M HCl and 0.3 M hydroxylamine hydrochloride (Appendix A). These mixtures were allowed to digest for a minimum of one hour and refrigerated at 4 °C thereafter for later analysis. The HCl lyse the cells and prevents abiotic oxidation of the Fe in the sample, allowing the Fe^{2+} concentration to be preserved for analysis. The hydroxylamine hydrochloride acts as a reducing agent, converting Fe^{3+} to Fe^{2+} and giving a value for total Fe concentration in the cultures. By comparing the Fe^{2+} and total Fe concentrations, the Fe^{2+}/Fe^{3+} ratio can therefore be determined at regular time points and thus the rate of Fe oxidation calculated. For this, 20 µl of the HCl and hydroxylamine hydrochloride digests were transferred into seperate 1 mL cuvettes containing 980 µl of ferrozine solution (Appendix A), and were mixed using a pipette. The absorbance was measured using a Camspec M107 visible spectrophotometer at a wavelength of 592 nm.

Standards were prepared by mixing 20 µl of 10 mM, 5 mM, 1 mM and 500 µM $FeSO_4$ solutions with 980 µl of 0.5 M HCl in 1.5 mL microcentrifuge tubes. Ferrozine solution

was then added to these mixtures in the same manner as the samples and read at 592 nm. The standard curve was produced as a calibration graph. Fe^{2+} and Fe_{total} concentrations were calculated from the line equation and Fe^{2+}/Fe_{total} ratios determined subsequently (Appendix B).

3.2.3.3.2 Nitrate measurement

The concentration of nitrate ions in each of the cultures was measured post-inoculation and at the endpoint of the experiment using an ELIT 0821 ion selective NO_3^- electrode and ELIT 003 lithium acetate reference electrode (Nico2000) connected to a conductivity meter (HANNA instruments). A calibration curve was prepared with 10 µM, 100 µM and 1 mM of $NaNO_3$ dissolved in milliQ water, with the concentration plotted against conductivity (mV). The nitrate concentrations were determined using the equation from the standard curve of the calibration graph (Appendix B) and the end point presented relative to the initial concentration.

3.2.3.3.3 Griess reagent assay for nitrite

The Griess reagent assay is a colourimetric method, which is used to determine nitrite ion concentration in a solution, whereby the reaction of sulfanilic acid with 1-naphthylamine to produce red-pink azo compounds in the presence of nitrite ions is used as a proxy for nitrite concentration (Griess, 1879; Ivanov, 2004).

For monitoring nitrite concetrations, a 100 µl aliquot of culture was transferred into sterile 1.5 mL microcentrifuge tubes and centrifuged at 15,500 × *g* for 10 minutes. In parallel, nitrite standards were prepared by diluting 100 mM $NaNO_2$ with 0.1 M NaOH solution, to give 100 µM, 50 µM, 25 µM, 10 µM, 5 µM, 2.5 µM and 1 µM $NaNO_2$ concentrations.

Standards (in triplicate) and the supernatants from the culture samples (50 µL) were transferred to individual wells of a 96-well flat-bottomed, optically clear ELISA microplate. 100 µL of 1 × Griess reagent solution (Sigma-Aldrich) was added to each well, giving a total reaction volume of 150 µ. After 15 minutes, the plate was read using a Bio-tek ELx808 microplate reader with a 540 nm filter and using KC4 software for data output. Nitrite concentrations were calculated using the line equation from the calibration curve of standards (Appendix B).

3.2.3.3.4 Inductively coupled plasma optical emission spectrometry

Inductively coupled plasma optical emission spectrometry (ICP-OES) was used to measure the chemical composition of the media immediately after inoculation and at the conclusion of the experiment (day 10). Aliquots (9 mL) of cultures and controls were extracted under anaerobic conditions using a N_2-flushed sterile syringe at day 10. The samples were filtered through 0.2 µm sterile filters into 1 mL aliquots of 20 % HNO_3 solution (Appendix A), resulting in 2 % final HNO_3 concentration. These samples were then diluted to 100× and 1000× in 2 % HNO_3. ICP-OES was conducted using an Agilent 5110 ICP-OES in axial view by Tim Barton at the Open University as per Macey et al. (2020). Accuracy of major element results was estimated using a 28 component multi-element standard solution for ICP (Fisher Chemical MS102050) and minor elements using a tailored 10 component standard solution. The specified wavelength for each element was selected for repeatability and performance. Check standards for ppm (0.5, 1, 2.5) and ppb (10, 100, 250, 500), blanks and drifts checks were run for quality control and data repeatability. Limits of detection are given in Table 3.4.

Table 3.4. Detection limits by element for the Agilent 5110 ICP-OES system.

Element	Detection limit (ppb)	Element	Detection limit (ppb)
Al	5.0	Nd	2.8
As	6.3	Ni	2.0
Ba	0.5	P	139.0
Ca	4.0	Pb	2.1
Ce	2.0	S	28.0
Co	0.5	Sb	6.4
Cr	0.3	Sc	1.3
Cs	282.0	Se	5.9
Cu	0.4	Si	6.0
Fe	1.0	Sn	9.6
Ga	4.3	Sr	0.3
K	0.0	Ti	0.6
Mg	1.0	V	0.6
Mn	1.0	W	7.1
Mo	5.7	Zn	7.7
Na	69.0	Zr	0.8

3.2.3.3.5 pH

pH was measured using a Thermo Scientific Orion Three Star pH meter with a two-point calibration using Omega Buffer solutions at pH 4 and 7 at the start and end points of the experiment.

3.2.4 Inhibition and co-substrate experiments

Growth experiments were conducted to assess the ability of NDFO microorganisms to grow in the CM brine, when supplemented with additional organic carbon and nutrient sources (Figure 3.1).

For this experiment, the focus was the CM brine because the composition was based on the Yellowknife Bay site in Gale crater, which is claimed to have been habitable during the existence of a lake which once partially filled the crater (Grotzinger et al., 2014a; Ramkissoon et al., 2019). *Acidovorax sp.* strain BoFeN1 was selected as a strain, because it grew on the olivine substrate in Chapter 2.

The first step was to determine whether the CM medium had any inhibitory effect on microbial growth. For this, the CM medium was mixed with an anoxic nutrient medium (containing peptone 5.0 g L^{-1}, meat extract 3.0 g L^{-1}) (Section 2.2.2) at ratios of 90:10 and 10:90, to provide a range of organic carbon sources and trace elements at different concentrations.

Subsequently, *Acidovorax sp*. strain BoFeN1 was grown in CM brine with an organic co-substrate (acetate) and additional soluble Fe^{2+} to test the effect they had on growth rate and maximum cell density. Acetate was selected having been previously used as an organic co-substrate for *Acidovorax sp*. strain BoFeN1 and other strains in mixotrophic NDFO experiments (Miot et al., 2009; Muehe et al., 2009). For this, CM media were created unamended, amended with sodium acetate (2 mM) or with both sodium acetate (2 mM) and $FeSO_4$ (10 mM). Anoxic nutrient medium was used as a positive control.

The media was prepared by aliquoting 30 mL of CM media (prepared as in Section 3.2.1.1) into 50 mL Wheaton bottles, under a N_2 headspace. The bottles were then sealed with a butyl rubber stoppers and crimped aluminium caps (described in Section 3.2.3.1).

The inoculum (10^5 cells mL^{-1}) was prepared by growing *Acidovorax sp*. strain BoFeN1 in an anoxic nutrient media at 30 °C for 2 days. The cells were harvested during exponential growth phase, washed twice in the corresponding medium (see Section 3.2.3.1) to remove extracellular nutrients. Cultures were inoculated to give a starting concentration of 10^5 cells mL^{-1} (volumes calculated from cell counts of the inoculum) and an equal volume of sterile CM media was added to controls.

The mixed CM/nutrient media cultures and respective uninoculated negative controls in the inhibition experiment were incubated at 25 °C for 4 days and observed for turbidity.

Identification of visible turbidity in the media column is commonly used to check for microbial growth in enrichment cultures..

The unamended CM cultures, amended CM cultures, positive controls and uninoculated negative controls were incubated at 25 °C for 6 days. The Baclight Live/Dead stain method (Section 2.2.4) was used to monitor microbial growth. Cell counts were performed in the co-substrate experiment, which involved a smaller total number of cultures and controls compared with the chemolithotrophic experiment (as described in Section 3.2.3).

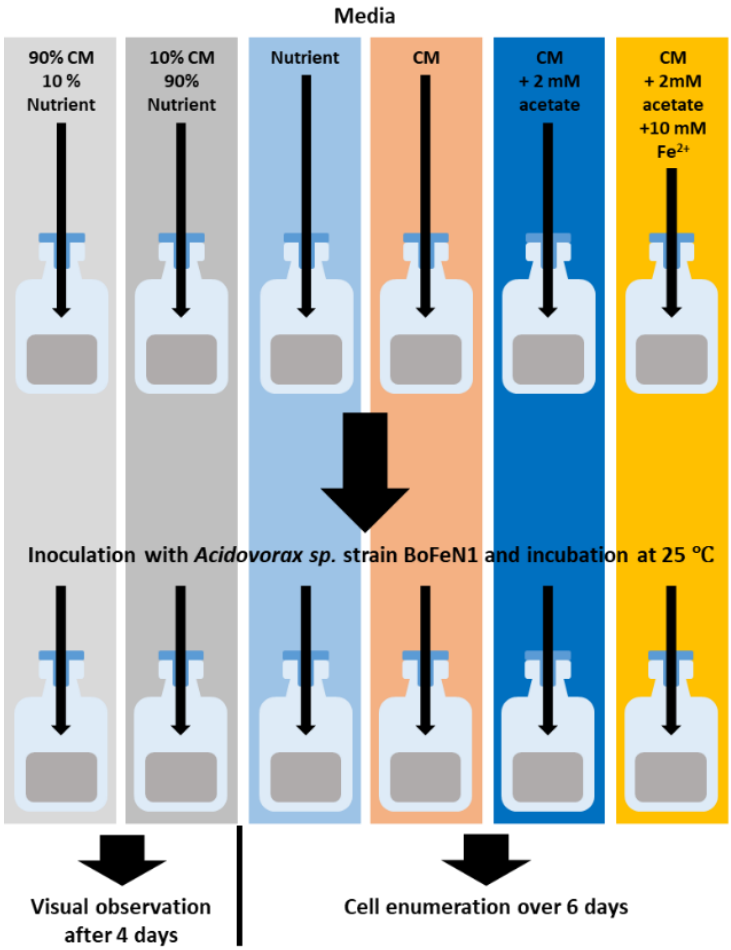

Figure 3.1. Preparation of inhibition and co-substrate experiments. Anaerobic nutrient and Contemporary Mars (CM) media were mixed and amended with acetate and Fe^{2+}, then inoculated with *Acidovorax sp*. strain BoFeN1. Two series (90% CM 10% Nutrient and 10% CM 90% Nutrient) were incubated at 25°C for 4 days and visually observed for growth. All other cultures were incubated at 25°C for 6 days, with regular samples taken for cell enumeration.

Cell densities were determined using equation (1) and specific growth rates were calculated from exponential growth phases using equation (2).

3.2.5 Statistics

Results from nitrate and nitrite assays, the protein assay, ferrozine assay, ICP-MS and viable cell counting were tested for significance using a 2-tailed paired Student's t-test. Pooled biotic samples were tested for significance against controls using a 2-tailed 2-sample t-test assuming equal variance. Correlations were calculated using Pearson's coefficient of linear correlation.

3.3 Results

3.3.1 Growth under simulated martian chemical conditions

3.3.1.1 Chemolithotrophic growth experiment

Microbial growth was monitored using the Bradford protein assay. Growth was detected for all of the isolates when grown in SG media and for *Acidovorax sp.* strain BoFeN1 and *Pseudogulbenkiania sp.* strain 2002 when grown in CM media (Figure 3.2).

Protein was detected for all three strains after 10 days in the SG medium. There was no lag phase observed for *Paracoccus sp.* strain KS1 (1.53 ± 0.74 µg mL^{-1}) and *Acidovorax sp.* strain BoFeN1 (1.12 ± 0.47 µg mL^{-1}); whereas a lag phase was observed for *Pseudogulbenkiania sp.* strain 2002 between inoculation and day 1. This was followed by a period of exponential phase from days 1 to 7. A growth maximum (1.00 ± 0.47 µg mL^{-1}) was reached at day 7. The specific growth rates were 1.3 day^{-1} for *Paracoccus sp.* strain KS1, 1.9 day^{-1} for *Acidovorax sp.* strain BoFeN1 and 2.5 day^{-1} for *Pseudogulbenkiania sp.* strain 2002.

Within the CM medium, no lag phase was observed for *Acidovorax sp*. strain BoFeN1 and *Pseudogulbenkiania sp*. strain 2002. *Acidovorax sp*. strain BoFeN1 (0.53 ± 0.26 µg mL^{-1}) and *Pseudogulbenkiania sp*. strain 2002 (0.66 ± 0.15 µg mL^{-1}) reached maximum detected protein concentration at day 10 with respective specific growth rates of 1.5 day^{-1} and 2.1 day^{-1}. Despite increasing mean protein concentration between days 2 and 10 for *Paracoccus sp*. strain KS1 in the CM medium, protein was not significantly higher than in the controls at any point, so this apparent growth cannot be confirmed. No growth was detected in the CM or SG controls.

In the SR medium, no significant growth was detected for any of the strains throughout the experiment. *Pseudogulbenkiania sp*. strain 2002 grown in HR media initially demonstrated growth; however, no protein was detected after day 4. None of the other strains were able to grow in the HR media and no detectable protein was produced at any point. The initial protein detection could be due to microbial activity based on a carry-over of intracellular nutrients from the pre-experiment growth medium, after which the cells died off over the first 4 days of the experiment.

A caveat is that the protein concentrations detected were very much at the lower detection limits of the Bradford assay, despite modifications to improve sensitivity. For this reason, the culture values have been normalised against the controls to help separate protein trends from instrument noise.

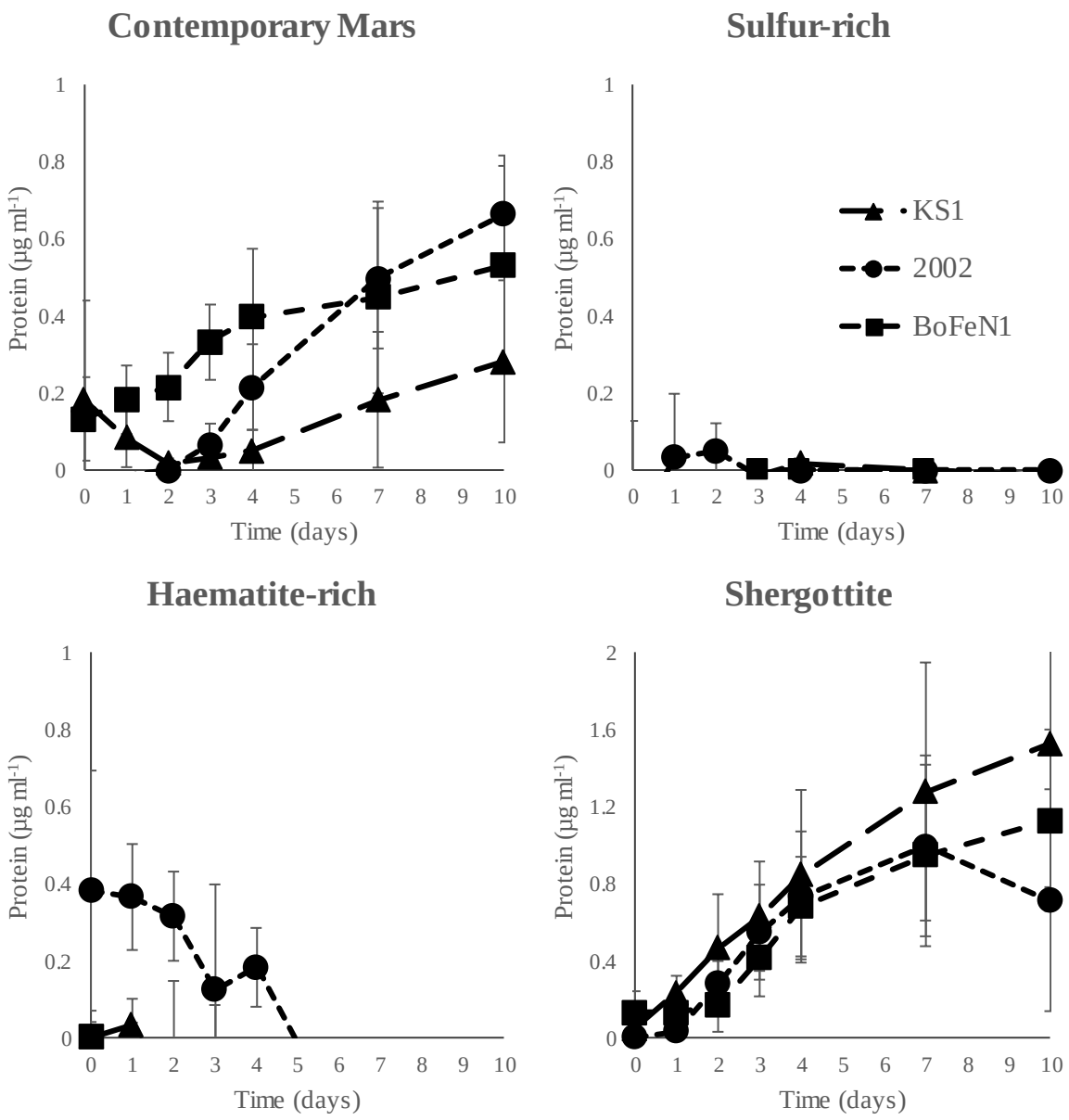

Figure 3.2. Protein concentration over time in Contemporary Mars (CM), Sulfur-rich (SR), Haematite-rich (SR) and Shergottite (SG) brines for *Paracoccus sp*. strain KS1, *Pseudogulbenkiania sp*. strain 2002, *Acidovorax sp*. strain BoFeN1 (± standard error). Values are normalised against the abiotic control.

3.3.1.2 Inhibition and co-substrate experiments

After four days of incubation, microbial growth was observed in the 90:10 and 10:90 CM brine/Nutrient media cultures of *Acidovorax sp*. strain BoFeN1, demonstrating that the composition of the CM brine was not inhibitory to the growth of *Acidovorax sp*. strain BoFeN1.

Table 3.5. Determination of *Acidovorax sp*. strain BoFeN1 growth by visible turbidity (+) after 4 days in culture at 25 °C.

Inoculum	Media			
	90:10 Brine: Nutrient media	10:90 Brine: Nutrient media	Nutrient media	Sterile water
Acidovorax sp. strain BoFeN1	+	+	+	-
Control	-	-	-	-

Growth of *Acidovorax sp*. strain BoFeN1 was significan in the CM medium, and the cell concentration increased from 10^5 cells mL^{-1} (at inoculation) to a maximum cell number of $4.2 \pm 1.2 \times 10^5$ cells mL^{-1} after four days (Figure 3.3). The cell numbers then dropped below that of the initial concentration ($4.8 \pm 4.0 \times 10^4$ cells mL^{-1}). The specific growth rate during exponential phase was 6.5 day^{-1}.

The addition of the acetate (2 mM) to the CM brine, enhanced the growth rate (7.1 day^{-1}) and maximum cell numbers for *Acidovorax sp*. strain BoFeN1 in comparison to the unamended brine cultures. The maximum cell concentration of $2.2 \pm 0.1 \times 10^6$ cells mL^{-1} was reached after 3 days, significantly higher than the maximum cell concentration in the unamended medium (p=0.02). The growth of *Acidovorax sp*. strain BoFeN1 with addition of both acetate (2 mM) and Fe^{2+} (10mM) to the medium followed a similar pattern to cultures amended with only acetate (2 mM), but with a specific growth rate of 7.4 day^{-1} and a significantly higher (p=0.04) maximum concentration of $7.2 \pm 0.7 \times 10^6$ cells mL^{-1} at day 4. In nutrient media, the strain grew heterotrophically with a specific growth rate of 14.0 day^{-1}. A maximum cell number of 1.3×10^6 cells mL^{-1} was reached at day 1 and the cultures entered stationary phase and remained at around 10^6 cells mL^{-1} thereafter.

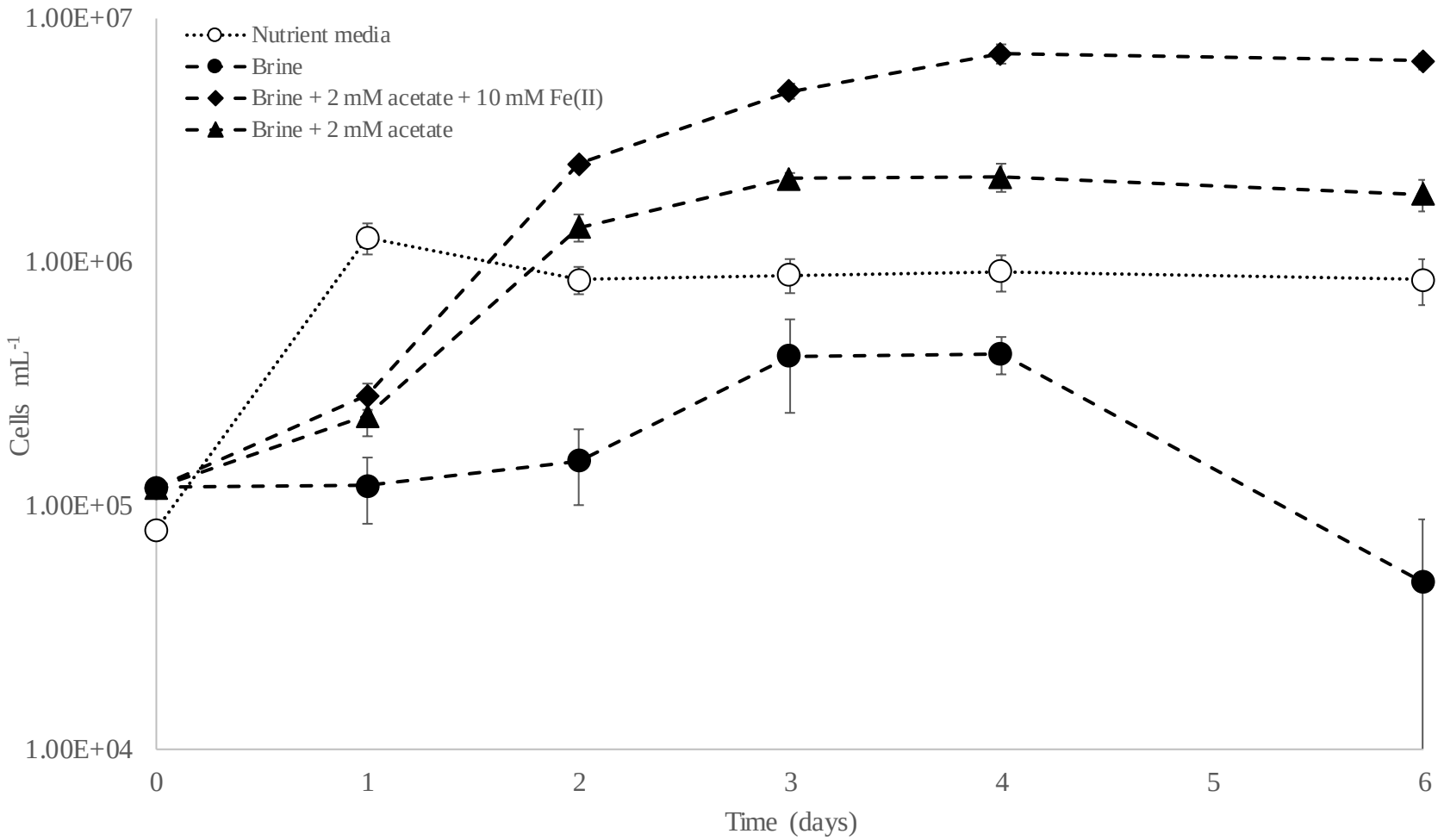

Figure 3.3. Viable cell counts over time for *Acidovorax sp.* strain BoFeN1 in Contemporary Mars (CM) brine. Growth in the unamended brine is shown in comparison to brines amended with 2 mM acetate, 2 mM acetate and 10 mM Fe^{2+} and to nutrient media (± standard error).

3.3.2 Fe oxidation state

The total Fe and the Fe^{2+} was measured throughout the experiment using the ferrozine assay. In the CM, the other series besides SG with microbial growth, Fe became more reduced over the course of the experiment in all inoculated cultures and controls from ~0.2 at inoculation to 0.4-0.5 by day 10 (Figure 3.4). Between day 0 and 10, the Fe^{2+}/Fe_{total} ratio increased from 0.25 ± 0.03 to 0.41 ± 0.03 in *Paracoccus sp.* strain KS1, from 0.25 ± 0.02 in *Pseudogulbenkiania sp.* strain 2002, from 0.25 ± 0.03 to 0.43 ± 0.02 in *Acidovorax sp.* strain BoFeN1 and from 0.22 ± 0.03 to 0.48 ± 0.04 in the control. This contrasted with the expectation that NDFO metabolism would result in an overall trend of Fe oxidation (Miot et al., 2014a). The growth observed here may be insufficient to generate significant Fe oxidation, relative to the control. The final Fe^{2+}/Fe_{total} ratios do appear lower in the three biotic culture sets than in the control, which may suggest a relative oxidation effect. However, no significant differences were found between the CM cultures and controls, either when cultures were considered in organism-specific groups (*Acidovorax sp.* strain BoFeN1 p=0.22, *Pseudogulbenkiania sp.* strain 2002 p=0.36, *Paracoccus sp.* strain KS1 p=0.06) or a pooled biotic sample set (p=0.09).

In both SR and HR media there was an initial trend in Fe oxidation across for both the biotic experiments and the abiotic controls, until day 2, after which the Fe^{2+}/Fe_{total} ratios plateau over the next 8 days. The exception to this are the *Paracoccus sp.* strain KS1 cultures in HR brine, which remain stable at ~0.9 Fe^{2+}/Fe_{total} throughout.

The initial Fe concentration of the SG media was entirely in the form of low solubility precipitates, and therefore dissolved total Fe and Fe^{2+} was below the detection limits of the ferrozine assay.

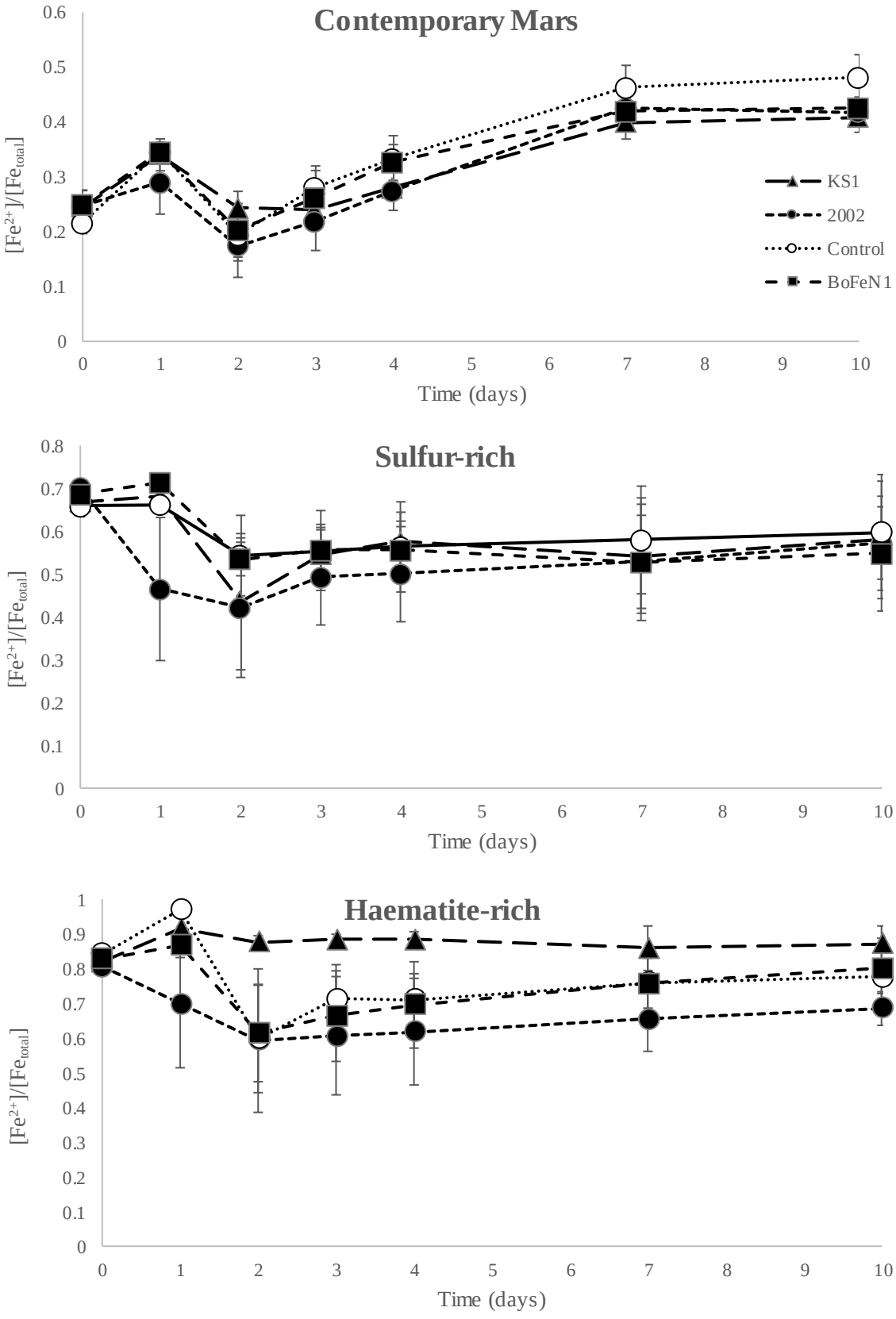

Figure 3.4. Fe^{2+}/Fe_{total} over time in Contemporary Mars, Sulfur-rich and Haematite-rich brines for *Paracoccus sp.* strain KS1, *Pseudogulbenkiania sp.* strain 2002, *Acidovorax sp.* strain BoFeN1 and an abiotic control (± standard error).

When the Fe redox is displayed relative to the control and plotted against microbial growth (Figure 3.5), there are inverse correlations in the CM media for *Paracoccus sp*. strain KS1 (ρ = -0.43), *Pseudogulbenkiania sp*. strain 2002 (ρ = -0.45) and *Acidovorax sp*. strain BoFeN1 (ρ = -0.92). This suggests that a greater extent of microbial growth is associated with oxidation of Fe in the CM media, relative to the control, which could be a microbially-mediated NDFO effect.

In the HR media, there was no strong correlation between Fe redox state and microbial growth for *Pseudogulbenkiania sp*. strain 2002 (ρ = -0.07), despite protein detected over the first 4 days. There were no correlations in the SR media due to the lack of microbial growth.

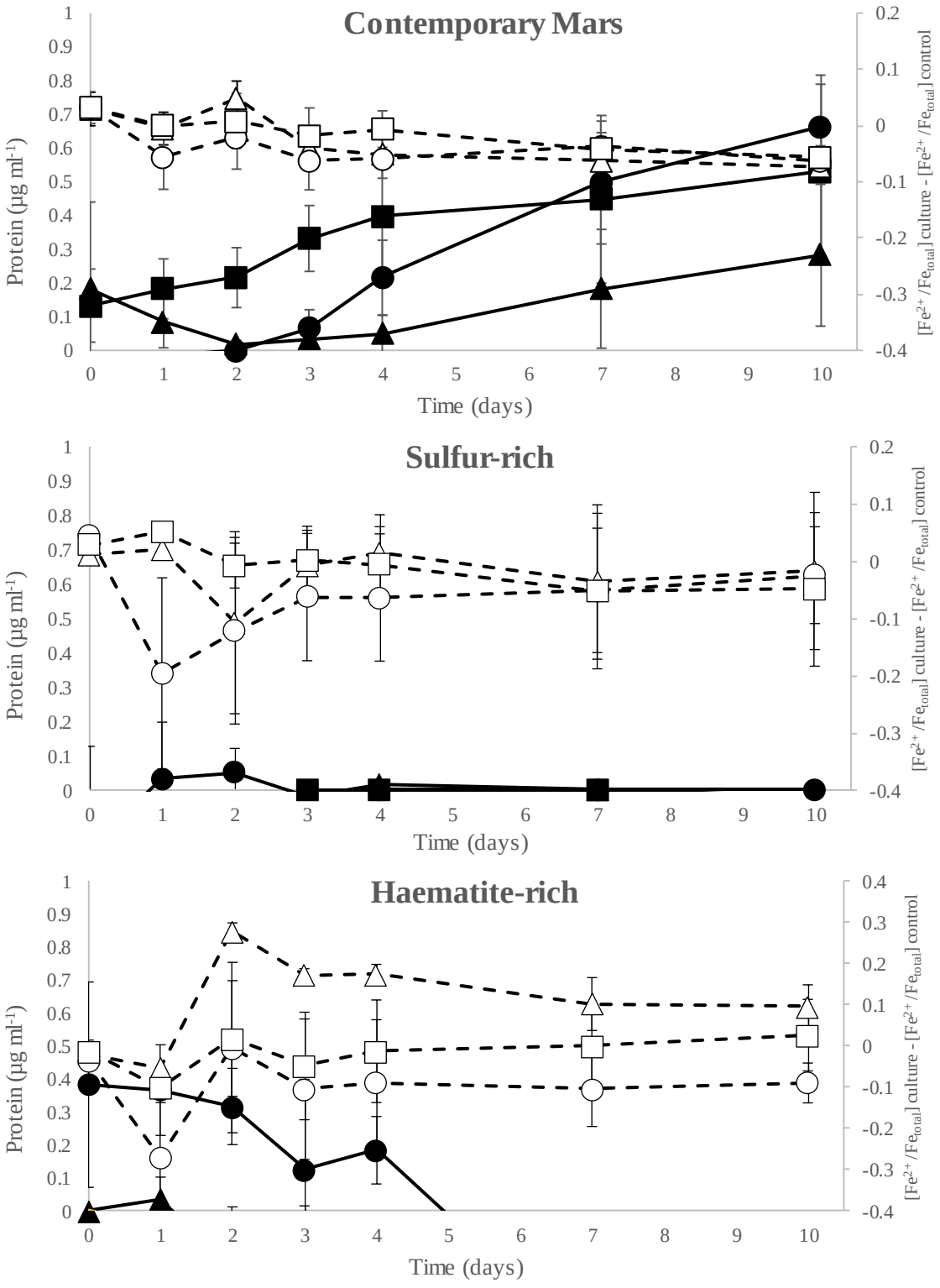

Figure 3.5. Protein (filled symbols, solid lines) and Fe^{2+}/Fe_{total} relative to the control (open symbols, dotted lines) over time in Contemporary Mars, Sulfur-rich and Haematite-rich media for *Paracoccus sp*. strain KS1 (triangles), *Pseudogulbenkiania sp*. strain 2002 (circles) and *Acidovorax sp*. strain BoFeN1 (squares) (± standard error).

3.3.3 pH

The pH decreased between the start and end point (day 10) of the experiment for all of the culture and control experiments as shown in Table 3.6. There were no significant differences between the inoculated cultures and abiotic controls after 10 days (Appendix C), across the four media, except for *Pseudogulbenkiania sp.* strain 2002 grown in the SG brine (p=0.02), indicating no role for biological activity in this downward trend.

The mean pH values for *Pseudogulbenkiania sp.* strain 2002 cultures and the abiotic controls after 10 days in SG brine were significantly different (p<0.05). However, the error margins as calculated for standard error for these two data points are overlapping and therefore this may represent a statistical anomaly or an isolated temperature-dependent effect during measurement.

Table 3.6. Initial and final pH values for Mars brine cultures and abiotic controls (± standard error).

Brine	Inoculum	Initial pH	End point pH
Contemporary Mars	*Paracoccus sp.* strain KS1	6.75	6.28 (±0.06)
	Pseudogulbenkiania sp. strain 2002	6.75	6.39 (±0.07)
	Acidovorax sp. strain BoFeN1	6.75	6.21 (±0.03)
	Control	6.75	6.28 (±0.07)
Sulfur-rich	*Paracoccus sp.* strain KS1	6.69	5.85 (±0.02)
	Pseudogulbenkiania sp. strain 2002	6.69	5.86 (±0.02)
	Acidovorax sp. strain BoFeN1	6.69	5.76 (±0.05)
	Control	6.69	5.79 (±0.01)
Haematite Slope	*Paracoccus sp.* strain KS1	6.72	6.36 (±0.03)
	Pseudogulbenkiania sp. strain 2002	6.72	6.34 (±0.02)
	Acidovorax sp. strain BoFeN1	6.72	6.30 (±0.04)
	Control	6.72	6.31 (±0.02)
Shergottite	*Paracoccus sp.* strain KS1	7.00	6.70 (±0.01)
	Pseudogulbenkiania sp. strain 2002	7.00	6.74 (±0.06)
	Acidovorax sp. strain BoFeN1	7.00	6.63 (±0.03)
	Control	7.00	6.67 (±0.07)

3.3.4 Nitrate consumption and nitrite production

Nitrite concentration correlates with microbial growth in both the CM and SG culture series (Figure 3.7), indicating a growth phase based on nitrate reduction (which produces biogenic nitrite as a metabolite). The nitrate concentrations at the end of the experiment (Figure 3.6) appear lowest in those cultures with the highest concentrations of nitrite and protein produced, indicating more extensive consumption of nitrate in growing cultures. However, this finding is limited by the minimal growth and the sensitivity of the nitrate measurement, which only revealed a significantly greater (p<0.05) consumption of nitrate by the *Paracoccus sp*. strain KS1 cultures relative to the abiotic control over the 10-day experiment.

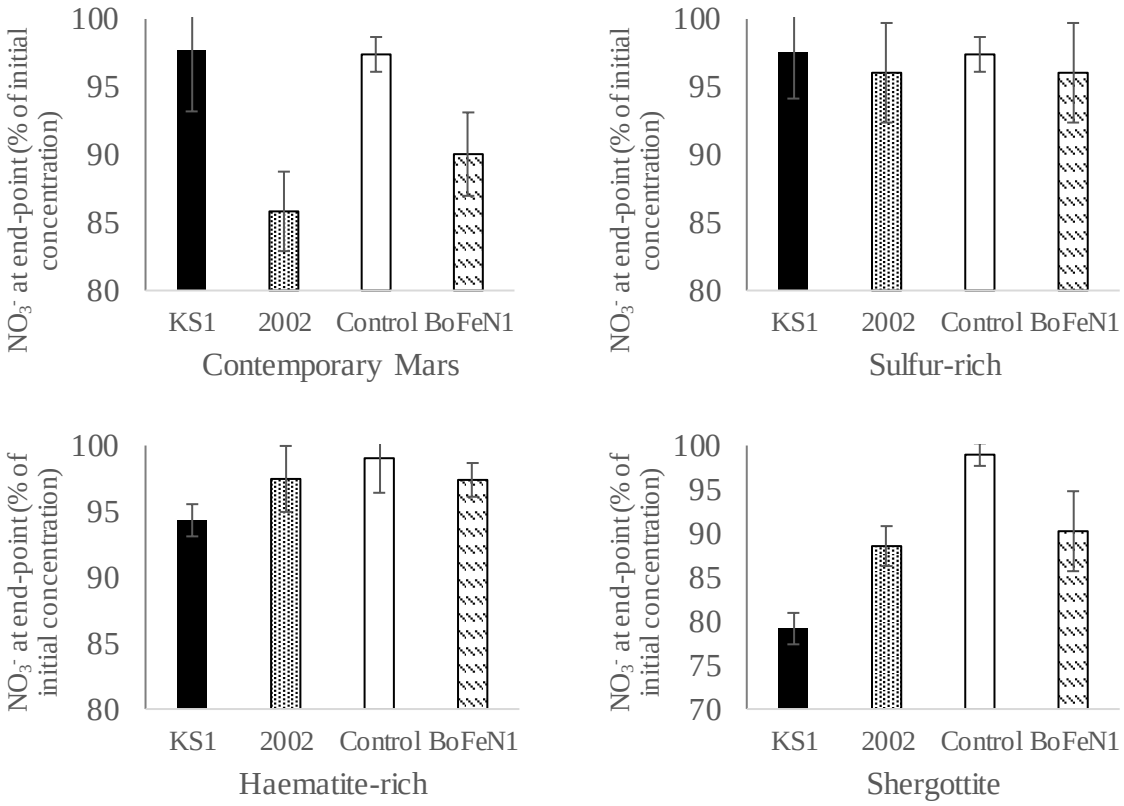

Figure 3.6. Relative nitrate concentrations after 10 days in Rocknest, Paso Robles, Haematite Slope and Shergottite brines for *Paracoccus sp*. strain KS1 (KS1), *Pseudogulbenkiania sp*. strain 2002 (2002), *Acidovorax sp*. strain BoFeN1 (BoFeN1) and an abiotic control (Control) (± standard error).

In CM, the nitrite concentrations gradually increased from day 3 and 4 for *Pseudogulbenkiania sp*. strain 2002 and *Acidovorax sp*. strain BoFeN1 respectively. The maximum concentrations were 1.26 (±0.05) and 0.90 (±0.05) µM at day 7. There was no clear evidence of nitrite production by *Paracoccus sp*. strain KS1 in CM cultures. The consumption of nitrate in cultures reflects the extent of nitrite production, with *Pseudogulbenkiania sp*. strain 2002 and *Acidovorax sp*. strain BoFeN1 cultures at 85.8 % (±2.9) and 90.0 % (±3.1) of the initial values, respectively. This contrasts with the *Paracoccus sp*. strain KS1 cultures (97.7 % ±4.5) and control (97.4 % ±1.3), which were both higher.

Nitrite concentrations in SG media increased for all three strains and reached maximum values of 3.10 (±0.13) µM in *Paracoccus sp*. strain KS1, 2.33 (±0.13) µM in *Pseudogulbenkiania sp*. strain 2002 and 2.39 (±0.34) µM in *Acidovorax sp*. strain BoFeN1, at day 7. No significant detections of nitrite were made in the control series. The most significant effect on the nitrate concentration was observed in *Paracoccus sp*. strain KS1 SG cultures, which decreased to 79.2 % (±1.8) over the 10 days, which also produced the highest maximum protein concentration of any culture in the chemolithotrophic experiment. This was significantly lower ($p<0.05$) than the end point nitrate concentration of 99.0 % (±1.3) in the control.

There were no significant differences in either nitrite or nitrate from the values of the abiotic controls, across the inoculated SR and HR cultures ($p<0.05$). Along with the lack of evidence for microbial growth in the protein data for SR and HR cultures, this finding suggests no growth by nitrate reduction to nitrite in the SR and HR media.

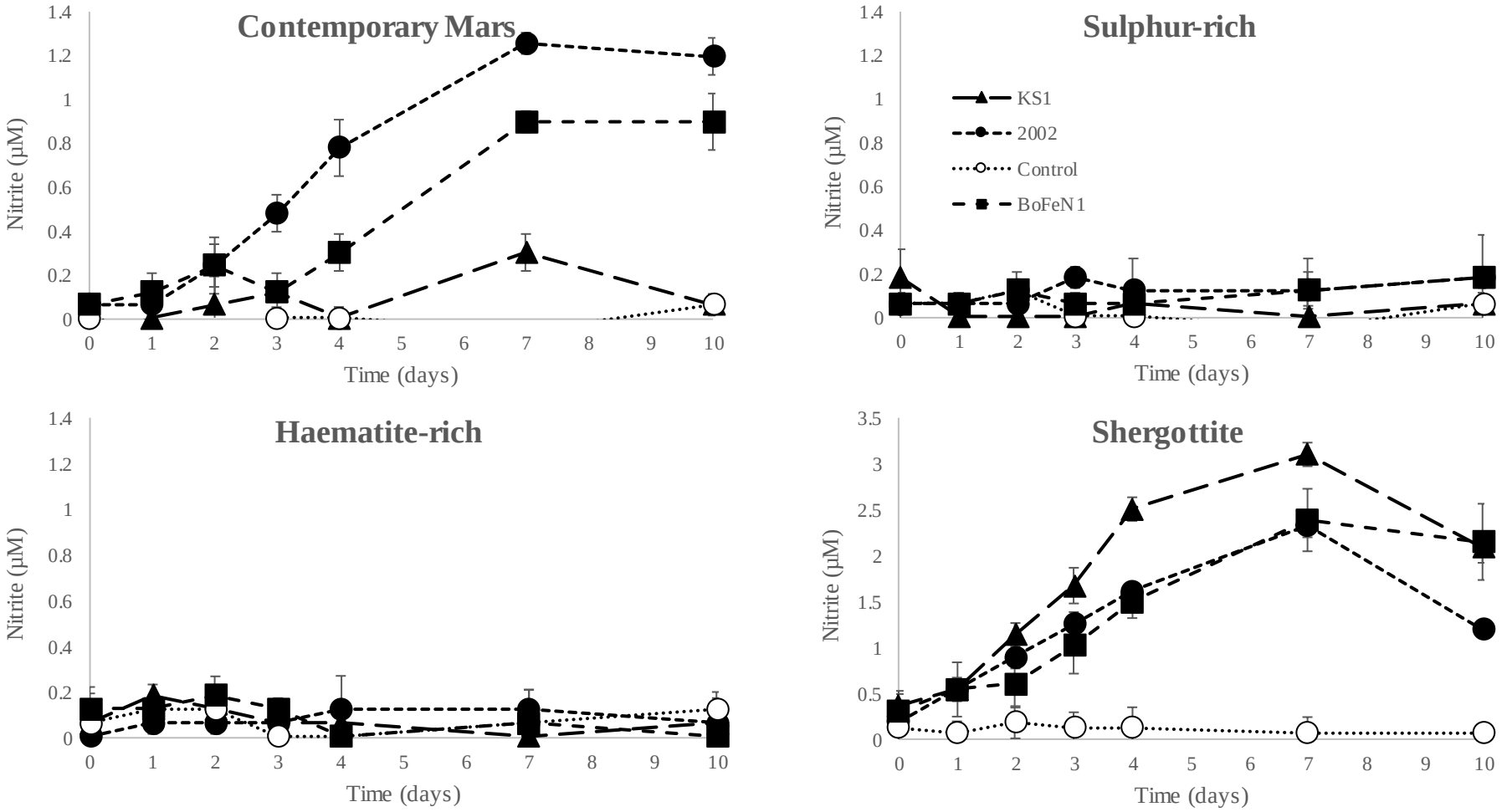

Figure 3.7. Nitrite concentrations over time in Rocknest, Paso Robles, Haematite Slope and Shergottite brines for *Paracoccus sp.* strain KS1, *Pseudogulbenkiania sp.* strain 2002, *Acidovorax sp.* strain BoFeN1 and an abiotic control (± standard error).

3.3.5 Dissolved elemental composition

In contrast to the results of Chapter 2, there were few significant differences in the concentration of dissolved Fe between cultures and abiotic controls after 10 days (Figure 3.8).

Immediately after inoculation, no significant differences in terms of Fe were found between the three strains or controls any of the media (Figure 3.9). The overall trend within SR and HR media was a decline of ~5.5-9 ppm Fe across all cultures and controls over 10 days. Decreases from the Fe concentrations at the point of inoculation were significant ($p<0.05$) in the control and *Paracoccus sp*. strain KS1 cultures for HR, and in all cultures and controls except *Paracoccus sp*. strain KS1 for the SR brine.

There were no significant differences between the dissolved Fe concentration in the three strains and the abiotic controls in any of the media after 10 days, besides that between *Acidovorax sp*. strain BoFeN1 cultures and the abiotic control in HR ($p<0.05$). Given that there is no supporting evidence for growth or active metabolism in these cultures, it is reasonable to conclude that this solitary result is an outlier rather than an effect of microbial metabolism in *Acidovorax sp*. strain BoFeN1 HR cultures.

There is a similar pattern across other metabolically important elements such as Mg, Mn and S, which show no significant removal from solution in biotic cultures relative to the controls at either point. There does appear to be an elevated Cu concentration in the SR (141.9 ± 112.3) and HR (45.6 ± 22.8 ppb) controls, relative to the biotic cultures immediately after inoculation, but the difference is not significant and outliers in the triplicate data (416.9 ppb in HR and 99.5 ppb in SR) may be primarily responsible.

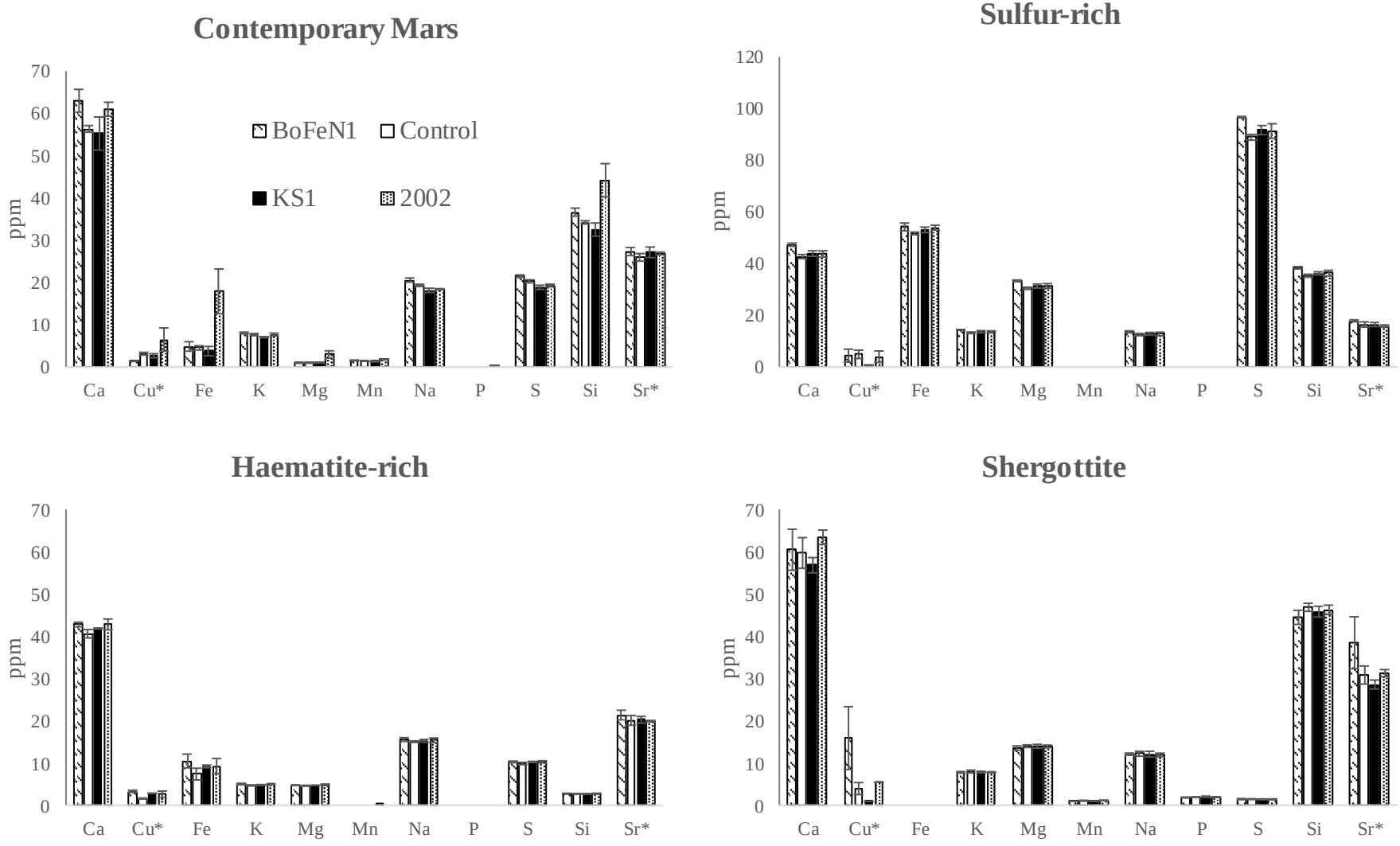

Figure 3.8. Dissolved elemental concentrations after 10 days in the martian simulant brines for *Paracoccus sp.* strain KS1, *Pseudogulbenkiania sp.* strain 2002, *Acidovorax sp.* strain BoFeN1 and an abiotic control (± standard error). *denotes that this column represents ppb.

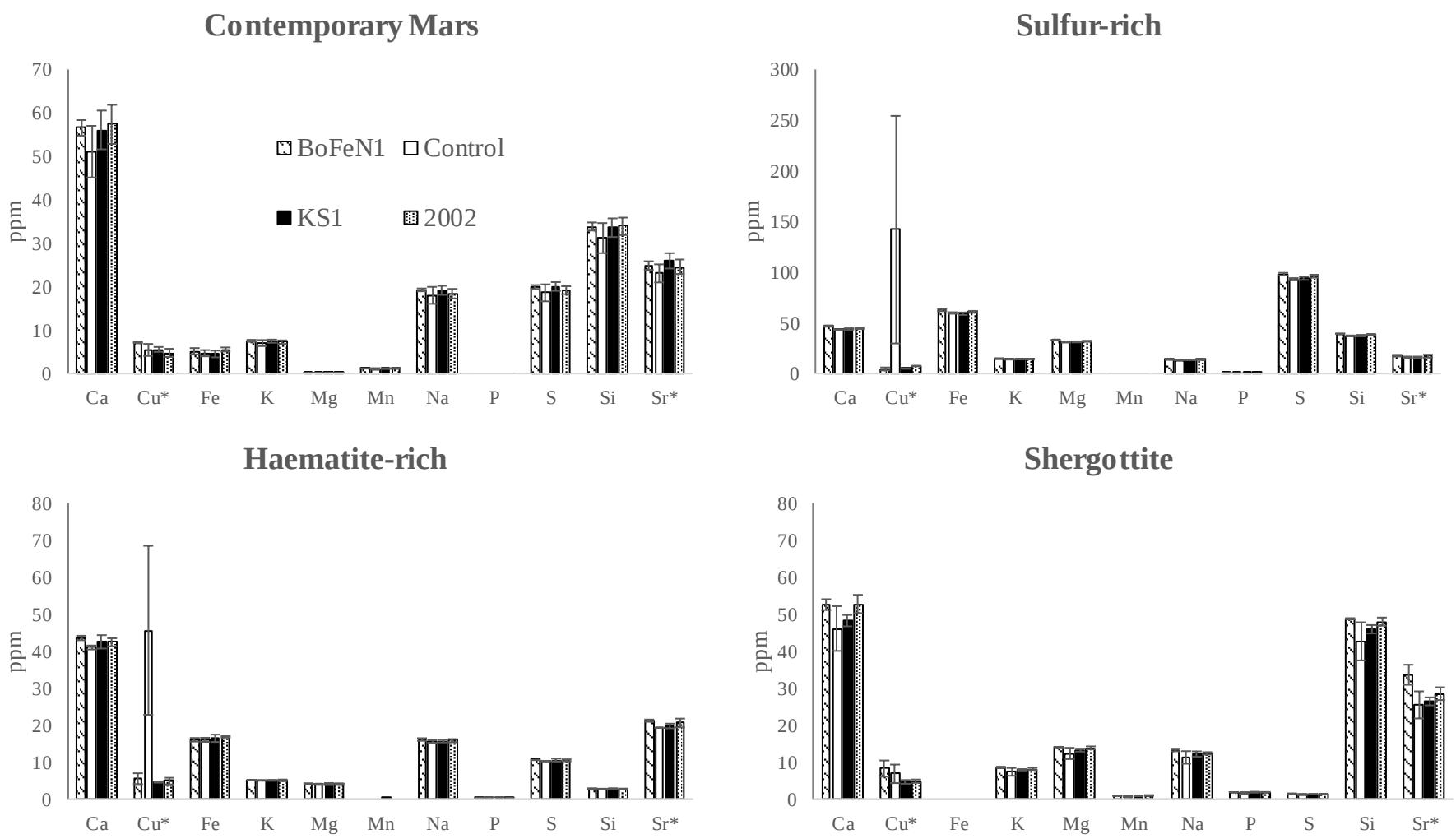

Figure 3.9. Dissolved elemental concentrations immediately after inoculation in the martian simulant brines for *Paracoccus sp*. strain KS1, *Pseudogulbenkiania sp*. strain 2002, *Acidovorax sp*. strain BoFeN1 and an abiotic control (± standard error). *denotes that this column represents ppb.

3.4 Discussion

3.4.1 Microbial growth in martian chemical conditions

It must be noted that the microbial growth in the chemolithotrophic experiment was carried out under autotrophic conditions. The trends in biomass production, nitrate consumption and nitrite production all indicate some growth for *Pseudogulbenkiania sp*. strain 2002 and *Acidovorax sp*. strain BoFeN1 in CM media, whereas all three NDFO strains have exhibited some growth in the SG media. The caveat to this is that the results from the protein and nitrite assays are at the lower limits of detection for those methods, demonstrating that these cultures are low-biomass even following an exponential growth phase. This could provide an explanation for the lack of discernible biological effects on the Fe oxidation state and dissolved elemental composition. While it is likely that some intracellular nutrients were carried over during inoculation despite the wash steps, it is unlikely that metabolism using these would be sufficient to allow for the sustained production of protein - and thus biomass - over the duration of the experiment.

What is clear is the ability of *Acidovorax sp*. strain BoFeN1 to grow in CM brine, in the presence and absence of additional organics. The growth of this strain in the nutrient media-CM mixtures demonstrates that the brine itself is not prohibitive to the growth of NDFO strains. Meanwhile, cell counts from cultures show acetate is effective in promoting growth exceeding that observed in autotrophic conditions. The addition of Fe^{2+} in combination with acetate promoted further growth. This growth dependence on an organic co-substrate and the associated benefit of additional Fe^{2+} agrees with previously reported results for *Acidovorax sp*. strain BoFeN1 and other strains (Benz et al., 1998; Kappler et al., 2005; Muehe et al., 2009).

The successful autotrophic microbial colonisation of CM and SG media here has implications for NDFO metabolism on Mars, both geographically and through time.

The Shergottite meteorites on which the SG brine is based, are proposed to be representative of the extensive basaltic terrains observed throughout martian history. With that in mind, the growth of all three strains in SG culture indicates that these environments would not inhibit the proliferation of NDFO microbes, when sufficient nitrate is present as a result of the formation mechanisms discussed in Chapter 1. This finding has implications for life at both the surface and in subsurface of early Mars, where basalts of this type have been abundant throughout history (Bertka and Fei, 1998; Bridges and Warren, 2006; Steele et al., 2012a).

The CM brine is modelled originally from aeolian dust at Gale Crater and better represents the modern global composition of the weathered martian surface, so the growth of *Pseudogulbenkiania sp.* strain 2002 and *Acidovorax sp*. strain BoFeN1 could mean that any near-surface aqueous environment with regolith of this composition could host NDFO organisms. Considering indigenous microbes, the inhabitation of hypothetical modern fluids by NDFO microbes is made more relevant by the recent evidence for Amazonian hydrological activity (Adeli et al., 2016; Butcher et al., 2017). Butcher et al. (2017) described eskers, subglacial landforms caused by basal melting and subsequent erosion, revealed by retreating glaciers in areas of elevated geothermal heat flux. The existence of these features indicates that Mars has hosted large-scale mixing of meltwater with modern surface geology, potentially providing environments similar to the CM cultures in this experiment.

This finding is also significant when considering issues around planetary protection. Most plans for human habitation on Mars include mining for water-ice from the near subsurface

(Linne et al., 2019); the energy introduced in this process could generate habitable liquid microenvironments for organisms carried on equipment from Earth. This potential forward contamination highlights the need for effective sterilisation procedures.

3.4.2 Fe oxidation

Despite evidence for growth and reduction of nitrate to nitrite (Figure 3.2, Figure 3.6 and Figure 3.7), growth is not associated with significant oxidation of Fe^{2+}, which could be expected from active NDFO-based energy metabolisms in the growing cultures. For example, Weber et al. (2006b) observed that *Pseudogulbenkiania sp.* strain 2002 oxidised ~2 mM Fe^{2+} - of a medium containing 10 mM Fe^{2+} - over 7 days during autotrophic growth. *Acidovorax sp.* strain BoFeN1 oxidised ~2 mM of 4 mM total Fe^{2+} during autotrophic culture over 20 days (Kappler et al., 2005). These studies included higher concentrations of both Fe^{2+} and nitrate than any of the media in the chemolithotrophic media tested here, which may account for some of the difference in the extent of Fe^{2+} oxidation along with inhibitory growth effects of the martian simulant media.

The statistically indistinguishable patterns of Fe oxidation state of inoculated cultures and controls within each of the four brine series suggest that the shifts observed over time in the Fe^{2+}/Fe_{total} ratios are predominantly abiotic chemical processes. However, the mean Fe oxidation balances, in the biotic CM culture series showing evidence for microbial growth, appear more oxidised at the end of the experiment than the controls. Additionally, there were negative correlations between microbial growth and the Fe^{2+}/Fe_{total} ratio relative to the control in CM cultures. This finding suggests that sufficient microbial growth by nitrate reduction to nitrate in this media could produce detectable patterns of Fe oxidation, if the link is causal.

It is possible that with a longer experiment duration or a more sensitive method for monitoring Fe oxidation state, that a significant trend of oxidation - relative to the controls - may be found.

3.4.3 Abiotic acidification

By the conclusion of the experiment, pH had dropped below the reported range (<6) for NDFO metabolism in the SR brine. More acidic pH reduces the energetic favourability of the redox potential NDFO couple (discussed in Chapter 1) for sustaining microbial growth and carbon fixation (Weber et al., 2006a). Therefore, it is unsurprising that the results of this experiment report no definite NDFO-based autotrophic growth in this brine.

Acidification is a commonly observed effect of fermentative heterotrophic growth, due to the organic acids produced during metabolism (Madigan et al., 2008; Sauer et al., 2008). If microbes in anoxic growth medium were growing by fermentation prior to washing and inoculation into the chemolithotrophic media, there may logically have been some internal carry-over of biogenic acids. However, fermentation could not have continued in the chemolithotrophic media here due to the lack of organic carbon compounds as substrates. Additionally, the comparable acidification of controls indicates that this process is abiotic rather than a consequence of biogenic acids.

The acidification observed is likely to be due to the reaction of the 10 % CO_2 headspace component with water to form carbonic acid. The martian atmosphere is, and has been, primarily composed of CO_2 throughout history, so the acidifying effects of this on long-lived hydrological systems are important to note when considering habitability for pH-dependent metabolisms such as NDFO. Indeed, acidified oceans (pH <6.2) have been proposed on early Mars as a consequence of a carbon dioxide (0.8-4 bar) atmosphere (Fairén et al., 2004). If true, these conditions would inhibit NDFO as a viable metabolism

across large swathes of early Mars. However, direct geochemical analysis of rocks *in situ* at Gale crater show that circumneutral systems did persist on early Mars (Grotzinger et al., 2014a), particularly in the subsurface, where they could even be available today (Michalski et al., 2013).

With this in mind, it may be appropriate to conduct future experiments of this type under an inert atmosphere, such as the pure N_2 headspaces used in previous brine survival studies (Fox-Powell et al., 2016) to remove this effect. The CO_2 in these experiments and in Chapter 2 was included as an inorganic carbon source for autotrophic growth by NDFO. However, the discovery of complex, endogenous organics at Gale crater (Eigenbrode et al., 2018) has changed previous assumptions about the carbon sources available in early Mars environments and future work should be adapted to reflect these discoveries.

3.4.4 Future Work

The inhibition experiment showed that the CM brine components were not inhibitory to growth of *Acidovorax sp*. strain BoFeN1 in the presence of organic carbon sources and additional nutrients. Therefore, inhibition experiments should be conducted with the remaining three brines using the *Acidovorax sp*. strain BoFeN1 as well as other NDFO microorganisms. The habitability of the SR and HR brines are of particular interest, given the absence of growth in the autotrophic cultures here.

Given the evident positive impact of an additional organic co-substrate to growth of in CM media, future experiments could incorporate organics at a range of concentrations, including those reported from Gale crater, Mars (10-100 nmol), present as thiophenic, aromatic, aliphatic and C_1 and C_2 sulfur molecules (Eigenbrode et al., 2018). A good analogue for martian surface organics may be to use material from carbonaceous chondrites as a carbon source, given the influx of carbonaceous meteorites to the martian

surface over time and prior evidence for Fe oxidation by NDFO bacteria in meteorites under experimental conditions (Yen et al., 2006; Gronstal et al., 2009). If extensive growth by mixotrophic NDFO is possible when using similar organic compounds to those detected on contemporary Mars as co-substrates, that growth may be associated with detectable Fe oxidation trends. In which case, application of the full analytical inventory described here, as well as the addition of scanning electron microscopy and mineralogical analyses to characterise the Fe^{3+} oxides produced in association with the cells, would further our understanding of the behaviour of NDFO strains under simulated martian conditions.

3.4.5 Conclusions

All three strains grew in the SG brine and two strains in the CM brine, based on combined protein, nitrite and nitrate data. However, there was no evidence of significant Fe oxidation or removal of soluble Fe from solution to form Fe^{3+} oxide precipitates in any of the cultures relative to the abiotic controls, suggesting that NDFO was not a dominant process in the brine chemistry in actively growing cultures.

Addition of both complex organics and acetate (2 mM) as co-substrates allowed *Acidovorax sp*. strain BoFeN1 to grow more extensively in the CM brine. Further addition of Fe^{2+} (10 mM) to acetate-amended cultures accelerated growth relative to the acetate-only cultures, suggesting that Fe^{2+} is a more effective electron donor in the presence of an organic co-substrate such as acetate.

Therefore, some aqueous environments on Early Mars were likely habitable to NDFO microorganisms, but the presence of organics may have been required in order to metabolise efficiently enough so as to alter the Fe redox chemistry and leave detectable traces as biosignatures in the sedimentary record.

4. NDFO draft genome analysis and *nar* gene knockout experiments

4.1 Introduction

In order to truly assess the viability of nitrate-dependent Fe^{2+} oxidation (NDFO) on early Mars, it is first necessary to gain a greater understanding of the process in its terrestrial context. There is ongoing debate around the status of NDFO as a true metabolism, as opposed to a consequence of denitrification, which has no direct benefit to growth (Weber et al., 2006a; Hedrich et al., 2011).

The mechanisms of NDFO have remained elusive since the process was first described (Straub et al., 1996). Several hypotheses have been advanced to account for both the oxidation of Fe during nitrate reduction and the reported associated benefit for growth (Temple and Colmer, 1951; Weber et al., 2006b; Blöthe and Roden, 2009; Weber et al., 2009; Laufer et al., 2016b). Carlson et al. (2012) postulated that the energetic gain from NDFO metabolism for microorganisms is along a spectrum. At one end of the spectrum (most energetically beneficial) are microorganisms that efficiently accept electrons from Fe^{2+} for energetic gain; whilst managing the toxic effects of intracellular Fe^{2+} oxidation. At the other end of the spectrum (least energetically beneficial) are those that manage toxicity but gain no energetic benefit and those that oxidise Fe^{2+} inadvertently but suffer from energy metabolism inhibition and toxicity.

Four mechanisms have been proposed that can energetically benefit microorganisms by Fe^{2+} oxidation coupled to nitrate reduction as shown in Figure 4.1 (Carlson et al., 2012). The most energetically beneficial mechanism would be a dedicated Fe^{2+} oxidoreductase, which would enzymatically catalyse the oxidation of Fe^{2+} to Fe^{3+}. This would result in the release and conservation of electrons for energy metabolism (Figure 4.1A). The second potential mechanism is that Fe^{2+} oxidation is catalysed by the secondary action of the respiratory nitrate reductase (Nar) enzyme, present in all denitrifying bacteria, which

provides a less efficient pathway for electron acquisition (Figure 4.1B). The final biotic mechanism that Carlson et al (2012) suggested is where a cytochrome bc_1 complex accepts electrons from Fe^{2+} to reduce the quinone pool and generates a proton motive force by coupling to quinol dehydrogenase activity (Figure 4.1C). An alternative mechanism would be an abiotic reaction. This would entirely be due to abiotic interactions of Fe^{2+} with the oxidised nitrogen species, such as nitrite, generated by microbial nitrate reduction. This could still lead to a growth benefit *via* electron sparing, whereby the removal of accumulated nitrite by Fe^{2+} results in accelerated proton translocation by respiratory complex I during heterotrophic nitrate reduction (Figure 4.1D). However, it is also possible that this nitrite-mediated Fe^{2+} oxidation would result in Fe^{3+} formation with no conservation of electrons and subsequently no energetic benefit for the cell.

Several proteins have been proposed as mediators of enzymatic Fe^{2+} oxidation among NDFO species. A system of electron transfer from Fe^{2+} using a membrane cytochrome (Cyc2) and rusticyanin (rus) - described by Liu et al. (2011) - has been proposed to drive lithotrophic NDFO within two mixed denitrifying cultures and one NDFO strain (He et al., 2016; He et al., 2017; Wang et al., 2020). Another involves a porin-cytochrome *c* protein complex (PCCC) - Pio/Mtr/MtoAB - which uses a cytochrome *c* (MtoA) embedded within a transmembrane porin (MtoB) in the outer membrane to shuttle electrons. Homologs for this system have been previously found in a NDFO microbe, *Dechloromonas aromatica* strain RCB (He et al., 2017). The PcoAB porin-periplasmic multicopper oxidase (MCO) complex is an alternative mechanism of electron transfer, structurally and functionally analogous to the PCCC system (He et al., 2017). OmpB and MofA are homologous Fe^{3+} and Mn oxidation MCOs, respectively. MofA/OmpB homologs, which may facilitate Fe^{2+} oxidation, have been identified in the *Gallionellaceae sp*. from the autotrophic KS mixed NDFO culture, as well as other aerobic Fe oxidisers (He et al., 2016; He et al., 2017).

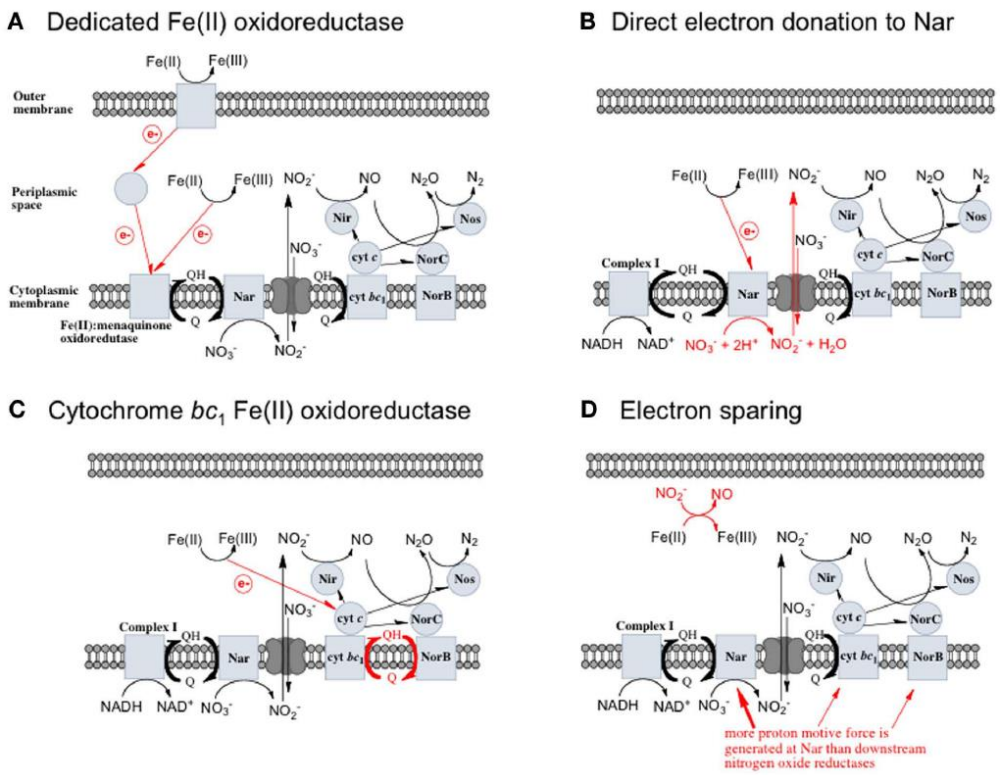

Figure 4.1. Four possible mechanisms of Fe^{2+} electron donation for energetic benefit in NDFO (Carlson et al., 2012): (A) the action of a putative periplasmic oxidoreductase; (B) electron donation to the Nar nitrate reductase; (C) reduction of the quinone pool via cytochrome bc_1; (D) electron sparing by accelerated activity of the Nar respiratory nitrate reductase relative to other nitrogen oxide reductases. In each case nitrate is reduced by the action of the Nar enzyme.

The presence of dedicated Fe^{2+} oxidoreductases and potential cytochrome bc_1-based mechanisms in NDFO organisms can be assessed by the sequencing and analysis of genomes. The genome sequences of two of the four organisms used in Chapter 2, *Thiobacillus denitrificans* and *Pseudogulbenkiania sp.* strain 2002, have already been published (Beller et al., 2006; Byrne-Bailey et al., 2012); in the case of *T. denitrificans*, a number of cytochromes of unknown function were identified which could be related to NDFO (Beller et al., 2006). However, the wider genomic dataset among NDFO microorganisms is limited to only a few strains, the majority of which were investigated by He et al. (2017) for potential NDFO related genes. Therefore, the addition of draft genomes for *Acidovorax sp.* strain BoFeN1 and *Paracoccus sp.* strain KS1 will contribute

to both the investigations of this thesis and future metagenomic studies across NDFO strains.

The influence of the Nar enzyme in NDFO can be examined by a knockout study, whereby a specific gene is deleted from the genome of an organism to investigate the effects of loss of function for the associated translated protein on a biological process. In this instance focusing on the contribution of Nar to NDFO. If Nar activity is the basis of, or a major contributor, to NDFO then all nitrate-reducing bacteria should be capable of the process as previously suggested by Carlson et al. (2013). For this reason, I chose *Salmonella enterica* Serovar Typhimurium strain SL1344 as a model organism for the knockout study, as a nitrate-reducing strain without prior reported evidence of NDFO. The comparison of the wild-type microorganism to a Nar knockout mutant under conditions promoting NDFO could be expected to reveal a disparity in the rate and extent of Fe oxidation.

The overarching goal of this Chapter is to investigate three of these hypothetical underlying mechanisms of NDFO metabolism through culture-dependent and independent methods.

This will be achieved by:

1) Sequencing and comparing the genomes of two microorganisms used in Chapters 2 and 3 (*Acidovorax sp.* strain BoFeN1 and *Paracoccus sp.* strain KS1) with previously published NDFO genomes to establish the presence or absence of common genes for putative oxidoreductases and systems of enzymatic Fe^{2+} oxidation using various analytical pipelines;

2) Quantifying the contribution of the Nar enzyme to NDFO metabolism in a heterotrophic nitrate-reducing bacterium, *Salmonella enterica* Serovar Typhimurium strain SL1344 (Hoiseth and Stocker, 1981) using a *Nar* gene knockout;

3) Assessing the contribution of nitrite accumulation and subsequent abiotic Fe^{2+} oxidation to NDFO by monitoring the effect of nitrite addition on Fe oxidation state in abiotic controls.

4.2 Methods

4.2.1 Genome analysis

4.2.1.1 Strain source and maintenance

The *Acidovorax sp.* strain BoFeN1 and *Paracoccus sp.* strain KS1, used in Chapters 2 & 3, were sourced from the Mineralogy, Material Physics and Cosmochemistry Institute (IMPMC) in Paris and the DSMZ culture collection in Leibniz, respectively. The two strains were maintained in pure culture in aerobic nutrient media (peptone 5.0 g L^{-1}, meat extract 3.0 g L^{-1}) at 30 °C prior to DNA extraction and sequencing of the genomes.

4.2.1.2 Draft genome sequencing and analysis

DNA extraction and sequencing of the genomes from pure cultures was performed externally by MicrobesNG (https://microbesng.uk/) using the Illumina Miseq platform using 2x250bp paired-end reads. Trimmed reads were produced using Trimmomatic version 0.30 (http://www.usadellab.org/cms/?page=trimmomatic) with a sliding window quality cut-off of Q15 and de novo assembly performed using SPAdes version 3.7 (http://cab.spbu.ru/software/spades/) (Bankevich et al., 2012; Bolger et al., 2014). Coverage of 30x was achieved during sequencing. Draft genome annotations were performed with the Rapid Annotation using Subsystem Technology (RAST) server version 2.0 (http://rast.nmpdr.org/rast.cgi) *via* the Classic RAST pipeline (Aziz et al., 2008), Blast KEGG Orthology And Links Annotation (BlastKOALA) tool version 2.2 (https://www.kegg.jp/blastkoala/) (Kanehisa et al., 2016) and using the NCBI Prokaryotic

Genome Annotation Pipeline (PGAP) tool (https://www.ncbi.nlm.nih.gov/genome/annotation_prok/) (Tatusova et al., 2016; Haft et al., 2018). tRNAs were identified from the annotated genome using the Aragorn version 1.1 tRNA detection program (http://mbio-serv2.mbioekol.lu.se/ARAGORN/) (Laslett and Canback, 2004).

Annotated genomes produced by these tools were screened for recognised enzymes that may catalyse Fe^{2+} oxidation and for putative ferroxidases. Genes of interest were then converted to amino acid sequences and matched to known proteins on the NCBI database using the Basic Local Alignment Search Tool (BLAST) (https://blast.ncbi.nlm.nih.gov/Blast.cgi) protein program (Altschul et al., 1990). Finally, nucleotide sequences for genes proposed as drivers of enzymatic NDFO (He et al., 2017) were aligned with the draft genomes from this study and complete genomes of the *Salmonella enterica* Serovar Typhimurium strain SL1344 used in this Chapter and of known NDFO microorganisms using the nucleotide BLAST program.

4.2.2 Nar enzyme knockout experiment

4.2.2.1 Source and maintenance of microorganisms

Cultures of *Salmonella enterica* Serovar Typhimurium strain SL1344 WT and the Δ*narGHIJ* mutant, in which the *nar* genes coding for the Nar respiratory nitrate reductase enzyme are deleted, were donated by the Rowley lab at the University of East Anglia (Rowley et al., 2012). The complete genome of the SL1344 strain has been sequenced previously (Kröger et al., 2012) and the wild-type genome contains two copies of the Nar respiratory nitrate reductase, which are absent in the mutant. The SL1344 genome also contains genes for the Nap periplasmic nitrate reductase, which will remain unaffected in both wild type and the mutant strains. The Nap enzyme is located within the periplasm,

unlike the transmembrane Nar enzyme, meaning Nap does not generate a proton motive force and thus does not contribute to ATP production (Kuypers et al., 2018). Therefore, the presence of this enzyme will not yield energy for growth as Nap is not able to generate a proton motive force (except when coupled to formate oxidation, which is not the case here) (Kern and Simon, 2009; Sparacino-Watkins et al., 2014). Indeed, the kinetics of nitrate reduction and nitrite accumulation in a Nap-deficient mutant of this strain were found to be not significantly different from the wild-type, further demonstrating the peripheral role of Nap in this organism (Rowley et al., 2012).

The mutant was created Rowley et al. (2012) using the lambda red recombination method (Datsenko and Wanner, 2000) targeting the *narG*, *narH*, *narI* and *narJ* genes coding for subunits of the Nar nitrate reductase enzyme, which were replaced with a kanamycin-resistance gene (Rowley et al., 2012). These strains were transported as agar stabs and maintained in aerobic LB (Lysogeny Broth) media (10 g L^{-1} tryptone, 10 g L^{-1} NaCl, 5 g L^{-1} yeast extract) at 37°C.

The vector pKD4, which was used to replace the *narGHIJ* genes, contains a kanamycin resistance gene. Therefore, screening for resistance to kanamycin (100 µg mL^{-1}) was used to identify the mutant.

4.2.3 Anaerobic growth

Anaerobic cultures were prepared by growing the strains in anoxic LB media (general anaerobic techniques are discussed in Section 2.2.2) (Bertani, 1951). The medium was prepared by adding 10 g L^{-1} tryptone, 5 g L^{-1} yeast extract, 10 g L^{-1} NaCl to boiled distilled water, which was cooled under a continuous flow of N_2 gas. A series of 10 mL aliquots were pipetted into Wheaton bottles under a continuous flow of N_2, and then stoppered and crimped with aluminium seals. These were flushed with a 90:10 N_2:CO_2 gas mixture *via*

the butyl rubber septa, with an unconnected needle to allow excess pressure to escape. The medium was inoculated with 100 µl of the SL1344 WT or Δ*narGHIJ* aerobic cultures using sterile syringes and needles, and incubated at 37 °C.

4.2.3.1 Preparation and inoculation

For the knockout experiment, triplicate cultures of SL1344 WT and SL1344 Δ*narGHIJ*, an abiotic nitrite-amended control and a negative control series were prepared (Figure 4.2).

Anoxic LB media (19.3 mL) was dispensed into 12 serum Wheaton bottles under an 80:15:5 N_2:CO_2:H_2 atmosphere in a COY anaerobic glove box. Nitrate was added to the SL1344 WT and Δ*narGHIJ* cultures and to the abiotic control series, whilst nitrite was added to the abiotic nitrite-amended series. The final concertation of nitrate (or nitrite for the abiotic nitrite series) in the medium was 4 mM (400 µL of a 200 mM stocks solution of $NaNO_3$ or $NaNO_2$, respectively was added). The media were inoculated with 100 µL aliquots of the two strains (anaerobically grown SL1344 WT and Δ*narGHIJ*) (4.2.3) and sterile LB media (abiotic nitrite-amended and nitrate control series). The final Fe^{2+} concentration in the medium was 10 mM (200 µL of a 1 M anoxic $FeSO_4$ stock solution was added). The Wheaton bottles were sealed with a butyl rubber stoppers and aluminium crimping, before flushing with 90:10 N_2:CO_2 and incubation at 37°C (Figure 4.2).

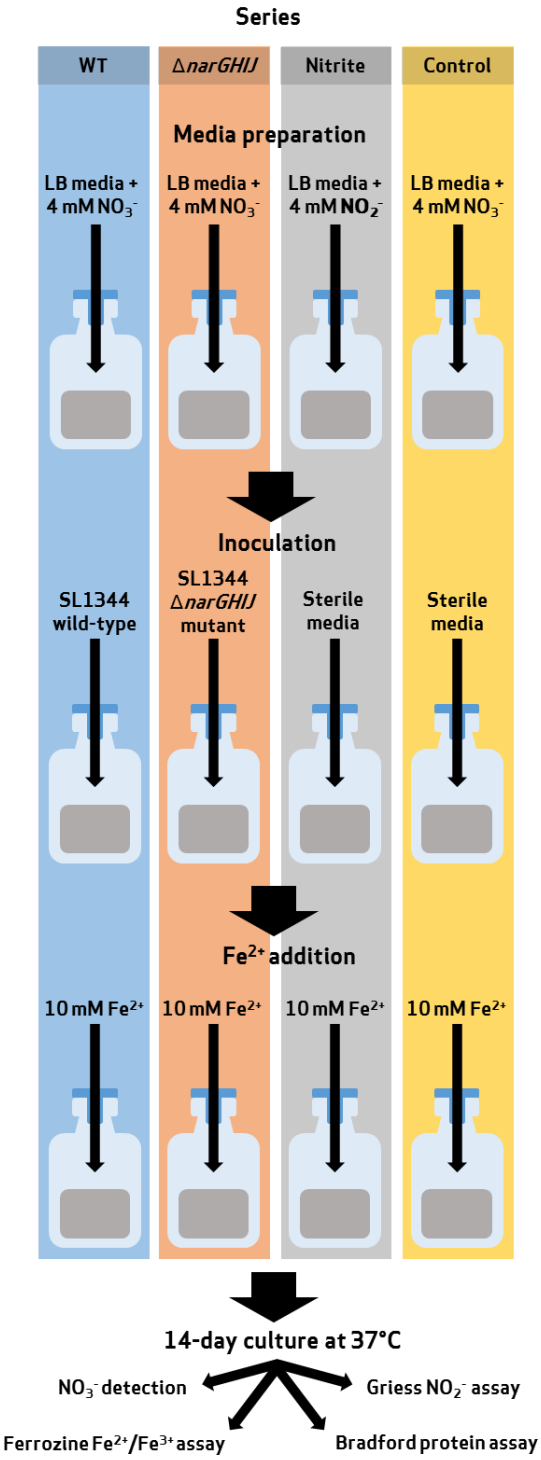

Figure 4.2. Preparation of Nar enzyme knockout experiment. Anaerobic lysogeny broth (amended with 4 mM NO_3^-) batch culture series are inoculated with either sterile LB (abiotic nitrite and nitrate control series), the wild-type (WT) or the Nar-deficient (Δ*narGHIJ*) mutant SL1344 organism. One series is amended with 4 mM NO_2^- (Nitrite) and inoculated with sterile LB. All cultures and controls are amended with 10 mM Fe^{2+} following the inoculation step and incubated at 37°C for 14 days, with regular samples taken for chemical analyses.

4.2.3.2 Chemical analyses

4.2.3.2.1 Sample collection

From each of the Wheaton bottles, 1.5 mL of sample was aseptically collected using a sterile N_2-flushed syringe at time-points of 0, 1, 2, 3, 4, 7 and 14 days, for chemical analysis. Unless otherwise stated, samples were sealed in 2 mL microcentrifuge tubes and stored at -20°C until removal for analysis. In addition, observations were made throughout the experiment regarding visible turbidity (indicating growth), precipitate formation and colour changes (associated with Fe oxidation).

4.2.3.2.2 Ferrozine assay

The ferrozine colourimetric assay (Stookey, 1970) was used to measure the reduced and total Fe concentration in the media. Incubation with HCl lyses cells and prevents abiotic oxidation of the Fe in the sample, allowing the Fe^{2+} concentration to be preserved for analysis. Hydroxylamine hydrochloride is added to a second sample along with HCl. This acts as a reducing agent, converting the Fe^{3+} present to Fe^{2+} and giving a representation of total Fe concentration in the cultures and controls. By comparing the Fe^{2+} and total Fe concentrations, we can determine the Fe^{2+}/Fe^{3+} ratio at regular time points and thus the rate of Fe oxidation.

For this analysis, 20 µL of medium was transferred immediately from the 1.5 ml main sample to two 1.5 mL microcentrifuge tubes, which contained 980 µL of 0.5 M HCl or 980 µL 0.5 M HCl and 0.3 M hydroxylamine hydrochloride. The tubes were incubated at room temperature for a minimum of one hour and then refrigerated at 4 °C for later analysis.

Ferrozine solution (1 g L^{-1} 3-(2-Pyridyl)-5,6-diphenyl-1,2,4-triazine-p,p′-disulfonic acid monosodium salt hydrate, 11.96 g L^{-1} HEPES) was prepared using milliQ water. 980 µL of ferrozine solution was added to 1 mL cuvettes and 20 µL of the HCl and hydroxylamine

hydrochloride digests was added and mixed by pipette. The optical density of the solution was measured using a Camspec M107 visible spectrophotometer at a wavelength of 592 nm.

Standards were prepared of 10 mM, 5 mM, 1 mM and 500 µM $FeSO_4$ and 20 µL was mixed with 980 µL of 0.5 M HCl in 1.5 mL microcentrifuge tubes. Ferrozine solution was added to the standards in the same manner as the samples and the absorbance was read at 592 nm. The standard curve was produced as a linear regression graph using Microsoft Excel and the line equation used to determine the Fe^{2+} concentration of the treated samples.

4.2.3.2.3 Bradford protein assay

The Bradford protein assay, described fully in Section 2.2.5, measured protein as a proxy for biomass production over the course of the experiment. This method was preferred to optical density measurements in monitoring growth because of the potential for the abiotic formation of Fe^{3+} oxide precipitates to give false positives.

Samples of 500 µL from each bottle were mixed with 420 µL of Tamm reagent (0.14 M oxalic acid, 0.2 M ammonium oxalate), which dissolved the amorphous Fe-bearing phases and lysed the cells. The protein was precipitated by adding 160 µL of 6.1 N trichloroacetic acid and the mixture centrifuged at 15, 500 × *g* for 30 minutes. The supernatant was removed *via* pipetting and the pellet (protein) resuspended in 500 µL 0.1 M NaOH. The resuspended protein was heated to 60 °C in a dry bath for 6 minutes in order to disrupt the secondary and tertiary structure of the proteins, allowing the dye to bind more effectively. As such, 250 µL of the sample was then mixed with an equal volume of Bradford reagent and the absorbance measured after 5 minutes in a Camspec M107 visible

spectrophotometer. γ-globulin was used as the protein standard, with 0 to 25 µg mL^{-1} prepared in 0.1 M NaOH solution. Standard curves were calculated as per Appendix B.

4.2.3.2.4 Griess reagent assay for nitrite

The Griess reagent assay is a colourimetric method of determining nitrite ion concentration in a solution, whereby the reaction of sulfanilic acid with 1-naphthylamine to produce red-pink azo compounds in the presence of nitrite ions is used as a proxy for nitrite concentration (Griess, 1879; Ivanov, 2004).

For the assay, 100 µL of sample was centrifuged at 15,500 × *g* for 10 minutes to pellet the solid components and the supernatant (50 µL) was transferred into a well of a 96-well flat-bottomed, optically clear ELISA microplate. 100 µL of 1 × Griess reagent solution (Sigma-Aldrich) was added to each well (150 µL total volume) and incubated at room temperature for 15 minutes. The absorbance was measured using a Bio-tek ELx808 microplate reader with a 540 nm filter KC4 software used for data output (Figure 4.3).

For this work, 100 µM, 50 µM, 25 µM, 10 µM, 5 µM, 2.5 µM and 1 µM $NaNO_2$ standards were prepared by diluting 100 mM $NaNO_2$ with 0.1 M NaOH solution. Standards were not centrifuged as there were no suspended solids to be removed.

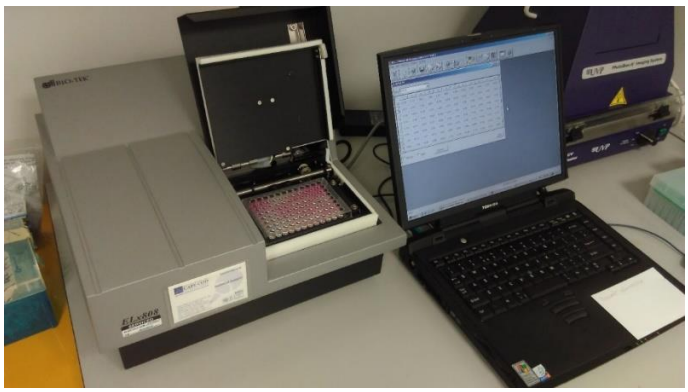

Figure 4.3. Griess regent assay for nitrite being carried out using a 96-well microplate, read in a Bio-tek ELx808 microplate reader at 540 nm.

4.2.3.2.5 Nitrate measurement

The concentration of nitrate ions was measured, prior to inoculation, in the nitrate-amended media and in each of the inoculated cultures and controls at 14 days using an ELIT 0821 ion selective $NO3^-$ electrode and ELIT 003 lithium acetate reference electrode (Nico2000) connected to a conductivity meter (HANNA instruments). Standards of 10 µM, 100 µM, 1 mM and 10 mM of $NaNO_3$ where prepared by dissolving $NaNO_3$ salt in milliQ water. A standard curve was prepared by plotting concentration against conductivity (mV). The nitrate concentration was determined using the line equation from the standard curve.

4.3 Results

4.3.1 Genome analysis

The draft genome of strain *Acidovorax sp*. strain BoFeN1 consisted of 4.06 Mb in 184 contigs (N50 = 37384), with a guanine-cytosine (GC) content of 63.77%. A total of 3,794 protein-coding sequences were predicted from the annotated genome, with 50 tRNAs identified. The closest match (% sequence similarity) for the 16S rRNA gene was (as identified in the GenBank database, using the BlastN program (https://blast.ncbi.nlm.nih.gov/Blast.cgi)) *Acidovorax defluvii* strain BSB411 (99% similarity; accession number NR_026506.1). The draft genome of *Paracoccus sp*. strain KS1 consisted of 4.16 Mb in 227 contigs (N50 = 36889), with a GC content of 67.69%. A total of 3,941 protein-coding sequences and 54 tRNAs were predicted from the annotated genome. The nearest 16S rRNA gene sequence was (as identified using BlastN) *Paracoccus pantotrophus* (100%; accession number AB098590.1). DDBJ/ENA/GenBank accession numbers have been assigned for *Acidovorax sp*. strain BoFeN1 (QOZT00000000) and *Paracoccus sp*. strain KS1 (QOZU00000000). Raw sequencing

reads for *Acidovorax sp.* strain BoFeN1 (SRP157586) and *Paracoccus sp.* strain KS1 (SRP157588) are available in the NCBI Sequence Read Archive.

Mapping of protein sequences to the most closely related genomes available on RAST revealed greater conservation between *Paracoccus sp.* strain KS1 and *Paracoccus denitrificans* strain PD1222 (Figure 4.5) than between *Acidovorax sp.* strain BoFeN1 and *Acidovorax sp.* strain JS42 and *Acidovorax avenae* subsp. *citrulli* strain AAC00-1, albeit with some highly conserved regions between BoFeN1 and JS42 (Figure 4.4). The most highly conserved regions between KS1 and *Paracoccus denitrificans* were related to methanol utilisation, periplasmic permeases, iron binding and transport. The few highly conserved regions between BoFeN1 and JS42 included a ferrodoxin reductase and tellurium resistance genes.

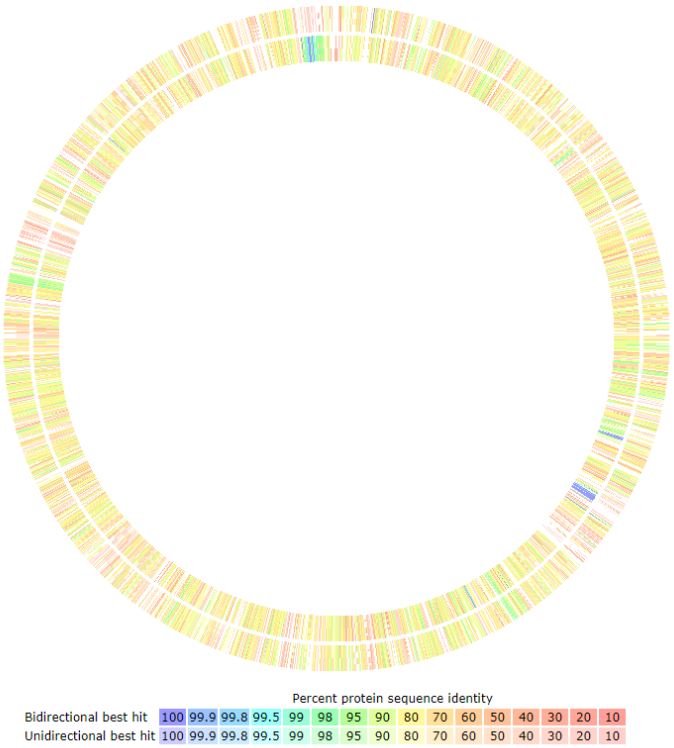

Figure 4.4. Protein sequence identity map of the Acidovorax sp. strain BoFeN1 genome against Acidovorax sp. strain JS42 (inner) and Acidovorax avenae subsp. citrulli strain AAC00-1 (outer).

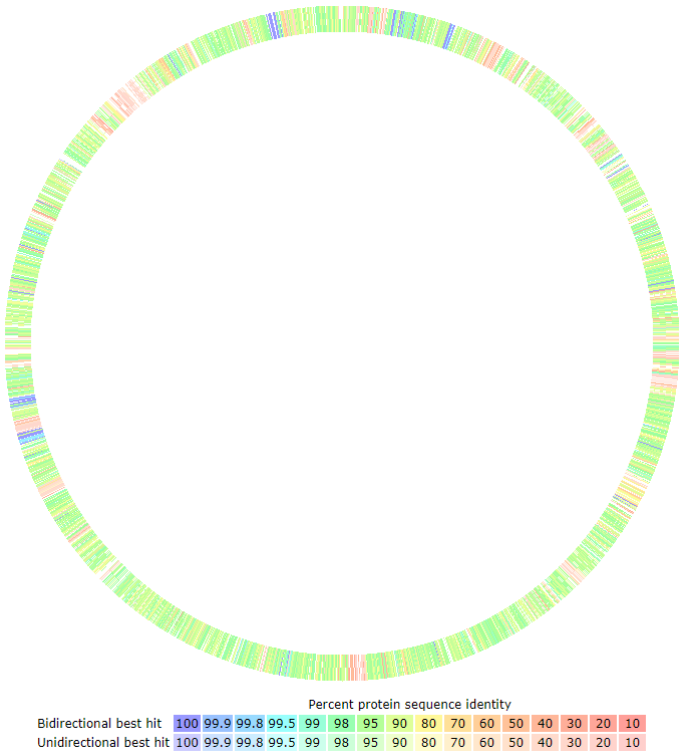

Figure 4.5. Protein sequence identity map of the Paracoccus sp. strain KS1 genome against Paracoccus denitrificans strain PD1222.

Full denitrification pathways were confirmed in both strains by the presence of nitrogen species reductase genes (*nar, nir, nor, nos*), with additional genes for a periplasmic nitrate reductase (*nap*) in the *Paracoccus pantotrophus* strain KS1 genome.

Both genomes contain numerous genes coding for cytochrome *b*- and *c*-type proteins as well as for enzymes related to iron uptake and metabolism, as identified by the three pipelines used. RAST detected a dedicated ferroxidase in BoFeN1 and KS1, but this was not replicated by the other tools. The BlastKOALA and PGAP annotation identified a ferrous iron transport protein (*feo*AB) in BoFeN1, and BlastKOALA found the same putative oxidoreductase (KEGG orthology: K15977) in both strains. However, neither was found in the RAST annotation. Bacterioferritin was found in the annotations of both genomes produced by BlastKOALA and PGAP (but not RAST), including three and two copies respectively in BoFeN1. PGAP and RAST did find a single copy of an iron-binding

ferritin-like antioxidant protein in both genomes at locations not matching the position of the bacterioferritin genes.

When the amino acid sequence for the RAST-identified ferroxidase was run through BLASTp, the protein was identified as "DNA starvation/stationary phase protection protein Dps", a ferritin homolog which protects DNA by sequestering Fe ions (Grant et al., 1998). Comparisons of the Fe redox and transport genes as identified by each annotation pipeline are shown in Table 4.1 and Table 4.2.

Table 4.1. Fe redox and transport-related genes of interest in Acidovorax sp. strain BoFeN1 as identified in different genome annotation pipelines.

Genes	**Function**	**RAST**	**BlastKOALA**	**PGAP**
feoAB	Fe^{2+} transport		✓	✓
Putative oxidoreductase	Unknown		✓	
hemH Ferrochelatase	Heme production	✓	✓	✓
Ferroxidase	Fe^{2+} oxidation	✓		
afuABC	Fe^{3+} transport			
Bacterioferritin	Fe^{2+} oxidation		✓	✓
Ferritin-like protein	Fe^{2+} oxidation	✓		✓
Ferric reductase	Fe uptake			✓
Iron ABC transporter permease	Fe uptake	✓		✓

Table 4.2. Fe redox and transport-related genes of interest in Paracoccus sp. strain KS1 as identified in different genome annotation pipelines.

Genes	**Function**	**RAST**	**BlastKOALA**	**PGAP**
feoAB	Fe^{2+} transport			
Putative oxidoreductase	Unknown		✓	
hemH Ferrochelatase	Heme production	✓	✓	✓
Ferroxidase	Fe^{2+} oxidation	✓		
afuABC	Fe^{3+} transport		✓	
Bacterioferritin	Fe^{2+} oxidation		✓	✓
Ferritin-like protein	Fe^{2+} oxidation	✓		
Ferric reductase	Fe uptake			
Iron ABC transporter permease	Fe uptake	✓		✓

Hypothetical oxidoreductases and within the two draft genomes - as identified by the annotation pipelines - were translated to amino acid sequences and identified using BLASTp. In *Acidovorax sp.* strain BoFeN1, a cytochrome c_4 and a transmembrane Fe permease were discovered. Cytochrome c_4 enzymes have been implicated in the Fe^{2+} oxidation pathway in *Thiobacillus ferrooxidans*, an acidophilic Fe^{2+} oxidiser (Cavazza et al., 1996), while Fe permeases - such as FeoAB - are involved in efficient Fe uptake from the immediate environment (Cartron et al., 2006). BLASTp did not identify putative membrane-associated oxidoreductase and in *Paracoccus sp.* strain KS1, there were no putative oxidoreductases with relevance to Fe acquisition or oxidation.

Nucleotide sequences coding for proteins of interest – those identified above and from proposed pathways of enzymatic Fe^{2+} oxidation in NDFO microorganisms (He et al., 2017) – were aligned against the draft genomes described here and other complete NDFO genomes. Neither *cyc2*, nor *rus*, nor significantly similar genes were identified in the sequenced or existing NDFO genomes analysed here. Both *Paracoccus* sp. strain KS1 and *T. denitrificans* returned significant hits for *pioAB* and *mofA* gene homologs and *pcoAB* returned a significant hit within the *T. denitrificans* genome. These results are summarised in Table 4.3.

Table 4.3. Fe redox and transport related genes identified across NDFO genomes sourced from this study and NCBI.

Genes	**Function**	**KS1**	**BoFeN1**	**2002**	***T. denitrificans***	**SL1344**	***F. placidus***	***A. oryzae* PS**
feoAB	Fe^{2+} transport		✓			✓	✓	✓
Putative oxidoreductase	Unknown	✓	✓	✓				✓
hemH Ferrochelatase	Heme production	✓	✓	✓	✓	✓		✓
Ferroxidase	Fe^{2+} oxidation	✓	✓	✓				
afuABC	Fe^{3+} transport	✓						
Bacterioferritin	Fe^{2+} oxidation	✓	✓	✓	✓	✓		✓
Ferritin	Fe^{2+} oxidation						✓	✓
Ferritin-like protein	Fe^{2+} oxidation	✓	✓	✓	✓	✓		✓
Ferric reductase	Fe uptake		✓	✓		✓		✓
Iron ABC transporter permease	Fe uptake	✓	✓	✓	✓		✓	✓
fieF	Fe^{2+} efflux					✓		
pio/mto/mtrAB	Fe^{2+} oxidation	✓			✓			
cyc2-rus	Fe^{2+} oxidation							
ompB/mofA	Metal oxidation	✓			✓			
pcoAB	Fe^{2+} oxidation				✓			

4.3.2 Nar knockout and abiotic nitrite experiments

The effect of the Nar enzyme on microbial growth and NDFO was investigated in the nitrate-reducing bacterium *Salmonella enterica* Serovar Typhimurum strain SL1344. This was assessed by comparing visible changes, protein concentration, Fe^{2+}/Fe^{3+} ratio and dissolved elemental composition during growth of the wild-type and a mutant lacking Nar enzyme production.

4.3.2.1 Visual observations

The progression of colour change of the blank medium from yellow to orange-brown (an indication of Fe^{3+} oxide formation) was the first observable difference between the four series during the experiment (Figure 4.6). At day 1, the nitrite-amended controls had become orange in colouration in comparison with the yellow of the other series, but this faded marginally at day 2, whereas an orange-brown colouration developed in the SL1344 WT cultures at day 2 and persisted throughout the remaining time points. Some slight orange-yellow colouration was observed in the liquid phase of the SL1344 Δ*narGHIJ* cultures at day 2 which gradually became less pronounced towards the end of the experiment. No colour change was observed in the nitrate control series.

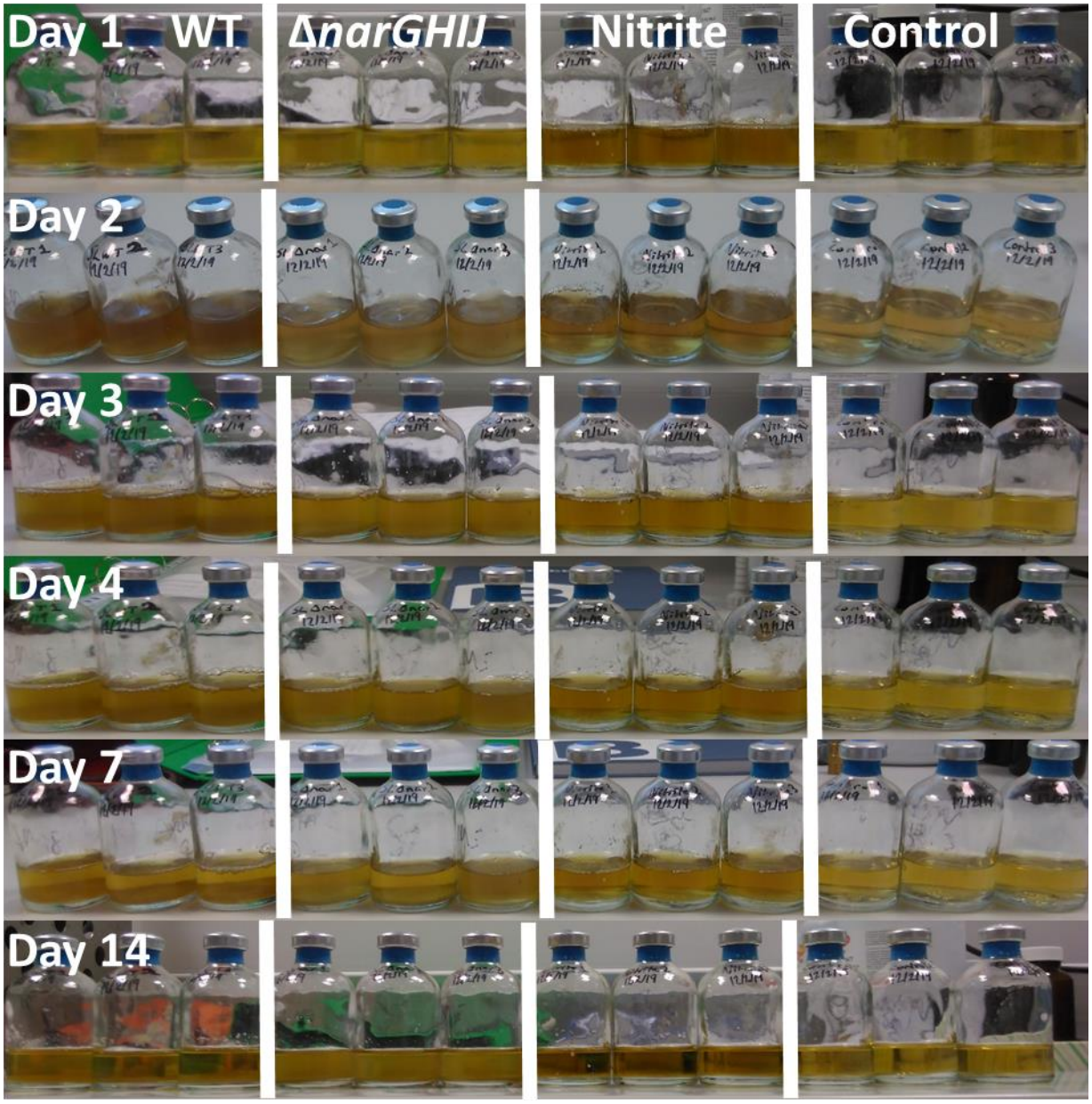

Figure 4.6. SL1344 WT, SL1344 Δ*narGHIJ*, nitrite-amended and control culture series at days 1-14. Orange colouration seen throughout in nitrite-amended series, developing from day 2 in SL1344 WT series. Turbidity evident from day 2 in SL1344 WT and Δ*narGHIJ* series.

Both the SL1344 WT and Δ*narGHIJ* culture series initially showed turbidity at day 2, which persisted at days 3 and 4 but became less intense thereafter, with the media column in two out of the three SL1344 WT cultures almost clear at day 14 (Figure 4.7). No turbidity was observed in either the abiotic nitrite-amended or nitrate control series.

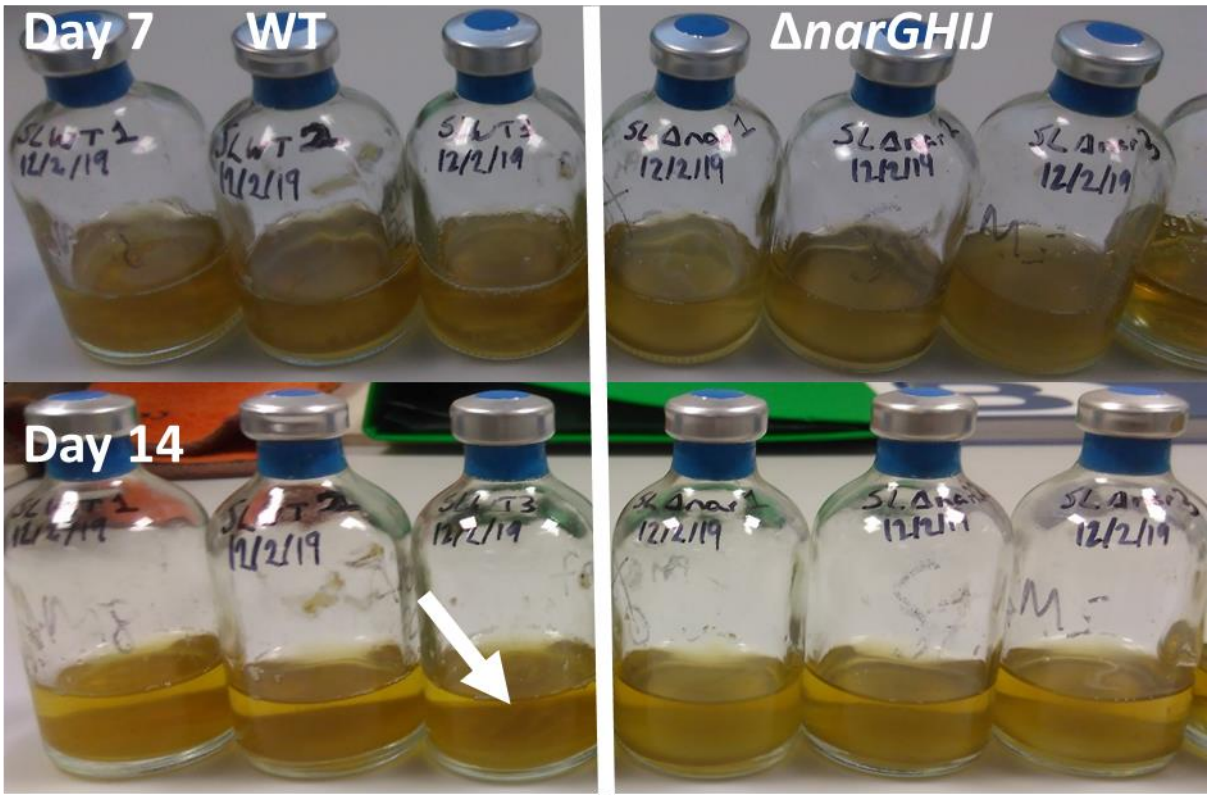

Figure 4.7. SL1344 WT and Δ*narGHIJ* cultures at day 7 and 14, displaying an accumulation of material at the base of the cultures. Wrinkling indicated by white arrow.

Though turbidity appeared to decrease at days 7 and 14 in the SL1344 WT and Δ*narGHIJ* cultures, orange or orange-yellow precipitate, respectively, accumulated at the base of the cultures towards the end of the experiment and formed a continuous layer by day 14. The precipitate displayed some wrinkling and mild elasticity when disturbed for sampling (Figure 4.7).

4.3.2.2 Microbial growth

Growth of the SL1344 WT and Δ*narGHIJ* strains was monitored throughout the experiment using the Bradford protein assay. Figure 4.8 demonstrates the mean protein concentration (normalised to the blank medium) for the two strains and the nitrate control. Both strains entered the exponential growth phase between inoculation and the first time point, displaying sharp increases in protein concentration over the first two days of the experiment. For both strains, the protein concentration plateaued after two days at

approximately 35 µg mL^{-1} and remained relatively constant, suggesting that the cells had reached stationary phase. By contrast, no notable variation was observed in the nitrite-amended control series from the protein concentration in the blank medium, remaining <3 µg mL^{-1}.

Given that turbidity - which might indicate contamination - was not observed in either abiotic series, it can be surmised that the ~5 µg mL^{-1} normalised baseline for protein concentration measured at day 0 in all culture series (Appendix C) is attributable to proteinaceous components of the LB media, yeast extract and tryptone.

From the results of the protein assay (Figure 4.8) and turbidity observations (Figure 4.6), clear growth is evident in both strains, with the wrinkled and elastic layers (Figure 4.7) forming at a later time point. This suggests the formation of biofilms (Serra et al., 2013; Cairns et al., 2014).

4.3.2.3 Nitrite concentration

The Griess assay was used to measure the production of nitrite through biological nitrate reduction and the depletion of nitrite due to abiotic reactions in the nitrite-amended control series (Figure 4.9). In the SL1344 WT cultures, the nitrite concentration increased rapidly between day 1 and day 2 where the concentration peaked at 132.4 µM (±15.2), coinciding with the end of the exponential growth phase in both strains and linking growth phase to nitrate reduction in these organisms.

The concentration then gradually declined to 41.1 µM during the stationary growth phase and remained below 50 µM until the end of the experiment. The SL1344 Δ*narGHIJ* cultures followed the same trend as the WT cultures, albeit a lower concentration of nitrite (65.9 µM ± 3.0) was measured at day 2 followed by a gradual decline continuing to 7.7 µM (±0.3) at day 14.

The nitrite concentration in the nitrite controls, decreased from a 4 mM initial concentration to 89.4 µM (±4.3) at day 1 and eventually to 15.6 µM (±1.2) by day 14, as shown in Figure 4.9. This suggests a period of rapid abiotic reactions after which the nitrite concentration became a limiting factor and slowed the subsequent reaction rate. Though Fe^{2+} was depleted between day 0 and 1, this reactant was not rate-limiting at later timepoints when the Fe^{2+}/Fe_{total} ratio was between 0.7.and 0.8 (Figure 4.9).

The nitrite in the abiotic control series remained around 1 µM throughout, near the lower detection limit of the assay, indicating abiotic oxidation of Fe^{2+} by nitrate was minimal or absent.

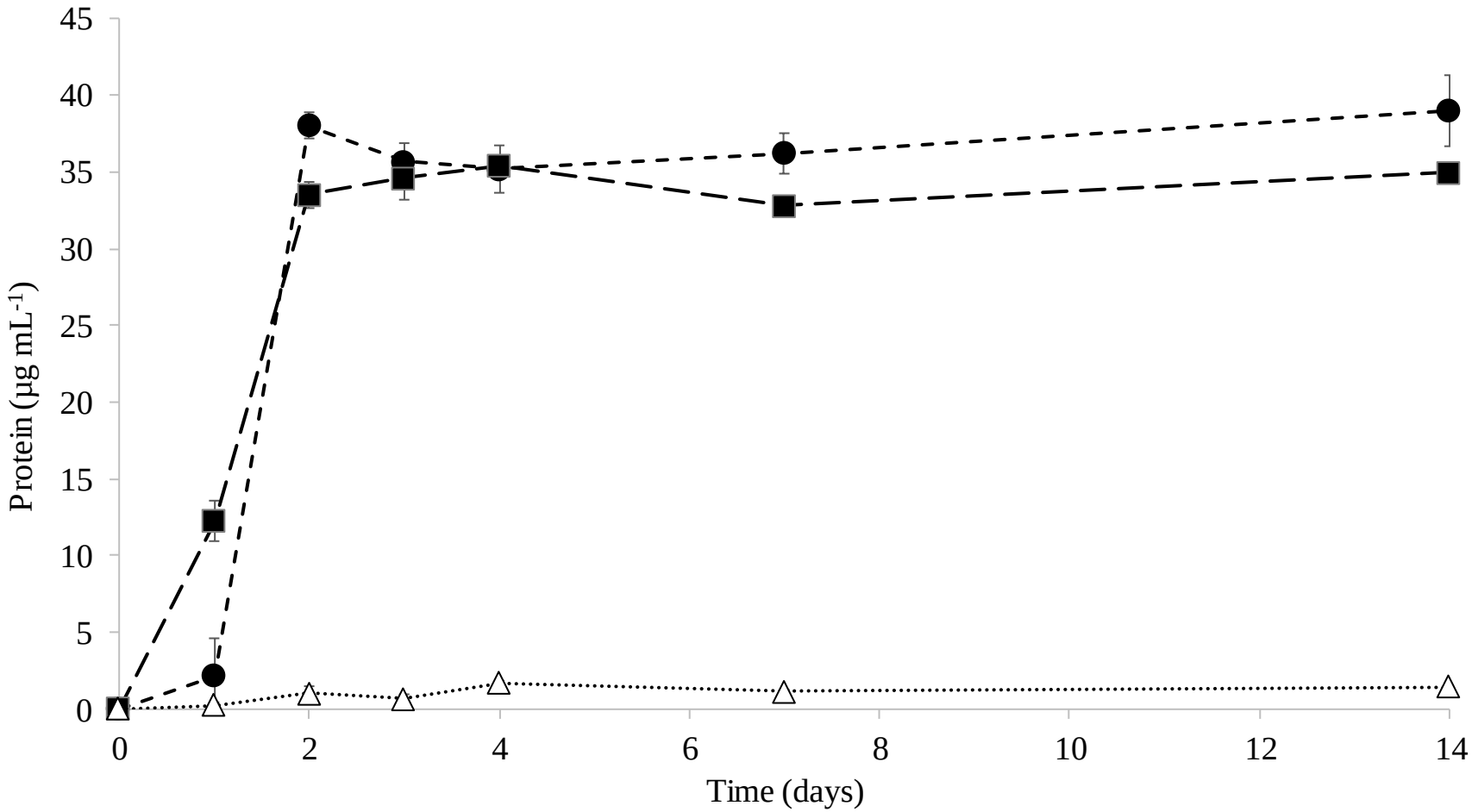

Figure 4.8. Protein concentration over time for SL1344 WT (filled circles), SL1344 *ΔnarGHIJ* (filled squares) and abiotic nitrite-amended (open triangles) series. Values are normalised against the blank medium. Error bars represent ±SE.

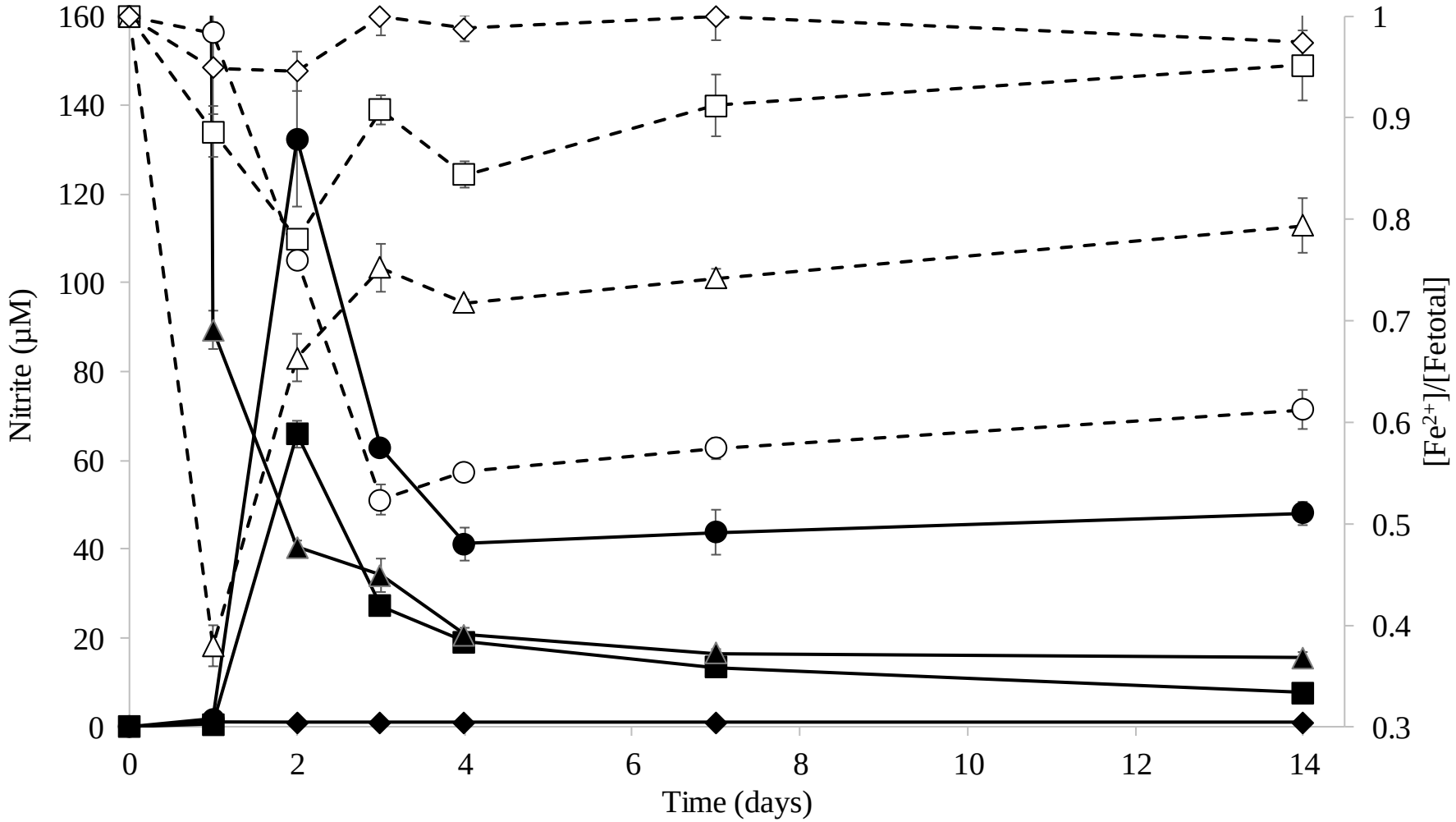

Figure 4.9. Fe^{2+}/Fe_{total} (open symbols, dotted lines) and nitrite (filled symbols, solid lines) ion concentration over time for SL1344 WT (circles), SL1344 Δ*narGHIJ* (squares), abiotic nitrite-amended (triangles) and control (diamonds) series. NO_2^- value at day 0 for the nitrite-amended series was 4 mM = 4000 µM. Error bars represent ±SE.

4.3.2.4 Fe oxidation state

The Ferrozine assay tracked the ratio of Fe^{2+} to Fe_{total} and thus the oxidation state of the Fe present in cultures and controls throughout the 14-day experimental period (Figure 4.9). For example, an Fe^{2+}/Fe_{total} value of 1 indicates 100% Fe^{2+}, whereas 0.5 indicates 50% Fe^{2+} and 50% Fe^{3+}.

There was an immediate decrease in the Fe^{2+}/Fe_{total} ratio from 1 to 0.38 (±0.02) after the first 24 hours in the nitrite-amended abiotic series, which indicates that 62% of the Fe was oxidised at this point, approximately agreeing with the extent of abiotic Fe^{2+} oxidation achieved by 4 mM nitrite under acidic conditions as reported by Klueglein and Kappler (2013). The Fe^{2+}/Fe_{total} ratio then recovered to 0.75 (±0.02) by day 3 and did not change significantly throughout the remaining time points. After the depletion of nitrite from 4 mM to <50 µM by day 2, it is likely that Fe^{2+} oxidation by the remaining nitrite was overtaken by the rate at which Fe^{3+} was abiotically reduced by organic components in the LB media.

Fe oxidation (Figure 4.9) progressed until day 3 in SL1344 WT cultures before stabilising at an Fe^{2+}/Fe_{total} value of 0.52 (±0.01), with a minor reversal to 0.61 (±0.02) by day 14. The continued increase in Fe^{3+} after the nitrite peak at day 2 in SL1344 WT cultures could be because the rate of Fe oxidation by nitrite ions at micromolar concentrations continued to exceed abiotic reduction until a dynamic equilibrium was reached. Biogenic nitrite ions were rapidly produced during growth between day 1 and day 2, in excess of the abiotic oxidation rate. When growth slowed, so did the production of nitrite ions, which began to deplete by further oxidising dissolved Fe^{2+} up to day 3. After this point, the reducing media and oxidation from the continued Nar-driven supply of nitrite reached an equilibrium, allowing Fe to remain partially oxidised even under reducing conditions.

In contrast, exponential growth of the SL1344 Δ*narGHIJ* knock out mutant caused the Fe^{2+}/Fe_{total} ratio to decrease from 1 to 0.78 (±0.01) between day 0 and day 2. The ratio then increased again to 0.91 (±0.03) at day 3 and was at 0.95 (±0.03) by the conclusion of the experiment, providing an inverse of the trend in nitrite accumulation for that organism.

The Fe^{2+}/Fe_{total} ratio in the abiotic control series remained between 1 (±0.02) and 0.95 (±0.05) throughout the experiment.

4.3.2.5 Nitrate Depletion

Over the 14 days, the nitrate concentration in the SL1344 WT cultures depleted by 56.9% (±1.7%) relative to the 4 mM starting concentration (Figure 4.10). The depletion over the same period was 19.7% (±3.7%) for the SL1344 Δ*narGHIJ* series and 4.0% (±1.0%) in the control.

The nitrate depletion correlates proportionally to the extent of nitrite production in the same cultures, providing further evidence for both microbial nitrate reduction and the partial inhibition of this process in the *nar*-deficient mutant. Nitrate consumption and nitrite production, but not growth, also mirrored the Fe^{2+} oxidation observed in each series in the SL1344 WT and Δ*narGHIJ* series. This indicates that microbial nitrate reduction and Fe^{2+} oxidation are intrinsically linked to one another in this instance, but not to increased biomass production.

The nitrite-amended control series is not shown as no nitrate was present in the initial media composition.

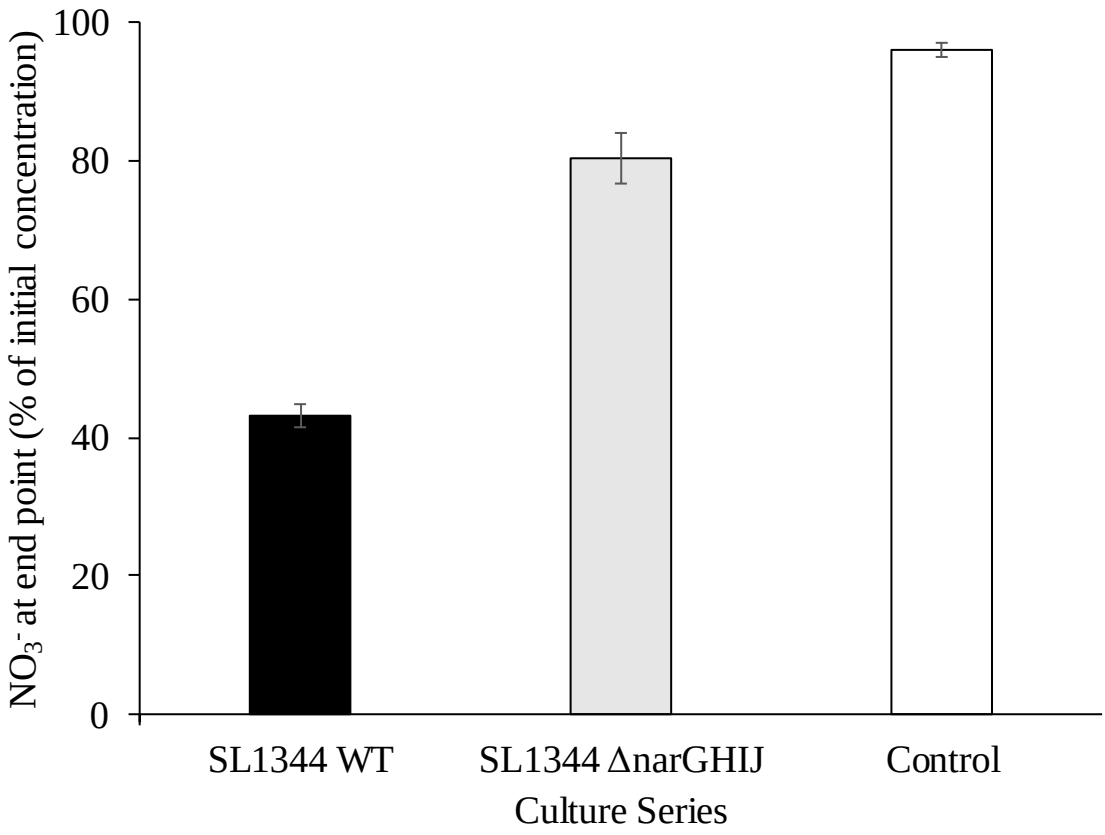

Figure 4.10. End-point nitrate concentrations as a percentage of the initial media concentration (4 mM) by culture series Salmonella enterica Serovar Typhimurium strain SL1344 wild-type (SL1344 WT), *ΔnarGHIJ* (SL1344 ΔnarGHIJ) and the control. Error bars represent ±SE.

4.4 Discussion

This Chapter has investigated three of the proposed mechanisms of microbial NDFO. Genome analysis was used to search for evidence of a hypothesised dedicated Fe^{2+} oxidoreductase which would allow conservation of electrons from Fe^{2+} for ATP generation and growth. The knockout study assessed the importance of the Nar respiratory nitrate reductase in NDFO and whether this enzyme could drive growth based on electrons directly donated from Fe^{2+}. Finally, the involvement of abiotic reactions between biogenic nitrite and Fe^{2+} was quantified in a parallel series by monitoring Fe oxidation states when spiked with nitrite.

4.4.1 Hypothesis 1 – enzymatic Fe^{2+} oxidation

To investigate the enzymatic hypotheses of NDFO illustrated in Figure 4.1A and C, existing genomes from NDFO strains were examined and two new draft genomes were sequenced.

Multiple enzymes associated with the control of the redox state and transport of iron are present in both published and newly-sequenced genomes, suggesting that an enzymatically-mediated mechanism NDFO in these organisms remains a possibility. Ferroxidases (also known as Fe^{2+}: oxygen oxidoreductases) were identified in both KS1 and BoFeN1 genomes by RAST, as well as in the annotated genome for *Pseudogulbenkiania sp.* strain 2002. These three strains were shown to grow under autotrophic conditions in Chapter 2. Ferroxidase enzymes catalyse the oxidation of Fe^{2+} by oxygen (Sarkar et al., 2003). This confirms that some enzymatic means of Fe^{2+} oxidation exists in both KS1 and BoFeN1, albeit linked to oxygen rather than nitrate. However, the primary function of Dps – the protein identified to the ferroxidases through BLAST – is to bind and protect DNA by catalysing Fe^{2+} oxidation as a detoxification strategy (Ren et al.,

2003). It is not clear, therefore, whether the release of electrons during this process would contribute to the electron transport chain at the periplasm. Other enzymes with ferroxidase activity include bacterioferritin (Andrews, 1998), identified in both strains by BlastKOALA and PGAP. However, ferritin proteins are a near-universal system of Fe storage among all three domains of life and cannot be specifically correlated to NDFO (Seckback, 1982; Theil, 2004). Indeed, bacterioferritin or ferritin protein genes were found in every NDFO genome available, including both bacterial and archaeal genomes.

Finding the same putative oxidoreductase in both draft genomes, along with *Pseudogulbenkiania sp.* strain 2002 and *Azospira oryzae* strain PS, is noteworthy in screening for a common mechanism across NDFO organisms. However, this gene does not appear to be linked to Fe^{2+} oxidation based on the function of the surrounding coding regions in the organisms in which it was characterised (Töwe et al., 2007; Van Duy et al., 2007).

The presence of ferric reductase in the BoFeN1 genome hints at Fe^{3+} reduction capability for respiratory or assimilatory purposes in this organism. The BoFeN1 genome also contains multiple genes for flavin reductases, which are the most common form of enzyme with ferric reductase activity (Schröder et al., 2003).

Disparities between multiple annotations of the same draft genome are not uncommon because of the different analytical pipelines and databases used, therefore it is unsurprising that the RAST, BlastKOALA and PGAP tools feature some differences. Additionally, the investigation of draft genomes always carries a risk that some genes may be split over two contigs. This disruption of sequences can result in annotation programs missing otherwise recognisable genes. This problem is mitigated in complete prokaryotic genomes, where contig ends are matched to provide a fully closed chromosome.

Using available genomes of NDFO microorganisms, it is possible to gain a broader context for the commonality of the iron redox and transport-related genes identified in the genomes of KS1 and BoFeN1 here. It is evident that there is a common presence for ferroxidase genes and orthologous ferritin and bacterioferritin, which can catalyse the oxidation of Fe^{2+} to Fe^{3+} (Le Brun et al., 1995) across the strains shown to grow autotrophically in the experiments of Chapter 2.

Among the NDFO genomes analysed here, *T. denitrificans* and *Paracoccus sp*. strain KS1 were the only organisms to return significant hits for genes identified in the potential electron transfer systems for NDFO put forward by He et al. (2017). In the absence of other candidate mechanisms for autotrophic growth by NDFO in *Paracoccus sp*. strain KS1, it can be proposed that one or a combination of the MtoAB and MofA systems may allow for enzymatic Fe^{2+} oxidation in this strain.

If these are indeed the underlying mechanisms of enzymatic NDFO, it is unexpected that the genomes of neither *Acidovorax sp*. strain BoFeN1 nor *Pseudogulbenkiania sp*. strain 2002 -both of which grew autotrophically in Chapters 2 and 3 – appear to contain these genes. It is possible, then, that NDFO in these organisms is reliant upon a system of electron acquisition and transfer from Fe^{2+} that remains undetermined. The discovery of an uncharacterised membrane-associated oxidoreductase and cytochrome c_4-family enzymes within the draft genome of *Acidovorax sp*. strain BoFeN1 suggests there is yet more to be discovered regarding enzyme-mediated mechanisms of lithoautotrophic NDFO.

4.4.2 Hypothesis 2 – electron donation from Fe^{2+} to the Nar enzyme

If NDFO were linked by direct electron donation to Nar from Fe^{2+} as hypothesised, it should be expected that the WT cultures would have generated greater biomass than the Δ*narGHIJ* cultures, in proportion to the consumption of nitrate and oxidation of Fe^{2+}. The

concentrations of biomass in SL1344 WT and Δ*narGHIJ* cultures are comparable throughout the growth experiment. However, Fe oxidation progressed to a significantly greater extent in the WT series than in Δ*narGHIJ* (Figure 4.9), which suggests that NDFO is not linked to growth of SL1344 in this experiment.

The explanation for the similar trends of Fe oxidation and nitrite accumulation between the SL1344 WT and Δ*narGHIJ* series could be that the periplasmic nitrate reductase capacity in the Δ*narGHIJ* mutant still allows for some accumulation of nitrite and oxidation of Fe^{2+} during the exponential growth phase up to day 2. After this point,qs the abiotic oxidation of Fe^{2+} by nitrite outstrips nitrite production in the stationary phase culture and Fe^{2+} is abiotically reduced to Fe^{3+} as described for the nitrite-amended series. Whereas, the undiminished nitrate reducing ability of the SL1344 WT allowed the stationary phase culture to maintain 40-50 µM nitrite in solution between day 3 and 14, a sufficient concentration to reach dynamic equilibrium with the abiotic Fe^{3+} reduction processes. Given the absence of Nar and the presence of only the Nap periplasmic nitrate reductase in SL1344 Δ*narGHIJ*, Nap activity may be linked to the exponential growth phase and nitrite production is stopped or slowed in stationary phase to such an extent that abiotic reactions with Fe^{2+} consume the remaining nitrite in a correlation with the depletion of the abiotic nitrite-amended control.

4.4.3 Hypothesis 3 – abiotic reactions of Fe^{2+} with biogenic nitrite

Nitrite ion accumulation (Figure 4.9) peaked at day 2 for both SL1344 cultures, suggesting biogenic nitrite production is associated with the exponential growth phase. The nitrite concentration continuously fell after day 2 in SL1344 Δ*narGHIJ* cultures until the end point, which tracked the depletion of nitrite ions of the abiotic nitrite-amended control series. This indicates that the biological mechanism for nitrite formation (Nap) was

reduced beyond day 2 in the SL1344 Δ*narGHIJ* cultures, whereas the nitrite was continually produced after day 4 in the SL1344 WT cultures. The plateau in nitrite concentration after day 4 in SL1344 WT contrasts with depletion in the abiotic nitrite-amended series and necessitates a continually active formation mechanism in stationary phase. In this case, that mechanism is likely to be respiratory nitrate reduction catalysed by the Nar enzyme.

The persistent partial oxidation of Fe in the presence of the SL1344 WT organism suggests that it is the presence and activity of Nar as a source of nitrite ions that drives the greater extent of observed NDFO, compared with SL1344 Δ*narGHIJ*, in this experiment. In the absence of evidence for the other hypotheses in this organism, nitrite-mediated oxidation is likely to be the sole or dominant mechanism for the Fe^{2+} oxidation observed.

4.4.4 The overall picture

From the combined results of this experiment, it is possible to say that the activity of the Nar respiratory nitrate reductase, *via* the production of nitrite ions, contributes to Fe oxidation and maintenance of Fe^{3+} under chemically reducing conditions that favour the existence of Fe^{2+}. This result has several implications, first among which is the confirmation that the interaction of biogenic nitrites with Fe^{2+} ions is likely to be a key contributor to NDFO. This supports previous findings in suggesting that all nitrate-reducing species are likely capable of NDFO (Carlson et al., 2013) *via* the abiotic reaction of nitrite with Fe^{2+} (Klueglein and Kappler, 2013; Klueglein et al., 2014; Klüglein et al., 2015). Taken together with the protein measurements, which showed parallel growth in SL1344 WT and Δ*narGHIJ*, this study does not support a growth benefit from Fe oxidation in this species or others with the same mechanism of NDFO. This is in contrast to previous studies (Hafenbradl et al., 1996; Straub et al., 1996; Weber et al., 2006b) and

indicates another mechanism is at play if chemolithoautotrophic growth by NDFO is a true phenomenon, as suggested by the results of Chapter 2.

4.4.5 The martian perspective

The relevance of these results within the context of early martian environments is that NDFO, in the form exhibited here by SL1344, would not be able to drive chemolithotrophic primary production as proposed in Chapter 1. However, this does not remove the potential for NDFO to be a mechanism of Fe^{3+} production and associated biomineralisation under reducing conditions. Heterotrophic nitrate reducers utilising the endogenous organic carbon sources within the martian surface and near-subsurface environments (Eigenbrode et al., 2018) would still produce biogenic nitrite, which is shown here to be an effective oxidant of Fe^{2+} under reducing conditions.

Further, the identification of numerous established and candidate iron redox proteins across the KS1 and BoFeN1 draft genomes and other previously published NDFO genomes ensures that a mechanism of electron conservation from NDFO that could have driven microbial growth on past Mars. More extensive experimental analysis is required in order to fully investigate those potential metabolic pathways.

4.4.6 Future work

In terms of finding common Fe redox-related genes, new tools currently in development, such as FeGenie (Garber et al., 2019), which specifically targets iron metabolic pathways in genomes, and metagenomic datasets will greatly enhance capability for comparative genomic analyses among distantly related NDFO microorganisms.

The genes of interest identified here could be targeted by future knockout experiments in species reported by other studies to grow lithotrophically using NDFO, such as *Pseudogulbenkiania sp.* strain 2002 (Weber et al., 2006b). An attempt to silence NDFO

has been attempted for the closely-related *Pseudogulbenkiania sp*. strain NH8B using transposon mutagenesis, without success (Ishii et al., 2016).

The conclusions of the knockout experiment are limited by the presence of an alternative nitrate reductase (Nap) in the genome of SL1344, which complicates the interpretation of results. The SL1344 wild-type genome contains two copies of the *narGHIJ* genes coding for the Nar respiratory nitrate reductase and *napABCDFGH* for the Nap periplasmic nitrate reductase. Though the *nar* genes have been deleted in the SL1344 mutant used in the knockout experiment, the *nap* operon remains intact. The activity of NapA, the terminal reductase can be linked to respiration by nitrate reduction by the presence of NapC and NapH quinone oxidases (Sparacino-Watkins et al., 2014), the genes for which are present in the SL1344 genome. It is possible then, that the knockout mutant could have retained some capacity for respiratory nitrate reduction without ATP generation, as has been suggested previously (Jepson et al., 2007). A future experiment could create a knockout mutant from a strain with no alternative nitrate reductase capabilities in order to fully isolate the impact of the loss of nitrate reductase activity on Fe^{2+} oxidation.

Additionally, the SL1344 is not previously described as performing NDFO in the environment and requires rich media for growth. To make more robust conclusions about the role of Nar in NDFO under more environmentally relevant conditions, it would be preferable to create a Nar knockout from one of the strains previously reported to conduct NDFO under autotrophic conditions.

4.4.7 Conclusions

Multiple NDFO microbe genomes contain genes coding for enzymes potentially capable of catalysing Fe^{2+} oxidation. Therefore, the proposed involvement of direct enzymatic activity in the donation of electrons to microbial energy metabolism during NDFO for some organisms cannot yet be ruled out. Future knockout experiments should target these genes of interest to investigate the effect upon growth rate and NDFO in these species.

The deletion of *narGHIJ* genes, which code for the Nar respiratory nitrate reductase, inhibited the oxidation of Fe^{2+} but not growth in the nitrate-reducing bacterium *Salmonella enterica* Serovar Typhimurium strain SL1344 relative to a wild-type of this strain under heterotrophic conditions. The presence of a Nap periplasmic nitrate reductase in the SL1344 genome allowed nitrate reduction to occur in the SL1344 Δ*narGHIJ* knockout mutant to a lesser extent than in SL1344 WT, mirrored in a smaller Fe^{2+}/Fe_{total} shift indicating a limited amount of oxidation. The increased extent of Fe^{2+} oxidation in the presence of Nar supports the integral involvement of this enzyme in NDFO. However, the lack of divergence in biomass production between the wild-type and mutant suggest that there was no direct electron donation from Fe^{2+} to Nar for respiration in this example. Therefore, the most likely explanation for the role of Nar in NDFO here is the production of nitrite ions which subsequently oxidise Fe^{2+} abiotically.

Addition of abiotic nitrite can produce similar extents of Fe^{2+}oxidation as the growth of NDFO strains under anaerobic heterotrophic conditions. Together with the results of the Nar knockout study, this suggests NDFO observed in heterotrophic species with no growth benefit is likely to be predominantly due to the abiotic reaction of biogenic nitrite with Fe^{2+} ions.

5. Discussion and Future Work

This thesis has assessed the ability of nitrate dependent Fe^{2+} oxidation (NDFO) metabolism, driven by the redox pairing of Fe^{2+} oxidation and nitrate reduction, to support life in the context of early martian environments. The work undertaken examined:

1) The underlying mechanisms of NDFO energy metabolism and therefore the feasibility for NDFO-based primary production to drive an early martian biosphere.

2) The ability of nitrate-dependent Fe^{2+} oxidising (NDFO) strains to utilise Fe^{2+} for growth from a Mars-relevant mineral substrate.

3) The capability of NDFO strains to metabolise and grow under the simulated chemical conditions of ancient martian fluids.

4) The extent of biomineralisation processes associated with NDFO growth in the above conditions as a formation mechanism for morphological biomarkers.

5.1 Biochemical mechanisms of NDFO

Though NDFO has been recognised since the 1990s (Hafenbradl et al., 1996; Straub et al., 1996), the underlying biochemical mechanisms have been an ongoing source of controversy with multiple competing hypotheses for the putative pathway of electron transfer (Carlson et al., 2012). The results of this thesis add to the growing body of literature that seeks to elucidate these biochemical pathways and the contribution of the Fe^{2+} oxidation half-reaction to microbial energy metabolism.

A nitrate reductase gene knockout study - using *Salmonella enterica* serovar Typhimurium strain SL1344 - revealed that NDFO is a side effect of heterotrophic nitrate reduction. In this organism, nitrite ions – produced by nitrate reductases - abiotically oxidise dissolved Fe^{2+} as suggested in previous studies (Klueglein and Kappler, 2013; Klueglein et al., 2014; Klüglein et al., 2015; Ishii et al., 2016). This conclusion agrees with the prediction of

Carlson et al. (2012) that all nitrate reducers may be innately capable of Fe^{2+} oxidation, which has also been supported by studies in other species (Carlson et al., 2013). It should be noted that the secondary nitrate reductase (Nap) present in the SL1344 strain and life cycle as a mammalian pathogen limits the usefulness of this strain as a model organism, and this could be substituted in future NDFO studies.

The hypothesis that NDFO-based energy metabolism can be driven by direct donation of electrons from Fe^{2+} to the Nar respiratory nitrate reductase was not supported by the knockout study in Chapter 4. NDFO was inhibited in the mutated SL1344 strain lacking Nar, whereas growth rate was comparable to the wild-type organism, thereby demonstrating that Nar was not a route for electrons entering the transport chain within the SL1344 strain used. There is some evidence to suggest that the Nar enzyme can still contribute directly to oxidation, without retaining electrons for energy metabolism (Carlson et al., 2013), though the efficient oxidation of Fe^{2+} by an abiotic nitrite control - and mirrored patterns of nitrite accumulation and Fe^{2+} oxidation - suggest that nitrite reactions are the dominant mechanism in the Chapter 4 knockout study.

Despite the findings of the knockout study, investigations of newly-sequenced NDFO genomes – *Acidovorax sp.* strain BoFeN1 and *Paracoccus sp.* strain KS1 - identified several genes potentially linked to a Fe^{2+} oxidation mechanism in strains which appeared to grow autotrophically by NDFO. This suggests that a direct enzymatic Fe^{2+} oxidation pathway is possible for some NDFO strains, but this requires more extensive investigation.

A mechanism involving electron donation between a membrane cytochrome (cyc2) and rusticyanin (rus) has been described by Liu et al. (2011) and is proposed to drive lithotrophic NDFO in *Hyphomicrobium* within mixed denitrifying cultures (Wang et al., 2020). Though *cyc2* and *rus* or significantly similar genes were not identified in the newly

sequenced or existing NDFO genomes analysed in Chapter 4, this example demonstrates a template for enzymatic Fe^{2+} oxidation which may be analogous to the mechanism in other species. Such a mechanism could allow for the lithotrophic growth seen in Chapters 2 and 3, which primarily tested metabolic activity and growth of NDFO organisms in relation to martian substrates and brines, respectively.

Active metabolism and growth were demonstrated in two simulated martian brines and with olivine (as a source of Fe^{2+}), a finding which supports the existence of a mechanism for electron acquisition from Fe^{2+} and retention in the electron transport chain. Specifically, growth of *Acidovorax sp*. strain BoFeN1 cultures using Fe^{2+} from olivine in Chapter 2 (in which soluble Fe^{2+} was detectably consumed) was significantly greater than when grown in the Shergottite and Contemporary Mars brines in Chapter 3 (in which microbial Fe^{2+} consumption was not detectable).

The addition of a carbon source increased the specific growth rate of *Acidovorax sp*. strain BoFeN1 in comparison to lithoautotrophic cultures, and this was further increased by spiking with soluble Fe^{2+}. This increase in growth through the presence of additional Fe^{2+}, when supplemented with an organic co-substrate, is supportive of a contribution of electrons from Fe^{2+} oxidation into the energy metabolism of this strain, with nitrate as the terminal electron acceptor. This suggests that the most effective form of NDFO metabolism is with Fe^{2+} as a co-substrate. This was certainly the case when nitrate-reducers were grown in organic-rich growth media with Fe^{2+} present (Chapter 4), where large shifts toward oxidised Fe were observed in inoculated cultures under mixotrophic conditions.

These findings build on the wealth of literature that reports that NDFO metabolism is stimulated to higher rates of productivity when conducted as a mixotrophic process (Straub

et al., 1996; Buchholz-Cleven et al., 1997; Benz et al., 1998; Straub et al., 2004), with the added consequence that our understanding of the potential for life in habitable martian environments can now extend beyond a reliance on obligate lithotrophy.

5.2 A revised NDFO model for Mars

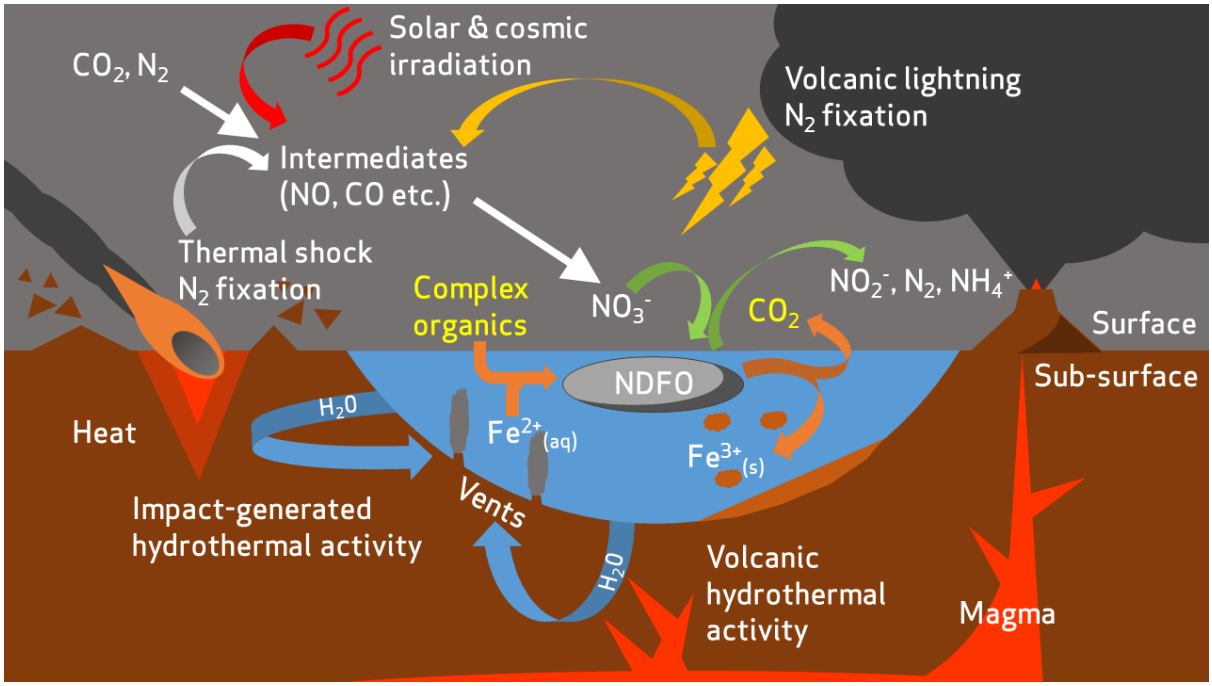

Figure 5.1. Overview of potential redox substrate sources for nitrate-dependent Fe^{2+}-oxidising microorganisms in the early Mars environment (modified from Figure 1.9). Complex organics are present as an additional electron donor and carbon source for microbial life. Organics act as a co-substrate with Fe^{2+} to drive respiratory nitrate reduction and ATP production in NDFO-performing microorganisms. CO_2 is produced as a metabolite from oxidation of organics.

The addition of confirmed complex organics to the catalogue of martian energy and carbon sources (Eigenbrode et al., 2018) necessitates amendment of the hypothetical Fe and N cycle proposed in Chapter 1. Based on the collective results within this thesis, NDFO would likely progress as a mixotrophic process, with Fe^{2+} acting as an electron donor in tandem with reduced organic molecules (Figure 5.1). In this case, CO_2 would be a product of organic oxidation and be either released to the atmosphere, sequestered into carbonates or reincorporated as biomass by autotrophic microorganisms. Biological fixation of

atmospheric carbon is one route by which the organic reservoirs of martian environments could be replenished for further use by heterotrophic and organotrophic microbes, creating a biologically mediated carbon cycle.

5.3 Nitrate reduction can fuel a martian biosphere

The presence of nitrates in modern and ancient martian surface samples (Stern et al., 2015) greatly diversified the range of metabolisms hypothetically possible, bringing autotrophic and heterotrophic forms of nitrate reduction and denitrification to the fore.

The abundances of nitrate on Mars in scooped dust and drilled sediment are in the range of 70-1,100 ppm (Stern et al., 2015), equivalent to ~1-16 mM and sufficient to drive nitrogen-based metabolisms in the presence of active nitrate formation mechanisms, such as volcanic lightning, impact-generated and radiation-catalysed nitrogen fixation reactions (described in Chapter 1). Denitrifying microbes are typically active from much lower nitrate concentrations (>1 ppm) and have been described performing denitrification at up to 36,000 ppm (0.58 M) on Earth, albeit at an impaired rate (Glass and Silverstein, 1999; Tomasek et al., 2017).

The autotrophic growth of *Acidovorax sp*. strain BoFeN1, *Pseudogulbenkiania sp*. strain 2002 and *Paracoccus sp*. strain KS1 with olivine in Chapter 2 and in an early basaltic brine in Chapter 3, and the two former strains in a contemporary martian brine (Chapter 3), reveals that growth by nitrate reduction is possible on both martian mineral substrates and in simulated brine chemistries. This is an important finding for early biospheres on Mars, as nitrate is a key electron acceptor past and present, given the near absence of molecular oxygen.

5.4 Targets for life detection

With the approaching launches of new rovers to the martian surface, it is worth taking account of what the results presented here mean for biosignature location and detection. The Mars 2020 rover, Perseverance, and the ExoMars Rosalind Franklin rover are both shifting the paradigm of Mars exploration from investigating habitable environments to direct detection of past and present life. This change in collective mindset represents an opportunity to search for specific biosignatures of relevant microbial processes, underlining the importance of the results reported in this thesis.

Biomineralised structures were identified after desiccation of cultures grown with olivine in Chapter 2, demonstrating the potential for mineralised NDFO microbes to form morphological biosignatures on grain surfaces. The largest aggregations of mineralised cells also retained detectable, elevated carbon signatures. The biomineralised microbial structures observed in Chapter 2 demonstrate a mechanism of morphological biosignature production from purely lithoautotrophic NDFO cultures. The difficulty in terms of detection, however, is the scale of these structures (~1-200 µm). For reference, the spot sizes on the Raman Laser Spectrometer (Rosalind Franklin rover) and Scanning Habitable Environments With Raman & Luminescence for Organics & Chemicals (SHERLOC) instrument (Perseverance rover) are both 50 µm (Beegle et al., 2015; Rull et al., 2017). The consequence of this is that most biomineralised structures would be undetectable, even if located perfectly in the path of the beam. For identification of structures on this scale, Mars sample return is vital; the Perseverance rover will cache up to 43 samples at the martian surface ahead of a series of joint NASA/ESA missions targeting eventual sample return to Earth, where more powerful instruments are available to analyse these samples at the highest possible resolution. If successful, samples will be returned to Earth by 2032 at the

earliest (Clery and Voosen, 2019). It is, therefore, pertinent to identify alternative targets for the upcoming rovers in the intervening years.

For example, a significant Fe oxidation trend was observed analytically and visually in tandem with nitrate reduction in Chapter 4, when under heterotrophic conditions in the presence of soluble Fe^{2+}. This suggests that Fe^{3+} precipitates could be extensively produced by nitrate reducing microorganisms if organic co-substrates were present on early Mars, as is now thought likely (Eigenbrode et al., 2018). However, it was not possible - using the same assays and observations - to find differences in the overall Fe oxidation states of growing autotrophic NDFO brine cultures in Chapter 3, relative to abiotic controls and non-growing cultures. This non-detection may be due to the sensitivity of the assay and length of the experiment, rather than an absence of an oxidation effect during growth.

The extent of Fe^{2+} oxidation in lithoautotrophic cultures was minimal to undetectable in the microbial growth experiments (Chapters 2 and 3), indicating that macroscopic Fe^{3+} precipitates in a martian context would be unlikely to accumulate from NDFO when in the presence of either abiotic reduction processes or Fe^{3+} reducing microorganisms such as those proposed by Nixon (2014), which could reduce Fe^{3+} and prevent precipitation. In that scenario, aggregates of microfossils - such as those discovered in Chapter 2 - may be a more plausible biosignature of lithoautotrophic NDFO.

Large-scale Fe oxidation patterns in reducing geological contexts may not only act as a biosignature in and of themselves but may also protect associated organic signatures during sedimentation. The co-preservation of biogenic Fe oxides and polysaccharides has already been proposed for neutrophilic Fe oxidisers that respire oxygen in a terrestrial context (Chan et al., 2011).

Lalonde et al. (2012) demonstrated that 13-30% of organic carbon in sediments on Earth is bound - either through chelation or co-precipitation - to reactive Fe phases such as goethite, forming a “rusty sink” for organic carbon. This remained true across sulphidic, anoxic, continental margin, deep sea, deltaic and estuarine sediments (Lalonde et al., 2012). In fact, sediments overlain by oxygen-depleted waters - analogous to what we expect on early Mars, (Hurowitz et al., 2017) - were found to host organometallic structures with the highest ratios of organic carbon to Fe, and were most resistant to chemical and microbial degradation during sediment maturation (~1,500 years). Lalonde et al. also found that organic compounds associated with Fe were N-enriched, suggesting preferential binding of biogenic proteins and carbohydrates.

Applying these findings to the hypothetical context of an NDFO-driven microbial biosphere clearly indicates that Fe^{3+}-rich mineral veins and sediments from reducing Noachian aqueous environments are prime targets for astrobiological investigation of Mars.

5.5 Looking beyond Mars

Logically, the relevance of lithotrophic and mixotrophic forms of NDFO may not be limited to Mars, but any habitable location where the requisite redox couple, carbon sources and neutral-alkaline environment exist.

In the last decade, revelations made by ground-based observations and space missions such as Galileo, Cassini and New Horizons have drawn focus within astrobiology onto the icy moons and dwarf planets of the outer Solar System and a succession of liquid water oceans have been discovered beneath the ice shells of multiple planetary bodies (Carr et al., 1998; Kivelson et al., 2000; McCord and Sotin, 2005; Porco et al., 2006; Roberts and Nimmo, 2008; Saur et al., 2015; Nimmo et al., 2016). Of these locations, the Jovian satellite

Europa and Saturnian moon Enceladus show the most promise for astrobiological exploration (Taubner et al., 2020). There are two primary reasons for this, the first of which is that these oceans are in direct contact with the rocky interiors of their respective moons (Postberg et al., 2009; Trumbo et al., 2019), allowing for more complex and rapid chemical reactions to take place within putative hydrothermal systems there (Waite et al., 2017). The second is that material is ejected from the subsurface of these worlds in plumes (Hansen et al., 2006; Waite et al., 2006; Roth et al., 2014; Jia et al., 2018), providing samples of these environments for collection without the practical and planetary protection complications of landing on a potentially habitable target.

Taking what we know about the distribution of NDFO across terrestrial environments, particularly species such as *Ferroglobus placidus* in deep ocean hydrothermal vents (Hafenbradl et al., 1996), it is possible to imagine that this chemotrophic metabolism could be applied to these extraterrestrial aquatic environments, given the requisite conditions. Courtesy of Cassini, we already have some indication of Enceladus' ocean composition, where CO_2 and macromolecular organic molecules are likely to be in contact with Fe^{2+}-bearing silicates (Seewald, 2017; Postberg et al., 2018; Glein and Waite, 2020). However, early estimates of 4% N species in the plume material were later revised down to <0.5 % (Waite et al., 2006; Hansen et al., 2011), potentially posing a problem for N cycling-based metabolisms such as NDFO. However, microbial denitrification on Earth is known to occur under nitrogen-limited conditions, given some input of organic carbon (Holmes et al., 1996)

5.6 Terrestrial applications

The conclusions of the work undertaken here are not limited to answering astrobiological questions. NDFO is a potentially important process within the deep biosphere of Earth, as well as holding potential uses within bioremediation and water treatment.

The identification of NDFO microorganisms capable of chemolithoautotrophic growth on solid ferrous phases such as olivine (Chapter 2), siderite, pyrite and basaltic glass (Edwards et al., 2003; Xiong et al., 2015) implies that any habitable, deep environment with sufficient nitrate to support metabolism will likely host some population of NDFO-capable microbes. However, there is a gap in our knowledge of Earth's Fe cycle, as a route for oxidation and mineralisation in the anaerobic subsurface could act as a control on the dissolved Fe^{2+} concentration of fluids reaching the surface.

NDFO will also concomitantly remove nitrate in deep environments, which informs not only our full understanding of the global N cycle but also our approach to a specific environmental issue of our own making, i.e. the growing concern around anthropogenic nitrates (primarily from agriculture). These nitrates are accumulating in the vadose zone (between the surface and water table), with potential to inflict large-scale pollution of aquifers for decades to come (Ascott et al., 2017). Though Ascott et al. take account of denitrification within anaerobic, organic-rich environments, the model developed assumes negligible denitrification rates elsewhere. Autotrophic NDFO, as was observed in Chapters 2 and 3, provides a mechanism by which microorganisms can remove nitrate from anaerobic, organic-poor environments. Therefore, more extensive studies into the extent of global NDFO-based N-cycling are essential to fully understand the fate of leached nitrates, which has far-reaching impacts on our natural environment and human health.

For example, Wang et al. (2020) investigated the potential for NDFO-based water treatment, in which the removal of nitrate is a key process. The use of organic influents, such as acetate as electron donors, is costly so an abundant alternative, such as Fe, is highly attractive. The acceleration of growth seen in microbial growth experiments in simulated martian brines (Chapter 3), when excess Fe^{2+} was added as a co-substrate with acetate, agrees with there being a role for Fe^{2+} in complementing nitrate removal processes.

5.7 Future work

This thesis advances our knowledge of NDFO mechanisms and suitability as a metabolism for early martian primary production. However, the studies described herein are not exhaustive, and further questions remain.

5.7.1 Role of serpentinization in growth with olivine as an Fe^{2+} source

Though the growth of three organisms in culture with olivine (Chapter 2) suggests that a lithotrophic form of NDFO can support cell growth, the abiotic process of serpentinisation (the chemical alteration of olivine by water) may have provided cells with a secondary electron donor in the form of H_2. If confirmed, Fe^{2+} would likely act as a co-electron donor, as seems to be the case in heterotrophic cultures (Chapters 3 and 4). To resolve this uncertainty, the experiment could be repeated to include monitoring of the headspace gas for H_2 release or consumption. If serpentinisation is an active process in this experiment, H_2 should accumulate in abiotic controls and be consumed in active biotic cultures if used as an electron donor.

5.7.2 Incorporation of organics into martian fluid simulants

Limited lithotrophic growth was apparent in early basaltic and contemporary martian brines, but not in either sulfur-rich or haematite-rich cultures (Chapter 3). Though

lithoautotrophic growth was not observed in the sulfur-rich or haematite-rich brines, an additional electron donor may allow growth. The full range of monitoring techniques described for the main lithoautotrophic study in Chapter 3 should be employed to monitor the Fe oxidation states and nitrate reduction in active mixotrophic cultures, as well as electron microscopy to characterise the microstructure of Fe^{3+} oxides precipitated with cells.

In the co-substrate study, the addition of an organic co-electron donor (acetate) led to a five-fold increase in maximum cell numbers for *Acidovorax sp.* strain BoFeN1 in the contemporary martian brine, with a further three-fold increase when soluble Fe^{2+} was quadrupled. This line of investigation should be followed and widened to investigate not only the effect of acetate, but a range of organic compounds in stimulating NDFO in all organisms used in this thesis when cultured within the full suite of martian analogue brines.

Carbonaceous chondritic material, similar in composition to that delivered to the martian surface in large quantities (Sephton et al., 2002; Yen et al., 2006), has previously been used to test the Fe^{2+} oxidation capacity of an acidophilic Fe^{2+} oxidiser as well as tests using a mixed NDFO culture (Gronstal et al., 2009). Carbonaceous chondritic material could be investigated as a carbon source for organisms within the simulated martian brines used in Chapter 3, thereby creating high-fidelity simulated martian environments.

5.7.3 Deepening the search for a lithotrophic NDFO mechanism

The genome analysis of *Acidovorax sp.* strain BoFeN1 and *Paracoccus sp.* strain KS1 (Chapter 4) revealed potential oxidoreductase proteins which may be implicated in enzymatic Fe^{2+} oxidation. Isolation and purification of these proteins would allow fuller

identification their biochemical roles, when combined with knockout studies comparing the Fe^{2+} oxidation capacity of wild-type and deletion mutant NDFO microorganisms.

As mentioned previously, the SL1344 strain used for the knockout study in Chapter 4 was limited by both the presence of a second nitrate reductase (leading to some confounding NDFO performed by the Nar-deficient mutant) and relevance as a mammalian pathogen - rather than environmental - bacterium. Future knockout studies should create targeted deletion mutants in environmentally relevant microbes, such as the *Acidovorax*, *Paracoccus* and *Pseudogulbenkiania spp.* used in this thesis. Ishii et al. (2016) used mutagenesis in *Pseudogulbenkiania* isolates to attempt to disrupt NDFO, without success. It is possible that a more targeted approach based on specific candidate genes identified by genome analysis may prove more fruitful.

Additionally, dedicated studies using comparative genomics and specialised programs to identify Fe metabolism genes (Garber et al., 2019) across all sequenced NDFO genomes would provide greater depth and confidence to the identification of potential oxidoreductases made in Chapter 4.

5.7.4 Identification of lithified NDFO on Mars

If we are to identify the traces of NDFO on Mars, we must first understand more fully how those traces are likely to appear in the present day. The mineralisation of microbes reported in Chapter 2 fits into a growing body of literature reporting the various Fe^{3+} precipitates found that entomb NDFO organisms (Kappler et al., 2005; Miot et al., 2009; Schädler et al., 2009; Pantke et al., 2012; Miot et al., 2014a; Miot et al., 2015; Zhou et al., 2016).

This is a useful starting point for biosignature-oriented mission such as the Rosalind Franklin and Perseverance rovers, which aim to investigate preserved Noachian sedimentary environments at Oxia Planum and Jezero crater (3.8-3.9 Ga), respectively

(Goudge et al., 2018; Quantin-Nataf et al., 2019). However, redox, aqueous, diagenetic, desiccative and irradiative processes could alter or destroy microbial structures in the billions of intervening years between sedimentation and investigation. For example, Glasauer et al. (2013) combined laboratory encrustation experiments using a NDFO isolate with field observations to highlight the importance of the redox environment in fossilisation, finding that reductive dissolution could inhibit Fe biomineralisation. In testing the diagenetic maturation of organo-ferric structures from microaerobic Fe oxidisers, Picard et al. (2015) found that Fe^{3+} oxides could enhance structural and chemical preservation of biological material under high temperature and pressure, and that spectroscopy could be used to identify these biosignatures in the rock record.

Experiments to simulate the long-term effects of desiccation and irradiation are a regular feature of Mars astrobiology research (Dartnell et al., 2007a; Dartnell et al., 2012; Gaboyer et al., 2017) but a strategy to more fully characterise the preservation potential of NDFO-driven biological activity should specifically assess the response of NDFO precipitates and encrustations to all these processes in simulated conditions. Encrusted microbial material could be mixed with early martian regolith simulants and: (1) exposed to redox shifts to simulate environmental change, (2) processed in high temperature, high pressure reactors to simulate burial and diagenesis, and (3) desiccated and irradiated to simulate exposure at the modern martian surface.

5.8 Summary

NDFO represents a redox process which can sustain nitrate-reducing microorganisms in simulated early basaltic and contemporary martian brine environments and on olivine, a common Fe^{2+} mineral at the martian surface.

Lithoautotrophic NDFO - based on Fe^{2+} as a sole electron donor - may sustain too few cells to produce readily detectable shifts in the geochemistry of the environment, posing a challenge for biosignature detection. However, biomineralised structures could be identified in samples returned by future missions using electron microscopy and associated mineralogical and elemental analyses.

A mixotrophic strategy combining organics and Fe^{2+} as electron donors would produce a larger amount of biomass than purely lithotrophic energy metabolisms, enhancing biomineralisation due to an associated increase in Fe^{3+} released. These Fe^{3+} minerals would be deposited as macroscopic features in lacustrine environments or rock fractures.

Therefore, future life detection missions should look for Fe^{3+} mineral formations within predominantly reduced sedimentary and vein formations, where preserved complex organics and biogenic minerals may be found in tandem and act as combined biosignatures.

References

Abramov, O., and Kring, D.A. (2005). Impact-induced hydrothermal activity on early Mars. *Journal of Geophysical Research: Planets* 110**,** E12S09.

Adeli, S., Hauber, E., Kleinhans, M., Le Deit, L., Platz, T., Fawdon, P., and Jaumann, R. (2016). Amazonian-aged fluvial system and associated ice-related features in Terra Cimmeria, Mars. *Icarus* 277**,** 286-299.

Allen, C.C., Morris, R.V., Lindstrom, D.J., Lindstrom, M., and Lockwood, J. (1997). JSC Mars-1-Martian regolith simulant. *Lunar and Planetary Science Conference 1997, Houston*.

Altschul, S.F., Gish, W., Miller, W., Myers, E.W., and Lipman, D.J. (1990). Basic local alignment search tool. *Journal of Molecular Biology* 215**,** 403-410.

Amador, E.S., Bandfield, J.L., Brazelton, W.J., and Kelley, D. (2017). The Lost City Hydrothermal Field: A Spectroscopic and Astrobiological Analogue for Nili Fossae, Mars. *Astrobiology* 17**,** 1138-1160.

Amils, R., González-Toril, E., Aguilera, A., Rodrıguez, N., Fernández-Remolar, D., Gómez, F., Garcıa-Moyano, A., Malki, M., Oggerin, M., and Sánchez-Andrea, I. (2011). From Rıo Tinto to Mars: the terrestrial and extraterrestrial ecology of acidophiles. *Advances in Applied Microbiology* 77**,** 41-70.

Amils, R., González-Toril, E., Fernández-Remolar, D., Gómez, F., Aguilera, Á., Rodríguez, N., Malki, M., García-Moyano, A., Fairén, A.G., and De La Fuente, V. (2007). Extreme environments as Mars terrestrial analogs: the Rio Tinto case. *Planetary and Space Science* 55**,** 370-381.

Anand, M., Russell, S.S., Blackhurst, R.L., and Grady, M.M. (2006). Searching for signatures of life on Mars: an Fe-isotope perspective. *Philosophical Transactions of the Royal Society B: Biological Sciences* 361**,** 1715-1720.

Andrews-Hanna, J.C., and Lewis, K.W. (2011). Early Mars hydrology: 2. Hydrological evolution in the Noachian and Hesperian epochs. *Journal of Geophysical Research: Planets* 116**,** E02007.

Andrews, S.C. (1998). Iron storage in bacteria. *Advances in microbial physiology* 40**,** 281-351.

Arnold, M., and Sheppard, S.M. (1981). East Pacific Rise at latitude 21 N: isotopic composition and origin of the hydrothermal sulphur. *Earth and Planetary Science Letters* 56**,** 148-156.

Arvidson, R.E., Ashley, J.W., Bell Iii, J.F., Chojnacki, M., Cohen, J., Economou, T.E., Farrand, W.H., Fergason, R., Fleischer, I., Geissler, P., Gellert, R., Golombek, M.P., Grotzinger, J.P., Guinness, E.A., Haberle, R.M., Herkenhoff, K.E., Herman, J.A., Iagnemma, K.D., Jolliff, B.L., Johnson, J.R., Klingelhöfer, G., Knoll, A.H., Knudson, A.T., Li, R., Mclennan, S.M., Mittlefehldt, D.W., Morris, R.V., Parker, T.J., Rice, M.S., Schröder, C., Soderblom, L.A., Squyres, S.W., Sullivan, R.J., and Wolff, M.J. (2011). Opportunity Mars Rover mission: Overview and selected results from Purgatory ripple to traverses to Endeavour crater. *Journal of Geophysical Research: Planets* 116**,** E00F15.

Arvidson, R.E., Squyres, S.W., Bell, J.F., Catalano, J.G., Clark, B.C., Crumpler, L.S., De Souza, P.A., Fairén, A.G., Farrand, W.H., Fox, V.K., Gellert, R., Ghosh, A., Golombek, M.P., Grotzinger, J.P., Guinness, E.A., Herkenhoff, K.E., Jolliff, B.L., Knoll, A.H., Li, R., Mclennan, S.M., Ming, D.W., Mittlefehldt, D.W., Moore, J.M., Morris, R.V., Murchie, S.L., Parker, T.J., Paulsen, G., Rice, J.W., Ruff, S.W., Smith, M.D., and Wolff, M.J. (2014). Ancient Aqueous Environments at Endeavour Crater, Mars. *Science* 343**,** 1248097.

Ascott, M.J., Gooddy, D.C., Wang, L., Stuart, M.E., Lewis, M.A., Ward, R.S., and Binley, A.M. (2017). Global patterns of nitrate storage in the vadose zone. *Nature Communications* 8**,** 1416.

Aziz, R.K., Bartels, D., Best, A.A., Dejongh, M., Disz, T., Edwards, R.A., Formsma, K., Gerdes, S., Glass, E.M., Kubal, M., Meyer, F., Olsen, G.J., Olson, R., Osterman, A.L., Overbeek, R.A., Mcneil, L.K., Paarmann, D., Paczian, T., Parrello, B., Pusch, G.D., Reich, C., Stevens, R., Vassieva, O., Vonstein, V., Wilke, A., and Zagnitko, O. (2008). The RAST Server: Rapid Annotations using Subsystems Technology. *BMC Genomics* 9**,** 75.

Balci, N., Bullen, T.D., Witte-Lien, K., Shanks, W.C., Motelica, M., and Mandernack, K.W. (2006). Iron isotope fractionation during microbially stimulated Fe(II) oxidation and Fe(III) precipitation. *Geochimica et Cosmochimica Acta* 70**,** 622-639.

Bankevich, A., Nurk, S., Antipov, D., Gurevich, A.A., Dvorkin, M., Kulikov, A.S., Lesin, V.M., Nikolenko, S.I., Pham, S., Prjibelski, A.D., Pyshkin, A.V., Sirotkin, A.V., Vyahhi, N., Tesler, G., Alekseyev, M.A., and Pevzner, P.A. (2012). SPAdes: A New Genome Assembly Algorithm and Its Applications to Single-Cell Sequencing. *Journal of Computational Biology* 19**,** 455-477.

Bauermeister, A., Rettberg, P., and Flemming, H.-C. (2014). Growth of the acidophilic iron–sulfur bacterium Acidithiobacillus ferrooxidans under Mars-like geochemical conditions. *Planetary and Space Science* 98**,** 205-215.

Beegle, L., Bhartia, R., White, M., Deflores, L., Abbey, W., Yen-Hung, W., Cameron, B., Moore, J., Fries, M., Burton, A., Edgett, K.S., Ravine, M.A., Hug, W., Reid, R., Nelson, T., Clegg, S., Wiens, R., Asher, S., and Sobron, P. (2015). SHERLOC: Scanning habitable environments with Raman & luminescence for organics & chemicals. *2015 IEEE Aerospace Conference, Big Sky***,** 1-11.

Beller, H.R., Chain, P.S.G., Letain, T.E., Chakicherla, A., Larimer, F.W., Richardson, P.M., Coleman, M.A., Wood, A.P., and Kelly, D.P. (2006). The Genome Sequence of the Obligately Chemolithoautotrophic, Facultatively Anaerobic Bacterium *Thiobacillus denitrificans*. *Journal of Bacteriology* 188**,** 1473-1488.

Benz, M., Brune, A., and Schink, B. (1998). Anaerobic and aerobic oxidation of ferrous iron at neutral pH by chemoheterotrophic nitrate-reducing bacteria. *Archives of Microbiology* 169**,** 159-165.

Bertani, G. (1951). Studies on lysogenesis. I. The mode of phage liberation by lysogenic *Escherichia coli*. *Journal of bacteriology* 62**,** 293-300.

Bertka, C.M., and Fei, Y. (1998). Density profile of an SNC model Martian interior and the moment-of-inertia factor of Mars. *Earth and Planetary Science Letters* 157**,** 79-88.

Bibring, J.-P., Langevin, Y., Mustard, J.F., Poulet, F., Arvidson, R., Gendrin, A., Gondet, B., Mangold, N., Pinet, P., and Forget, F. (2006). Global mineralogical and aqueous Mars history derived from OMEGA/Mars Express data. *Science* 312**,** 400-404.

Bish, D.L., Blake, D.F., Vaniman, D.T., Chipera, S.J., Morris, R.V., Ming, D.W., Treiman, A.H., Sarrazin, P., Morrison, S.M., Downs, R.T., Achilles, C.N., Yen, A.S., Bristow, T.F., Crisp, J.A., Morookian, J.M., Farmer, J.D., Rampe, E.B., Stolper, E.M., and Spanovich, N. (2013). X-ray Diffraction Results from Mars Science Laboratory: Mineralogy of Rocknest at Gale Crater. *Science* 341**,** 1238932.

Blake, D.F., Morris, R.V., Kocurek, G., Morrison, S.M., Downs, R.T., Bish, D., Ming, D.W., Edgett, K.S., Rubin, D., Goetz, W., Madsen, M.B., Sullivan, R., Gellert, R., Campbell, I., Treiman, A.H., Mclennan, S.M., Yen, A.S., Grotzinger, J., Vaniman, D.T., Chipera, S.J., Achilles, C.N., Rampe, E.B., Sumner, D., Meslin, P.-Y., Maurice, S., Forni, O., Gasnault, O., Fisk, M., Schmidt, M., Mahaffy, P., Leshin, L.A., Glavin, D., Steele, A., Freissinet, C., Navarro-González, R., Yingst, R.A.,

Kah, L.C., Bridges, N., Lewis, K.W., Bristow, T.F., Farmer, J.D., Crisp, J.A., Stolper, E.M., Des Marais, D.J., and Sarrazin, P. (2013). Curiosity at Gale Crater, Mars: Characterization and Analysis of the Rocknest Sand Shadow. *Science* 341**,** 1239505.

Blöthe, M., and Roden, E.E. (2009). Composition and activity of an autotrophic Fe (II)-oxidizing, nitrate-reducing enrichment culture. *Applied and environmental microbiology* 75**,** 6937-6940.

Bolger, A.M., Lohse, M., and Usadel, B. (2014). Trimmomatic: a flexible trimmer for Illumina sequence data. *Bioinformatics* 30**,** 2114-2120.

Böttger, U., De Vera, J.P., Fritz, J., Weber, I., Hübers, H.W., and Schulze-Makuch, D. (2012). Optimizing the detection of carotene in cyanobacteria in a martian regolith analogue with a Raman spectrometer for the ExoMars mission. *Planetary and Space Science* 60**,** 356-362.

Boynton, W.V., Ming, D.W., Kounaves, S.P., Young, S.M.M., Arvidson, R.E., Hecht, M.H., Hoffman, J., Niles, P.B., Hamara, D.K., Quinn, R.C., Smith, P.H., Sutter, B., Catling, D.C., and Morris, R.V. (2009). Evidence for Calcium Carbonate at the Mars Phoenix Landing Site. *Science* 325**,** 61-64.

Bradford, M.M. (1976). A rapid and sensitive method for the quantitation of microgram quantities of protein utilizing the principle of protein-dye binding. *Analytical Biochemistry* 72**,** 248-254.

Brazelton, W.J., Schrenk, M.O., Kelley, D.S., and Baross, J.A. (2006). Methane- and Sulfur-Metabolizing Microbial Communities Dominate the Lost City Hydrothermal Field Ecosystem. *Applied and Environmental Microbiology* 72**,** 6257-6270.

Bridges, J.C., and Grady, M.M. (2000). Evaporite mineral assemblages in the nakhlite (martian) meteorites. *Earth and Planetary Science Letters* 176**,** 267-279.

Bridges, J.C., and Schwenzer, S.P. (2012). The nakhlite hydrothermal brine on Mars. *Earth and Planetary Science Letters* 359-360**,** 117-123.

Bridges, J.C., Schwenzer, S.P., Leveille, R., Westall, F., Wiens, R.C., Mangold, N., Bristow, T., Edwards, P., and Berger, G. (2015). Diagenesis and clay mineral formation at Gale Crater, Mars. *Journal of Geophysical Research: Planets* 120**,** 1-19.

Bridges, J.C., and Warren, P.H. (2006). The SNC meteorites: basaltic igneous processes on Mars. *Journal of the Geological Society* 163**,** 229-251.

Bristow, T.F., Bish, D.L., Vaniman, D.T., Morris, R.V., Blake, D.F., Grotzinger, J.P., Rampe, E.B., Crisp, J.A., Achilles, C.N., Ming, D.W., Ehlmann, B.L., King, P.L., Bridges, J.C., Eigenbrode, J.L., Sumner, D.Y., Chipera, S.J., Moorokian, J.M., Treiman, A.H., Morrison, S.M., Downs, R.T., Farmer, J.D., Marais, D.D., Sarrazin, P., Floyd, M.M., Mischna, M.A., and Mcadam, A.C. (2015). The origin and implications of clay minerals from Yellowknife Bay, Gale crater, Mars†. *American Mineralogist* 100**,** 824-836.

Bruce, R.A., Achenbach, L.A., and Coates, J.D. (1999). Reduction of (per) chlorate by a novel organism isolated from paper mill waste. *Environmental Microbiology* 1**,** 319-329.

Bruslind, L. (2019). "Chemolithotrophy & Nitrogen Metabolism," in *Microbiology*. Pressbooks).

Buchholz-Cleven, B.E.E., Rattunde, B., and Straub, K.L. (1997). Screening for Genetic Diversity of Isolates of Anaerobic Fe(II)-oxidizing Bacteria Using DGGE and Whole-cell Hybridization. *Systematic and Applied Microbiology* 20**,** 301-309.

Busigny, V., Lebeau, O., Ader, M., Krapež, B., and Bekker, A. (2013). Nitrogen cycle in the Late Archean ferruginous ocean. *Chemical Geology* 362**,** 115-130.

Butcher, F.E.G., Balme, M.R., Gallagher, C., Arnold, N.S., Conway, S.J., Hagermann, A., and Lewis, S.R. (2017). Recent Basal Melting of a Mid-Latitude Glacier on Mars. *Journal of Geophysical Research: Planets* 122**,** 2445-2468.

Byrne-Bailey, K.G., Weber, K.A., and Coates, J.D. (2012). Draft Genome Sequence of the Anaerobic, Nitrate-Dependent, Fe(II)-Oxidizing Bacterium *Pseudogulbenkiania ferrooxidans* Strain 2002. *Journal of Bacteriology* 194**,** 2400-2401.

Cabrol, N.A., and Grin, E.A. (1999). Distribution, classification, and ages of Martian impact crater lakes. *Icarus* 142**,** 160-172.

Cairns, L.S., Hobley, L., and Stanley-Wall, N.R. (2014). Biofilm formation by *Bacillus subtilis*: new insights into regulatory strategies and assembly mechanisms. *Molecular Microbiology* 93**,** 587-598.

Canfield, D.E., Rosing, M.T., and Bjerrum, C. (2006). Early anaerobic metabolisms. *Philosophical Transactions of the Royal Society of London B: Biological Sciences* 361**,** 1819-1836.

Cannon, K.M., Britt, D.T., Smith, T.M., Fritsche, R.F., and Batcheldor, D. (2019). Mars global simulant MGS-1: A Rocknest-based open standard for basaltic martian

regolith simulants. *Icarus* 317**,** 470-478.

Carlson, H.K., Clark, I.C., Blazewicz, S.J., Iavarone, A.T., and Coates, J.D. (2013). Fe (II) oxidation is an innate capability of nitrate-reducing bacteria that involves abiotic and biotic reactions. *Journal of bacteriology* 195**,** 3260-3268.

Carlson, H.K., Clark, I.C., Melnyk, R.A., and Coates, J.D. (2012). Toward a mechanistic understanding of anaerobic nitrate-dependent iron oxidation: balancing electron uptake and detoxification. *Frontiers in Microbiology* 3**,** 57.

Carr, M.H., Belton, M.J.S., Chapman, C.R., Davies, M.E., Geissler, P., Greenberg, R., Mcewen, A.S., Tufts, B.R., Greeley, R., Sullivan, R., Head, J.W., Pappalardo, R.T., Klaasen, K.P., Johnson, T.V., Kaufman, J., Senske, D., Moore, J., Neukum, G., Schubert, G., Burns, J.A., Thomas, P., and Veverka, J. (1998). Evidence for a subsurface ocean on Europa. *Nature* 391**,** 363-365.

Carr, M.H., and Head, J.W. (2010). Geologic history of Mars. *Earth and Planetary Science Letters* 294**,** 185-203.

Cartron, M.L., Maddocks, S., Gillingham, P., Craven, C.J., and Andrews, S.C. (2006). Feo – Transport of Ferrous Iron into Bacteria. *Biometals* 19**,** 143-157.

Cavazza, C., Giudici-Orticoni, M.-T., Nitschke, W., Appia, C., Bonnefoy, V., and Bruschi, M. (1996). Characterisation of a Soluble Cytochrome c4 Isolated from *Thiobacillus ferrooxidans*. *European Journal of Biochemistry* 242**,** 308-314.

Chakraborty, A., and Picardal, F. (2013). Neutrophilic, nitrate-dependent, Fe(II) oxidation by a Dechloromonas species. *World Journal of Microbiology and Biotechnology* 29**,** 617-623.

Chakraborty, A., Roden, E.E., Schieber, J., and Picardal, F. (2011). Enhanced Growth of Acidovorax sp. Strain 2AN during Nitrate-Dependent Fe(II) Oxidation in Batch and Continuous-Flow Systems. *Applied and Environmental Microbiology* 77**,** 8548-8556.

Chan, C.S., Fakra, S.C., Emerson, D., Fleming, E.J., and Edwards, K.J. (2011). Lithotrophic iron-oxidizing bacteria produce organic stalks to control mineral growth: implications for biosignature formation. *The ISME Journal* 5**,** 717-727.

Changela, H.G., and Bridges, J.C. (2010). Alteration assemblages in the nakhlites: Variation with depth on Mars. *Meteoritics & Planetary Science* 45**,** 1847-1867.

Charlou, J.L., and Donval, J.P. (1993). Hydrothermal methane venting between 12° N and 26° N along the Mid-Atlantic Ridge. *Journal of Geophysical Research: Solid Earth*

98, 9625-9642.

Chassefière, E., and Leblanc, F. (2004). Mars atmospheric escape and evolution; interaction with the solar wind. *Planetary and Space Science* 52, 1039-1058.

Chassefière, E., and Leblanc, F. (2011). Methane release and the carbon cycle on Mars. *Planetary and Space Science* 59, 207-217.

Chastain, B.K., and Kral, T.A. (2010). Zero-valent iron on Mars: An alternative energy source for methanogens. *Icarus* 208, 198-201.

Chaudhuri, S.K., Lack, J.G., and Coates, J.D. (2001). Biogenic magnetite formation through anaerobic biooxidation of Fe (II). *Applied and environmental microbiology* 67, 2844-2848.

Chevrier, V., Mathé, P.-E., Rochette, P., Grauby, O., Bourrie, G., and Trolard, F. (2006). Iron weathering products in a CO 2+(H 2 O or H 2 O 2) atmosphere: Implications for weathering processes on the surface of Mars. *Geochimica et Cosmochimica Acta* 70, 4295-4317.

Chevrier, V., Poulet, F., and Bibring, J.-P. (2007). Early geochemical environment of Mars as determined from thermodynamics of phyllosilicates. *Nature* 448, 60-63.

Clarke, A., Morris, G.J., Fonseca, F., Murray, B.J., Acton, E., and Price, H.C. (2013). A Low Temperature Limit for Life on Earth. *PLOS ONE* 8, e66207.

Clery, D., and Voosen, P. (2019). Bold plan to retrieve Mars samples takes shape. *Science* 366, 932.

Cockell, C.S., Kelly, L.C., Summers, S., and Marteinsson, V. (2011). Following the kinetics: Iron-oxidizing microbial mats in cold Icelandic volcanic habitats and their rock-associated carbonaceous signature. *Astrobiology* 11, 679-694.

Cockell, C.S., and Raven, J.A. (2004). Zones of photosynthetic potential on Mars and the early Earth. *Icarus* 169, 300-310.

Cockell, C.S., Schuerger, A.C., Billi, D., Friedmann, E.I., and Panitz, C. (2005). Effects of a simulated martian UV flux on the cyanobacterium, Chroococcidiopsis sp. 029. *Astrobiology* 5, 127-140.

Comeau, A.M., Harding, T., Galand, P.E., Vincent, W.F., and Lovejoy, C. (2012). Vertical distribution of microbial communities in a perennially stratified Arctic lake with saline, anoxic bottom waters. *Scientific Reports* 2, 604.

Connon, S.A., Lester, E.D., Shafaat, H.S., Obenhuber, D.C., and Ponce, A. (2007). Bacterial diversity in hyperarid Atacama Desert soils. *Journal of Geophysical*

Research: Biogeosciences 112**,** G04S17.

Craddock, R.A., and Howard, A.D. (2002). The case for rainfall on a warm, wet early Mars. *Journal of Geophysical Research: Planets* 107**,** 5111.

Croal, L.R., Johnson, C.M., Beard, B.L., and Newman, D.K. (2004). Iron isotope fractionation by Fe (II)-oxidizing photoautotrophic bacteria. *Geochimica et Cosmochimica Acta* 68**,** 1227-1242.

Crosby, H.A., Roden, E.E., Johnson, C.M., and Beard, B.L. (2007). The mechanisms of iron isotope fractionation produced during dissimilatory Fe(III) reduction by *Shewanella putrefaciens* and *Geobacter sulfurreducens*. *Geobiology* 5**,** 169-189.

Curtis-Harper, E., Pearson, V.K., Summers, S., Bridges, J.C., Schwenzer, S.P., and Olsson-Francis, K. (2018). The Microbial Community of a Terrestrial Anoxic Inter-Tidal Zone: A Model for Laboratory-Based Studies of Potentially Habitable Ancient Lacustrine Systems on Mars. *Microorganisms* 6**,** 61.

Czaja, A.D., Johnson, C.M., Beard, B.L., Roden, E.E., Li, W., and Moorbath, S. (2013). Biological Fe oxidation controlled deposition of banded iron formation in the ca. 3770Ma Isua Supracrustal Belt (West Greenland). *Earth and Planetary Science Letters* 363**,** 192-203.

Dartnell, L.R., Desorgher, L., Ward, J.M., and Coates, A.J. (2007a). Martian sub-surface ionising radiation: biosignatures and geology. *Biogeosciences Discussions* 4**,** 455-492.

Dartnell, L.R., Desorgher, L., Ward, J.M., and Coates, A.J. (2007b). Modelling the surface and subsurface Martian radiation environment: Implications for astrobiology. *Geophysical Research Letters* 34**,** L02207.

Dartnell, L.R., Page, K., Jorge-Villar, S.E., Wright, G., Munshi, T., Scowen, I.J., Ward, J.M., and Edwards, H.G.M. (2012). Destruction of Raman biosignatures by ionising radiation and the implications for life detection on Mars. *Analytical and Bioanalytical Chemistry* 403**,** 131-144.

Datsenko, K.A., and Wanner, B.L. (2000). One-step inactivation of chromosomal genes in *Escherichia coli* K-12 using PCR products. *Proceedings of the National Academy of Sciences* 97**,** 6640-6645.

Davis, J.M., Balme, M., Grindrod, P.M., Williams, R.M.E., and Gupta, S. (2016). Extensive Noachian fluvial systems in Arabia Terra: Implications for early Martian climate. *Geology* 44**,** 847-850.

Davis, J.M., Gupta, S., Balme, M., Grindrod, P.M., Fawdon, P., Dickeson, Z.I., and Williams, R.M.E. (2019). A Diverse Array of Fluvial Depositional Systems in Arabia Terra: Evidence for mid-Noachian to Early Hesperian Rivers on Mars. *Journal of Geophysical Research: Planets* 124**,** 1913-1934.

Dodd, M.S., Papineau, D., Grenne, T., Slack, J.F., Rittner, M., Pirajno, F., O'neil, J., and Little, C.T. (2017). Evidence for early life in Earth's oldest hydrothermal vent precipitates. *Nature* 543**,** 60-64.

Edwards, C.S., and Ehlmann, B.L. (2015). Carbon sequestration on Mars. *Geology* 43**,** 863-866.

Edwards, C.S., and Piqueux, S. (2016). The water content of recurring slope lineae on Mars. *Geophysical Research Letters* 43**,** 8912-8919.

Edwards, K.J., Bach, W., Mccollom, T.M., and Rogers, D.R. (2004). Neutrophilic iron-oxidizing bacteria in the ocean: their habitats, diversity, and roles in mineral deposition, rock alteration, and biomass production in the deep-sea. *Geomicrobiology Journal* 21**,** 393-404.

Edwards, K.J., Rogers, D.R., Wirsen, C.O., and Mccollom, T.M. (2003). Isolation and characterization of novel psychrophilic, neutrophilic, Fe-oxidizing, chemolithoautotrophic α-and γ-Proteobacteria from the deep sea. *Applied and Environmental Microbiology* 69**,** 2906-2913.

Ehlmann, B.L., and Edwards, C.S. (2014). Mineralogy of the Martian Surface. *Annual Review of Earth and Planetary Sciences* 42**,** 291-315.

Ehlmann, B.L., Mustard, J.F., Fassett, C.I., Schon, S.C., Head Iii, J.W., Des Marais, D.J., Grant, J.A., and Murchie, S.L. (2008a). Clay minerals in delta deposits and organic preservation potential on Mars. *Nature Geoscience* 1**,** 355-358.

Ehlmann, B.L., Mustard, J.F., Murchie, S.L., Bibring, J.-P., Meunier, A., Fraeman, A.A., and Langevin, Y. (2011). Subsurface water and clay mineral formation during the early history of Mars. *Nature* 479**,** 53-60.

Ehlmann, B.L., Mustard, J.F., Murchie, S.L., Poulet, F., Bishop, J.L., Brown, A.J., Calvin, W.M., Clark, R.N., Marais, D.J.D., Milliken, R.E., Roach, L.H., Roush, T.L., Swayze, G.A., and Wray, J.J. (2008b). Orbital Identification of Carbonate-Bearing Rocks on Mars. *Science* 322**,** 1828-1832.

Ehlmann, B.L., Mustard, J.F., Swayze, G.A., Clark, R.N., Bishop, J.L., Poulet, F., Des Marais, D.J., Roach, L.H., Milliken, R.E., Wray, J.J., Barnouin-Jha, O., and

Murchie, S.L. (2009). Identification of hydrated silicate minerals on Mars using MRO-CRISM: Geologic context near Nili Fossae and implications for aqueous alteration. *Journal of Geophysical Research: Planets* 114**,** E00D08.

Ehrenreich, A., and Widdel, F. (1994). Anaerobic oxidation of ferrous iron by purple bacteria, a new type of phototrophic metabolism. *Applied and Environmental microbiology* 60**,** 4517-4526.

Eigenbrode, J.L., Summons, R.E., Steele, A., Freissinet, C., Millan, M., Navarro-González, R., Sutter, B., Mcadam, A.C., Franz, H.B., Glavin, D.P., Archer, P.D., Mahaffy, P.R., Conrad, P.G., Hurowitz, J.A., Grotzinger, J.P., Gupta, S., Ming, D.W., Sumner, D.Y., Szopa, C., Malespin, C., Buch, A., and Coll, P. (2018). Organic matter preserved in 3-billion-year-old mudstones at Gale crater, Mars. *Science* 360**,** 1096-1101.

Emerson, D., and Floyd, M.M. (2005). Enrichment and Isolation of Iron-Oxidizing Bacteria at Neutral pH. *Methods in Enzymology* 397**,** 112-123.

Emerson, D., and Moyer, C.L. (2002). Neutrophilic Fe-oxidizing bacteria are abundant at the Loihi Seamount hydrothermal vents and play a major role in Fe oxide deposition. *Applied and Environmental Microbiology* 68**,** 3085-3093.

Emerson, D., Scott, J.J., Benes, J., and Bowden, W.B. (2015). Microbial Iron Oxidation in the Arctic Tundra and Its Implications for Biogeochemical Cycling. *Applied and Environmental Microbiology* 81**,** 8066-8075.

Emerson, D., and Weiss, J.V. (2004). Bacterial Iron Oxidation in Circumneutral Freshwater Habitats: Findings from the Field and the Laboratory. *Geomicrobiology Journal* 21**,** 405-414.

Etique, M., Jorand, F.D.R.P., Zegeye, A., GréGoire, B., Despas, C., and Ruby, C. (2014). Abiotic process for Fe (II) oxidation and green rust mineralization driven by a heterotrophic nitrate reducing bacteria (*Klebsiella mobilis*). *Environmental science & technology* 48**,** 3742-3751.

Ettwig, K.F., Shima, S., Van De Pas-Schoonen, K.T., Kahnt, J., Medema, M.H., Op Den Camp, H.J.M., Jetten, M.S.M., and Strous, M. (2008). Denitrifying bacteria anaerobically oxidize methane in the absence of Archaea. *Environmental Microbiology* 10**,** 3164-3173.

Ewing, S., Macalady, J., Warren-Rhodes, K., Mckay, C., and Amundson, R. (2008). Changes in the soil C cycle at the arid-hyperarid transition in the Atacama Desert.

Journal of Geophysical Research: Biogeosciences 113**,** G02S90.

Fairén, A.G., Fernández-Remolar, D., Dohm, J.M., Baker, V.R., and Amils, R. (2004). Inhibition of carbonate synthesis in acidic oceans on early Mars. *Nature* 431**,** 423-426.

Fairén, A.G., Schulze-Makuch, D., Rodríguez, A.P., Fink, W., Davila, A.F., Uceda, E.R., Furfaro, R., Amils, R., and Mckay, C.P. (2009). Evidence for Amazonian acidic liquid water on Mars—A reinterpretation of MER mission results. *Planetary and Space Science* 57**,** 276-287.

Fassett, C.I., and Head, J.W. (2008). The timing of martian valley network activity: Constraints from buffered crater counting. *Icarus* 195**,** 61-89.

Filiberto, J., and Schwenzer, S.P. (2018). *Volatiles in the Martian Crust.* Elsevier.

Fisk, M.R., and Giovannoni, S.J. (1999). Sources of nutrients and energy for a deep biosphere on Mars. *Journal of Geophysical Research: Planets* 104**,** 11805-11815.

Formisano, V., Atreya, S., Encrenaz, T., Ignatiev, N., and Giuranna, M. (2004). Detection of Methane in the Atmosphere of Mars. *Science* 306**,** 1758-1761.

Fowler, D., Coyle, M., Skiba, U., Sutton, M.A., Cape, J.N., Reis, S., Sheppard, L.J., Jenkins, A., Grizzetti, B., and Galloway, J.N. (2013). The global nitrogen cycle in the twenty-first century. *Philosophical Transactions of the Royal Society B* 368**,** 20130164.

Fox-Powell, M.G., Hallsworth, J.E., Cousins, C.R., and Cockell, C.S. (2016). Ionic strength is a barrier to the habitability of Mars. *Astrobiology* 16**,** 427-442.

Fox, J.L. (1993). The production and escape of nitrogen atoms on Mars. *Journal of Geophysical Research: Planets* 98**,** 3297-3310.

Fox, V.K., Arvidson, R.E., Guinness, E.A., Mclennan, S.M., Catalano, J.G., Murchie, S.L., and Powell, K.E. (2016). Smectite deposits in Marathon Valley, Endeavour Crater, Mars, identified using CRISM hyperspectral reflectance data. *Geophysical Research Letters* 43**,** 4885-4892.

Franz, H.B., Trainer, M.G., Wong, M.H., Mahaffy, P.R., Atreya, S.K., Manning, H.L.K., and Stern, J.C. (2015). Reevaluated martian atmospheric mixing ratios from the mass spectrometer on the Curiosity rover. *Planetary and Space Science* 109-110**,** 154-158.

Frydenvang, J., Gasda, P.J., Hurowitz, J.A., Grotzinger, J.P., Wiens, R.C., Newsom, H.E., Edgett, K.S., Watkins, J., Bridges, J.C., Maurice, S., Fisk, M.R., Johnson, J.R.,

Rapin, W., Stein, N.T., Clegg, S.M., Schwenzer, S.P., Bedford, C.C., Edwards, P., Mangold, N., Cousin, A., Anderson, R.B., Payré, V., Vaniman, D., Blake, D.F., Lanza, N.L., Gupta, S., Van Beek, J., Sautter, V., Meslin, P.Y., Rice, M., Milliken, R., Gellert, R., Thompson, L., Clark, B.C., Sumner, D.Y., Fraeman, A.A., Kinch, K.M., Madsen, M.B., Mitrofanov, I.G., Jun, I., Calef, F., and Vasavada, A.R. (2017). Diagenetic silica enrichment and late-stage groundwater activity in Gale crater, Mars. *Geophysical Research Letters* 44**,** 4716-4724.

Gaboyer, F., Le Milbeau, C., Bohmeier, M., Schwendner, P., Vannier, P., Beblo-Vranesevic, K., Rabbow, E., Foucher, F., Gautret, P., Guégan, R., Richard, A., Sauldubois, A., Richmann, P., Perras, A.K., Moissl-Eichinger, C., Cockell, C.S., Rettberg, P., Marteinsson, Monaghan, E., Ehrenfreund, P., Garcia-Descalzo, L., Gomez, F., Malki, M., Amils, R., Cabezas, P., Walter, N., and Westall, F. (2017). Mineralization and Preservation of an extremotolerant Bacterium Isolated from an Early Mars Analog Environment. *Scientific Reports* 7**,** 8775.

Garber, A.I., Nealson, K.H., Okamoto, A., Mcallister, S.M., Chan, C.S., Barco, R.A., and Merino, N. (2019). FeGenie: a comprehensive tool for the identification of iron genes and iron gene neighborhoods in genomes and metagenome assemblies. *bioRxiv***,** 777656.

Gendrin, A., Mangold, N., Bibring, J.-P., Langevin, Y., Gondet, B., Poulet, F., Bonello, G., Quantin, C., Mustard, J., and Arvidson, R. (2005). Sulfates in Martian layered terrains: the OMEGA/Mars Express view. *Science* 307**,** 1587-1591.

Gilichinsky, D., Wilson, G., Friedmann, E., Mckay, C., Sletten, R., Rivkina, E., Vishnivetskaya, T., Erokhina, L., Ivanushkina, N., and Kochkina, G. (2007). Microbial populations in Antarctic permafrost: biodiversity, state, age, and implication for astrobiology. *Astrobiology* 7**,** 275-311.

Glasauer, S., Mattes, A., and Gehring, A. (2013). Constraints on the Preservation of Ferriferous Microfossils. *Geomicrobiology Journal* 30**,** 479-489.

Glass, C., and Silverstein, J. (1999). Denitrification of high-nitrate, high-salinity wastewater. *Water Research* 33**,** 223-229.

Glavin, D.P., Freissinet, C., Miller, K.E., Eigenbrode, J.L., Brunner, A.E., Buch, A., Sutter, B., Archer, P.D., Atreya, S.K., and Brinckerhoff, W.B. (2013). Evidence for perchlorates and the origin of chlorinated hydrocarbons detected by SAM at the Rocknest aeolian deposit in Gale Crater. *Journal of Geophysical Research: Planets*

118**,** 1955-1973.

Glein, C.R., and Waite, J.H. (2020). The Carbonate Geochemistry of Enceladus' Ocean. *Geophysical Research Letters* 47**,** e2019GL085885.

Goetz, W., Brinckerhoff, W.B., Arevalo, R., Freissinet, C., Getty, S., Glavin, D.P., Siljeström, S., Buch, A., Stalport, F., Grubisic, A., Li, X., Pinnick, V., Danell, R., Van Amerom, F.H.W., Goesmann, F., Steininger, H., Grand, N., Raulin, F., Szopa, C., Meierhenrich, U., and Brucato, J.R. (2016). MOMA: the challenge to search for organics and biosignatures on Mars. *International Journal of Astrobiology* 15**,** 239-250.

Goudge, T.A., Mohrig, D., Cardenas, B.T., Hughes, C.M., and Fassett, C.I. (2018). Stratigraphy and paleohydrology of delta channel deposits, Jezero crater, Mars. *Icarus* 301**,** 58-75.

Grady, M.M., Wright, I., and Pillinger, C.T. (1995). A search for nitrates in Martian meteorites. *Journal of Geophysical Research: Planets* 100**,** 5449-5455.

Grant, R.A., Filman, D.J., Finkel, S.E., Kolter, R., and Hogle, J.M. (1998). The crystal structure of Dps, a ferritin homolog that binds and protects DNA. *Nature Structural Biology* 5**,** 294-303.

Griess, P. (1879). Griess reagent: a solution of sulphanilic acid and 1-Naphthylamine in acetic acid which gives a pink colour on reaction with the solution obtained after decomposition of nitrosyl complexes. *Berichte der deutschen chemischen Gesellschaft* 12**,** 427.

Gronstal, A., Pearson, V., Kappler, A., Dooris, C., Anand, M., Poitrasson, F., Kee, T.P., and Cockell, C.S. (2009). Laboratory experiments on the weathering of iron meteorites and carbonaceous chondrites by iron-oxidizing bacteria. *Meteoritics & Planetary Science* 44**,** 233-247.

Grotzinger, J.P., Gupta, S., Malin, M.C., Rubin, D.M., Schieber, J., Siebach, K., Sumner, D.Y., Stack, K.M., Vasavada, A.R., Arvidson, R.E., Calef, F., Edgar, L., Fischer, W.F., Grant, J.A., Griffes, J., Kah, L.C., Lamb, M.P., Lewis, K.W., Mangold, N., Minitti, M.E., Palucis, M., Rice, M., Williams, R.M.E., Yingst, R.A., Blake, D., Blaney, D., Conrad, P., Crisp, J., Dietrich, W.E., Dromart, G., Edgett, K.S., Ewing, R.C., Gellert, R., Hurowitz, J.A., Kocurek, G., Mahaffy, P., Mcbride, M.J., Mclennan, S.M., Mischna, M., Ming, D., Milliken, R., Newsom, H., Oehler, D., Parker, T.J., Vaniman, D., Wiens, R.C., and Wilson, S.A. (2015). Deposition,

exhumation, and paleoclimate of an ancient lake deposit, Gale crater, Mars. *Science* 350**,** aac7575.

Grotzinger, J.P., Sumner, D., Kah, L., Stack, K., Gupta, S., Edgar, L., Rubin, D., Lewis, K., Schieber, J., and Mangold, N. (2014a). A habitable fluvio-lacustrine environment at Yellowknife Bay, Gale Crater, Mars. *Science* 343**,** 1242777.

Grotzinger, J.P., Sumner, D.Y., Kah, L.C., Stack, K., Gupta, S., Edgar, L., Rubin, D., Lewis, K., Schieber, J., Mangold, N., Milliken, R., Conrad, P.G., Desmarais, D., Farmer, J., Siebach, K., Calef, F., Hurowitz, J., Mclennan, S.M., Ming, D., Vaniman, D., Crisp, J., Vasavada, A., Edgett, K.S., Malin, M., Blake, D., Gellert, R., Mahaffy, P., Wiens, R.C., Maurice, S., Grant, J.A., Wilson, S., Anderson, R.C., Beegle, L., Arvidson, R., Hallet, B., Sletten, R.S., Rice, M., Bell, J., Griffes, J., Ehlmann, B., Anderson, R.B., Bristow, T.F., Dietrich, W.E., Dromart, G., Eigenbrode, J., Fraeman, A., Hardgrove, C., Herkenhoff, K., Jandura, L., Kocurek, G., Lee, S., Leshin, L.A., Leveille, R., Limonadi, D., Maki, J., Mccloskey, S., Meyer, M., Minitti, M., Newsom, H., Oehler, D., Okon, A., Palucis, M., Parker, T., Rowland, S., Schmidt, M., Squyres, S., Steele, A., Stolper, E., Summons, R., Treiman, A., Williams, R., Yingst, A., and Team, M.S. (2014b). A Habitable Fluvio-Lacustrine Environment at Yellowknife Bay, Gale Crater, Mars. *Science* 343**,** 1242777.

Hafenbradl, D., Keller, M., Dirmeier, R., Rachel, R., Roßnagel, P., Burggraf, S., Huber, H., and Stetter, K.O. (1996). *Ferroglobus placidus* gen. nov., sp. nov., a novel hyperthermophilic archaeum that oxidizes Fe^{2+} at neutral pH under anoxic conditions. *Archives of Microbiology* 166**,** 308-314.

Haft, D.H., Dicuccio, M., Badretdin, A., Brover, V., Chetvernin, V., O'neill, K., Li, W., Chitsaz, F., Derbyshire, M.K., Gonzales, N.R., Gwadz, M., Lu, F., Marchler, G.H., Song, J.S., Thanki, N., Yamashita, R.A., Zheng, C., Thibaud-Nissen, F., Geer, L.Y., Marchler-Bauer, A., and Pruitt, K.D. (2018). RefSeq: an update on prokaryotic genome annotation and curation. *Nucleic Acids Res* 46**,** D851-d860.

Halevy, I., and Head Iii, J.W. (2014). Episodic warming of early Mars by punctuated volcanism. *Nature Geoscience* 7**,** 865-868.

Hansen, C.J., Esposito, L., Stewart, A.I.F., Colwell, J., Hendrix, A., Pryor, W., Shemansky, D., and West, R. (2006). Enceladus' Water Vapor Plume. *Science* 311**,** 1422.

Hansen, C.J., Shemansky, D.E., Esposito, L.W., Stewart, A.I.F., Lewis, B.R., Colwell, J.E.,

Hendrix, A.R., West, R.A., Waite Jr, J.H., Teolis, B., and Magee, B.A. (2011). The composition and structure of the Enceladus plume. *Geophysical Research Letters* 38**,** L11202.

Hartmann, W.K., and Neukum, G. (2001). *Cratering Chronology and the Evolution of Mars*. Dordrecht: Springer Netherlands.

He, S., Barco, R.A., Emerson, D., and Roden, E.E. (2017). Comparative Genomic Analysis of Neutrophilic Iron(II) Oxidizer Genomes for Candidate Genes in Extracellular Electron Transfer. *Frontiers in Microbiology* 8**,** 1584.

He, S., Tominski, C., Kappler, A., Behrens, S., and Roden, E.E. (2016). Metagenomic analyses of the autotrophic Fe (II)-oxidizing, nitrate-reducing enrichment Culture KS. *Applied and Environmental Microbiology***,** AEM. 03493-03415.

Hecht, M.H., Kounaves, S.P., Quinn, R.C., West, S.J., Young, S.M.M., Ming, D.W., Catling, D.C., Clark, B.C., Boynton, W.V., Hoffman, J., Deflores, L.P., Gospodinova, K., Kapit, J., and Smith, P.H. (2009). Detection of Perchlorate and the Soluble Chemistry of Martian Soil at the Phoenix Lander Site. *Science* 325**,** 64-67.

Hedrich, S., Schlömann, M., and Johnson, D.B. (2011). The iron-oxidizing proteobacteria. *Microbiology* 157**,** 1551-1564.

Hicks, L.J., Bridges, J.C., and Gurman, S. (2014). Ferric saponite and serpentine in the nakhlite martian meteorites. *Geochimica et Cosmochimica Acta* 136**,** 194-210.

Hoefen, T.M., Clark, R.N., Bandfield, J.L., Smith, M.D., Pearl, J.C., and Christensen, P.R. (2003). Discovery of olivine in the Nili Fossae region of Mars. *Science* 302**,** 627-630.

Hoehler, T.M., and Jørgensen, B.B. (2013). Microbial life under extreme energy limitation. *Nature Reviews Microbiology* 11**,** 83-94.

Hoiseth, S.K., and Stocker, B.a.D. (1981). Aromatic-dependent Salmonella typhimurium are non-virulent and effective as live vaccines. *Nature* 291**,** 238-239.

Holm, N.G., Oze, C., Mousis, O., Waite, J.H., and Guilbert-Lepoutre, A. (2015). Serpentinization and the Formation of H2 and CH4 on Celestial Bodies (Planets, Moons, Comets). *Astrobiology* 15**,** 587-600.

Holmes, R.M., Jones, J.B., Fisher, S.G., and Grimm, N.B. (1996). Denitrification in a nitrogen-limited stream ecosystem. *Biogeochemistry* 33**,** 125-146.

Hoppert, M. (2011). "Metalloenzymes," in *Encyclopedia of Geobiology*, eds. R. Reitner &

V. Thiel. Springer Netherlands), 558-563.

Hsu, H.-W., Postberg, F., Sekine, Y., Shibuya, T., Kempf, S., Horányi, M., Juhász, A., Altobelli, N., Suzuki, K., Masaki, Y., Kuwatani, T., Tachibana, S., Sirono, S.-I., Moragas-Klostermeyer, G., and Srama, R. (2015). Ongoing hydrothermal activities within Enceladus. *Nature* 519**,** 207.

Hungate, R. (1950). The anaerobic mesophilic cellulolytic bacteria. *Bacteriological Reviews* 14**,** 1.

Hurowitz, J.A., Grotzinger, J.P., Fischer, W.W., Mclennan, S.M., Milliken, R.E., Stein, N., Vasavada, A.R., Blake, D.F., Dehouck, E., Eigenbrode, J.L., Fairén, A.G., Frydenvang, J., Gellert, R., Grant, J.A., Gupta, S., Herkenhoff, K.E., Ming, D.W., Rampe, E.B., Schmidt, M.E., Siebach, K.L., Stack-Morgan, K., Sumner, D.Y., and Wiens, R.C. (2017). Redox stratification of an ancient lake in Gale crater, Mars. *Science* 356**,** 6849.

Ilbert, M., and Bonnefoy, V. (2013). Insight into the evolution of the iron oxidation pathways. *Biochimica et Biophysica Acta (BBA)-Bioenergetics* 1827**,** 161-175.

Ionescu, D., Heim, C., Polerecky, L., Thiel, V., and De Beer, D. (2015). Biotic and abiotic oxidation and reduction of iron at circumneutral pH are inseparable processes under natural conditions. *Geomicrobiology Journal* 32**,** 221-230.

Iordan, S.L., Kraczkiewicz-Dowjat, A.J., Kelly, D.P., and Wood, A.P. (1995). Novel eubacteria able to grow on carbon disulfide. *Archives of Microbiology* 163**,** 131-137.

Irwin, R.P., Howard, A.D., Craddock, R.A., and Moore, J.M. (2005). An intense terminal epoch of widespread fluvial activity on early Mars: 2. Increased runoff and paleolake development. *Journal of Geophysical Research: Planets* 110**,** E12S15.

Ishii, S., Joikai, K., Otsuka, S., Senoo, K., and Okabe, S. (2016). Denitrification and Nitrate-Dependent Fe(II) Oxidation in Various *Pseudogulbenkiania* Strains. *Microbes and Environments* 31**,** 293-298.

Ivanov, V.M. (2004). The 125th Anniversary of the Griess Reagent. *Journal of Analytical Chemistry* 59**,** 1002-1005.

Jakosky, B.M., and Phillips, R.J. (2001). Mars' volatile and climate history. *Nature* 412**,** 237-244.

Jakosky, B.M., Slipski, M., Benna, M., Mahaffy, P., Elrod, M., Yelle, R., Stone, S., and Alsaeed, N. (2017). Mars' atmospheric history derived from upper-atmosphere

measurements of $^{38}Ar/^{36}Ar$. *Science* 355**,** 1408-1410.

Jepsen, S.M., Priscu, J.C., Grimm, R.E., and Bullock, M.A. (2007). The potential for lithoautotrophic life on Mars: application to shallow interfacial water environments. *Astrobiology* 7**,** 342-354.

Jepson, B.J., Mohan, S., Clarke, T.A., Gates, A.J., Cole, J.A., Butler, C.S., Butt, J.N., Hemmings, A.M., and Richardson, D.J. (2007). Spectropotentiometric and structural analysis of the periplasmic nitrate reductase from *Escherichia coli*. *Journal of Biological Chemistry* 282**,** 6425-6437.

Jia, X., Kivelson, M.G., Khurana, K.K., and Kurth, W.S. (2018). Evidence of a plume on Europa from Galileo magnetic and plasma wave signatures. *Nature Astronomy* 2**,** 459-464.

Johnson, J.R., Bell, J.F., Bender, S., Blaney, D., Cloutis, E., Ehlmann, B., Fraeman, A., Gasnault, O., Kinch, K., and Le Mouélic, S. (2016). Constraints on iron sulfate and iron oxide mineralogy from ChemCam visible/near-infrared reflectance spectroscopy of Mt. Sharp basal units, Gale Crater, Mars. *American Mineralogist* 101**,** 1501-1514.

Jolliff, B.L., Mittlefehldt, D.W., Farrand, W.H., Knoll, A.H., Mclennan, S.M., and Gellert, R. (2019). "Chapter 10 - Mars Exploration Rover Opportunity: Water and Other Volatiles on Ancient Mars," in *Volatiles in the Martian Crust,* eds. J. Filiberto & S.P. Schwenzer. Elsevier), 285-328.

Juncher Jørgensen, C., Jacobsen, O.S., Elberling, B., and Aamand, J. (2009). Microbial oxidation of pyrite coupled to nitrate reduction in anoxic groundwater sediment. *Environmental science & technology* 43**,** 4851-4857.

Kanehisa, M., Sato, Y., and Morishima, K. (2016). BlastKOALA and GhostKOALA: KEGG Tools for Functional Characterization of Genome and Metagenome Sequences. *Journal of Molecular Biology* 428**,** 726-731.

Kappler, A., Johnson, C., Crosby, H., Beard, B., and Newman, D. (2010). Evidence for equilibrium iron isotope fractionation by nitrate-reducing iron (II)-oxidizing bacteria. *Geochimica et Cosmochimica Acta* 74**,** 2826-2842.

Kappler, A., Schink, B., and Newman, D.K. (2005). Fe (III) mineral formation and cell encrustation by the nitrate-dependent Fe (II)-oxidizer strain BoFeN1. *Geobiology* 3**,** 235-245.

Kappler, A., and Straub, K.L. (2005). Geomicrobiological cycling of iron. *Reviews in*

Mineralogy and Geochemistry 59**,** 85-108.

Kern, M., and Simon, J. (2009). Electron transport chains and bioenergetics of respiratory nitrogen metabolism in Wolinella succinogenes and other Epsilonproteobacteria. *Biochimica et Biophysica Acta* 1787**,** 646-656.

King, G.M. (2015). Carbon monoxide as a metabolic energy source for extremely halophilic microbes: implications for microbial activity in Mars regolith. *Proceedings of the National Academy of Sciences* 112**,** 4465-4470.

Kivelson, M.G., Khurana, K.K., Russell, C.T., Volwerk, M., Walker, R.J., and Zimmer, C. (2000). Galileo Magnetometer Measurements: A Stronger Case for a Subsurface Ocean at Europa. *Science* 289**,** 1340.

Kliore, A., Cain, D.L., Levy, G.S., Eshleman, V.R., Fjeldbo, G., and Drake, F.D. (1965). Occultation experiment: Results of the first direct measurement of Mars's atmosphere and ionosphere. *Science* 149**,** 1243-1248.

Klueglein, N., and Kappler, A. (2013). Abiotic oxidation of Fe(II) by reactive nitrogen species in cultures of the nitrate-reducing Fe(II) oxidizer *Acidovorax sp.* BoFeN1 – questioning the existence of enzymatic Fe(II) oxidation. *Geobiology* 11**,** 180-190.

Klueglein, N., Zeitvogel, F., Stierhof, Y.-D., Floetenmeyer, M., Konhauser, K.O., Kappler, A., and Obst, M. (2014). Potential role of nitrite for abiotic Fe (II) oxidation and cell encrustation during nitrate reduction by denitrifying bacteria. *Applied and Environmental Microbiology* 80**,** 1051-1061.

Klüglein, N., Picardal, F., Zedda, M., Zwiener, C., and Kappler, A. (2015). Oxidation of Fe (II)-EDTA by nitrite and by two nitrate-reducing Fe (II)-oxidizing *Acidovorax* strains. *Geobiology* 13**,** 198-207.

Konhauser, K.O., and Ferris, F.G. (1996). Diversity of iron and silica precipitation by microbial mats in hydrothermal waters, Iceland: Implications for Precambrian iron formations. *Geology* 24**,** 323-326.

Konhauser, K.O., Jones, B., Phoenix, V.R., Ferris, G., and Renaut, R.W. (2004). The Microbial Role in Hot Spring Silicification. *AMBIO: A Journal of the Human Environment* 33**,** 552-558.

Konn, C., Charlou, J.-L., Donval, J.-P., Holm, N., Dehairs, F., and Bouillon, S. (2009). Hydrocarbons and oxidized organic compounds in hydrothermal fluids from Rainbow and Lost City ultramafic-hosted vents. *Chemical Geology* 258**,** 299-314.

Korablev, O., Vandaele, A.C., Montmessin, F., Fedorova, A.A., Trokhimovskiy, A.,

Forget, F., Lefèvre, F., Daerden, F., Thomas, I.R., Trompet, L., Erwin, J.T., Aoki, S., Robert, S., Neary, L., Viscardy, S., Grigoriev, A.V., Ignatiev, N.I., Shakun, A., Patrakeev, A., Belyaev, D.A., Bertaux, J.-L., Olsen, K.S., Baggio, L., Alday, J., Ivanov, Y.S., Ristic, B., Mason, J., Willame, Y., Depiesse, C., Hetey, L., Berkenbosch, S., Clairquin, R., Queirolo, C., Beeckman, B., Neefs, E., Patel, M.R., Bellucci, G., López-Moreno, J.-J., Wilson, C.F., Etiope, G., Zelenyi, L., Svedhem, H., Vago, J.L., Alonso-Rodrigo, G., Altieri, F., Anufreychik, K., Arnold, G., Bauduin, S., Bolsée, D., Carrozzo, G., Clancy, R.T., Cloutis, E., Crismani, M., Da Pieve, F., D'aversa, E., Duxbury, N., Encrenaz, T., Fouchet, T., Funke, B., Fussen, D., Garcia-Comas, M., Gérard, J.-C., Giuranna, M., Gkouvelis, L., Gonzalez-Galindo, F., Grassi, D., Guerlet, S., Hartogh, P., Holmes, J., Hubert, B., Kaminski, J., Karatekin, O., Kasaba, Y., Kass, D., Khatuntsev, I., Kleinböhl, A., Kokonkov, N., Krasnopolsky, V., Kuzmin, R., Lacombe, G., Lanciano, O., Lellouch, E., Lewis, S., Luginin, M., Liuzzi, G., López-Puertas, M., López-Valverde, M., Määttänen, A., Mahieux, A., Marcq, E., Martin-Torres, J., Maslov, I., Medvedev, A., Millour, E., Moshkin, B., Mumma, Michael j., Nakagawa, H., Novak, R.E., Oliva, F., Patsaev, D., et al. (2019). No detection of methane on Mars from early ExoMars Trace Gas Orbiter observations. *Nature* 568**,** 517-520.

Kounaves, S.P., Carrier, B.L., O'neil, G.D., Stroble, S.T., and Claire, M.W. (2014). Evidence of martian perchlorate, chlorate, and nitrate in Mars meteorite EETA79001: Implications for oxidants and organics. *Icarus* 229**,** 206-213.

Kröger, C., Dillon, S.C., Cameron, A.D.S., Papenfort, K., Sivasankaran, S.K., Hokamp, K., Chao, Y., Sittka, A., Hébrard, M., Händler, K., Colgan, A., Leekitcharoenphon, P., Langridge, G.C., Lohan, A.J., Loftus, B., Lucchini, S., Ussery, D.W., Dorman, C.J., Thomson, N.R., Vogel, J., and Hinton, J.C.D. (2012). The transcriptional landscape and small RNAs of Salmonella enterica serovar Typhimurium. *Proceedings of the National Academy of Sciences of the United States of America* 109**,** E1277-E1286.

Kumaraswamy, R., Sjollema, K., Kuenen, G., Van Loosdrecht, M., and Muyzer, G. (2006). Nitrate-dependent [Fe (II) EDTA] 2− oxidation by *Paracoccus ferrooxidans* sp. nov., isolated from a denitrifying bioreactor. *Systematic and Applied Microbiology* 29**,** 276-286.

Kurokawa, H., Kurosawa, K., and Usui, T. (2018). A lower limit of atmospheric pressure on early Mars inferred from nitrogen and argon isotopic compositions. *Icarus* 299**,**

443-459.

Kuypers, M.M.M., Marchant, H.K., and Kartal, B. (2018). The microbial nitrogen-cycling network. *Nature Reviews Microbiology* 16**,** 263-276.

Lack, J.G., Chaudhuri, S.K., Chakraborty, R., Achenbach, L.A., and Coates, J.D. (2002). Anaerobic Biooxidation of Fe(II) by Dechlorosoma suillum. *Microbial Ecology* 43**,** 424-431.

Lalonde, K., Mucci, A., Ouellet, A., and Gélinas, Y. (2012). Preservation of organic matter in sediments promoted by iron. *Nature* 483**,** 198-200.

Lane, M.D., Bishop, J.L., Darby Dyar, M., Hyde, B.C., King, P.L., and Parente, M. (2008). Mineralogy of the Paso Robles soils on Mars. *American Mineralogist* 93**,** 728-739.

Lanza, N.L., Wiens, R.C., Arvidson, R.E., Clark, B.C., Fischer, W.W., Gellert, R., Grotzinger, J.P., Hurowitz, J.A., Mclennan, S.M., and Morris, R.V. (2016). Oxidation of manganese in an ancient aquifer, Kimberley formation, Gale crater, Mars. *Geophysical Research Letters* 43**,** 7398-7407.

Larese-Casanova, P., Haderlein, S.B., and Kappler, A. (2010). Biomineralization of lepidocrocite and goethite by nitrate-reducing Fe (II)-oxidizing bacteria: effect of pH, bicarbonate, phosphate, and humic acids. *Geochimica et Cosmochimica Acta* 74**,** 3721-3734.

Laslett, D., and Canback, B. (2004). ARAGORN, a program to detect tRNA genes and tmRNA genes in nucleotide sequences. *Nucleic Acids Research* 32**,** 11-16.

Laufer, K., Røy, H., Jørgensen, B.B., and Kappler, A. (2016a). Evidence for the existence of autotrophic nitrate-reducing Fe (II)-oxidizing bacteria in marine coastal sediment. *Applied and environmental microbiology* 82**,** 6120-6131.

Laufer, K., Røy, H., Jørgensen, B.B., and Kappler, A. (2016b). Evidence for the Existence of Autotrophic Nitrate-Reducing Fe(II)-Oxidizing Bacteria in Marine Coastal Sediment. *Applied and Environmental Microbiology* 82**,** 6120-6131.

Le Brun, N.E., Andrews, S.C., Guest, J.R., Harrison, P.M., Moore, G.R., and Thomson, A.J. (1995). Identification of the ferroxidase centre of *Escherichia coli* bacterioferritin. *The Biochemical Journal* 312**,** 385-392.

Leighton, R.B., Murray, B.C., Sharp, R.P., Allen, J.D., and Sloan, R.K. (1965). Mariner IV photography of Mars: Initial results. *Science* 149**,** 627-630.

Li, J., Bernard, S., Benzerara, K., Beyssac, O., Allard, T., Cosmidis, J., and Moussou, J. (2014). Impact of biomineralization on the preservation of microorganisms during

fossilization: An experimental perspective. *Earth and Planetary Science Letters* 400**,** 113-122.

Linne, D., Moses, R., Sanders, G., Kleinhenz, J., and Mueller, R. (2019). Mars ISRU & Civil Engineering Current Thinking and Approaches. *International Mars Exploration Working Group (IMEWG) 2019, Oslo*.

Liu, W., Lin, J., Pang, X., Cui, S., Mi, S., and Lin, J. (2011). Overexpression of Rusticyanin in *Acidithiobacillus ferrooxidans* ATCC19859 Increased Fe(II) Oxidation Activity. *Current Microbiology* 62**,** 320-324.

Lopez-Reyes, G., Rull, F., Venegas, G., Westall, F., Foucher, F., Bost, N., Sanz, A., Catalá-Espí, A., Vegas, A., and Hermosilla, I. (2013). Analysis of the scientific capabilities of the ExoMars Raman Laser Spectrometer instrument. *European Journal of Mineralogy* 25**,** 721-733.

Lovley, D.R., Baedecker, M.J., Lonergan, D.J., Cozzarelli, I.M., Phillips, E.J., and Siegel, D.I. (1989). Oxidation of aromatic contaminants coupled to microbial iron reduction. *Nature* 339**,** 297-300.

Lovley, D.R., Holmes, D.E., and Nevin, K.P. (2004). Dissimilatory Fe (III) and Mn (IV) reduction. *Advances in Microbial Physiology* 49**,** 219-286.

Lovley, D.R., and Phillips, E.J. (1988). Novel mode of microbial energy metabolism: organic carbon oxidation coupled to dissimilatory reduction of iron or manganese. *Applied and Environmental Microbiology* 54**,** 1472-1480.

Macey, M.C., Fox–Powell, M., Ramkissoon, N.K., Stephens, B.P., Barton, T., Schwenzer, S.P., Pearson, V.K., Cousins, C.R., and Olsson–Francis, K. (2020). The identification of sulfide oxidation as a potential metabolism driving primary production on late Noachian Mars. *Scientific Reports* 10**,** 10941.

Madigan, M.T., Martinko, J.M., Dunlap, P.V., and Clark, D.P. (2008). "Brock Biology of microorganisms 12th edn", in: *International Microbiology.*).

Mahaffy, P.R., Webster, C.R., Atreya, S.K., Franz, H., Wong, M., Conrad, P.G., Harpold, D., Jones, J.J., Leshin, L.A., and Manning, H. (2013). Abundance and isotopic composition of gases in the martian atmosphere from the Curiosity rover. *Science* 341**,** 263-266.

Malin, M.C., and Edgett, K.S. (2003). Evidence for persistent flow and aqueous sedimentation on early Mars. *Science* 302**,** 1931-1934.

Mancinelli, R.L., Fahlen, T.F., Landheim, R., and Klovstad, M.R. (2004). Brines and

evaporites: analogs for Martian life. *Advances in Space Research* 33**,** 1244-1246.

Mangold, N., Carter, J., Poulet, F., Dehouck, E., Ansan, V., and Loizeau, D. (2012). Late Hesperian aqueous alteration at Majuro crater, Mars. *Planetary and Space Science* 72**,** 18-30.

Manning, C.V., Zahnle, K.J., and Mckay, C.P. (2009). Impact processing of nitrogen on early Mars. *Icarus* 199**,** 273-285.

Martín-Torres, F.J., Zorzano, M.-P., Valentín-Serrano, P., Harri, A.-M., Genzer, M., Kemppinen, O., Rivera-Valentin, E.G., Jun, I., Wray, J., and Madsen, M.B. (2015). Transient liquid water and water activity at Gale crater on Mars. *Nature Geoscience* 8**,** 357-361.

Martin, W., Baross, J., Kelley, D., and Russell, M.J. (2008). Hydrothermal vents and the origin of life. *Nature Reviews Microbiology* 6**,** 805.

Marzo, G.A., Davila, A.F., Tornabene, L.L., Dohm, J.M., Fairén, A.G., Gross, C., Kneissl, T., Bishop, J.L., Roush, T.L., and Mckay, C.P. (2010). Evidence for Hesperian impact-induced hydrothermalism on Mars. *Icarus* 208**,** 667-683.

Mccord, T.B., and Sotin, C. (2005). Ceres: Evolution and current state. *Journal of Geophysical Research: Planets* 110**,** E05009.

Mckay, D.S., Gibson, E.K., Thomas-Keprta, K.L., Vali, H., Romanek, C.S., Clemett, S.J., Chillier, X.D.F., Maechling, C.R., and Zare, R.N. (1996). Search for Past Life on Mars: Possible Relic Biogenic Activity in Martian Meteorite ALH84001. *Science* 273**,** 924-930.

Mclennan, S.M., Anderson, R., Bell, J., Bridges, J., Calef, F., Campbell, J.L., Clark, B., Clegg, S., Conrad, P., and Cousin, A. (2014). Elemental geochemistry of sedimentary rocks at Yellowknife Bay, Gale crater, Mars. *Science* 343**,** 1244734.

Mcsween, H.Y., Taylor, G.J., and Wyatt, M.B. (2009). Elemental composition of the Martian crust. *Science* 324**,** 736-739.

Michalski, J.R., Cuadros, J., Niles, P.B., Parnell, J., Rogers, A.D., and Wright, S.P. (2013). Groundwater activity on Mars and implications for a deep biosphere. *Nature Geoscience* 6**,** 133-138.

Millero, F.J., Sotolongo, S., and Izaguirre, M. (1987). The oxidation kinetics of Fe (II) in seawater. *Geochimica et Cosmochimica Acta* 51**,** 793-801.

Ming, D.W., Archer, P.D., Glavin, D.P., Eigenbrode, J.L., Franz, H.B., Sutter, B., Brunner, A.E., Stern, J.C., Freissinet, C., Mcadam, A.C., Mahaffy, P.R., Cabane, M., Coll,

P., Campbell, J.L., Atreya, S.K., Niles, P.B., Bell, J.F., Bish, D.L., Brinckerhoff, W.B., Buch, A., Conrad, P.G., Des Marais, D.J., Ehlmann, B.L., Fairén, A.G., Farley, K., Flesch, G.J., Francois, P., Gellert, R., Grant, J.A., Grotzinger, J.P., Gupta, S., Herkenhoff, K.E., Hurowitz, J.A., Leshin, L.A., Lewis, K.W., Mclennan, S.M., Miller, K.E., Moersch, J., Morris, R.V., Navarro-González, R., Pavlov, A.A., Perrett, G.M., Pradler, I., Squyres, S.W., Summons, R.E., Steele, A., Stolper, E.M., Sumner, D.Y., Szopa, C., Teinturier, S., Trainer, M.G., Treiman, A.H., Vaniman, D.T., Vasavada, A.R., Webster, C.R., Wray, J.J., and Yingst, R.A. (2014). Volatile and Organic Compositions of Sedimentary Rocks in Yellowknife Bay, Gale Crater, Mars. *Science* 343**,** 1245267.

Ming, D.W., Mittlefehldt, D.W., Morris, R.V., Golden, D.C., Gellert, R., Yen, A., Clark, B.C., Squyres, S.W., Farrand, W.H., Ruff, S.W., Arvidson, R.E., Klingelhöfer, G., Mcsween, H.Y., Rodionov, D.S., Schröder, C., De Souza, P.A., and Wang, A. (2006). Geochemical and mineralogical indicators for aqueous processes in the Columbia Hills of Gusev crater, Mars. *Journal of Geophysical Research: Planets* 111**,** E02S12.

Miot, J., Benzerara, K., Morin, G., Kappler, A., Bernard, S., Obst, M., Férard, C., Skouri-Panet, F., Guigner, J.-M., and Posth, N. (2009). Iron biomineralization by anaerobic neutrophilic iron-oxidizing bacteria. *Geochimica et Cosmochimica Acta* 73**,** 696-711.

Miot, J., Jézéquel, D., Benzerara, K., Cordier, L., Rivas-Lamelo, S., Skouri-Panet, F., Férard, C., Poinsot, M., and Duprat, E. (2016). Mineralogical Diversity in Lake Pavin: Connections with Water Column Chemistry and Biomineralization Processes. *Minerals* 6**,** 24.

Miot, J., Li, J., Benzerara, K., Sougrati, M.T., Ona-Nguema, G., Bernard, S., Jumas, J.-C., and Guyot, F. (2014a). Formation of single domain magnetite by green rust oxidation promoted by microbial anaerobic nitrate-dependent iron oxidation. *Geochimica et Cosmochimica Acta* 139**,** 327-343.

Miot, J., Recham, N., Larcher, D., Guyot, F., Brest, J., and Tarascon, J.-M. (2014b). Biomineralized α-Fe_2O_3: texture and electrochemical reaction with Li. *Energy & Environmental Science* 7**,** 451-460.

Miot, J., Remusat, L., Duprat, E., Gonzalez, A., Pont, S., and Poinsot, M. (2015). Fe biomineralization mirrors individual metabolic activity in a nitrate-dependent Fe

(II)-oxidizer. *Frontiers in Microbiology* 6**,** 879.

Mojzsis, S.J., Arrhenius, G., Mckeegan, K.D., Harrison, T.M., Nutman, A.P., and Friend, C.R.L. (1996). Evidence for life on Earth before 3,800 million years ago. *Nature* 384**,** 55-59.

Montoya, L., Vizioli, C., Rodríguez, N., Rastoll, M.J., Amils, R., and Marin, I. (2013). Microbial community composition of Tirez lagoon (Spain), a highly sulfated athalassohaline environment. *Aquatic Biosystems* 9**,** 19.

Morgan, B., and Lahav, O. (2007). The effect of pH on the kinetics of spontaneous Fe (II) oxidation by O_2 in aqueous solution–basic principles and a simple heuristic description. *Chemosphere* 68**,** 2080-2084.

Morris, R.V., Ruff, S.W., Gellert, R., Ming, D.W., Arvidson, R.E., Clark, B.C., Golden, D., Siebach, K., Klingelhöfer, G., and Schröder, C. (2010). Identification of carbonate-rich outcrops on Mars by the Spirit rover. *Science* 329**,** 421-424.

Morris, R.V., Vaniman, D.T., Blake, D.F., Gellert, R., Chipera, S.J., Rampe, E.B., Ming, D.W., Morrison, S.M., Downs, R.T., and Treiman, A.H. (2016). Silicic volcanism on Mars evidenced by tridymite in high-SiO2 sedimentary rock at Gale crater. *Proceedings of the National Academy of Sciences* 113**,** 7071-7076.

Moyer, C.L., Dobbs, F.C., and Karl, D.M. (1995). Phylogenetic diversity of the bacterial community from a microbial mat at an active, hydrothermal vent system, Loihi Seamount, Hawaii. *Applied and Environmental Microbiology* 61**,** 1555-1562.

Muehe, E.M., Gerhardt, S., Schink, B., and Kappler, A. (2009). Ecophysiology and the energetic benefit of mixotrophic Fe (II) oxidation by various strains of nitrate-reducing bacteria. *FEMS Microbiology Ecology* 70**,** 335-343.

Myers, C.R., and Nealson, K.H. (1988). Microbial reduction of manganese oxides: interactions with iron and sulfur. *Geochimica et Cosmochimica Acta* 52**,** 2727-2732.

Nachon, M., Mangold, N., Forni, O., Kah, L.C., Cousin, A., Wiens, R.C., Anderson, R., Blaney, D., Blank, J.G., and Calef, F. (2017). Chemistry of diagenetic features analyzed by ChemCam at Pahrump Hills, Gale crater, Mars. *Icarus* 281**,** 121-136.

Navarro-González, R., Vargas, E., De La Rosa, J., Raga, A.C., and Mckay, C.P. (2010). Reanalysis of the Viking results suggests perchlorate and organics at midlatitudes on Mars. *Journal of Geophysical Research: Planets* 115**,** E12010.

Nealson, K.H. (1997). The limits of life on Earth and searching for life on Mars. *Journal of*

Geophysical Research: Planets 102**,** 23675-23686.

Nie, N.X., Dauphas, N., and Greenwood, R.C. (2017). Iron and oxygen isotope fractionation during iron UV photo-oxidation: Implications for early Earth and Mars. *Earth and Planetary Science Letters* 458**,** 179-191.

Nimmo, F., Hamilton, D.P., Mckinnon, W.B., Schenk, P.M., Binzel, R.P., Bierson, C.J., Beyer, R.A., Moore, J.M., Stern, S.A., Weaver, H.A., Olkin, C.B., Young, L.A., Smith, K.E., Moore, J.M., Mckinnon, W.B., Spencer, J.R., Beyer, R., Binzel, R.P., Buie, M., Buratti, B., Cheng, A., Cruikshank, D., Ore, C.D., Earle, A., Gladstone, R., Grundy, W., Howard, A.D., Lauer, T., Linscott, I., Nimmo, F., Parker, J., Porter, S., Reitsema, H., Reuter, D., Roberts, J.H., Robbins, S., Schenk, P.M., Showalter, M., Singer, K., Strobel, D., Summers, M., Tyler, L., White, O.L., Umurhan, O.M., Banks, M., Barnouin, O., Bray, V., Carcich, B., Chaikin, A., Chavez, C., Conrad, C., Hamilton, D.P., Howett, C., Hofgartner, J., Kammer, J., Lisse, C., Marcotte, A., Parker, A., Retherford, K., Saina, M., Runyon, K., Schindhelm, E., Stansberry, J., Steffl, A., Stryk, T., Throop, H., Tsang, C., Verbiscer, A., Winters, H., Zangari, A., Stern, S.A., Weaver, H.A., Olkin, C.B., Young, L.A., Smith, K.E., New Horizons Geology, G., and Imaging Theme, T. (2016). Reorientation of Sputnik Planitia implies a subsurface ocean on Pluto. *Nature* 540**,** 94-96.

Nixon, S.L. (2014). *Microbial iron reduction on Earth and Mars.* PhD thesis, University of Edinburgh.

Nixon, S.L., Cockell, C.S., and Tranter, M. (2012). Limitations to a microbial iron cycle on Mars. *Planetary and Space Science* 72**,** 116-128.

Nixon, S.L., Cousins, C.R., and Cockell, C.S. (2013). Plausible microbial metabolisms on Mars. *Astronomy & Geophysics* 54**,** 1.13-11.16.

Noffke, N., Christian, D., Wacey, D., and Hazen, R.M. (2013). Microbially induced sedimentary structures recording an ancient ecosystem in the ca. 3.48 billion-year-old Dresser Formation, Pilbara, Western Australia. *Astrobiology* 13**,** 1103-1124.

Nutman, A.P., Bennett, V.C., Friend, C.R., Van Kranendonk, M.J., and Chivas, A.R. (2016). Rapid emergence of life shown by discovery of 3,700-million-year-old microbial structures. *Nature* 537**,** 535-538.

Nyquist L.E., B.D.D., Shih Cy., Greshake A., Stöffler D., Eugster O. (2001). "Ages and Geologic Histories of Martian Meteorites", in: *Chronology and Evolution of Mars.*

Space Sciences Series of ISSI. (ed.) G.J. Kallenbach R., Hartmann W.K. . Springer, Dordrecht).

Ojha, L., Wilhelm, M.B., Murchie, S.L., Mcewen, A.S., Wray, J.J., Hanley, J., Massé, M., and Chojnacki, M. (2015). Spectral evidence for hydrated salts in recurring slope lineae on Mars. *Nature Geoscience* 8**,** 829-832.

Oren, A., Bardavid, R.E., and Mana, L. (2014). Perchlorate and halophilic prokaryotes: implications for possible halophilic life on Mars. *Extremophiles* 18**,** 75-80.

Osinski, G.R., Tornabene, L.L., Banerjee, N.R., Cockell, C.S., Flemming, R., Izawa, M.R.M., Mccutcheon, J., Parnell, J., Preston, L.J., Pickersgill, A.E., Pontefract, A., Sapers, H.M., and Southam, G. (2013). Impact-generated hydrothermal systems on Earth and Mars. *Icarus* 224**,** 347-363.

Palucis, M.C., Dietrich, W.E., Williams, R.M., Hayes, A.G., Parker, T., Sumner, D.Y., Mangold, N., Lewis, K., and Newsom, H. (2016). Sequence and relative timing of large lakes in Gale crater (Mars) after the formation of Mount Sharp. *Journal of Geophysical Research: Planets* 121**,** 472-496.

Pantke, C., Obst, M., Benzerara, K., Morin, G., Ona-Nguema, G., Dippon, U., and Kappler, A. (2012). Green rust formation during Fe (II) oxidation by the nitrate-reducing *Acidovorax sp.* strain BoFeN1. *Environmental Science & Technology* 46**,** 1439-1446.

Parnell, J., Lee, P., Cockell, C.S., and Osinski, G.R. (2004). Microbial colonization in impact-generated hydrothermal sulphate deposits, Haughton impact structure, and implications for sulphates on Mars. *International Journal of Astrobiology* 3**,** 247-256.

Peters, G.H., Abbey, W., Bearman, G.H., Mungas, G.S., Smith, J.A., Anderson, R.C., Douglas, S., and Beegle, L.W. (2008). Mojave Mars simulant—Characterization of a new geologic Mars analog. *Icarus* 197**,** 470-479.

Picard, A., Kappler, A., Schmid, G., Quaroni, L., and Obst, M. (2015). Experimental diagenesis of organo-mineral structures formed by microaerophilic Fe(II)-oxidizing bacteria. *Nature Communications* 6**,** 6277.

Pirajno, F. (2009). "Hydrothermal processes associated with meteorite impacts," in *Hydrothermal processes and mineral systems*. (Dordrecht: Springer), 1097-1130.

Popa, R., Smith, A.R., Popa, R., Boone, J., and Fisk, M. (2012). Olivine-respiring bacteria isolated from the rock-ice interface in a lava-tube cave, a Mars analog environment.

Astrobiology 12**,** 9-18.

Porco, C.C., Helfenstein, P., Thomas, P.C., Ingersoll, A.P., Wisdom, J., West, R., Neukum, G., Denk, T., Wagner, R., Roatsch, T., Kieffer, S., Turtle, E., Mcewen, A., Johnson, T.V., Rathbun, J., Veverka, J., Wilson, D., Perry, J., Spitale, J., Brahic, A., Burns, J.A., Delgenio, A.D., Dones, L., Murray, C.D., and Squyres, S. (2006). Cassini Observes the Active South Pole of Enceladus. *Science* 311**,** 1393.

Postberg, F., Kempf, S., Schmidt, J., Brilliantov, N., Beinsen, A., Abel, B., Buck, U., and Srama, R. (2009). Sodium salts in E-ring ice grains from an ocean below the surface of Enceladus. *Nature* 459**,** 1098-1101.

Postberg, F., Khawaja, N., Abel, B., Choblet, G., Glein, C.R., Gudipati, M.S., Henderson, B.L., Hsu, H.-W., Kempf, S., Klenner, F., Moragas-Klostermeyer, G., Magee, B., Nölle, L., Perry, M., Reviol, R., Schmidt, J., Srama, R., Stolz, F., Tobie, G., Trieloff, M., and Waite, J.H. (2018). Macromolecular organic compounds from the depths of Enceladus. *Nature* 558**,** 564-568.

Preston, L., Barber, S., and Grady, M. (2012). Introducing a new on-line resource for planning scientific field investigations in planetary analogue environments: CAFE. *Astrobiology Science Conference 2012, Atlanta*.

Preston, L., Shuster, J., Fernández-Remolar, D., Banerjee, N., Osinski, G., and Southam, G. (2011). The preservation and degradation of filamentous bacteria and biomolecules within iron oxide deposits at Rio Tinto, Spain. *Geobiology* 9**,** 233-249.

Preston, L.J., and Dartnell, L.R. (2014). Planetary habitability: lessons learned from terrestrial analogues. *International Journal of Astrobiology* 13**,** 81-98.

Price, A., Pearson, V.K., Schwenzer, S.P., Miot, J., and Olsson-Francis, K. (2018). Nitrate-Dependent Iron Oxidation: A Potential Mars Metabolism. *Frontiers in Microbiology* 9**,** 513.

Quantin-Nataf, C., Carter, J., Mandon, L., Balme, M., Fawdon, P., Davis, J., Thollot, P., Dehouck, E., Pan, L., and Volat, M. (2019). ExoMars at Oxia Planum, probing the aqueous-related Noachian environments. *Ninth International Conference on Mars 2019*.

Raghoebarsing, A.A., Pol, A., Van De Pas-Schoonen, K.T., Smolders, A.J.P., Ettwig, K.F., Rijpstra, W.I.C., Schouten, S., Damsté, J.S.S., Op Den Camp, H.J.M., Jetten, M.S.M., and Strous, M. (2006). A microbial consortium couples anaerobic methane

oxidation to denitrification. *Nature* 440**,** 918.

Raiswell, R., and Canfield, D.E. (2012). The iron biogeochemical cycle past and present. *Geochemical Perspectives* 1**,** 1-2.

Ramirez, R.M., Kopparapu, R., Zugger, M.E., Robinson, T.D., Freedman, R., and Kasting, J.F. (2014). Warming early Mars with CO_2 and H_2. *Nature Geoscience* 7**,** 59-63.

Ramkissoon, N.K., Pearson, V.K., Schwenzer, S.P., Schröder, C., Kirnbauer, T., Wood, D., Seidel, R.G.W., Miller, M.A., and Olsson-Francis, K. (2019). New simulants for martian regolith: Controlling iron variability. *Planetary and Space Science* 179**,** 104722.

Rampe, E.B., Ming, D.W., Blake, D.F., Bristow, T.F., Chipera, S.J., Grotzinger, J.P., Morris, R.V., Morrison, S.M., Vaniman, D.T., Yen, A.S., Achilles, C.N., Craig, P.I., Des Marais, D.J., Downs, R.T., Farmer, J.D., Fendrich, K.V., Gellert, R., Hazen, R.M., Kah, L.C., Morookian, J.M., Peretyazhko, T.S., Sarrazin, P., Treiman, A.H., Berger, J.A., Eigenbrode, J., Fairén, A.G., Forni, O., Gupta, S., Hurowitz, J.A., Lanza, N.L., Schmidt, M.E., Siebach, K., Sutter, B., and Thompson, L.M. (2017). Mineralogy of an ancient lacustrine mudstone succession from the Murray formation, Gale crater, Mars. *Earth and Planetary Science Letters* 471**,** 172-185.

Reid, I.N., Sparks, W.B., Lubow, S., Mcgrath, M., Livio, M., Valenti, J., Sowers, K.R., Shukla, H.D., Macauley, S., Miller, T., Suvanasuthi, R., Belas, R., Colman, A., Robb, F.T., Dassarma, P., Müller, J.A., Coker, J.A., Cavicchioli, R., Chen, F., and Dassarma, S. (2006). Terrestrial models for extraterrestrial life: methanogens and halophiles at Martian temperatures. *International Journal of Astrobiology* 5**,** 89-97.

Reimers, C.E., Fischer, K.M., Merewether, R., Smith, K., and Jahnke, R.A. (1986). Oxygen microprofiles measured in situ in deep ocean sediments. *Nature* 320**,** 741-744.

Ren, B., Tibbelin, G., Kajino, T., Asami, O., and Ladenstein, R. (2003). The Multi-layered Structure of Dps with a Novel Di-nuclear Ferroxidase Center. *Journal of Molecular Biology* 329**,** 467-477.

Revsbech, N.P., Sorensen, J., Blackburn, T.H., and Lomholt, J.P. (1980). Distribution of oxygen in marine sediments measured with microelectrodes. *Limnology and Oceanography* 25**,** 403-411.

Rieder, R., Gellert, R., Anderson, R.C., Brückner, J., Clark, B.C., Dreibus, G., Economou,

T., Klingelhöfer, G., Lugmair, G.W., Ming, D.W., Squyres, S.W., D'uston, C., Wänke, H., Yen, A., and Zipfel, J. (2004). Chemistry of Rocks and Soils at Meridiani Planum from the Alpha Particle X-ray Spectrometer. *Science* 306**,** 1746-1749.

Roberts, J.H., and Nimmo, F. (2008). Tidal heating and the long-term stability of a subsurface ocean on Enceladus. *Icarus* 194**,** 675-689.

Roden, E.E., Sobolev, D., Glazer, B., and Luther, G.W. (2004). Potential for microscale bacterial Fe redox cycling at the aerobic-anaerobic interface. *Geomicrobiology Journal* 21**,** 379-391.

Roth, L., Saur, J., Retherford, K.D., Strobel, D.F., Feldman, P.D., Mcgrath, M.A., and Nimmo, F. (2014). Transient Water Vapor at Europa's South Pole. *Science* 343**,** 171.

Rowley, G., Hensen, D., Felgate, H., Arkenberg, A., Appia-Ayme, C., Prior, K., Harrington, C., Field, Sarah j., Butt, Julea n., Baggs, E., and Richardson, David j. (2012). Resolving the contributions of the membrane-bound and periplasmic nitrate reductase systems to nitric oxide and nitrous oxide production in *Salmonella enterica* serovar Typhimurium. *Biochemical Journal* 441**,** 755-762.

Rull, F., Maurice, S., Hutchinson, I., Moral, A., Perez, C., Diaz, C., Colombo, M., Belenguer, T., Lopez-Reyes, G., Sansano, A., Forni, O., Parot, Y., Striebig, N., Woodward, S., Howe, C., Tarcea, N., Rodriguez, P., Seoane, L., Santiago, A., Rodriguez-Prieto, J.A., Medina, J., Gallego, P., Canchal, R., Santamaría, P., Ramos, G., Vago, J.L., and On Behalf of The, R.L.S.T. (2017). The Raman Laser Spectrometer for the ExoMars Rover Mission to Mars. *Astrobiology* 17**,** 627-654.

Santelli, C.M., Welch, S.A., Westrich, H.R., and Banfield, J.F. (2001). The effect of Fe-oxidizing bacteria on Fe-silicate mineral dissolution. *Chemical Geology* 180**,** 99-115.

Sarkar, J., Seshadri, V., Tripoulas, N.A., Ketterer, M.E., and Fox, P.L. (2003). Role of Ceruloplasmin in Macrophage Iron Efflux during Hypoxia. *Journal of Biological Chemistry* 278**,** 44018-44024.

Sauer, M., Porro, D., Mattanovich, D., and Branduardi, P. (2008). Microbial production of organic acids: expanding the markets. *Trends in Biotechnology* 26**,** 100-108.

Saur, J., Duling, S., Roth, L., Jia, X., Strobel, D.F., Feldman, P.D., Christensen, U.R., Retherford, K.D., Mcgrath, M.A., Musacchio, F., Wennmacher, A., Neubauer,

F.M., Simon, S., and Hartkorn, O. (2015). The search for a subsurface ocean in Ganymede with Hubble Space Telescope observations of its auroral ovals. *Journal of Geophysical Research: Space Physics* 120**,** 1715-1737.

Schädler, S., Burkhardt, C., Hegler, F., Straub, K., Miot, J., Benzerara, K., and Kappler, A. (2009). Formation of cell-iron-mineral aggregates by phototrophic and nitrate-reducing anaerobic Fe (II)-oxidizing bacteria. *Geomicrobiology Journal* 26**,** 93-103.

Schieber, J. (2002). Sedimentary pyrite: A window into the microbial past. *Geology* 30**,** 531-534.

Schröder, I., Johnson, E., and De Vries, S. (2003). Microbial ferric iron reductases. *FEMS Microbiology Reviews* 27**,** 427-447.

Schuerger, A.C., and Nicholson, W.L. (2016). Twenty Species of Hypobarophilic Bacteria Recovered from Diverse Soils Exhibit Growth under Simulated Martian Conditions at 0.7 kPa. *Astrobiology* 16**,** 964-976.

Schwenzer, S.P., Abramov, O., Allen, C.C., Bridges, J.C., Clifford, S.M., Filiberto, J., Kring, D.A., Lasue, J., Mcgovern, P.J., Newsom, H.E., Treiman, A.H., Vaniman, D.T., Wiens, R.C., and Wittmann, A. (2012). Gale Crater: Formation and post-impact hydrous environments. *Planetary and Space Science* 70**,** 84-95.

Schwenzer, S.P., Bridges, J.C., Wiens, R.C., Conrad, P.G., Kelley, S.P., Leveille, R., Mangold, N., Martín-Torres, J., Mcadam, A., Newsom, H., Zorzano, M.P., Rapin, W., Spray, J., Treiman, A.H., Westall, F., Fairén, A.G., and Meslin, P.Y. (2016). Fluids during diagenesis and sulfate vein formation in sediments at Gale crater, Mars. *Meteoritics & Planetary Science* 51**,** 2175-2202.

Schwenzer, S.P., and Kring, D.A. (2009). Impact-generated hydrothermal systems capable of forming phyllosilicates on Noachian Mars. *Geology* 37**,** 1091-1094.

Seckback, J. (1982). Ferreting out the secrets of plant ferritin - A review. *Journal of Plant Nutrition* 5**,** 369-394.

Seewald, J.S. (2017). Detecting molecular hydrogen on Enceladus. *Science* 356**,** 132.

Sephton, M.A., Wright, I.P., Gilmour, I., De Leeuw, J.W., Grady, M.M., and Pillinger, C.T. (2002). High molecular weight organic matter in martian meteorites. *Planetary and Space Science* 50**,** 711-716.

Serra, D.O., Richter, A.M., and Hengge, R. (2013). Cellulose as an Architectural Element in Spatially Structured *Escherichia coli* Biofilms. *Journal of Bacteriology* 195**,**

5540-5554.

Shelobolina, E.S., Vanpraagh, C.G., and Lovley, D.R. (2003). Use of Ferric and Ferrous Iron Containing Minerals for Respiration by Desulfitobacterium frappieri. *Geomicrobiology Journal* 20**,** 143-156.

Sholes, S.F., Smith, M.L., Claire, M.W., Zahnle, K.J., and Catling, D.C. (2017). Anoxic atmospheres on Mars driven by volcanism: Implications for past environments and life. *Icarus* 290**,** 46-62.

Smith, A.R. (2011). *Subsurface Igneous Mineral Microbiology: Iron-Oxidizing Organotrophs on Olivine Surfaces and the Significance of Mineral Heterogeneity in Basalts*. Master thesis, Portland State University.

Smith, M.L., Claire, M.W., Catling, D.C., and Zahnle, K.J. (2014). The formation of sulfate, nitrate and perchlorate salts in the martian atmosphere. *Icarus* 231**,** 51-64.

Sparacino-Watkins, C., Stolz, J.F., and Basu, P. (2014). Nitrate and periplasmic nitrate reductases. *Chemical Society Reviews* 43**,** 676-706.

Squyres, S., Grotzinger, J., Arvidson, R., Bell, J., Calvin, W., Christensen, P., Clark, B., Crisp, J., Farrand, W., and Herkenhoff, K.E. (2004a). In situ evidence for an ancient aqueous environment at Meridiani Planum, Mars. *Science* 306**,** 1709-1714.

Squyres, S.W., Arvidson, R.E., Bell, J., Calef, F., Clark, B., Cohen, B., Crumpler, L., De Souza, P., Farrand, W., and Gellert, R. (2012). Ancient impact and aqueous processes at Endeavour Crater, Mars. *Science* 336**,** 570-576.

Squyres, S.W., Grotzinger, J.P., Arvidson, R.E., Bell, J.F., Calvin, W., Christensen, P.R., Clark, B.C., Crisp, J.A., Farrand, W.H., Herkenhoff, K.E., Johnson, J.R., Klingelhöfer, G., Knoll, A.H., Mclennan, S.M., Mcsween, H.Y., Morris, R.V., Rice, J.W., Rieder, R., and Soderblom, L.A. (2004b). In Situ Evidence for an Ancient Aqueous Environment at Meridiani Planum, Mars. *Science* 306**,** 1709-1714.

Squyres, S.W., and Knoll, A.H. (2005). Sedimentary rocks at Meridiani Planum: Origin, diagenesis, and implications for life on Mars. *Earth and Planetary Science Letters* 240**,** 1-10.

Stamenković, V., Ward, L.M., Mischna, M., and Fischer, W.W. (2018). O2 solubility in Martian near-surface environments and implications for aerobic life. *Nature Geoscience* 11**,** 905-909.

Steele, A., Mccubbin, F., Fries, M., Kater, L., Boctor, N., Fogel, M., Conrad, P.,

Glamoclija, M., Spencer, M., and Morrow, A. (2012a). A reduced organic carbon component in martian basalts. *Science* 337**,** 212-215.

Steele, A., Mccubbin, F.M., Fries, M., Kater, L., Boctor, N.Z., Fogel, M.L., Conrad, P.G., Glamoclija, M., Spencer, M., Morrow, A.L., Hammond, M.R., Zare, R.N., Vicenzi, E.P., Siljeström, S., Bowden, R., Herd, C.D.K., Mysen, B.O., Shirey, S.B., Amundsen, H.E.F., Treiman, A.H., Bullock, E.S., and Jull, A.J.T. (2012b). A Reduced Organic Carbon Component in Martian Basalts. *Science* 337**,** 212-215.

Stern, J.C., Sutter, B., Freissinet, C., Navarro-González, R., Mckay, C.P., Archer, P.D., Buch, A., Brunner, A.E., Coll, P., and Eigenbrode, J.L. (2015). Evidence for indigenous nitrogen in sedimentary and aeolian deposits from the Curiosity rover investigations at Gale crater, Mars. *Proceedings of the National Academy of Sciences* 112**,** 4245-4250.

Stern, J.C., Sutter, B., Jackson, W.A., Navarro-González, R., Mckay, C.P., Ming, D.W., Archer, P.D., and Mahaffy, P.R. (2017). The nitrate/(per) chlorate relationship on Mars. *Geophysical Research Letters* 44**,** 2643-2651.

Stevens, A.H., Steer, E., Mcdonald, A., Amador, E.S., and Cockell, C.S. (2018). Y-Mars: An Astrobiological Analogue of Martian Mudstone. *Earth and Space Science* 5**,** 163-174.

Stevens, M.H., Evans, J., Schneider, N.M., Stewart, A.I.F., Deighan, J., Jain, S.K., Crismani, M., Stiepen, A., Chaffin, M.S., and Mcclintock, W.E. (2015). New observations of molecular nitrogen in the Martian upper atmosphere by IUVS on MAVEN. *Geophysical Research Letters* 42**,** 9050-9056.

Stookey, L.L. (1970). Ferrozine---a new spectrophotometric reagent for iron. *Analytical chemistry* 42**,** 779-781.

Straub, K.L., Benz, M., Schink, B., and Widdel, F. (1996). Anaerobic, nitrate-dependent microbial oxidation of ferrous iron. *Applied and Environmental Microbiology* 62**,** 1458-1460.

Straub, K.L., and Buchholz-Cleven, B.E. (1998). Enumeration and detection of anaerobic ferrous iron-oxidizing, nitrate-reducing bacteria from diverse European sediments. *Applied and Environmental Microbiology* 64**,** 4846-4856.

Straub, K.L., Schönhuber, W.A., Buchholz-Cleven, B.E., and Schink, B. (2004). Diversity of ferrous iron-oxidizing, nitrate-reducing bacteria and their involvement in oxygen-independent iron cycling. *Geomicrobiology Journal* 21**,** 371-378.

Strohm, T.O., Griffin, B., Zumft, W.G., and Schink, B. (2007). Growth yields in bacterial denitrification and nitrate ammonification. *Applied and environmental microbiology* 73**,** 1420-1424.

Summers, D.P., Basa, R.C., Khare, B., and Rodoni, D. (2012). Abiotic nitrogen fixation on terrestrial planets: Reduction of NO to ammonia by FeS. *Astrobiology* 12**,** 107-114.

Summers, D.P., and Khare, B. (2007). Nitrogen fixation on early Mars and other terrestrial planets: experimental demonstration of abiotic fixation reactions to nitrite and nitrate. *Astrobiology* 7**,** 333-341.

Summers, S. (2013). *The bacterial ecology and function from a sub-surface critical zone*. PhD thesis, Open University.

Sutter, B., Eigenbrode, J.L., Steele, A., Mcadam, A., Ming, D.W., Archer, D., Jr., and Mahaffy, P.R. (2016). "The Sample Analysis at Mars (SAM) Detections of CO_2 and CO in Sedimentary Material from Gale Crater, Mars: Implications for the Presence of Organic Carbon and Microbial Habitability on Mars", in: *AGU Fall Meeting Abstracts.*).

Swindle, T.D., Treiman, A.H., Lindstrom, D.J., Burkland, M.K., Cohen, B.A., Grier, J.A., Li, B., and Olson, E.K. (2000). Noble gases in iddingsite from the Lafayette meteorite: Evidence for liquid water on Mars in the last few hundred million years. *Meteoritics & Planetary Science* 35**,** 107-115.

Tanaka, K.L., Skinner, J.A., and Hare, T.M. (2005). Geologic map of the northern plains of Mars.

Tatusova, T., Dicuccio, M., Badretdin, A., Chetvernin, V., Nawrocki, E.P., Zaslavsky, L., Lomsadze, A., Pruitt, K.D., Borodovsky, M., and Ostell, J. (2016). NCBI prokaryotic genome annotation pipeline. *Nucleic Acids Research* 44**,** 6614-6624.

Taubner, R.-S., Leitner, J.J., Firneis, M.G., and Hitzenberger, R. (2016). Modelling the Interior Structure of Enceladus Based on the 2014's Cassini Gravity Data. *Origins of Life and Evolution of Biospheres* 46**,** 283-288.

Taubner, R.-S., Olsson-Francis, K., Vance, S.D., Ramkissoon, N.K., Postberg, F., De Vera, J.-P., Antunes, A., Camprubi Casas, E., Sekine, Y., Noack, L., Barge, L., Goodman, J., Jebbar, M., Journaux, B., Karatekin, Ö., Klenner, F., Rabbow, E., Rettberg, P., Rückriemen-Bez, T., Saur, J., Shibuya, T., and Soderlund, K.M. (2020). Experimental and Simulation Efforts in the Astrobiological Exploration of Exooceans. *Space Science Reviews* 216**,** 9.

Taubner, R.-S., Pappenreiter, P., Zwicker, J., Smrzka, D., Pruckner, C., Kolar, P., Bernacchi, S., Seifert, A.H., Krajete, A., Bach, W., Peckmann, J., Paulik, C., Firneis, M.G., Schleper, C., and Rittmann, S.K.M.R. (2018). Biological methane production under putative Enceladus-like conditions. *Nature Communications* 9**,** 748.

Tebo, B.M., Johnson, H.A., Mccarthy, J.K., and Templeton, A.S. (2005). Geomicrobiology of manganese(II) oxidation. *Trends in Microbiology* 13**,** 421-428.

Temple, K.L., and Colmer, A.R. (1951). The autotrophic oxidation of iron by a new bacterium: *Thiobacillus ferrooxidans*. *Journal of Bacteriology* 62**,** 605.

Theil, E.C. (2004). Iron, Ferritin and Nutrition. *Annual Review of Nutrition* 24**,** 327-343.

Tomasek, A., Kozarek, J.L., Hondzo, M., Lurndahl, N., Sadowsky, M.J., Wang, P., and Staley, C. (2017). Environmental drivers of denitrification rates and denitrifying gene abundances in channels and riparian areas. *Water Resources Research* 53**,** 6523-6538.

Tominski, C., Heyer, H., Lösekann-Behrens, T., Behrens, S., and Kappler, A. (2018). Growth and Population Dynamics of the Anaerobic Fe(II)-Oxidizing and Nitrate-Reducing Enrichment Culture KS. *Applied and Environmental Microbiology* 84**,** e02173-02117.

Toporski, J.K., Steele, A., Westall, F., Thomas-Keprta, K.L., and Mckay, D.S. (2002a). The simulated silicification of bacteria--new clues to the modes and timing of bacterial preservation and implications for the search for extraterrestrial microfossils. *Astrobiology* 2**,** 1-26.

Toporski, J.K.W., Steele, A., Westall, F., Avci, R., Martill, D.M., and Mckay, D.S. (2002b). Morphologic and spectral investigation of exceptionally well-preserved bacterial biofilms from the Oligocene Enspel formation, Germany. *Geochimica et Cosmochimica Acta* 66**,** 1773-1791.

Tosca, N.J., and Mclennan, S.M. (2006). Chemical divides and evaporite assemblages on Mars. *Earth and Planetary Science Letters* 241**,** 21-31.

Tosca, N.J., and Mclennan, S.M. (2009). Experimental constraints on the evaporation of partially oxidized acid-sulfate waters at the martian surface. *Geochimica et Cosmochimica Acta* 73**,** 1205-1222.

Tosca, N.J., Mclennan, S.M., Lamb, M.P., and Grotzinger, J.P. (2011). Physicochemical properties of concentrated Martian surface waters. *Journal of Geophysical*

Research: Planets 116**,** E05004.

Töwe, S., Leelakriangsak, M., Kobayashi, K., Van Duy, N., Hecker, M., Zuber, P., and Antelmann, H. (2007). The MarR-type repressor MhqR (YkvE) regulates multiple dioxygenases/glyoxalases and an azoreductase which confer resistance to 2-methylhydroquinone and catechol in *Bacillus subtilis*. *Molecular Microbiology* 66**,** 40-54.

Trumbo, S.K., Brown, M.E., and Hand, K.P. (2019). Sodium chloride on the surface of Europa. *Science Advances* 5**,** eaaw7123.

Tuff, J., Wade, J., and Wood, B. (2013). Volcanism on Mars controlled by early oxidation of the upper mantle. *Nature* 498**,** 342-345.

Vago, J.L., Westall, F., Pasteur Instrument Teams, L.S.S.W.G., Other, C., Coates, A.J., Jaumann, R., Korablev, O., Ciarletti, V., Mitrofanov, I., Josset, J.-L., De Sanctis, M.C., Bibring, J.-P., Rull, F., Goesmann, F., Steininger, H., Goetz, W., Brinckerhoff, W., Szopa, C., Raulin, F., Westall, F., Edwards, H.G.M., Whyte, L.G., Fairén, A.G., Bibring, J.-P., Bridges, J., Hauber, E., Ori, G.G., Werner, S., Loizeau, D., Kuzmin, R.O., Williams, R.M.E., Flahaut, J., Forget, F., Vago, J.L., Rodionov, D., Korablev, O., Svedhem, H., Sefton-Nash, E., Kminek, G., Lorenzoni, L., Joudrier, L., Mikhailov, V., Zashchirinskiy, A., Alexashkin, S., Calantropio, F., Merlo, A., Poulakis, P., Witasse, O., Bayle, O., Bayón, S., Meierhenrich, U., Carter, J., García-Ruiz, J.M., Baglioni, P., Haldemann, A., Ball, A.J., Debus, A., Lindner, R., Haessig, F., Monteiro, D., Trautner, R., Voland, C., Rebeyre, P., Goulty, D., Didot, F., Durrant, S., Zekri, E., Koschny, D., Toni, A., Visentin, G., Zwick, M., Van Winnendael, M., Azkarate, M., Carreau, C., and The Exomars Project, T. (2017). Habitability on Early Mars and the Search for Biosignatures with the ExoMars Rover. *Astrobiology* 17**,** 471-510.

Valdivia-Silva, J.E., Navarro-González, R., Ortega-Gutierrez, F., Fletcher, L.E., Perez-Montaño, S., Condori-Apaza, R., and Mckay, C.P. (2011). Multidisciplinary approach of the hyperarid desert of Pampas de La Joya in southern Peru as a new Mars-like soil analog. *Geochimica et Cosmochimica Acta* 75**,** 1975-1991.

Van Duy, N., Wolf, C., Mäder, U., Lalk, M., Langer, P., Lindequist, U., Hecker, M., and Antelmann, H. (2007). Transcriptome and proteome analyses in response to 2-methylhydroquinone and 6-brom-2-vinyl-chroman-4-on reveal different degradation systems involved in the catabolism of aromatic compounds in *Bacillus*

subtilis. *Proteomics* 7**,** 1391-1408.

Vanhaecke, F., Balcaen, L., De Wannemacker, G., and Moens, L. (2002). Capabilities of inductively coupled plasma mass spectrometry for the measurement of Fe isotope ratios. *Journal of Analytical Atomic Spectrometry* 17**,** 933-943.

Vaniman, D.T., Bish, D.L., Ming, D.W., Bristow, T.F., Morris, R.V., Blake, D.F., Chipera, S.J., Morrison, S.M., Treiman, A.H., Rampe, E.B., Rice, M., Achilles, C.N., Grotzinger, J., Mclennan, S.M., Williams, J., Bell, J., Newsom, H., Downs, R.T., Maurice, S., Sarrazin, P., Yen, A.S., Morookian, J.M., Farmer, J.D., Stack, K., Milliken, R.E., Ehlmann, B., Sumner, D.Y., Berger, G., Crisp, J.A., Hurowitz, J.A., Anderson, R., Desmarais, D., Stolper, E.M., Edgett, K.S., Gupta, S., Spanovich, N., and Team, M.S. (2013). Mineralogy of a Mudstone at Yellowknife Bay, Gale Crater, Mars. *Science* 343**,** 1243480.

Visscher, P.T., Beukema, J., and Van Gemerden, H. (1991). In situ characterization of sediments: measurements of oxygen and sulfide profiles with a novel combined needle electrode. *Limnology and Oceanography* 36**,** 1476-1480.

Vodyanitskii, Y.N. (2001). On the dissolution of iron minerals in Tamm's reagent. *Eurasian Soil Science* 34**,** 1086-1096.

Wacey, D., Mcloughlin, N., Kilburn, M.R., Saunders, M., Cliff, J.B., Kong, C., Barley, M.E., and Brasier, M.D. (2013). Nanoscale analysis of pyritized microfossils reveals differential heterotrophic consumption in the ~1.9-Ga Gunflint chert. *Proceedings of the National Academy of Sciences* 110**,** 8020-8024.

Waite, J.H., Combi, M.R., Ip, W.-H., Cravens, T.E., Mcnutt, R.L., Kasprzak, W., Yelle, R., Luhmann, J., Niemann, H., Gell, D., Magee, B., Fletcher, G., Lunine, J., and Tseng, W.-L. (2006). Cassini Ion and Neutral Mass Spectrometer: Enceladus Plume Composition and Structure. *Science* 311**,** 1419.

Waite, J.H., Glein, C.R., Perryman, R.S., Teolis, B.D., Magee, B.A., Miller, G., Grimes, J., Perry, M.E., Miller, K.E., Bouquet, A., Lunine, J.I., Brockwell, T., and Bolton, S.J. (2017). Cassini finds molecular hydrogen in the Enceladus plume: Evidence for hydrothermal processes. *Science* 356**,** 155-159.

Wang, R., Xu, S.-Y., Zhang, M., Ghulam, A., Dai, C.-L., and Zheng, P. (2020). Iron as electron donor for denitrification: The efficiency, toxicity and mechanism. *Ecotoxicology and Environmental Safety* 194**,** 110343.

Weber, K.A., Achenbach, L.A., and Coates, J.D. (2006a). Microorganisms pumping iron:

anaerobic microbial iron oxidation and reduction. *Nature Reviews Microbiology* 4**,** 752-764.

Weber, K.A., Hedrick, D.B., Peacock, A.D., Thrash, J.C., White, D.C., Achenbach, L.A., and Coates, J.D. (2009). Physiological and taxonomic description of the novel autotrophic, metal oxidizing bacterium, *Pseudogulbenkiania sp*. strain 2002. *Applied Microbiology and Biotechnology* 83**,** 555-565.

Weber, K.A., Pollock, J., Cole, K.A., O'connor, S.M., Achenbach, L.A., and Coates, J.D. (2006b). Anaerobic nitrate-dependent iron (II) bio-oxidation by a novel lithoautotrophic betaproteobacterium, strain 2002. *Applied and Environmental Microbiology* 72**,** 686-694.

Webster, C.R., Mahaffy, P.R., Atreya, S.K., Flesch, G.J., Mischna, M.A., Meslin, P.-Y., Farley, K.A., Conrad, P.G., Christensen, L.E., Pavlov, A.A., Martín-Torres, J., Zorzano, M.-P., Mcconnochie, T.H., Owen, T., Eigenbrode, J.L., Glavin, D.P., Steele, A., Malespin, C.A., Archer, P.D., Sutter, B., Coll, P., Freissinet, C., Mckay, C.P., Moores, J.E., Schwenzer, S.P., Bridges, J.C., Navarro-Gonzalez, R., Gellert, R., and Lemmon, M.T. (2015). Mars methane detection and variability at Gale crater. *Science* 347**,** 415-417.

Webster, C.R., Mahaffy, P.R., Atreya, S.K., Moores, J.E., Flesch, G.J., Malespin, C., Mckay, C.P., Martinez, G., Smith, C.L., Martin-Torres, J., Gomez-Elvira, J., Zorzano, M.-P., Wong, M.H., Trainer, M.G., Steele, A., Archer, D., Sutter, B., Coll, P.J., Freissinet, C., Meslin, P.-Y., Gough, R.V., House, C.H., Pavlov, A., Eigenbrode, J.L., Glavin, D.P., Pearson, J.C., Keymeulen, D., Christensen, L.E., Schwenzer, S.P., Navarro-Gonzalez, R., Pla-García, J., Rafkin, S.C.R., Vicente-Retortillo, Á., Kahanpää, H., Viudez-Moreiras, D., Smith, M.D., Harri, A.-M., Genzer, M., Hassler, D.M., Lemmon, M., Crisp, J., Sander, S.P., Zurek, R.W., and Vasavada, A.R. (2018). Background levels of methane in Mars' atmosphere show strong seasonal variations. *Science* 360**,** 1093-1096.

Welhan, J.A., and Craig, H. (1983). "Methane, hydrogen and helium in hydrothermal fluids at 21 N on the East Pacific Rise," in *Hydrothermal processes at seafloor spreading centers*, eds. P.A. Rona, K. Boström, L. Laubier & K.L. Smith. Springer), 391-409.

Westall, F., De Vries, S.T., Nijman, W., Rouchon, V., Orberger, B., Pearson, V., Watson, J., Verchovsky, A., Wright, I., and Rouzaud, J.-N. (2006). The 3.466 Ga "Kitty's

Gap Chert," an early Archean microbial ecosystem. *Geological Society of America Special Papers* 405**,** 105-131.

Westall, F., Foucher, F., Bost, N., Bertrand, M., Loizeau, D., Vago, J.L., Kminek, G., Gaboyer, F., Campbell, K.A., Bréhéret, J.-G., Gautret, P., and Cockell, C.S. (2015). Biosignatures on Mars: What, Where, and How? Implications for the Search for Martian Life. *Astrobiology* 15**,** 998-1029.

Wheat, C.G., Feely, R.A., and Mottl, M.J. (1996). Phosphate removal by oceanic hydrothermal processes: An update of the phosphorus budget in the oceans. *Geochimica et Cosmochimica Acta* 60**,** 3593-3608.

Widdel, F., Schnell, S., Heising, S., Ehrenreich, A., Assmus, B., and Schink, B. (1993). Ferrous iron oxidation by anoxygenic phototrophic bacteria. *Nature* 362**,** 834.

Williams, R.M.E., Grotzinger, J.P., Dietrich, W.E., Gupta, S., Sumner, D.Y., Wiens, R.C., Mangold, N., Malin, M.C., Edgett, K.S., and Maurice, S. (2013). Martian fluvial conglomerates at Gale crater. *Science* 340**,** 1068-1072.

Wogelius, R.A., and Walther, J.V. (1991). Olivine dissolution at 25 C: Effects of pH, CO_2, and organic acids. *Geochimica et Cosmochimica Acta* 55**,** 943-954.

Wordsworth, R.D. (2016). The Climate of Early Mars. *Annual Review of Earth and Planetary Sciences* 44**,** 381-408.

Wray, J.J., Murchie, S.L., Bishop, J.L., Ehlmann, B.L., Milliken, R.E., Wilhelm, M.B., Seelos, K.D., and Chojnacki, M. (2016). Orbital evidence for more widespread carbonate-bearing rocks on Mars. *Journal of Geophysical Research: Planets* 121**,** 652-677.

Wynn-Williams, D., and Edwards, H. (2000). Antarctic ecosystems as models for extraterrestrial surface habitats. *Planetary and Space Science* 48**,** 1065-1075.

Xiong, M.Y., Shelobolina, E.S., and Roden, E.E. (2015). Potential for microbial oxidation of ferrous iron in basaltic glass. *Astrobiology* 15**,** 331-340.

Yen, A.S., Ming, D.W., Vaniman, D.T., Gellert, R., Blake, D.F., Morris, R.V., Morrison, S.M., Bristow, T.F., Chipera, S.J., and Edgett, K.S. (2017). Multiple stages of aqueous alteration along fractures in mudstone and sandstone strata in Gale Crater, Mars. *Earth and Planetary Science Letters* 471**,** 186-198.

Yen, A.S., Mittlefehldt, D.W., Mclennan, S.M., Gellert, R., Bell, J., Mcsween, H.Y., Ming, D.W., Mccoy, T.J., Morris, R.V., and Golombek, M. (2006). Nickel on Mars: Constraints on meteoritic material at the surface. *Journal of Geophysical Research:*

Planets 111.

Zhao, L., Dong, H., Kukkadapu, R., Agrawal, A., Liu, D., Zhang, J., and Edelmann, R.E. (2013). Biological oxidation of Fe(II) in reduced nontronite coupled with nitrate reduction by Pseudogulbenkiania sp. Strain 2002. *Geochimica et Cosmochimica Acta* 119**,** 231-247.

Zhou, J., Wang, H., Yang, K., Ji, B., Chen, D., Zhang, H., Sun, Y., and Tian, J. (2016). Autotrophic denitrification by nitrate-dependent Fe(II) oxidation in a continuous up-flow biofilter. *Bioprocess and Biosystems Engineering* 39**,** 277-284.

Zolotov, M.Y., and Mironenko, M.V. (2007). Timing of acid weathering on Mars: A kinetic-thermodynamic assessment. *Journal of Geophysical Research: Planets* 112**,** E07006.

Appendices

A. Media and solutions

Chapter 2

Nutrient media

Peptone 5.0 g

Meat Extract 3.0 g

Distilled water 1000.0 ml

S-8 media for Thiobacillus

Solution A:

KH_2PO_4 2.0 g

KNO_3 2.0 g

NH_4Cl 1.0 g

$MgSO_4$ x 7 H_2O 0.8 g

Trace element solution SL-4 2.0 ml

Agar (for solid medium) 15.0 g

Distilled water 940.0 ml

Adjust pH to 7.0 with NaOH.

Solution B:

$Na_2S_2O_3$ x 5 H_2O 5.0 g

Distilled water 40.0 ml

Solution C:

$NaHCO_3$ 1.0 g

Distilled water 20.0 ml

Solution D:

$FeSO_4$ x 7 H_2O 2.0 mg

0.1 N H_2SO_4 1.0 ml

Solutions A, B and D are sterilized separately by autoclaving at 121°C for 15 min under 100% N_2 gas atmosphere. Solution C is sterilized by filtration under an atmosphere of 80% N_2 and 20% CO_2 gas mixture. Appropriate amounts of solutions B to D are added to the sterile solution A in the sequence as indicated.

Note: A small amount of white precipitate forms after autoclaving, but this has no negative effect on growth.

Trace element solution SL-4:

Na_2-EDTA 0.50 g

$FeSO_4$ x 7 H_2O 0.20 g

$ZnSO_4$ x 7 H_2O 0.10 g

$MnCl_2$ x 4 H_2O 0.03 g

H_3BO_3 0.30 g

$CoCl_2$ x 6 H_2O 0.20 g

$CuCl_2$ x 2 H_2O 0.01 g

$NiCl_2$ x 6 H_2O 0.02 g

Na_2MoO_4 x 2 H_2O 0.03 g

Distilled water 1000.0 ml

First dissolve EDTA in distilled water and adjust pH to 7.0 using 2 N NaOH; then add other compounds.

Minimal test media

NH_4Cl 0.3 g

$MgCl_2.6H_2O$ 0.4 g

$CaCl_2.2H_2O$ 0.1 g

K_2HPO_4 0.6 g

$MgSO_4$ 50 mg

Distilled water 1000.0 ml

Autoclave at 121 °C for 20 minutes.

SL-10 trace elements solution

HCl (25%) 10.0 ml

$FeCl_2$. 4H2O 1.5 g

$ZnCl_2$ 70.0 mg

$MnCl_2$. 4H2O 100.0 mg

H_3BO_3 6.0 mg

$CoCl_2$. 6H2O 190.0 mg

$CuCl_2$. 2H2O 2.0 mg

$NiCl_2$. 6H2O 24.0 mg

Na_2MoO_4 . 2H2O 36.0 mg

Distilled water 990.0 ml

Vitamin solution

Biotin 2 mg

Folic acid 2 mg

Pyridoxine HCl 10 mg

Riboflavin 5 mg

Thiamine 5 mg

Nicotinic acid 5 mg

Pantothenic acid 5 mg

Vitamin B 0.1 mg

p-aminobenzoic acid 5 mg

Thioctic acid 5 mg

Distilled water 1000.0 ml

Chapter 3

Stock solutions

Stock solutions for media components were prepared by the dissolution of the following masses of the components in deoxygenated sterile milliQ water under N_2 flushing and sealed with sterile butyl stoppers and aluminium crimps:

Table A A.1 Stock solutions for preparation of Mars simulant media.

Compound	Final concentration (mM)	Volume of water (mL)	Molecular weight	Volume to add (g)
$NaNO_3$	100	100	84.99	0.850
$Mg(NO_3)_2$	100	100	148.32	1.483
Na_2S	100	100	78.05	0.781
$MnCl_2$	10	100	125.84	0.126
K_2HPO_4	10	100	174.20	0.174
NaOH	100	100	40.00	0.400
KOH	100	100	56.11	0.561
$FeSO_4$	1000	50	151.91	7.596
$MnSO_4$	10	100	151.00	0.151
Na_2HPO_4	10	100	141.96	0.142
$Fe_2(SO4)_3$	100	100	399.88	3.999
KH_2PO_4	100	100	136.01	1.360
$MgSO_4$	1000	50	120.37	6.019

A **Ferrozine solution** stock was prepared by the dissolution of 200 mg 3-(2-Pyridyl)-5,6-diphenyl-1,2,4-triazine-p,p′-disulfonic acid monosodium salt hydrate and 2.39 g HEPES in milliQ sterile water.

Tamm reagent (0.14 M oxalic acid, 0.2 M ammonium oxalate) was prepared by dissolving 1.26 g oxalic acid and 2.48 g ammonium oxalate in 100 mL milliQ sterile water.

0.5 M HCl was prepared by diluting 50 mL 2M HCl in 150 mL milliQ sterile water

A stock of **0.5 M HCl with 0.3 M hydroxylamine hydrochloride** was prepared as 0.5 M HCl, with the addition of 4.17 g hydroxylamine hydrochloride to the 200 mL volume.

A 50 mL stock of 20 % **HNO_3 solution** was prepared by diluting 20 mL 70% HNO_3 with 30 mL milliQ sterile water.

Table A A.2. Chemical composition of each media based on Contemporary Mars (CM), Sulfur-rich (SR), Haematite-rich (HR) and Shergottite (SG) ion concentrations as listed in Table 3.1.

	Simulant			
	CM	SR	HR	SG
Component	Concentration (mg L^{-1})			
$NaNO_3$	84.995	52.550	63.410	-
$Mg(NO_3)_2$	-	28.305	18.831	74.150
Na_2S	-	-	0.903	2.465
$MnCl_2$	1.851	1.312	1.455	1.242
K_2HPO_4	3.455	-	12.549	13.710
NaOH	1.698	-	-	18.443
KOH	13.104	-	5.551	-
$Ca(OH)_2$	102.382	111.953	75.599	125.396
$FeSO_4$	34.375	349.524	81.094	-
FeO	171.858	41.573	102.685	161.910
Fe_2O_3	-	-	153.492	12.082
$3AL_2O_3.2SiO_2$	219.699	109.899	155.442	141.145
$3MgO.4SiO_2.H_2O$	192.117	-	605.691	259.920
SiO_2	280.329	196.567	-	325.666
TiOH	5.986	3.789	4.019	2.053
$MnSO_4$	2.875	0.853	-	2.808
Na_2HPO_4	-	-	-	0.232
$Fe_2(SO_4)_3$	88.136	84.034	-	-
KH_2PO_4	-	57.217	-	-
$MgSO_4$	-	136.251	-	-

Media limitations

Some challenges arose in recreating the calculated ionic composition in the media. There were some minor deviations from the ion balance in the overall media recipe, such as 20 µM surpluses of S^- in SR brine and of Si^+ in HR.

The greater challenges were primarily a consequence of limited availability of suitable soluble compounds. Compounds with low solubility (FeO, Fe_2O_3, $3AL_2O_3.2SiO_2$, $3MgO{\cdot}4SiO_2{\cdot}H_2O$, SiO_2, TiOH, $Ca(OH)_2$) were used to introduce the remaining ions to the overall media, meaning much of the Al, Ca, Si and Ti is not dissolved in solution but present as precipitate. This is not a major issue as none will have a major impact on microbial growth.

However, it was not possible to use fully soluble Fe^{2+} and Fe^{3+} sources while balancing the major anions such as SO_4^- and Cl^-, meaning that soluble Fe^{2+} is available at >2 mM in SR, 0.5 mM in HR, 0.2 mM in CM and not at all in EB, despite the modelling predicting 1.9-2.9 mM with full dissolution of the four simulants.

Chapter 4

Anoxic solutions

These were prepared by adding anoxic distilled water to chemical components in 50 ml Wheaton bottles under 85:10:5 N_2:CO_2:H_2 atmosphere in a COY anaerobic glove box.

1 M $FeSO_4$ solution: 8.34 g of $FeSO_4{\cdot}7H_2O$ in 30 ml anoxic distilled water

200 mM $NaNO_2$ solution: 2.07 g of $NaNO_2$ in 30 ml anoxic distilled water

200 mM $NaNO_3$ solution: 2.55 g of $NaNO_3$ in 30 ml anoxic distilled water

Wheaton bottles were sealed with butyl septa and crimped with aluminium caps until use.

B. Standards

Protein

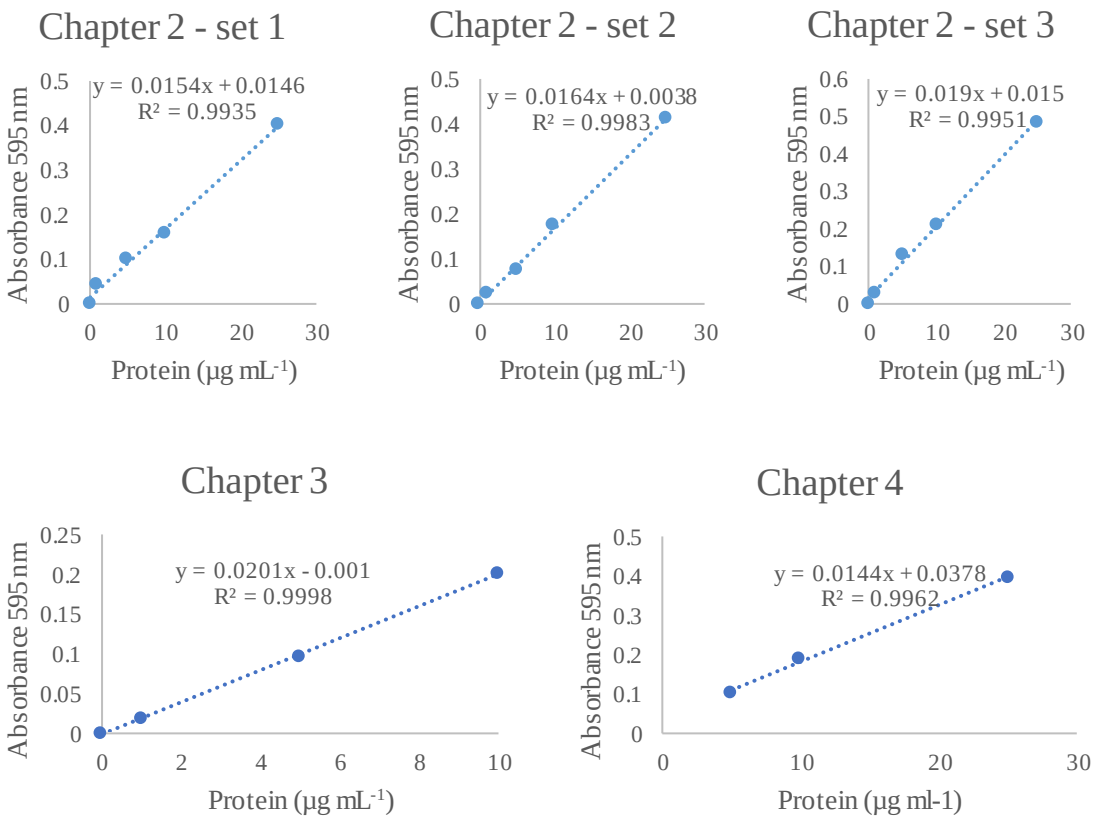

Figure A B.1 Standard curves used to determine protein concentration in samples for Chapters 2, 3 and 4.

Nitrate

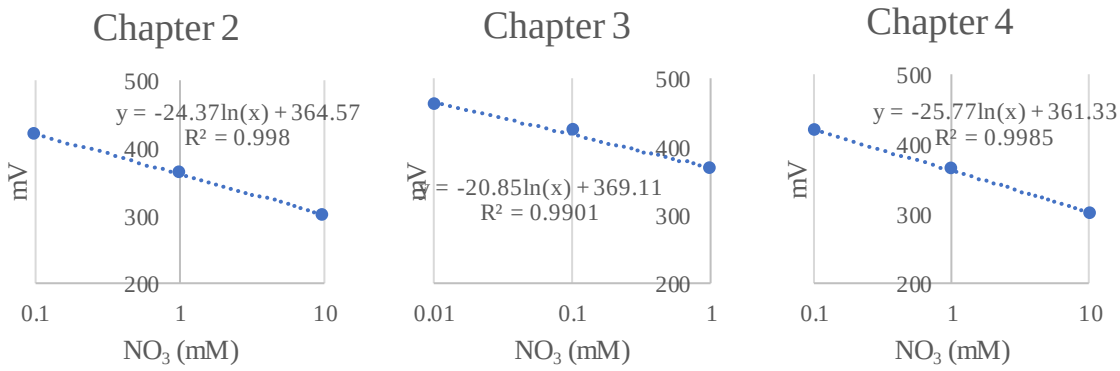

Figure A B.2 Standard curves used to determine nitrate concentration in samples for Chapters 2, 3 and 4.

Nitrite

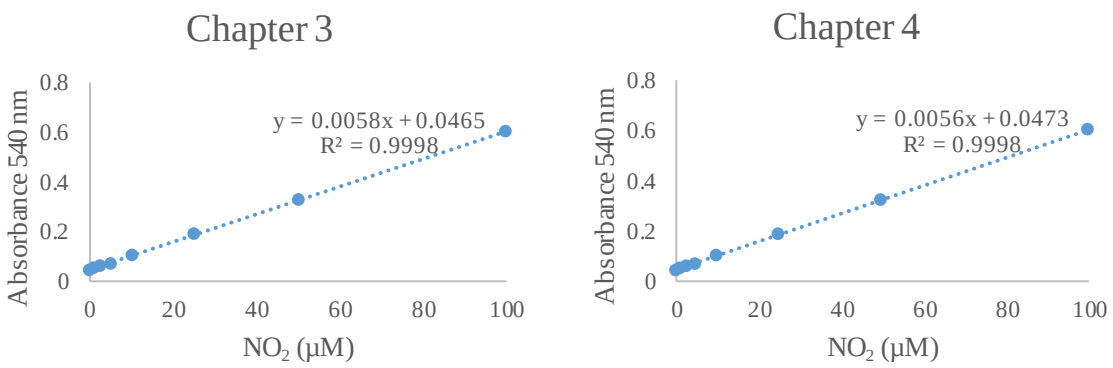

Figure A B.3 Standard curves used to determine nitrite concentration in samples for Chapters 3 and 4.

Fe

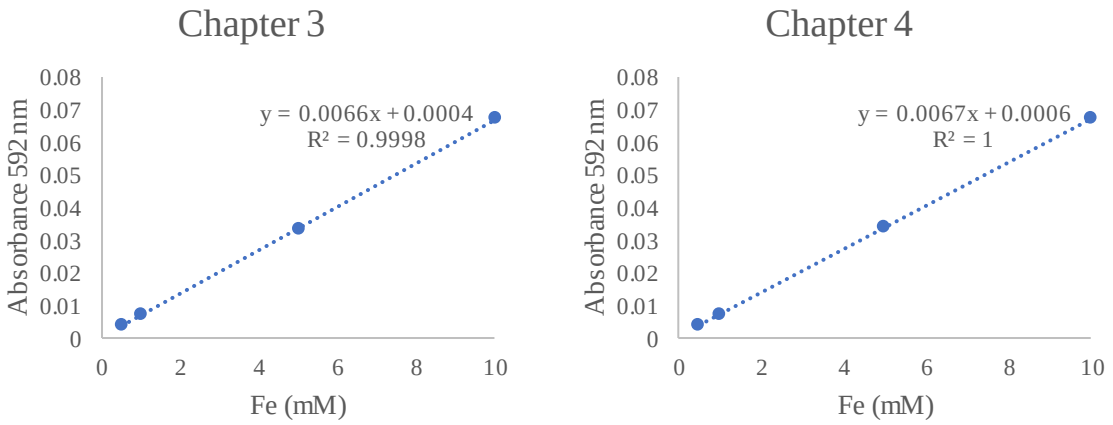

Figure A B.4 Standard curves used to determine Fe concentration in samples for Chapters 3 and 4.

C. Additional figures and tables

Table A C.1. Mean FeO/(MgO+FeO) values for individual analysed grains of the solid Fe^{2+} substrate and mineral identification of grains.

Grain no.	FeO/(MgO+FeO)	Mineral identification
3	0.162	Olivine
4	0.163	Olivine
5	0.162	Olivine
6	0.154	Diopside
7	0.156	Enstatite
8	0.162	Olivine
9	0.163	Olivine
10	0.150	Diopside

11	0.162	Olivine
12	0.161	Olivine
13	0.155	Enstatite
14	0.182	low total %
15	0.157	Mixed
16	0.163	Olivine
17	0.162	Olivine
18	0.162	Olivine
19	0.180	Diopside
20	0.162	Olivine
21	0.149	Diopside
22	0.154	Enstatite
23	0.162	Olivine
24	0.159	Mixed
25	0.162	Olivine
26	0.162	Olivine
27	0.162	Olivine
28	0.161	Olivine
29	0.162	Olivine
30	0.142	Diopside
31	0.162	Olivine
32	0.161	Olivine
33	0.153	Diopside
34	0.163	Olivine
35	0.158	Enstatite
36	0.161	Olivine
37	0.163	Olivine
38	0.156	Enstatite
39	0.161	Olivine
40	0.160	Mixed
41	0.163	Olivine
42	0.148	Diopside
43	0.162	Olivine
44	0.161	Olivine
45	0.153	Enstatite
46	0.153	Enstatite
47	0.163	Olivine
48	0.153	Diopside
49	0.163	Olivine
50	0.161	Olivine
51	0.163	Olivine
52	0.162	Olivine
53	0.150	Diopside
54	0.162	Olivine
55	0.163	Olivine
56	0.162	Olivine
57	0.162	Olivine
58	0.155	Enstatite

59	0.154	Diopside
60	0.163	Olivine
61	0.360	Al-rich
62	0.162	Olivine
63	0.163	Olivine
64	0.154	Enstatite
65	0.154	Enstatite
66	0.162	Olivine
67	0.162	Olivine
68	0.163	Olivine
69	0.161	Olivine
70	7.16769E-05	low total %
71	0.155	Enstatite
72	0.164	Olivine
73	0.162	Olivine
74	0.172	Mixed
75	0.154	Enstatite
76	0.160	Olivine
77	0.162	Olivine
78	0.161	Olivine
79	0.164	Olivine
80	0.162	Olivine
81	0.163	Olivine
82	0.163	Olivine
83	0.158	Mixed
84	0.162	Olivine
85	0.153	Mixed
86	0.156	Mixed
87	0.319	Al-rich
88	0.163	Olivine
89	0.162	Olivine
90	0.156	Enstatite
91	0.162	Olivine
92	0.154	Enstatite
93	0.164	Olivine
94	0.162	Olivine
95	0.155	Diopside
96	0.163	Olivine
97	0.163	Olivine
98	0.153	Diopside
99	0.163	Olivine
100	0.162	Olivine

Table A C.2. Mean data for the olivine grains from the solid Fe^{2+} substrate.

% grains identified as olivine	Mean [FeO/(MgO+FeO)] of olivine grains
73.95833	16.22513

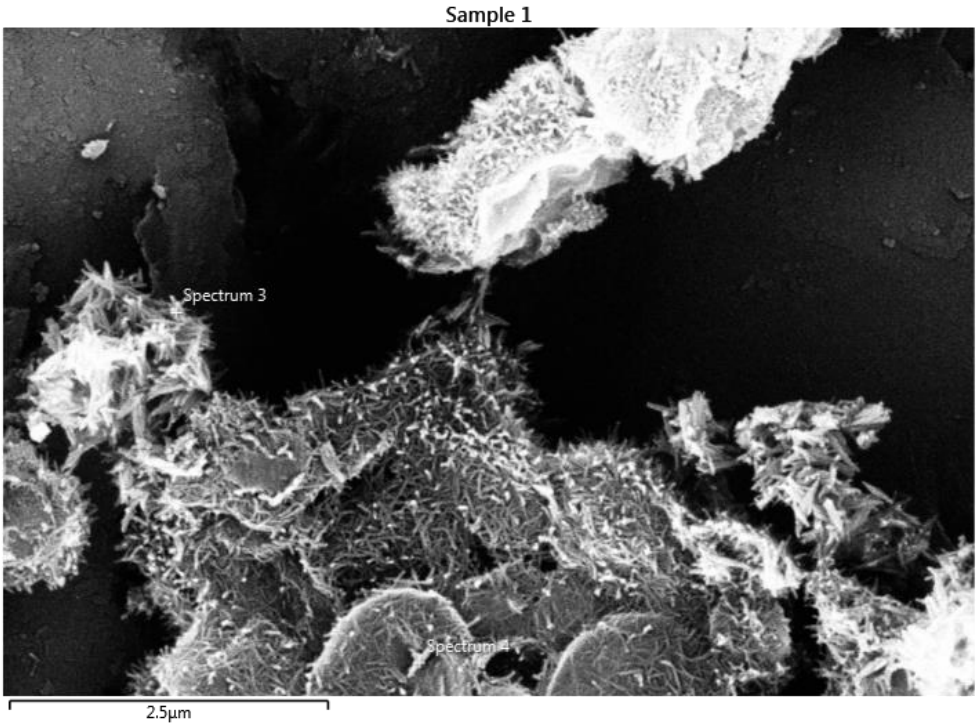

Figure A C.1 Electron micrograph of globular aggregations on olivine surface after culture with *Pseudogulbenkiania sp.* strain 2002. Target areas for electron dispersive X-ray spectroscopic (EDS) analysis are shown with white boxes.

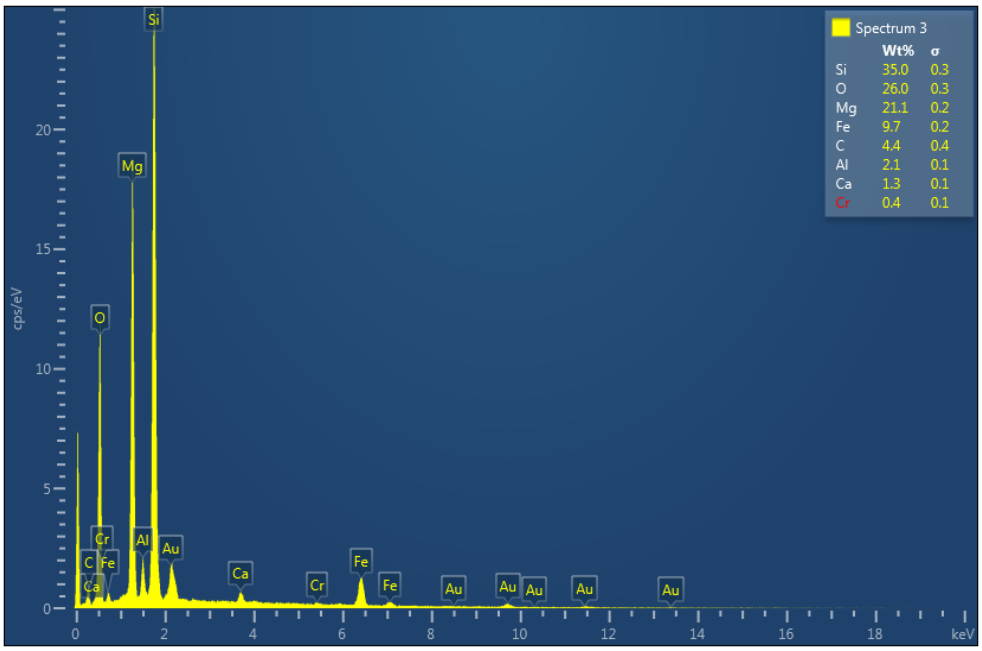

Figure A C.2. Energy dispersive X-ray spectroscopy (EDS) elemental composition output for target area "Spectrum 3" indicated in Figure A C.1.

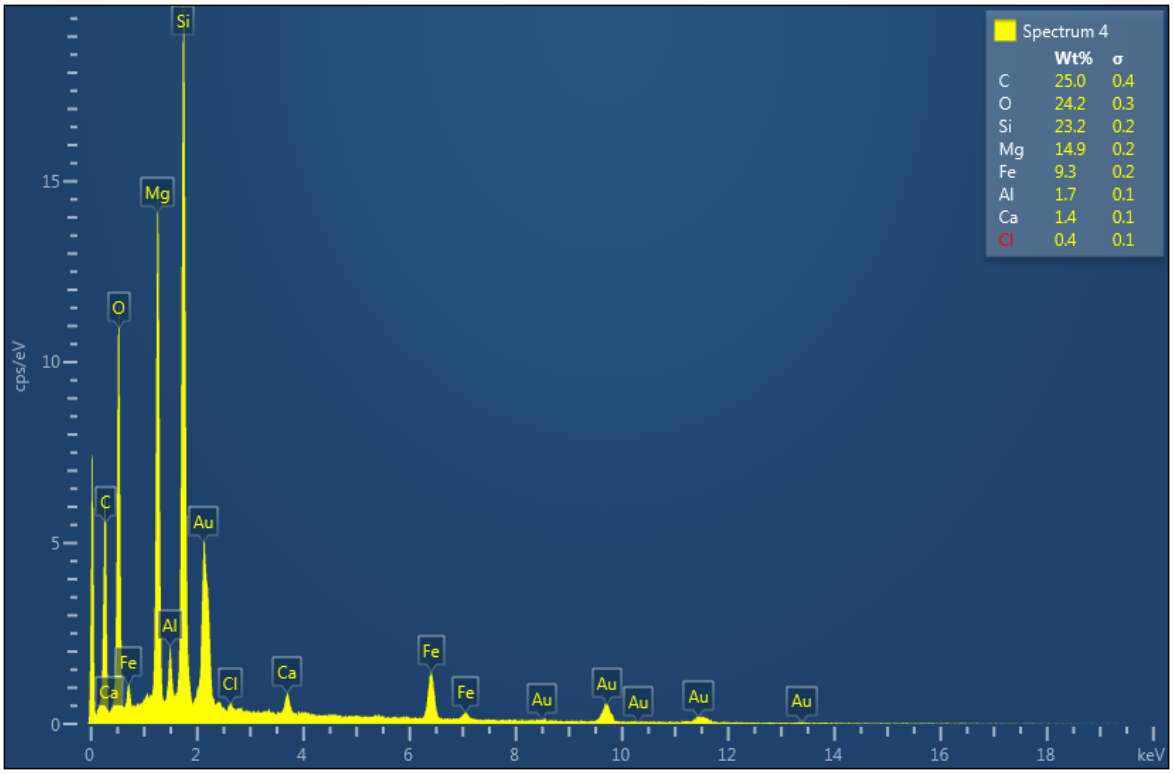

Figure A C.3. Energy dispersive X-ray spectroscopy (EDS) elemental composition output for target area "Spectrum 4" indicated in Figure A C.1.

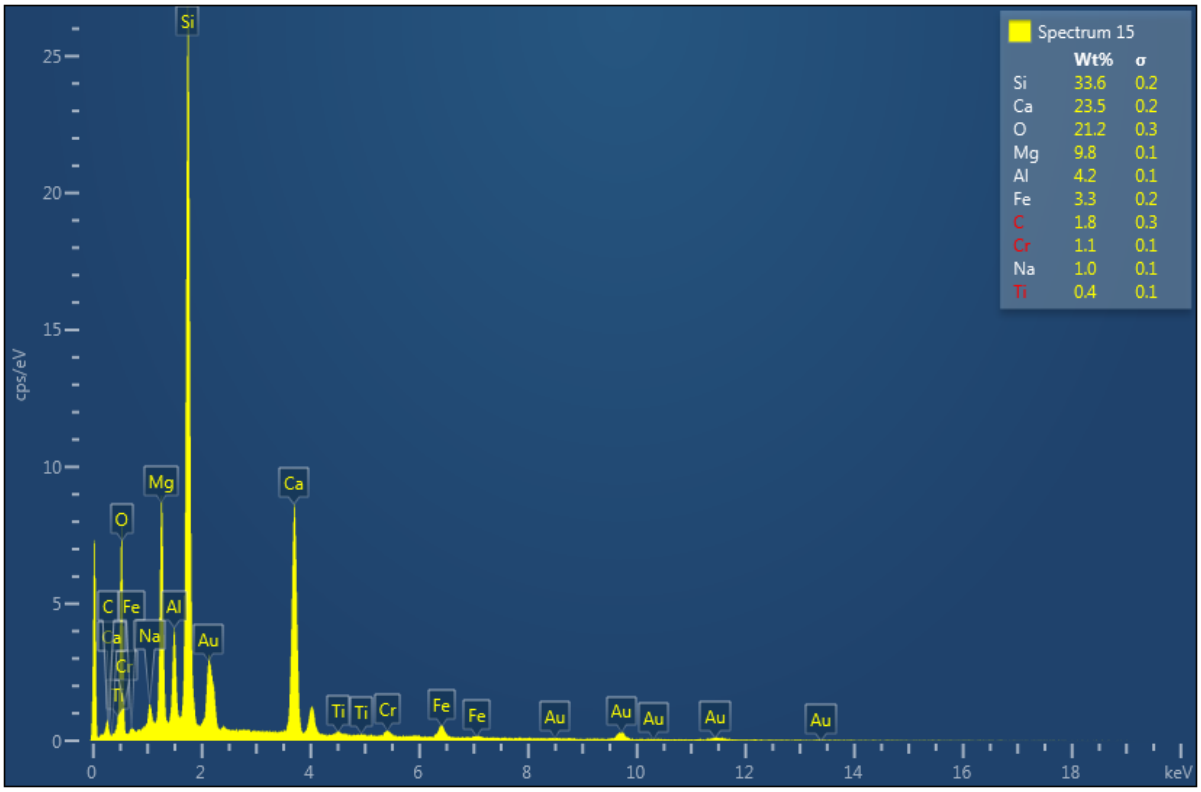

Figure A C.4. Energy dispersive X-ray spectroscopy (EDS) elemental composition output for target area "Spectrum 15" indicated in Figure 2.13.

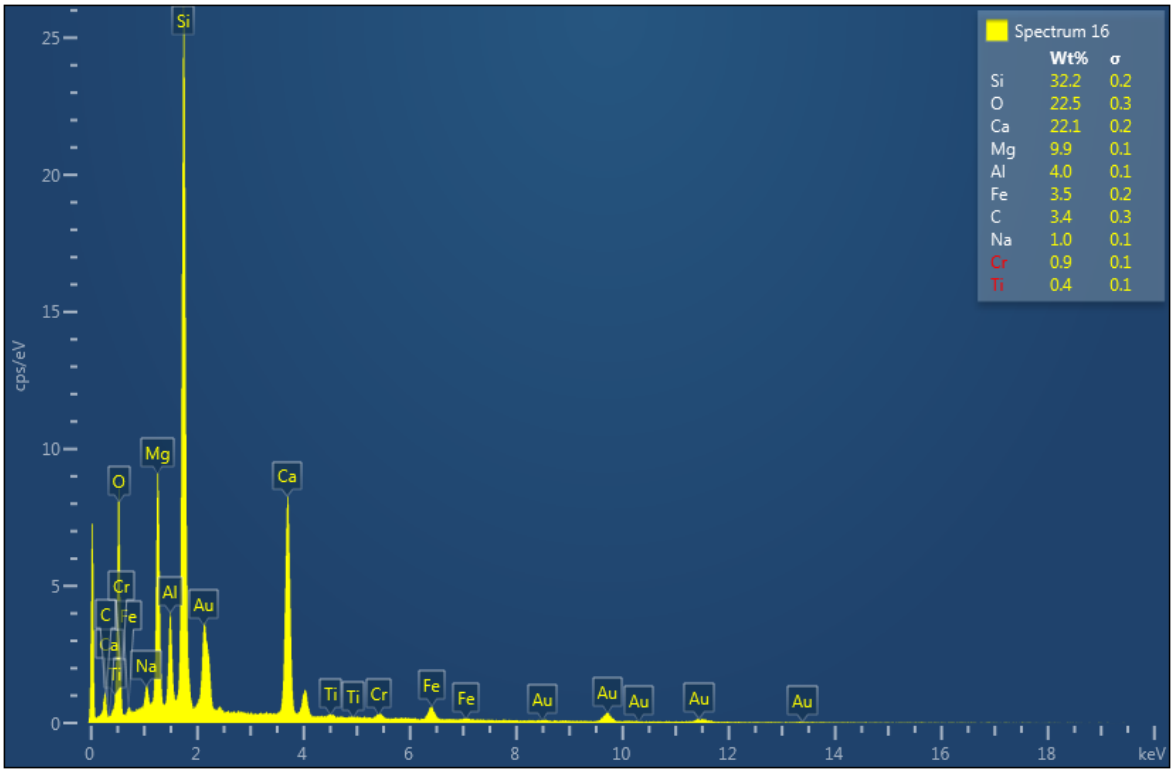

Figure A C.5. Energy dispersive X-ray spectroscopy (EDS) elemental composition output for target area "Spectrum 16" indicated in Figure 2.13.

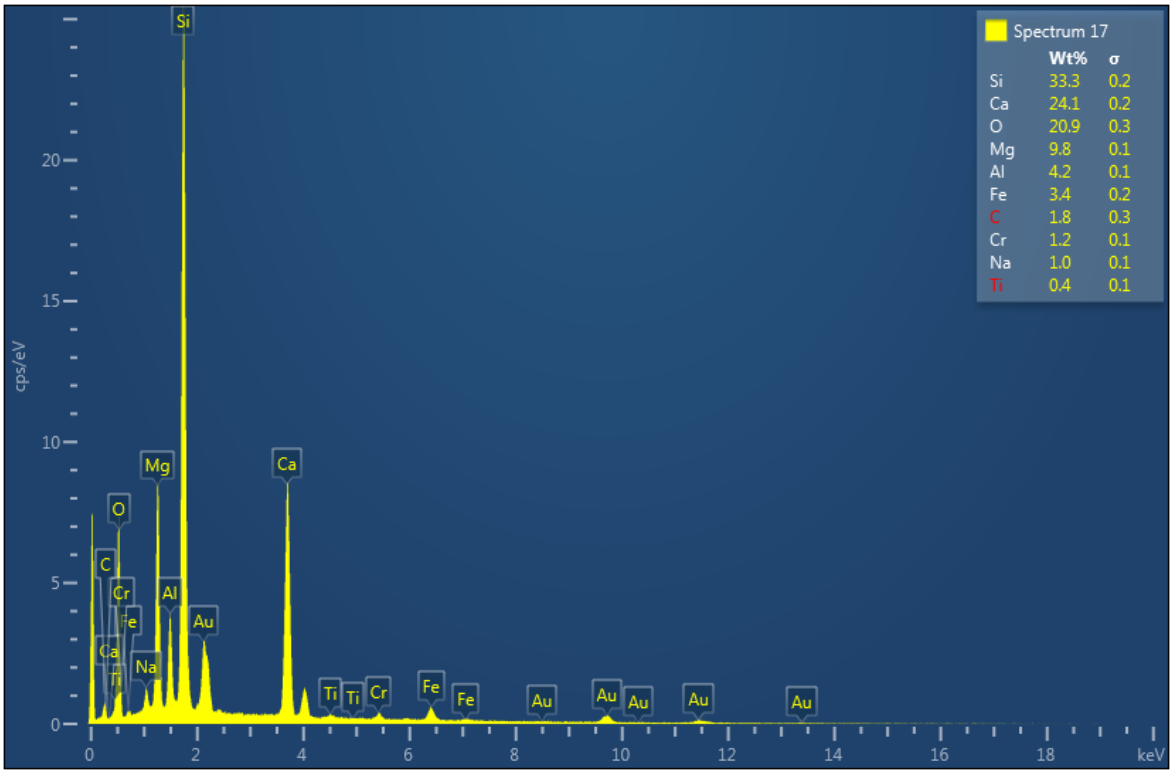

Figure A C.6. Energy dispersive X-ray spectroscopy (EDS) elemental composition output for target area "Spectrum 17" indicated in Figure 2.13.

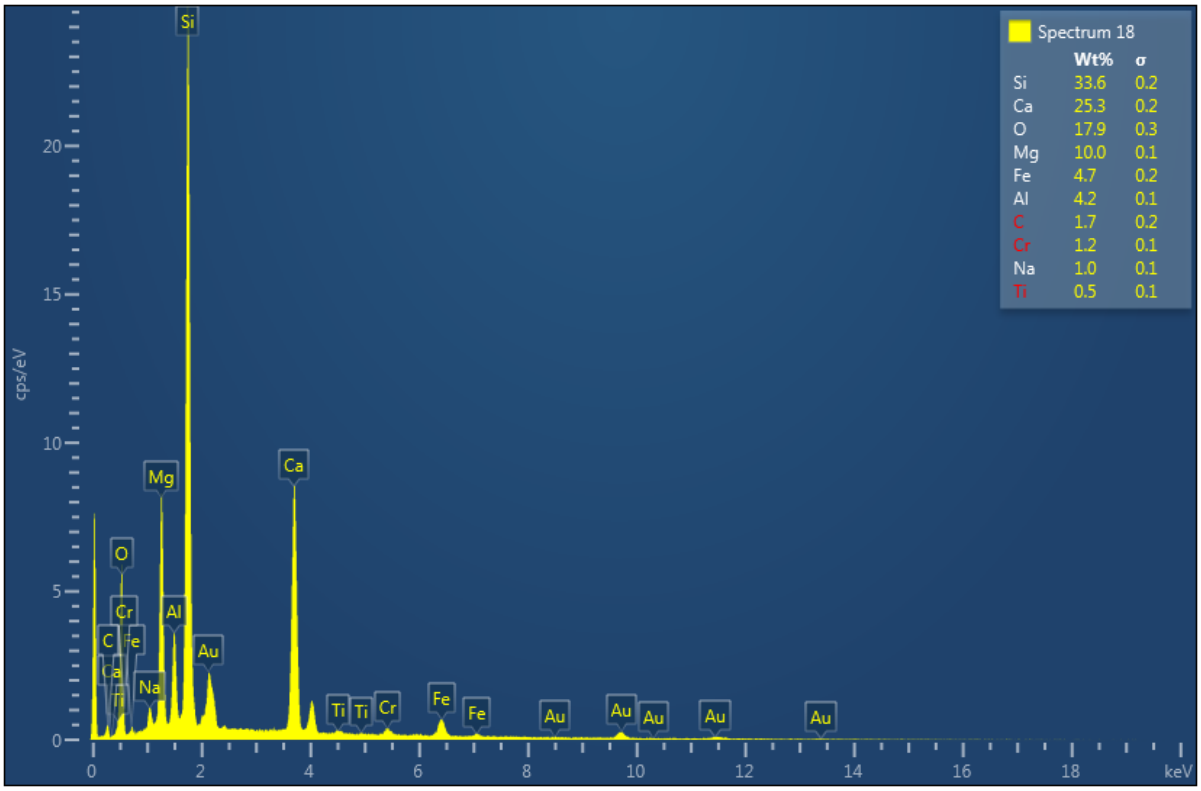

Figure A C.7. Energy dispersive X-ray spectroscopy (EDS) elemental composition output for target area "Spectrum 18" indicated in Figure 2.13.

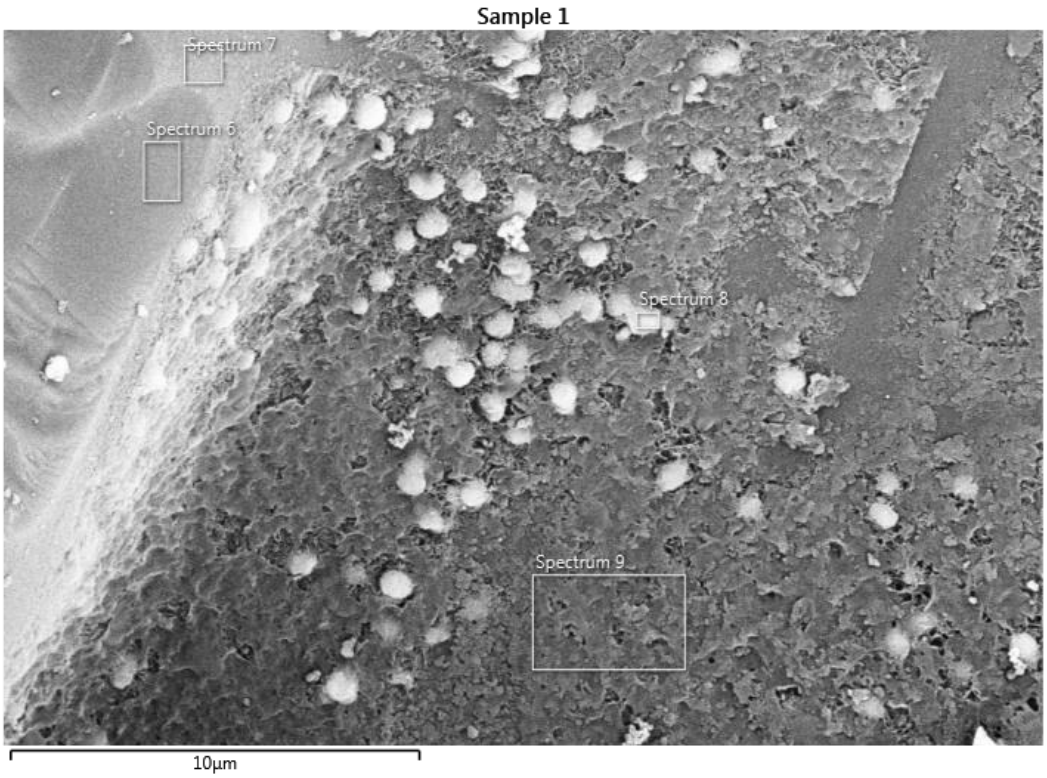

Figure A C.8. Electron micrograph of rounded features in a semi-porous matrix on olivine surface after culture with Pseudogulbenkiania sp. strain 2002. Target areas for electron dispersive X-ray spectroscopic (EDS) analysis are shown with white boxes.

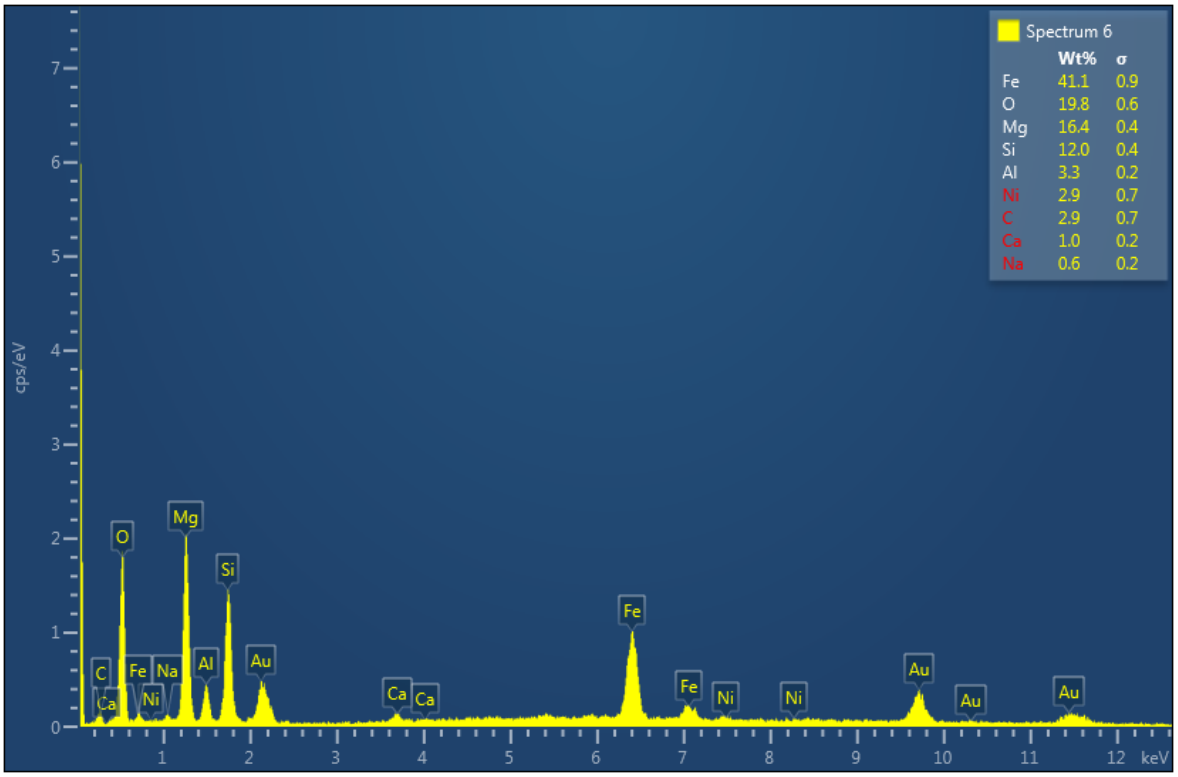

Figure A C.9. Energy dispersive X-ray spectroscopy (EDS) elemental composition output for target area "Spectrum 6" indicated in Figure A C.8.

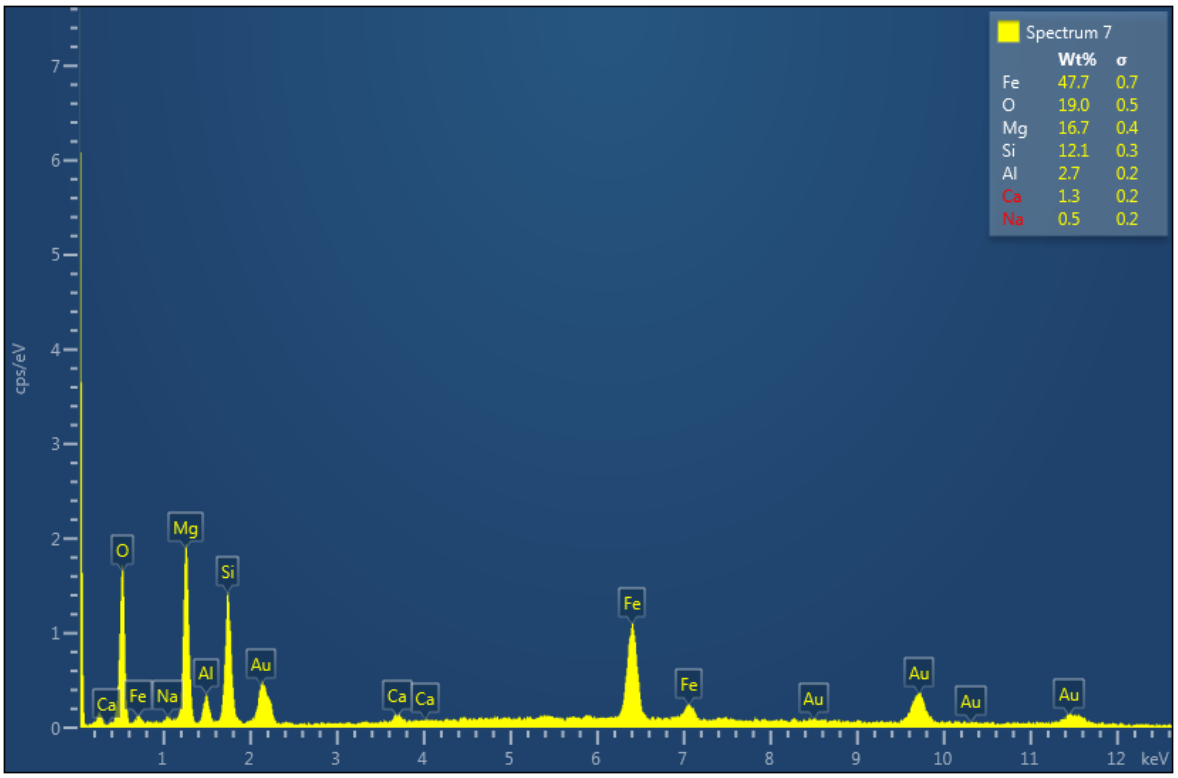

Figure A C.10. Energy dispersive X-ray spectroscopy (EDS) elemental composition output for target area "Spectrum 7" indicated in Figure A C.8.

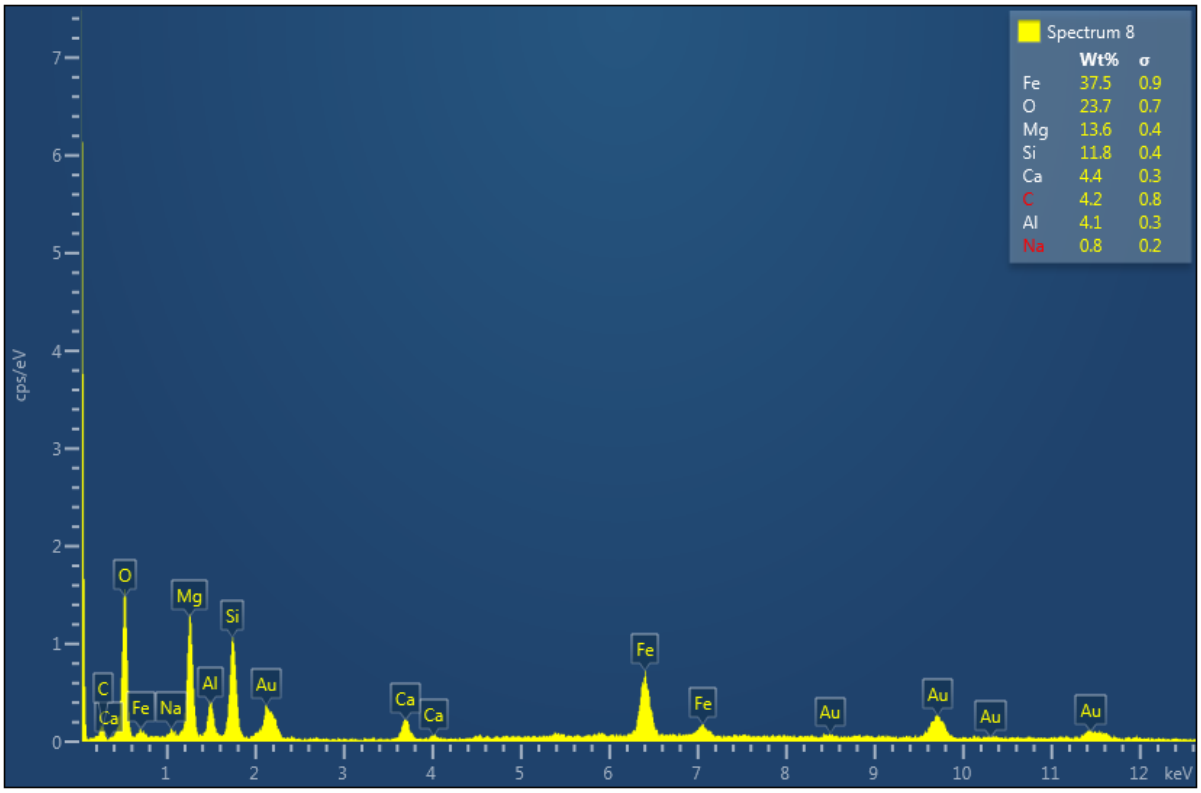

Figure A C.11. Energy dispersive X-ray spectroscopy (EDS) elemental composition output for target area "Spectrum 8" indicated in Figure A C.8.

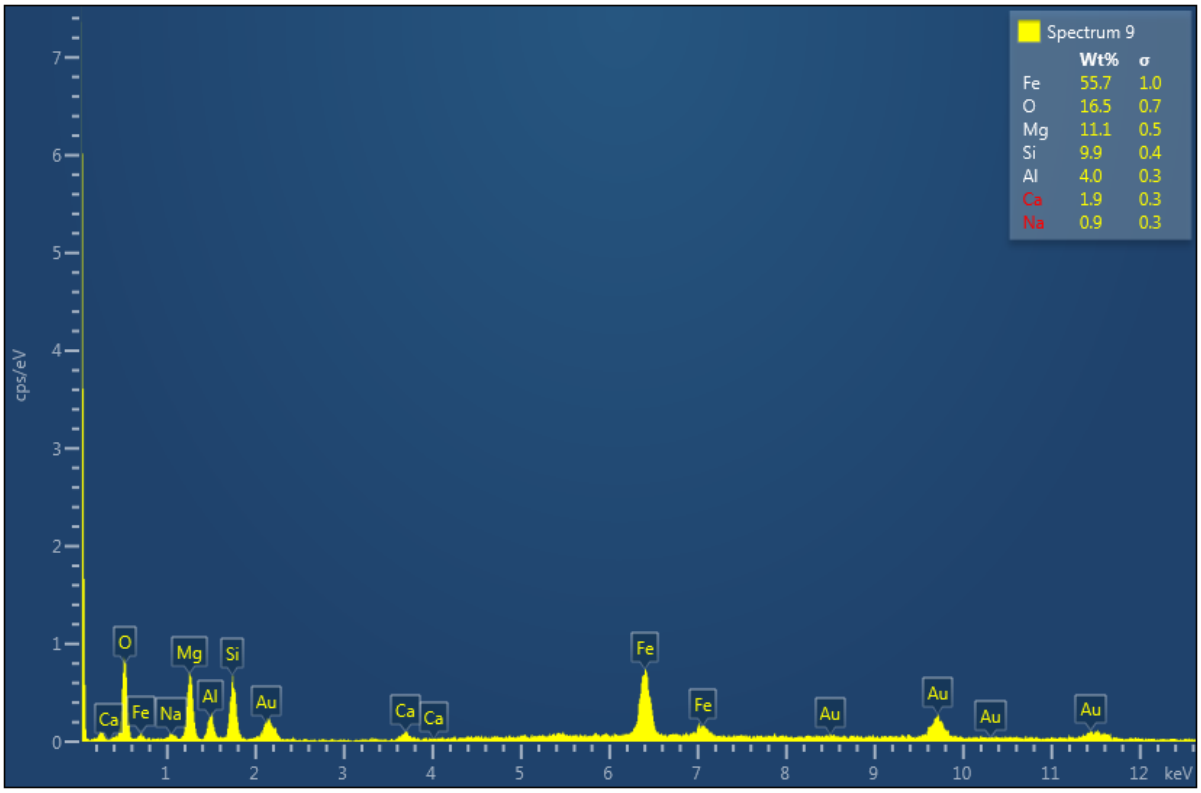

Figure A C.12. Energy dispersive X-ray spectroscopy (EDS) elemental composition output for target area "Spectrum 9" indicated in Figure A C.8.

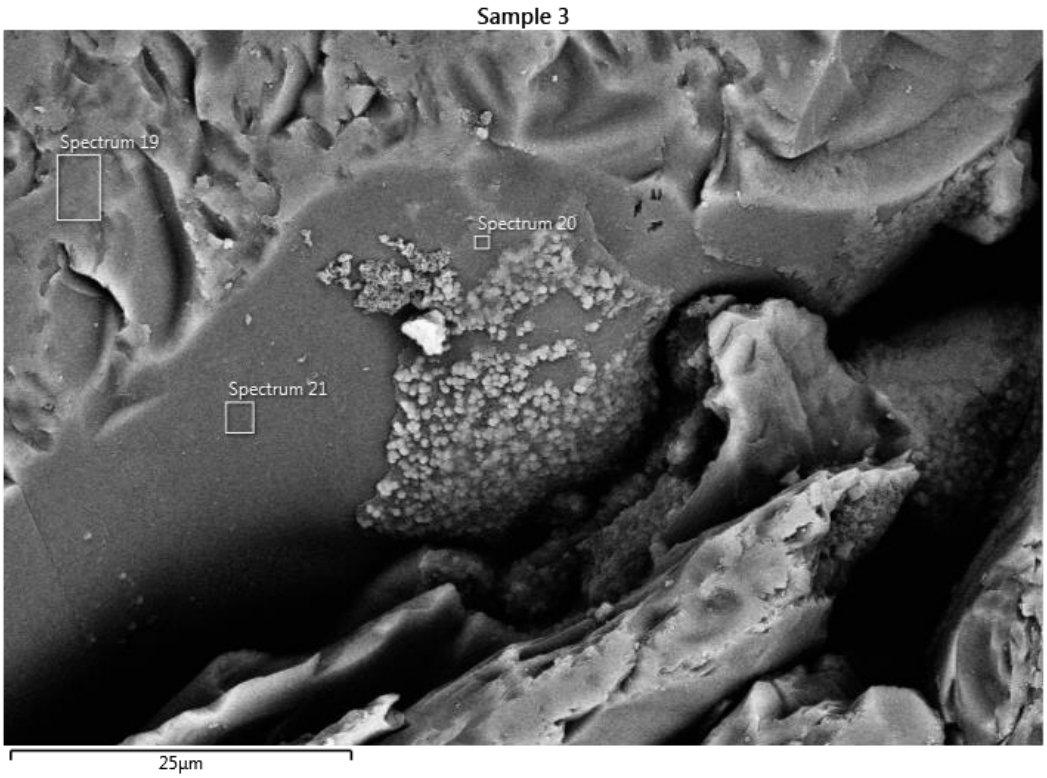

Figure A C.13. Electron micrograph of rounded features in a semi-porous matrix on olivine surface after culture with *Paracoccus sp.* strain KS1. Target areas for electron dispersive X-ray spectroscopic (EDS) analysis are shown with white boxes.

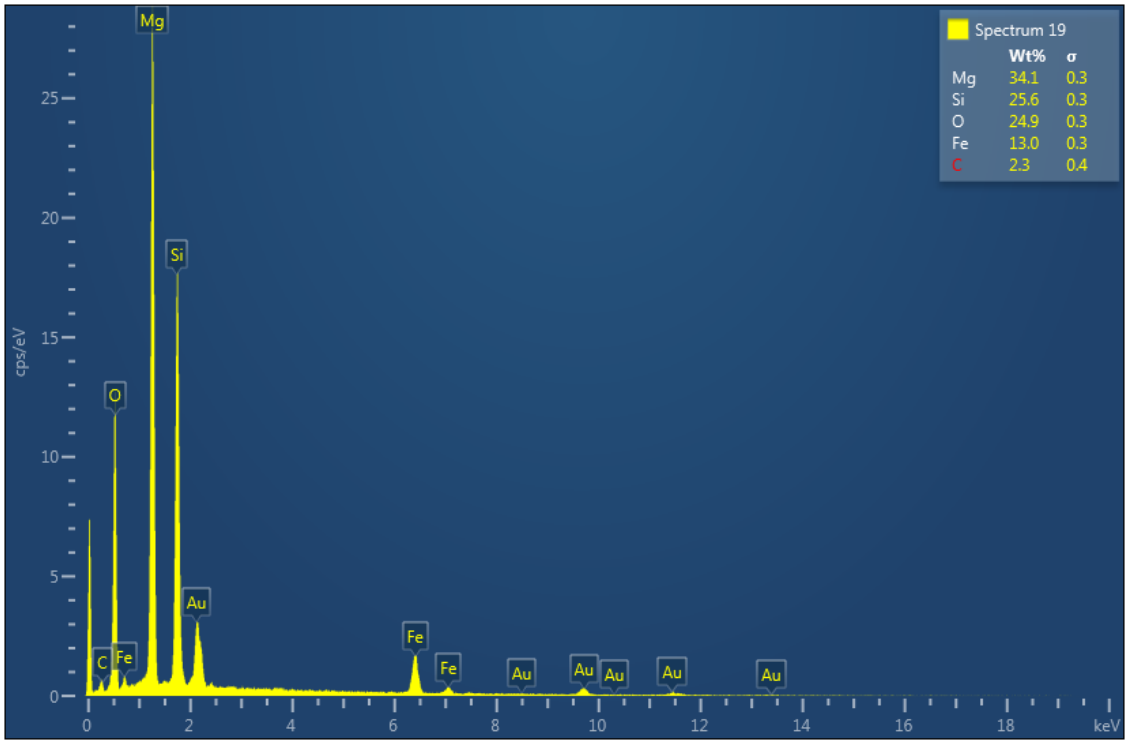

Figure A C.14 Energy dispersive X-ray spectroscopy (EDS) elemental composition output for target area "Spectrum 19" indicated in Figure A C.13.

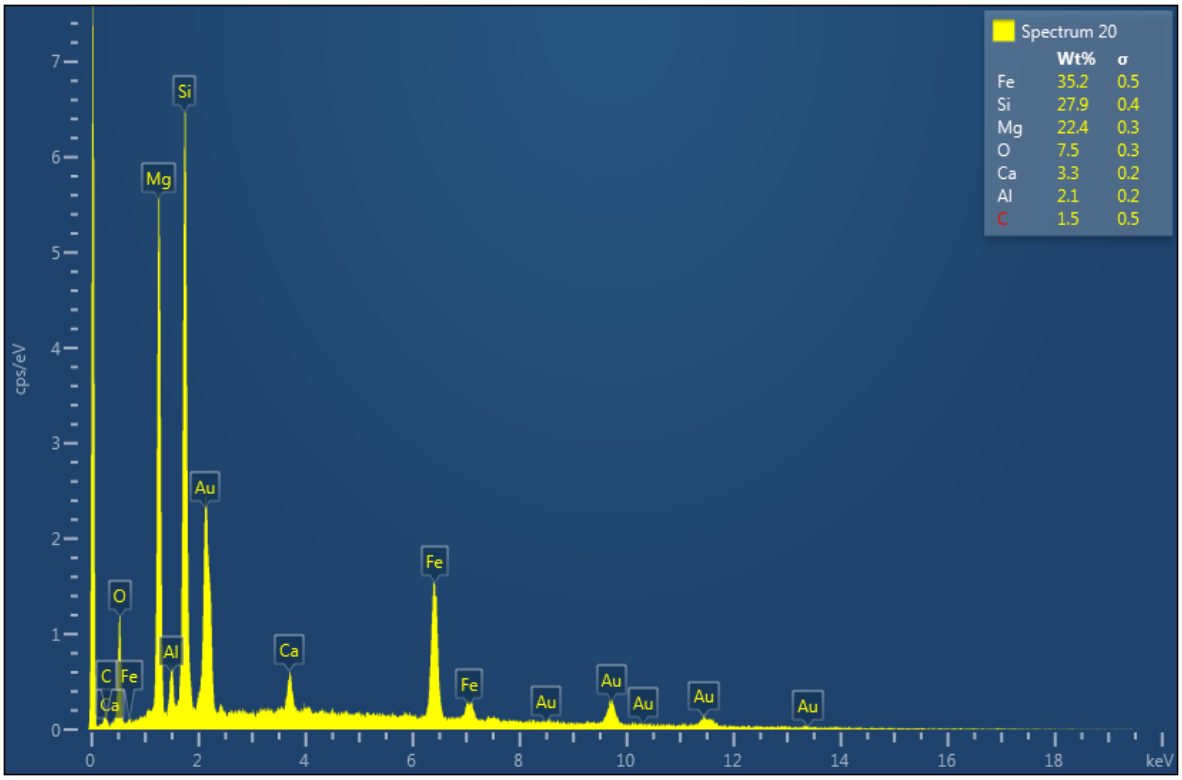

Figure A C.15. Energy dispersive X-ray spectroscopy (EDS) elemental composition output for target area "Spectrum 20" indicated in Figure A C.13.

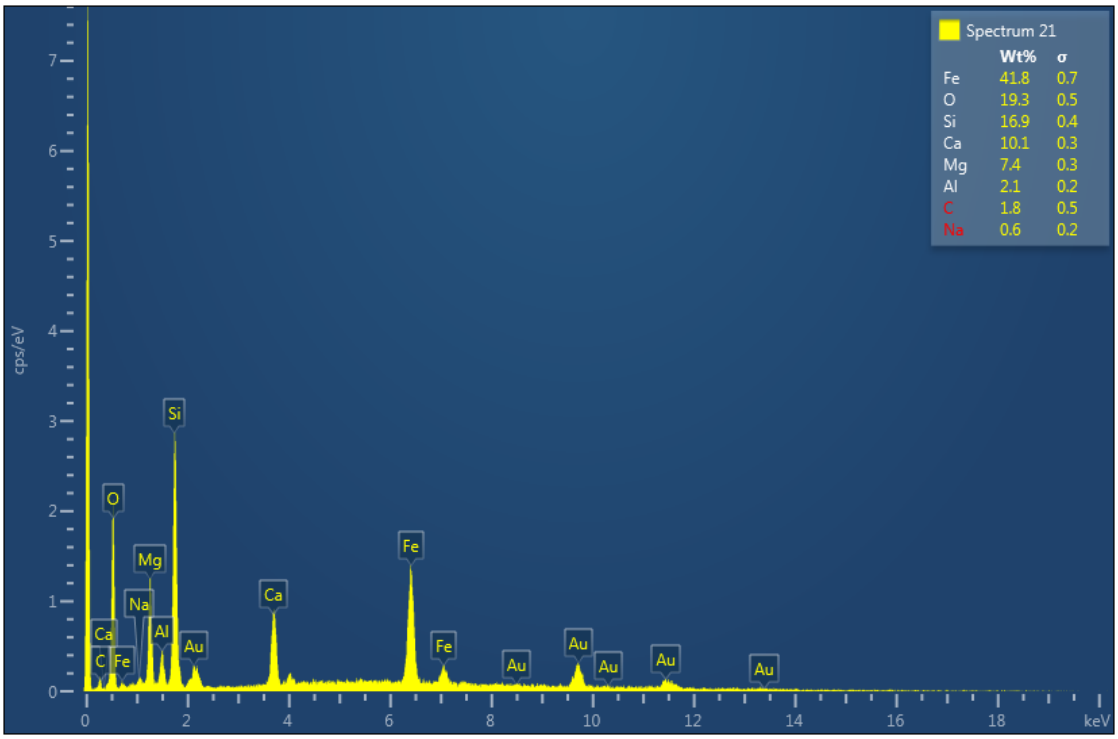

Figure A C.16. Energy dispersive X-ray spectroscopy (EDS) elemental composition output for target area "Spectrum 21" indicated in Figure A C.13.

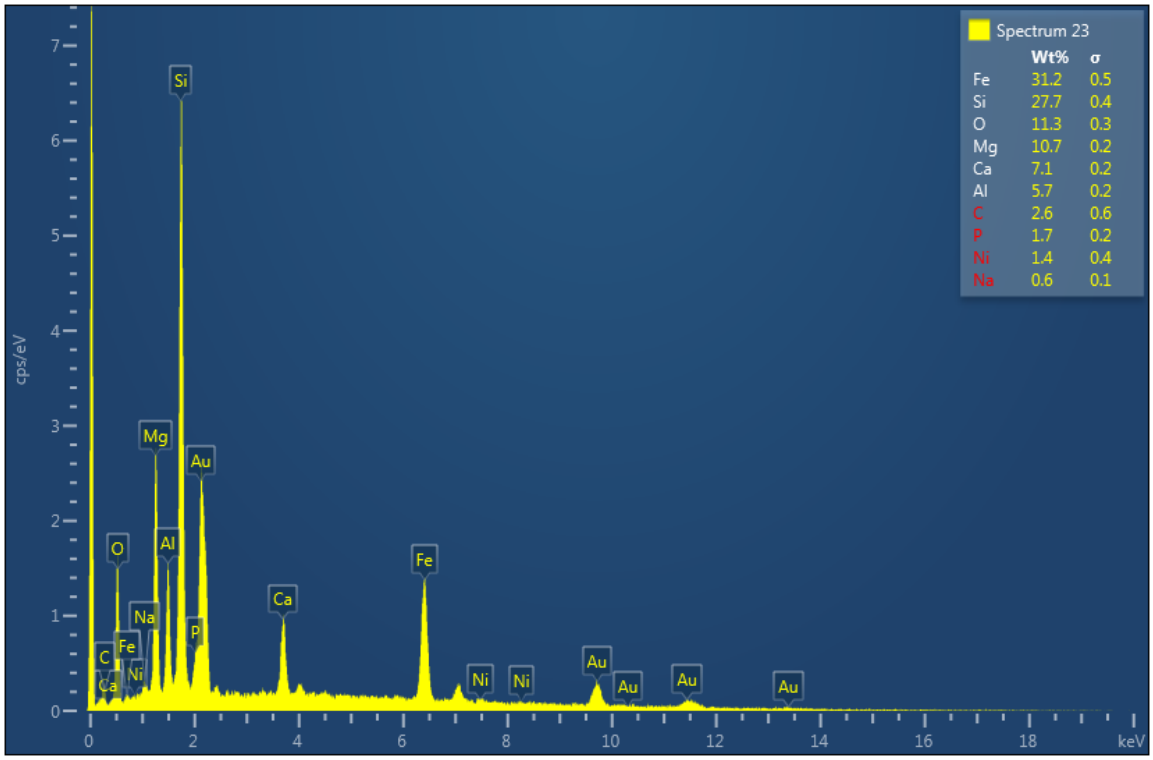

Figure A C.17. Energy dispersive X-ray spectroscopy (EDS) elemental composition output for target area "Spectrum 23" indicated in Figure 2.21.

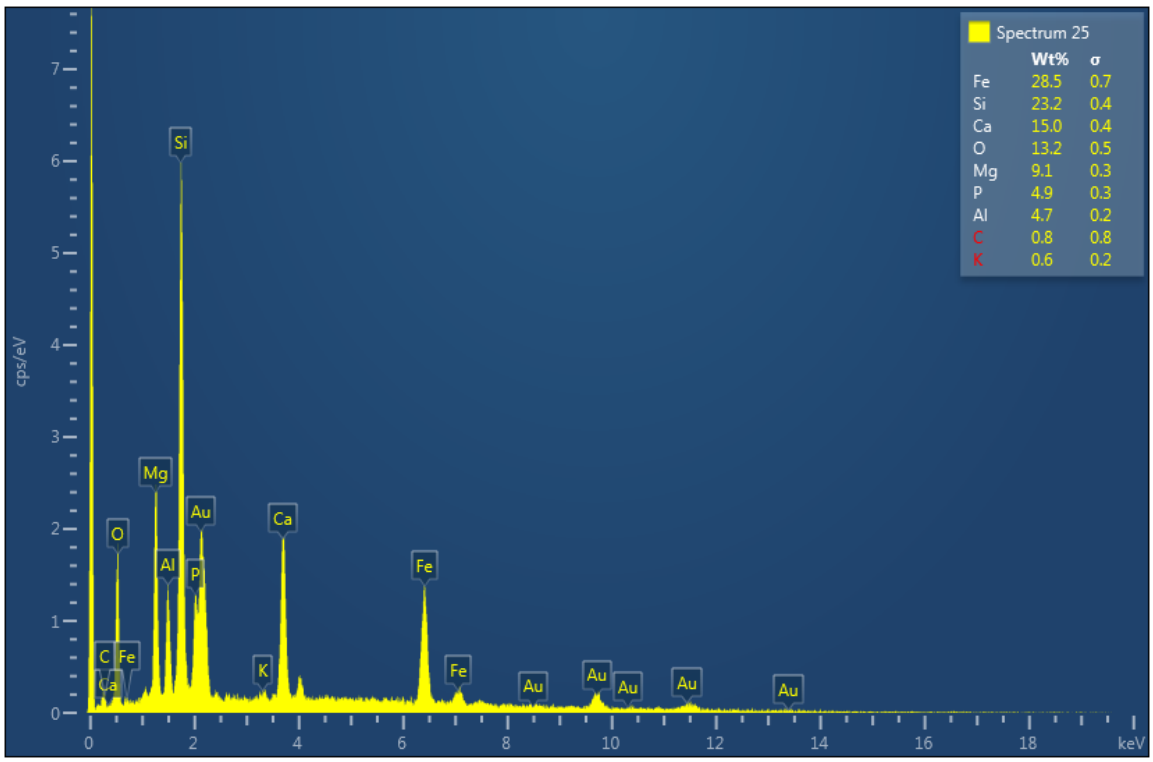

Figure A C.18. Energy dispersive X-ray spectroscopy (EDS) elemental composition output for target area "Spectrum 25" indicated in Figure 2.21.

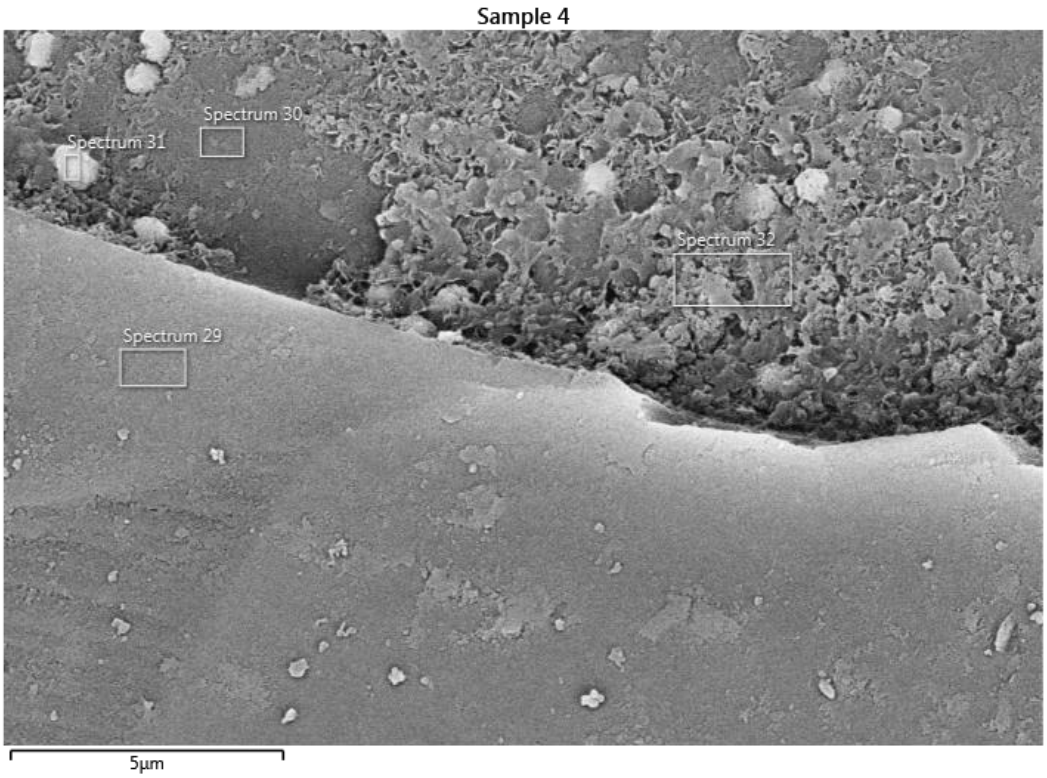

Figure A C.19. Electron micrograph of rounded features in a semi-porous matrix on olivine surface after culture with Acidovorax sp. strain BoFeN1. Target areas for electron dispersive X-ray spectroscopic (EDS) analysis are shown with white boxes.

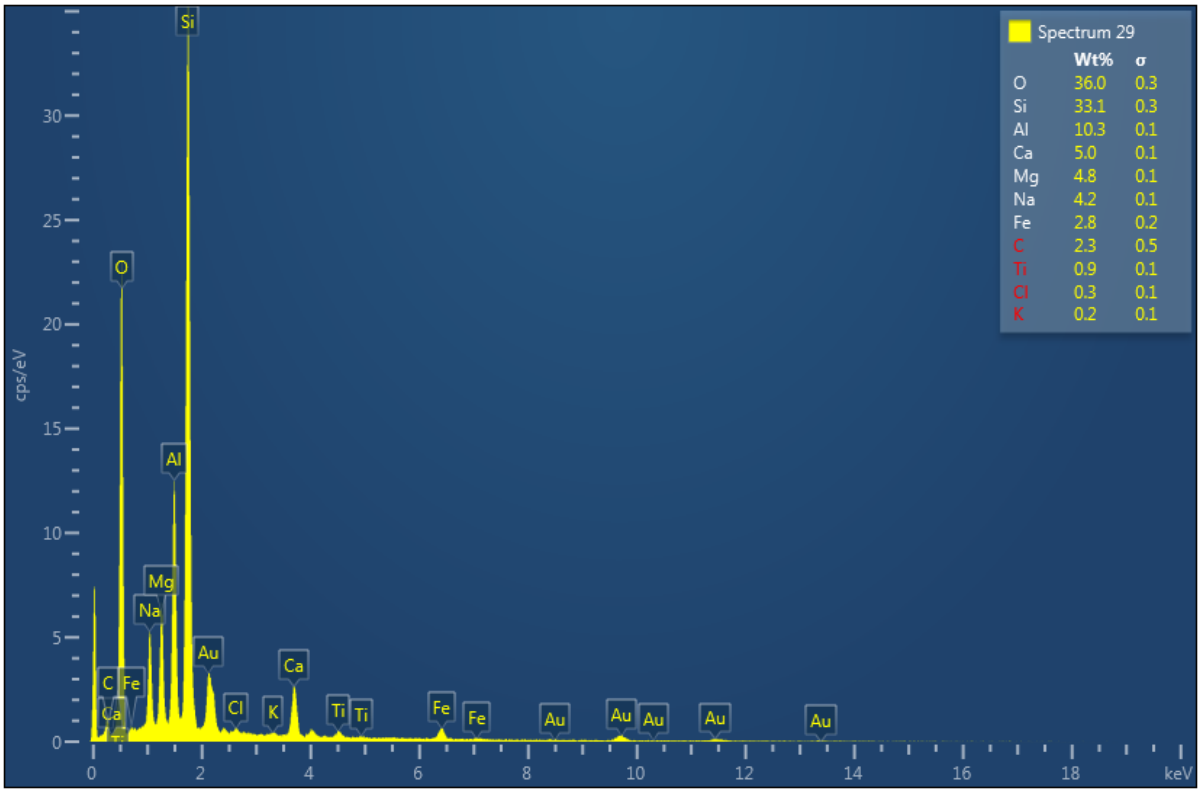

Figure A C.20. Energy dispersive X-ray spectroscopy (EDS) elemental composition output for target area "Spectrum 29" indicated in Figure A C.19.

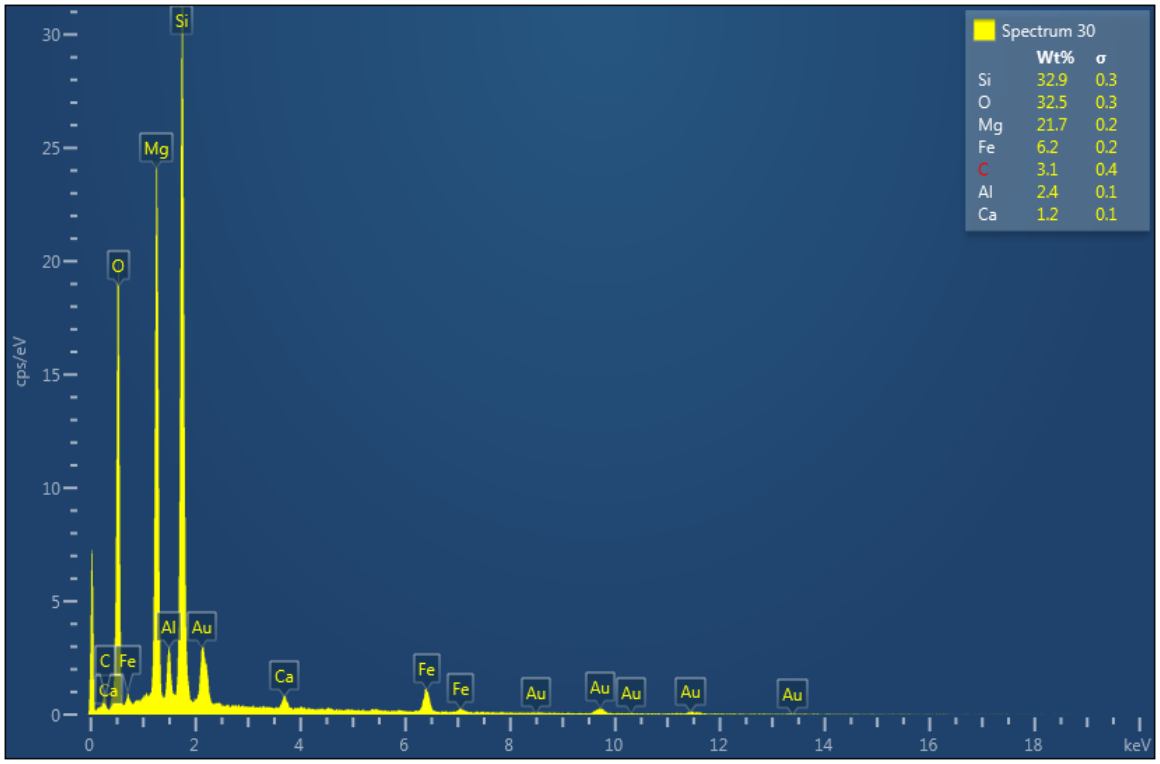

Figure A C.21. Energy dispersive X-ray spectroscopy (EDS) elemental composition output for target area "Spectrum 30" indicated in Figure A C.19.

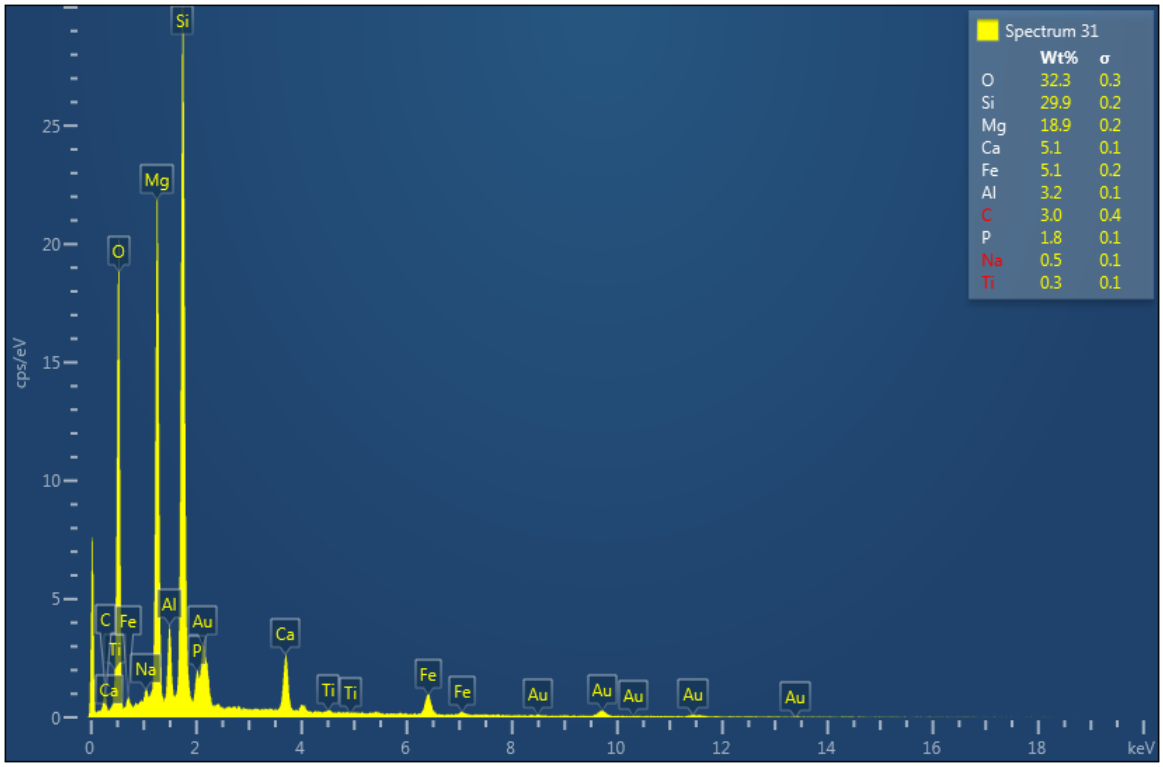

Figure A C.22. Energy dispersive X-ray spectroscopy (EDS) elemental composition output for target area "Spectrum 31" indicated in Figure A C.19.

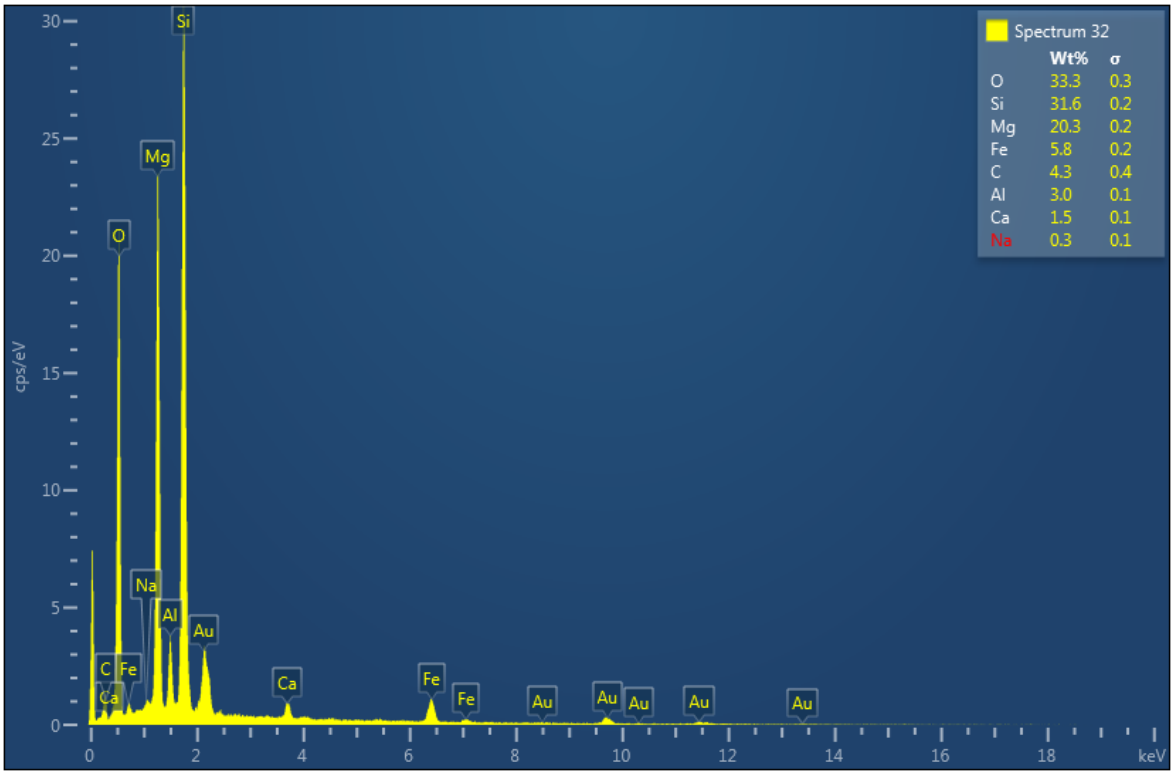

Figure A C.23. Energy dispersive X-ray spectroscopy (EDS) elemental composition output for target area "Spectrum 32" indicated in Figure A C.19.

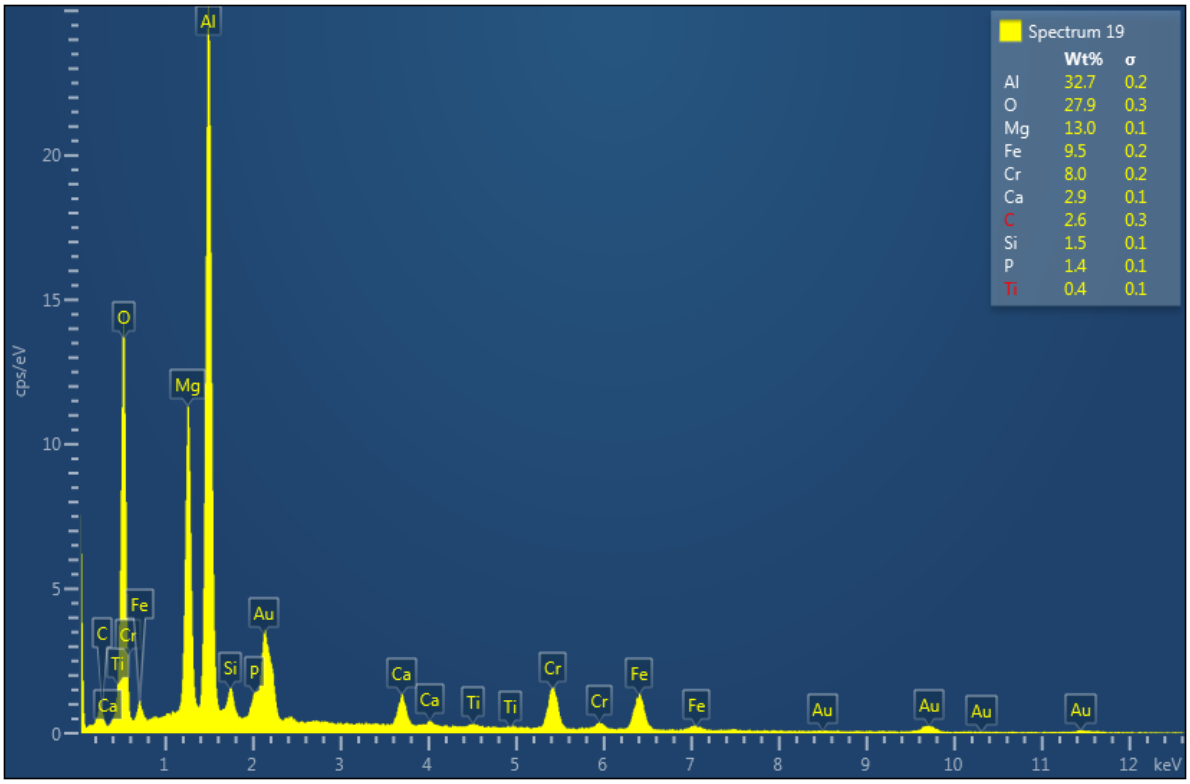

Figure A C.24. Energy dispersive X-ray spectroscopy (EDS) elemental composition output for target area "Spectrum 19" indicated in Figure 2.28.

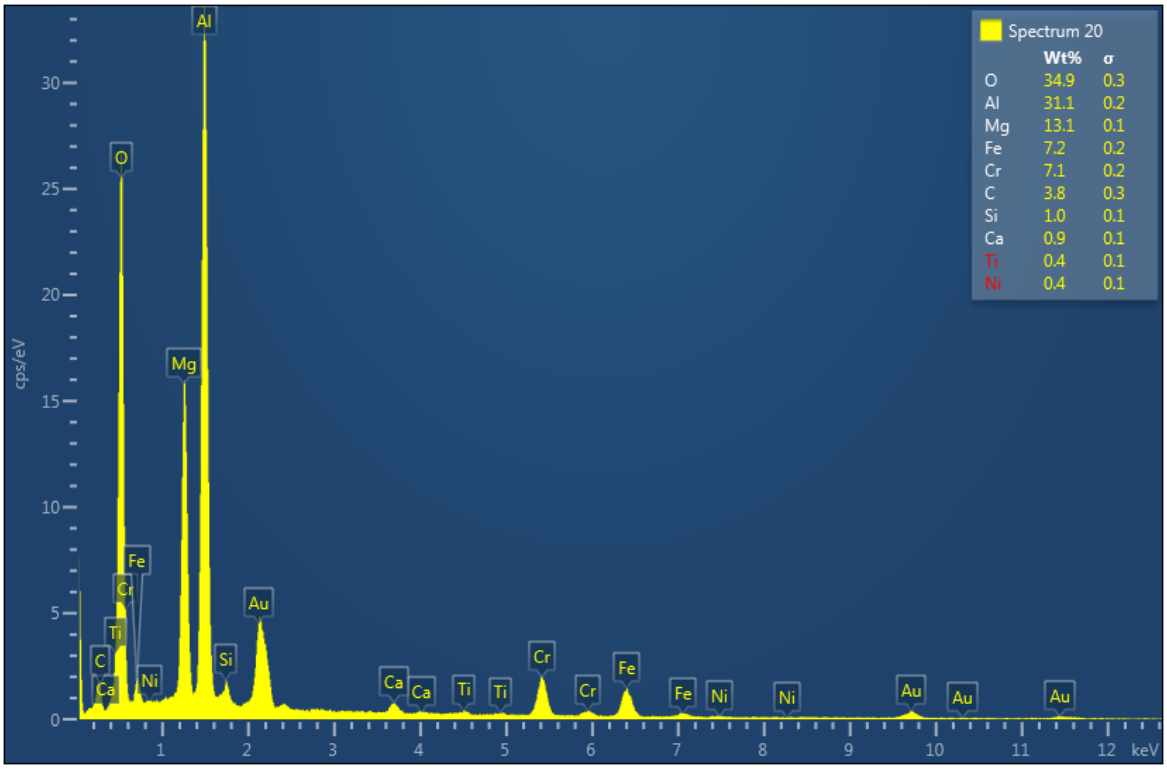

Figure A C.25. Energy dispersive X-ray spectroscopy (EDS) elemental composition output for target area "Spectrum 20" indicated in Figure 2.28.

Table A C.3 Raw ICP-MS data for analysis of olivine culture and control end-point filtrates. Series notation: PO=strain 2002, TO=*T. denitrificans*, KO=strain KS1, BO=strain BoFeN1, CO=control.

	He					No Gas	
	ppb						
Sample	**Mn**	**Fe-56**	**Fe-57**	**Cu**	**Mo**	**Mn**	**Mo**
PO1	17.8562	8.595639	11.13759	1.547744	15.31409	17.65527	12.59653
PO2	20.20211	5.610946	7.780992	1.511714	17.33237	20.84279	13.10704
PO3	20.49738	11.61293	13.56349	1.753999	16.94636	22.98154	12.86386
TO1	31.08078	45.88342	47.86655	0.690045	16.5661	33.00283	12.08827
TO2	34.64611	39.17765	40.81847	0.89616	15.4565	35.55027	12.1985
TO3	28.89173	49.92566	51.51689	1.181537	14.7412	30.54645	11.86973
KO1	20.98789	10.10439	11.90999	1.73417	15.29297	22.98573	12.83719
KO2	25.40154	13.59169	15.36696	0.772921	15.01761	26.7025	12.83807
KO3	21.01618	6.794112	8.692059	2.118481	14.01843	22.66491	12.59674
BO1	18.70218	5.935361	7.848834	3.6844	14.66441	20.79754	12.91237
BO2	19.69466	6.104499	8.120475	1.818324	14.41459	21.40139	13.18488
BO3	21.65804	11.49389	13.00036	1.145749	13.82586	23.18003	12.67092
CO1	31.97981	57.44925	58.22066	1.05418	12.79469	31.49385	12.47533
CO2	32.8098	53.64396	54.48553	1.312402	13.25147	33.36497	12.08453
CO3	32.53004	56.50158	57.22132	0.640137	12.77605	31.93205	12.19415

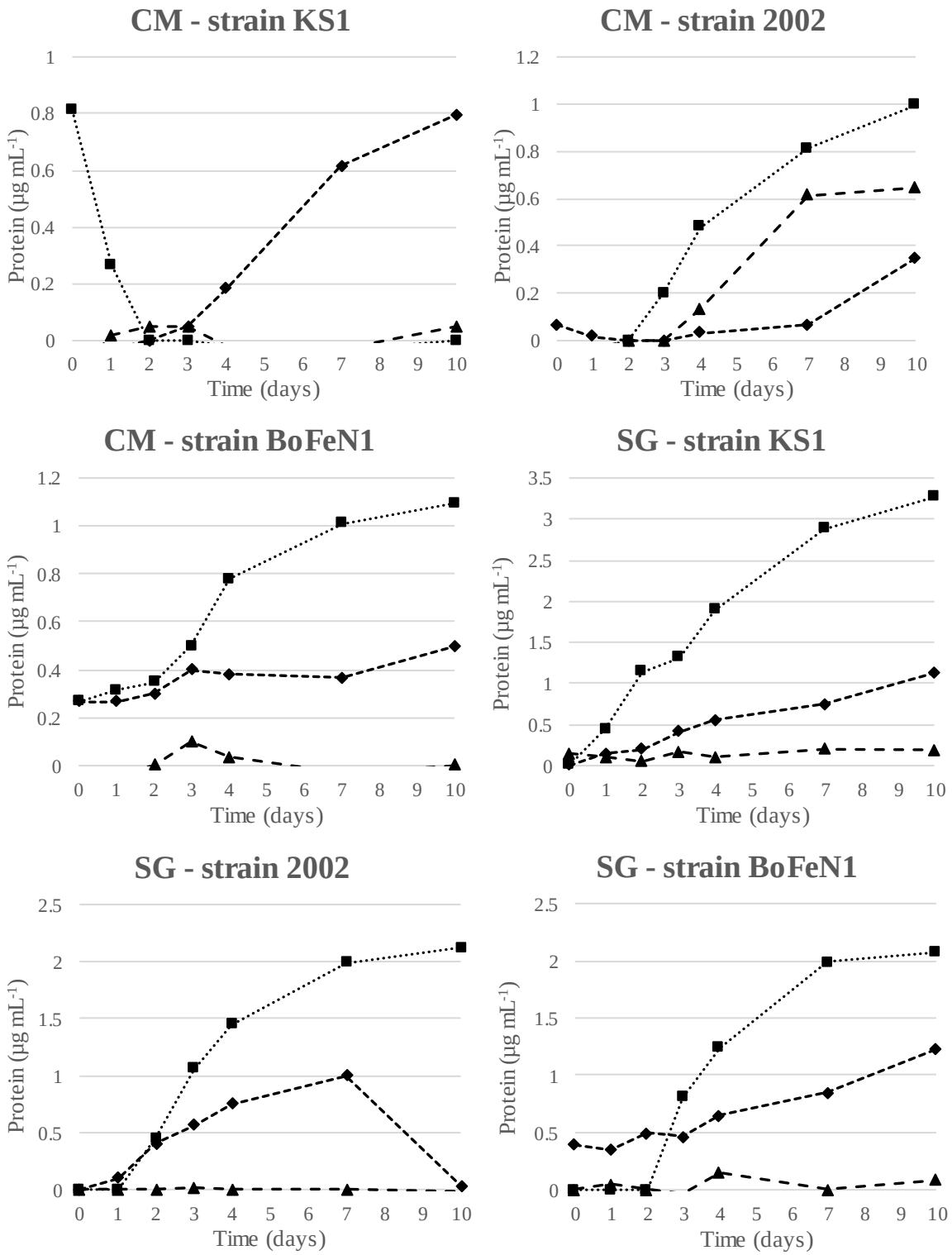

Figure A C.26. Protein concentrations for individual triplicate cultures of *Paracoccus sp*. strain KS1, *Pseudogulbenkiania sp*. strain 2002 and *Acidovorax sp*. strain BoFeN1 in Contemporary Mars (CM) and Shergottite (SG) brines.

Table A C.4. Significance tests for pH at 10 days between martian simulant media cultures and controls (shaded).

Media	Series	KS1	2002	Control
Contemporary Mars	KS1			
	2002	0.29435		
	Control	0.899496	0.379868	
	BoFeN1	0.38022	0.072843	0.49872
Sulfur-Rich	KS1			
	2002	0.03775		
	Control	0.134819	0.1086	
	BoFeN1	0.188292	0.127712	0.656193
Haematite-Rich	KS1			
	2002	0.337734		
	Control	0.424892	0.465162	
	BoFeN1	0.537832	0.597306	0.899496
Shergottite	KS1			
	2002	0.612782		
	Control	0.689615	0.026148	
	BoFeN1	0.26341	0.411867	0.754804

Chapter 4

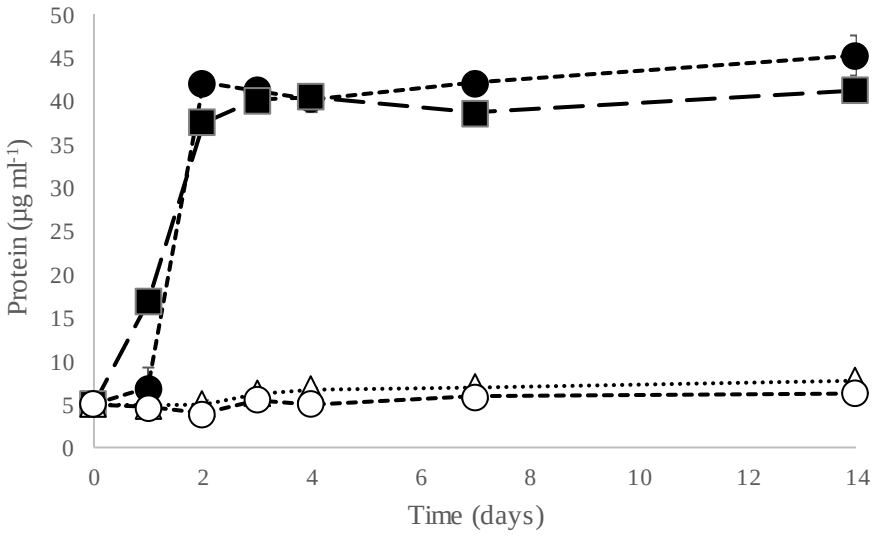

Figure A C.27 Unnormalised protein concentrations over time for *Salmonella enterica* Serovar Typhimurium strain SL1344 wild-type (filled circles) and Δ*narGHIJ* mutant (filled squares), abiotic nitrite control (open triangles) and negative control (open circles).